The formation and the stellar populations of dwarf galaxies

Dissertation
zur Erlangung des Doktorgrades (Dr. rer. nat.)
der
Mathematisch-Naturwissenschaftlichen Fakultät
der
Rheinischen Friedrich-Wilhelms-Universität Bonn

vorgelegt von
Jörg Dabringhausen
aus
Bonn

Bonn, 2013

Angefertigt mit Genehmigung der Mathematisch-Naturwissenschaftlichen Fakultät der Rheinischen Friedrich-Wilhelms-Universität Bonn.

1. Gutachter: Prof. Dr. Pavel Kroupa

2. Gutachter: Prof. Dr. Cristiano Porciani

Tag der Promotion: 23.09.2013

Erscheinungsjahr: 2013

Summary

This thesis is on the origin, the evolution and the stellar populations of ultra compact dwarf galaxies (UCDs) and dwarf elliptical galaxies (dEs), i.e. two kinds of stellar systems in the same mass range and with similar morphology, but very different extensions.

One of the most intriguing properties of UCDs are the mass-to-light ratios that are implied by their internal dynamics. These mass-to-light ratios are significantly higher than imaginable for any realistic pure stellar population, if the initial stellar mass function (IMF) is the same in all star-formation events. Thus, in contrast to the stellar population in the solar neighborhood, the UCDs furnish evidence for a varying IMF instead of a universal IMF.

Given that the UCDs are old stellar systems, there are two possibilities by which a varying IMF could lead to an enhanced mass-to-light ratio of present-day stellar populations, if they are compared to stellar populations that formed with the universal IMF. The first possibility is a bottom-heavy IMF, i.e. an IMF that is overabundant in faint low-mass stars in comparison to the universal IMF. The second possibility is a top-heavy IMF, i.e. an IMF that is overabundant in high-mass stars, which quickly evolve into stellar remnants that contribute mass, but almost no light to a stellar population.

These two possibilities can be distinguished by attempting to detect the remnants of massive stars independent of the effect that they would have on the mass-to-light ratio of a stellar population. For this reason, the frequency of bright X-ray sources in UCDs was studied, since a bright X-ray source can be interpreted as a low-mass X-ray binary (LMXB), which is composed of a low-mass star and a stellar remnant. Using archival data, it has been shown in this thesis that indeed a remarkably high fraction of the UCDs in the Virgo cluster are bright X-ray sources, which implies that UCDs contained a large population of high-mass stars when they formed, i.e. that the IMF in the UCDs was top-heavy. Moreover, the top-heavy IMF that was derived from the fraction of UCDs with a bright LMXB is consistent with the IMF that was derived from the mass-to-light ratios of the UCDs.

Since UCDs are likely to loose mass by the evolution of massive stars, the shape of the IMF has implications for their evolution and their initial conditions. Based on the estimates for the IMF in UCDs, it has been concluded that the UCDs must have been extremely dense when they formed. These extreme initial conditions may explain that UCDs formed with an IMF that deviates from the IMF in less extreme environments.

Regarding the origin of the UCDs, it has been argued in the literature that they are created by the interaction between gas-rich galaxies. However, the formation of dEs may have been triggered by the same process, since it has been shown in this thesis that young galaxies that form through the interaction between gas-rich galaxies, so-called tidal dwarf galaxies (TDGs), would evolve naturally into dEs as far as their masses and radii are concerned.

Moreover, the rather low rates for the production of long-lived TDGs would already be sufficient to account for the observed number of dEs. Neither the UCDs nor the dEs would contain non-baryonic cold dark matter if they formed through galaxies encounters. This is however in contradiction to the currently prevailing cosmological model, which predicts the existence of primordial stellar systems that formed within haloes of non-baryonic dark matter in the same mass range. The results presented here thus add to the growing body of evidence that this cosmological model needs to be revised.

Preface

This thesis is structured as follows:

- Chapter (1) gives an short introduction and an overview of the topics treated in chapters (2) to (7).
- Chapter (2) is based on Dabringhausen, Hilker & Kroupa, *" From star clusters to dwarf galaxies: The properties of dynamically hot stellar systems"*, (2008, MNRAS, 386, 864). In this chapter, the scaling relations of pressure supported stellar systems are discussed, with an emphasis on the mass-to-light ratios of ultra-compact dwarf galaxies (UCDs).
- Chapter (3) is based on Dabringhausen, Baumgardt & Kroupa, *"A top-heavy stellar initial mass function in starbursts as an explanation for the high mass-to-light ratios of ultra-compact dwarf galaxies"*, (2009, MNRAS, 394, 1529). In this chapter, it is quantified how a top-heavy stellar initial mass function (IMF) could explain the mass-to-light ratios of UCDs.
- Chapter (4) is based on Dabringhausen, Fellhauer & Kroupa, *"Mass loss and expansion of ultra compact dwarf galaxies through gas expulsion and stellar evolution for top-heavy stellar initial mass functions"*, (2010, MNRAS, 403, 1054). In this chapter, it is discussed how a top-heavy IMF would affect the evolution and the stability of UCDs.
- Chapter (5) is based on Dabringhausen, Kroupa, Pflamm-Altenburg & Mieske, *"Low-mass X-Ray Binaries Indicate a Top-heavy Stellar Initial Mass Function in Ultracompact Dwarf Galaxies"*, (2012, ApJ, 747, 72). In this chapter, the frequency of low-mass X-ray binaries is used as an additional test for the hypothesis of a top-heavy IMF in UCDs.
- Chapter (6) is based on Dabringhausen & Kroupa, *"Dwarf elliptical galaxies as ancient tidal dwarf galaxies"*, (2013, MNRAS, 429, 1858). In this chapter, it is discussed whether the dwarf elliptical galaxies formed as primordial galaxies or as tidal dwarf galaxies.
- Chapter (7) is based on Section (3) in Kroupa, Famaey, de Boer, Dabringhausen, Pawlowski, Boily, Jerjen, Forbes, Hensler & Metz, *"Local-Group tests of dark-matter concordance cosmology. Towards a new paradigm for structure formation"*, (2010, A&A, 523, 32). In this chapter, it is discussed whether the masses estimated for the satellite galaxies of the Milky Way are consistent with them being a population of primordial galaxies that formed in haloes of cold dark matter.
- Chapter (8) gives an outlook on possible future work.

Thus, chapters (2) to (6) are based on the first-author papers I have published during my time a PhD-student and chapter (7) is based on my contribution to a paper by Prof. Dr. Kroupa. These parts of the thesis have been published already in refereed astronomical journals. As the changes in chapters (2) to (7) with respect to the original publications have been kept to a minimum, some parts in these chapters may be redundant.

Bonn, June 2013

Contents

List of Figures

List of Tables

Chapter 1

Introduction and Overview

1.1 Types of spheroidal stellar systems

Many extra-Galactic stellar systems are not disk-shaped or irregular, but spheroidal. Their common morphology despite very different extensions and masses reflects a common physical property of these systems, namely that random motions of stars contribute at least as much to the total internal kinetic energy of the stellar system as ordered motions of stars. In an analogy to microscopic systems, where heat and pressure are phenomena linked to random motions of atoms and molecules, these stellar system are referred to dynamically hot or pressure-supported (as opposed to rotationally supported).

A closer inspection reveals that pressure-supported stellar systems can be distinguished into several subgroups, even though some of these distinctions may only exist for historical reasons instead of physical reasons:

- **normal elliptical galaxies (nEs).** The nEs have stellar populations with total masses $M_* \gtrsim 10^{10}\ \mathrm{M}_\odot$ and effective half-light radii $r_\mathrm{e} \gtrsim 10^3\ \mathrm{pc}$. In a 3-dimensional parameter space defined by the effective half-light radius, the effective surface brightness and the central velocity dispersion, the normal elliptical galaxies are aligned along a plane. This plane is known as the fundamental plane (Bender et al. 1992 and references therein).

- **dwarf elliptical galaxies (dEs).** The dEs have stellar populations with total masses $10^6\ \mathrm{M}_\odot \lesssim M_* \lesssim 10^{10}\ \mathrm{M}_\odot$ and effective half-light radii of the order of 10^3 pc. The dEs do not lie along the fundamental plane defined by the nEs. This motivates to consider dEs a population of their own, even though there is a transition between nEs and dEs at a total stellar mass of $M_* \approx 10^{10}\ \mathrm{M}_\odot$, where the objects cannot be classified unambiguously.

- **dwarf spheroidal galaxies (dSphs).** The dSphs have stellar populations with total masses $10^3\ \mathrm{M}_\odot \lesssim M \lesssim 10^6\ \mathrm{M}_\odot$ and effective half-light radii of the order of 10^2 pc. The mass-to-light ratios of the dSphs are usually much higher than the mass-to-light ratios of dEs, when the mass of the stellar systems is estimated from their internal dynamics under the assumptions of virial equilibrium and Newtonian dynamics. Other than this, the dSphs appear to be the low-mass extension of the population of 'normal' dEs (see Ferguson & Binggeli 1994), so that a distinction between dSphs and dEs would only have historical reasons.

  The high mass-to-light ratios derived for dSphs under the assumptions of virial equilibrium and Newtonian dynamics have often lead to the conclusion that the dSphs mostly consist of non-baryonic dark matter (e.g. Mateo 1998 and Wolf et al. 2010) and have formed as primordial galaxies in the early Universe. There is however also evidence that the dEs and the dSphs are not primordial galaxies, but galaxies that have been created by tidal interactions between gas-rich galaxies (Kroupa P. et al. 2010; Kroupa 2012), and as such they would not contain significant amounts of non-baryonic dark matter (Barnes & Hernquist 1992b; Bournaud 2010). This matter is discussed in greater detail in Section 1.9 and Chapter 6.

- **globular clusters (GCs).** The GCs have stellar populations with total masses $10^4\ \mathrm{M}_\odot \lesssim M \lesssim 10^6\ \mathrm{M}_\odot$ and effective half-light radii of a few pc. Thus, the GCs are much more compact than the afore mentioned galaxies and can thereby easily be distinguished from them (see Gilmore et al. 2007, Section 1.8 and Chapter 6).

- **ultra compact dwarf galaxies (UCDs).** The UCDs have stellar populations with total masses $10^6\ \mathrm{M}_\odot \lesssim M \lesssim 10^8\ \mathrm{M}_\odot$ and effective half-light radii 10 pc $\lesssim r_\mathrm{e}\ 100$ pc. With these parameters, UCDs are easy to detect in the local Universe, but difficult to observe in detail. Already at the distance of neighboring galaxy clusters, UCDs are only distinguishable from point sources if they are observed with the best available telescopes under excellent seeing conditions. Obtaining a detailed spectrum of a single UCD at that distance requires hours of observing time. In this respect, UCDs are similar to GCs, for which it is known since a long time that they also accompany galaxies beyond the Local group of galaxies. However, since observers did not expect to find objects with extensions similar to those of GCs but luminosities like the ones of dEs, the UCDs in the local Universe have been interpreted as faint stars in the Milky Way, or as bright and distant background galaxies. The true nature of these UCDs has only been discovered quite recently in surveys of the stellar systems in the Fornax galaxy cluster by Hilker et al. (1999) and by Drinkwater et al. (2000). In contrast to earlier studies, these authors did not preselect stellar systems as possible members of the Fornax cluster by their brightness and their structure, but estimated the distance of every object within their field of view from its red shift. They thereby established that the UCDs in that field of view are actually members of the Fornax cluster and concluded that they must be stellar systems that are unusually compact for their brightness. Since then, UCDs have also been discovered in other galaxy clusters.

  The origin of UCDs is still a matter of debate. As they are quite similar to GCs in many respects, they have been suggested to be extremely bright GCs (Mieske et al. 2002, 2012). This is consistent with the finding that their numbers are few compared to typical GCs with luminosities $L < 10^6\ \mathrm{L}_\odot$, and that most UCDs have been detected near galaxies with particularly rich GC systems, i.e. the nEs in neighboring galaxy clusters. However, the UCDs have also been suggested to be stellar systems that evolved from the merger of several GC-like stellar systems (Fellhauer & Kroupa 2002a). Based on the observation of systems of groups of young and bright star clusters in the Antennae galaxies, the existence of objects that would qualify as UCDs was already predicted by (Kroupa 1998). Yet another model for the formation of UCDs that has been found to be consistent with the observational data is that the UCDs are the nuclei of nucleated dwarf galaxies whose outer parts have been stripped by tidal fields as they moved through the potential of a major galaxy (Bekki et al. 2003). Finally, the UCDs have been proposed to be primordial stellar systems within haloes of non-baryonic dark matter (Drinkwater et al. 2004). On first sight, this last hypothesis explains why the typical mass-to-light ratios derived from the internal dynamics of the UCDs are clearly higher than those estimated for typical GCs with the same method. However, on second sight, a difference between the stellar populations that formed in UCDs and the stellar populations that formed in GCs seems to the the more promising explanation for the difference between the mass-to-light ratios estimated from the internal dynamics of these stellar systems, as is discussed in this thesis (see Section 1.7 and Chapter 5 in particular).

In this thesis, the emphasis lies on how the stellar populations of UCDs would influence observed properties, and to a lesser extent on the nature and origin of UCDs as well as dEs.

1.2 The stellar initial mass function

Besides the age, the star formation history and the metallicity, the properties of a stellar system are determined by the mass spectrum of its stellar population. This is because the properties of stars strongly depend on their mass.

The mass spectrum of stars in a stellar system is quantified by the present-day mass function (PDMF),

$$dN = \Xi(m)\, dm, \tag{1.1}$$

where dN is the number of stars in the mass interval $[m, m + dm]$. However, stars loose mass during their lifetime and eventually cease to exist. Therefore, the PDMF is different from the mass spectrum of newly born stars, which is quantified by the stellar initial mass function (IMF),

$$dN = \xi(m)\, dm, \tag{1.2}$$

where dN is the number of newly born stars in the mass interval $[m, m + dm]$.

Note that the IMF of a stellar system cannot be observed, but is a theoretical function that is derived from the observed PDMF (the 'IMF unmeasurability theorem', Kroupa et al. 2011). This is because a stellar system is composed of stars with different (even though possibly very similar) ages. Moreover, the time of birth of a star is a somewhat problematic concept, since a gas cloud evolves continuously into a main-sequence star. It would however be natural if the shape of the IMF is influenced by the conditions under which star formation takes place. For this reason, determining the IMF from the PDMF is worth the effort.

The most direct way to determine the PDMF of a stellar system is to estimate the masses of the individual stars in the stellar system. This can be done by comparing the observed photometric or spectroscopic properties with stellar models. If also the ages of the stars are estimated, the stellar models can be used to determine the IMF of the stellar system.

Determining the IMF from star counts is however tedious work and at the present even impossible for stellar systems beyond the Local group of galaxies, if low-mass stars (i.e. stars with masses $m \lesssim 1\ \mathrm{M}_\odot$) are to be included. This is because low-mass stars are faint and therefore difficult to resolve in observations. Stellar systems with old stellar populations only contain stars with masses $m \lesssim 1\ \mathrm{M}_\odot$. Thus, the PDMFs and thereby the IMFs of old stellar systems beyond the Local Group can only be estimated by the light that is emitted by its stellar population as a whole, so that these estimates of the IMF are rather speculative and uncertain.

In practice, the probable shape of the IMF of old and distant stellar systems is often considered as given, so that other parameters that characterize the stellar population (e.g. its metallicity, its age or its total mass) can be estimated based on the light emitted by the stellar population. This may seem surprising, since a variation of the IMF with initial conditions is expected in theory (see e.g. Larson 1998 for a variation of the IMF with ambient temperature and Murray & Lin 1996 for a variation of the IMF with density). The assumption of a universal IMF for all star-forming systems can however be justified with the resolved stellar populations of the Milky Way, which are consistent with having formed with an invariant IMF (Kroupa 2001, 2002).

This universal IMF is commonly referred to as the canonical IMF. It can be formulated as

$$\xi(m) = k\, k_i\, m^{-\alpha_i}, \tag{1.3}$$

with

$$\alpha_1 = 1.3, \qquad 0.07 \leq \frac{m}{\mathrm{M}_\odot} < 0.5,$$
$$\alpha_2 = 2.3, \qquad 0.5 \leq \frac{m}{\mathrm{M}_\odot} < m_{\max},$$

where m is the initial stellar mass in units of $\mathrm{M}_\odot$, the factor k_i ensures that the IMF is continuous where the power changes and k is a normalization constant. $\xi(m)$ equals 0 if $m < 0.07\,\mathrm{M}_\odot$ or $m > m_{\mathrm{max}}$ (Kroupa 2001; Kroupa et al. 2011). The upper mass limit of the IMF, m_{max}, is a function of the total mass of stars formed in a given star-forming event.

An alternative formulation of the canonical IMF is

$$\xi(m) = k \begin{cases} \frac{\mathrm{M}_\odot}{m} \exp\left[-\frac{1}{2}\left(\frac{\log_{10}\left(\frac{m}{\mathrm{M}_\odot}\right)-\log_{10}(0.055)}{0.75}\right)^2\right] & 0.07 \leq \frac{m}{\mathrm{M}_\odot} < 1, \\ A\left(\frac{m}{\mathrm{M}_\odot}^{-2.3}\right) & 1 \leq \frac{m}{\mathrm{M}_\odot} < m_{\mathrm{max}}, \end{cases} \tag{1.4}$$

where m is the initial stellar mass in units of $\mathrm{M}_\odot$, the factor A ensures that the IMF is continuous and k is a normalization constant. As in equation (1.3), $\xi(m)$ equals 0 if $m < 0.07\,\mathrm{M}_\odot$ or $m > m_{\mathrm{max}}$, and m_{max} is a function of the total mass of stars formed in a given star-forming event.

Both formulations of the canonical IMF are shown in Figure 1.1. They are equivalent for practical purposes, since the uncertainties to the canonical IMF are much larger than the difference between equations (1.3) and (1.4).

However, while the IMF appears to be universal in resolved stellar systems, observational evidence for the contrary has emerged from unresolved stellar populations in elliptical galaxies over the past years (see, e.g. Baugh et al. 2005; Nagashima et al. 2005; van Dokkum 2008; van Dokkum & Conroy 2010; Cappellari M. et al. 2012). Showing that the assumption of a universal IMF is also dubious for UCDs is a central part of this thesis. For a comprehensive overview on the IMF including its possible variation, see Kroupa et al. (2011).

1.3 The mass-to-light ratios of stellar systems

Mass-to-light ratios are a useful indicator for the composition of stellar systems. In this thesis, two different methods to estimate the mass-to-light ratios of UCDs are considered, and the results are compared to each other.

- The first method to estimate the mass-to-light ratio of a UCD is based on models for single-age and single-metallicity stellar populations that formed with a given IMF. Sets of such so-called simple stellar population models (SSP-models) are provided in the literature (e.g. Bruzual & Charlot 2003; Maraston 2005). The SSP-models appropriate for an observed UCD can be confined by using photometrical or spectroscopical data on the observed UCD. The estimates of the mass-to-light ratios of a UCD obtained by this method are called **stellar masses-to-light ratios** in the following.

- The second method to estimate the mass-to-light ratio of a UCD is based on the density profile of a given UCD and its internal velocity dispersion. This method relies on the fact that the internal velocity dispersion of a virialised, undisturbed stellar system is determined by its gravitational potential and thus on its total mass and this mass is distributed over space according to the given density profile. By dividing such an estimate for the mass of a UCD by its luminosity, an estimate for its mass-to-light ratio is obtained. The estimates for the mass-to-light ratio of a UCD obtained with this method are called **dynamical mass-to-light ratios** in the following.

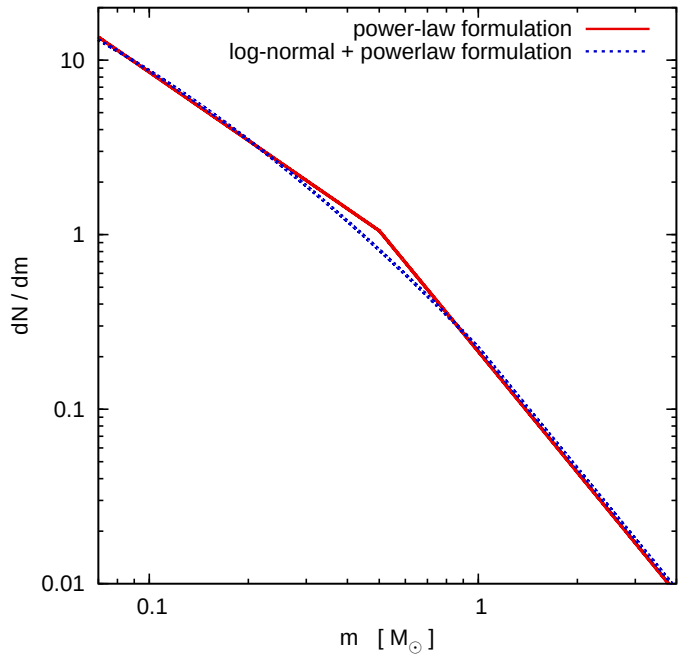

Figure 1.1: A comparison of the canonical IMF formulated with two power-law functions joined together at $m = 0.5\ \mathrm{M}_\odot$ (red solid line, equation 1.3) and formulated with a log-normal function and a power-law function joined together at $m = 1\ \mathrm{M}_\odot$ (blue dotted line, equation 1.4). Plotted is the number of stars per mass interval versus the stellar mass. The IMFs are normalized such that $\int_{0.07}^{150} m\xi(m)\, dm = 1\,\mathrm{M}_\odot$, where m is the mass in solar units. The two IMF forms are practically indistinguishable over the whole mass interval. Above a mass of $1\ \mathrm{M}_\odot$ the two IMFs are in fact identical except for a slightly different normalization factor (see Dabringhausen et al. 2008; Kroupa et al. 2011).

If the assumptions on the stellar population of the UCD are correct and the UCD does not contain significant amounts of gas or dark matter, the estimate of the stellar mass of the UCD should be consistent with the estimate of its dynamical mass. The comparison between the estimates for the mass-to-light ratios is therefore a means to test the assumption that have been made in the estimates.

Note that the data needed to estimate dynamical mass of a UCD is difficult to obtain. Excellent seeing is already required in order to spatially resolve a UCD in a neighboring galaxy cluster, so that a density profile can be fitted to it. Getting a spectrum that is good enough to estimate the internal velocity dispersion of a single UCD at that distance requires hours of observation time with a large telescope. Thus, there are only about 50 UCDs, for which estimates of their dynamical mass are available. They are listed in Mieske et al. (2008).

1.4 The Dynamical Masses of UCDs

($\rightarrow$ Chapters 2 and 3)

In this thesis, the dynamical mass-to-light ratios of the UCDs listed in Mieske et al. (2008) are compared to estimates for their stellar mass-to-light ratios. The SSP-models used for the estimates of the stellar mass-to-light ratios of the UCDs were chosen such that they are consistent with estimates of the metallicity of the UCDs and with the age of the Universe according to the prevailing cosmological model. With the additional assumption that the stellar populations of

the UCDs formed with the canonical IMF, the estimates of the dynamical mass-to-light ratios are higher than the estimates for the stellar mass-to-light ratios for a majority of the considered UCDs.

This discrepancy between the estimates of the stellar mass-to-light ratios and the estimates of the dynamical mass-to-light ratios of the UCDs could either indicate that the UCDs contain additional non-luminous matter or that their stellar populations did not form with the canonical IMF. It is unlikely that UCDs contain much gas, since this is also not the case for old stellar systems like elliptical galaxies or GCs, which are similar to UCDs in many respects. It is also unlikely that that UCDs contain a significant amount of non-baryonic dark matter, since the UCDs are very compact, and non-baryonic dark matter is expected to contribute to the total mass of a stellar system only on much larger scales (Murray 2009). A non-canonical IMF in UCDs thereby becomes the most promising explanation for their high dynamical mass-to-light ratios.

1.5 A top-heavy IMF in UCDs

($\rightarrow$ Chapter 3)

For an old stellar population with a given luminosity, a given age and given metallicity, there are two ways by which a variation of the IMF would make its actual mass-to-light ratio larger compared to the mass-to-light ratio expected for a stellar population that formed with the canonical IMF.

- The first way is an IMF that is compared to the canonical IMF overabundant with low-mass stars. Such an IMF is called **bottom-heavy**. The high mass-to-light ratio of a stellar population with a bottom-heavy IMF is due to the large number of low-mass main-sequence stars, which have a high mass-to-light ratio. A bottom-heavy IMF in UCDs and its possible detection through observations is discussed in Mieske & Kroupa (2008).

- The second way is an IMF that is compared to the canonical IMF overabundant with high-mass stars. Such an IMF is called **top-heavy**. The high mass-to-light ratio of an old stellar population that formed with a top-heavy IMF is due to the large number of white dwarfs, neutron stars and black holes. These objects are the remnants of evolved high-mass stars and have an extremely high mass-to-light ratio. A top-heavy IMF in UCDs is discussed in this thesis.

In order to quantify how top-heavy the IMF has to be in order to explain their dynamical mass-to-light ratios, a varying IMF is formulated as

$$\xi(m) = k\, k_i\, m^{-\alpha_i}, \tag{1.5}$$

with

$$\begin{aligned} \alpha_1 &= 1.3, & 0.1 &\leq \frac{m}{\mathrm{M}_\odot} < 0.5, \\ \alpha_2 &= 2.3, & 0.5 &\leq \frac{m}{\mathrm{M}_\odot} < 1.0, \\ \alpha_3 &\in \mathbb{R}, & 1.0 &\leq \frac{m}{\mathrm{M}_\odot} \leq m_{\max}, \end{aligned}$$

where m is the initial stellar mass in $\mathrm{M}_\odot$, the factors k_i ensure that the IMF is continuous where the power changes and k is a normalization constant and $\xi(m)$ equals 0 if $m < 0.1\,\mathrm{M}_\odot$ or $m > m_{\mathrm{max}}$. The number of stars more massive than $1\ \mathrm{M}_\odot$ depends on the free parameter α_3. Note that for $\alpha_3 = 2.3$, equation (1.5) equals equation (1.3), i.e. the canonical IMF.

Thus, the lower limit for stellar masses in equation 1.5 is chosen to be slightly higher than in equations (1.3) and (1.4), according to which the lower limit for stellar masses is $m = 0.07\,\mathrm{M}_\odot$. The reason for assuming $m = 0.1\ \mathrm{M}_\odot$ instead of $m = 0.07\ \mathrm{M}_\odot$ as a lower limit for the stellar masses in equation (1.5) is that this lower limit for stellar masses is consistent with the SSP-models by Bruzual & Charlot (2003) and Maraston (2005), on which the modeling of the mass-to-light ratios of the UCDs is based. In stellar systems as large as the UCDs, m_{max} is set by the upper mass limit for stars, i.e. $m_{\mathrm{max}} \approx 150\ \mathrm{M}_\odot$.

In stellar populations as old as the ones in UCDs, the massive stars have all evolved into dark stellar remnants. Thus, if the UCDs are assumed to have formed with the variable IMF that is formulated above, $\alpha_3 < 2.3$ (i.e. a top-heavy IMF) implies that their stellar mass-to-light ratios are higher than it would be expected for the canonical IMF.

If the dynamical mass-to-light ratio of a given UCD is above a lower limit that corresponds to $\alpha_3 = \infty$ (which implies that no stars with masses $m > 1\ \mathrm{M}_\odot$ are born), the stellar mass-to-light ratio of this UCD equals its dynamical mass-to-light ratio for a certain value for α_3. At this value for α_3, the dynamical mass-to-light ratio of the UCD can be fully explained with its stellar population.

Note that the value for α_3 where the stellar mass-to-light ratio equals the dynamical mass-to-light ratio of a given UCD is influenced by assumptions that are made on the age of the UCDs and the fraction of stellar remnants that are not expelled. However, also very conservative assumptions (i.e. all UCDs are 13 Gyr old and all stellar remnants are retained by them) imply $\alpha_3 \lesssim 2$, i.e. an IMF that is clearly flatter than the canonical IMF ($\alpha_3 = 2.3$). More realistic assumptions (i.e. some UCDs younger than 13 Gyr old and many stellar remnants are expelled from them) suggest $1 \lesssim \alpha_3 < 2$.

1.6 Stability of UCDs with a top-heavy IMF

($\rightarrow$ Chapter 4)

There are two mechanisms by which a young UCD probably loses mass as it evolves:

1. Short-lived massive stars end their evolution with a supernova explosion, in which most of the matter previously bound to the star is accelerated to velocities much higher than the escape velocity from the UCD.

2. Gas that has not been used up in star formation can be driven out of of the UCDs through the energy input from the massive stars through radiation and supernova explosions.

If the UCDs formed with IMFs that are as top-heavy as suggested in Section (1.5), they might thereby loose more than 90 per cent of their initial mass within some 10^8 years. Such a mass-loss might even destroy a forming UCD, since a stellar system completely dissolves if it looses most of its initial mass on a short enough time-scale (Boily & Kroupa 2003).

It is therefore investigated in this thesis which initial conditions would lead to objects that would be identified as UCDs today when the initial mass-loss is taken into account. For this

reason, the influence of the initial mass-loss on stellar systems with different initial conditions is calculated numerically with SUPERBOX. The results suggest that UCDs formed with initial densities up to $10^8\ \mathrm{M}_\odot\,\mathrm{pc}^{-3}$, while stellar systems recently formed in the Milky Way are characterized by initial densities below $10^6\ \mathrm{M}_\odot\,\mathrm{pc}^{-3}$.

At densities of $10^8\ \mathrm{M}_\odot\,\mathrm{pc}^{-3}$, collisions between protostars become common (Bonnell & Bate 2002), This process would distinguish star formation in UCDs from star formation in less massive stellar systems and may alter the shape of the stellar mass function. The notion of a top-heavy IMF in UCDs and the notion of extremely high initial densities in UCDs are therefore consistent with each other. The resolved stellar populations in the Milky Way from which Kroupa (2001) argued the universality of the IMF may have formed under conditions that were not extreme enough to cause a variation of the IMF.

1.7 Probing the IMF in UCDs with LMXBs

($\rightarrow$ Chapter 5)

A massive star ends its evolution by becoming a neutron star (NS) or a black hole (BH). If such a NS or BH belongs to a tight binary system where the other component is a evolving star, it can accrete gas from the expanding atmosphere of the evolving star. The NS or the BH thereby becomes a bright X-ray source, since the gas is heated up as it is accreted. As a consequence, such binaries can be detected with X-ray telescopes.

In a GC or a UCD, the evolving companion star from which a NS or a BH can accrete matter must be a low-mass star, since in old stellar systems like GCs and UCDs all other stars have already completed their evolution. Such X-ray emitting systems consisting of an evolving low-mass star and the remnant of a massive star are called low-mass X-ray binaries (LMXBs).

The number of LMXBs that are present a any given time depends on their formation rate and their depletion rate. The lifetime of a LMXB is a few 10^8 years, which corresponds to the duration of the giant phase of a $0.8\ \mathrm{M}_\odot$-star. The rate at which binaries that eventually become LMXBs are formed in a GC or a UCD depends on the encounter rate Γ, which is a function of the number density of NSs and BHs, the number density of low-mass stars, the radius of the GC or the UCD and the mass of the GC or the UCD. The average radius of GCs and UCDs as a function of their mass can be estimated from observed values and the number density of low-mass stars and the number density of NSs and BHs can be calculated for a given IMF. Γ can therefore be used to test assumptions on the IMF in UCDs.

If the IMF is assumed to be canonical in all GCs and UCDs and the same fraction of stellar remnants is retained by all GCs and UCDs, Γ and thus the fraction of GCs and UCDs that have a LMXB is expected to increase with mass for GCs and to decrease with mass for UCDs. This is however in strong contradiction with the observations published by Sivakoff et al. (2007), according to which the frequency of LMXBs increases with mass not only for GCs, but also for UCDs. The discrepancy between the observed LMXB-frequency in UCDs and the expected LMXB-frequency under the assumption of the canonical IMF can be explained with a varying IMF that becomes increasingly top-heavy with the mass of the UCDs. This varying IMF is consistent with the varying IMF that was independently derived from the mass-to-light ratios of the UCDs. This agreement is illustrated in Figure (1.2).

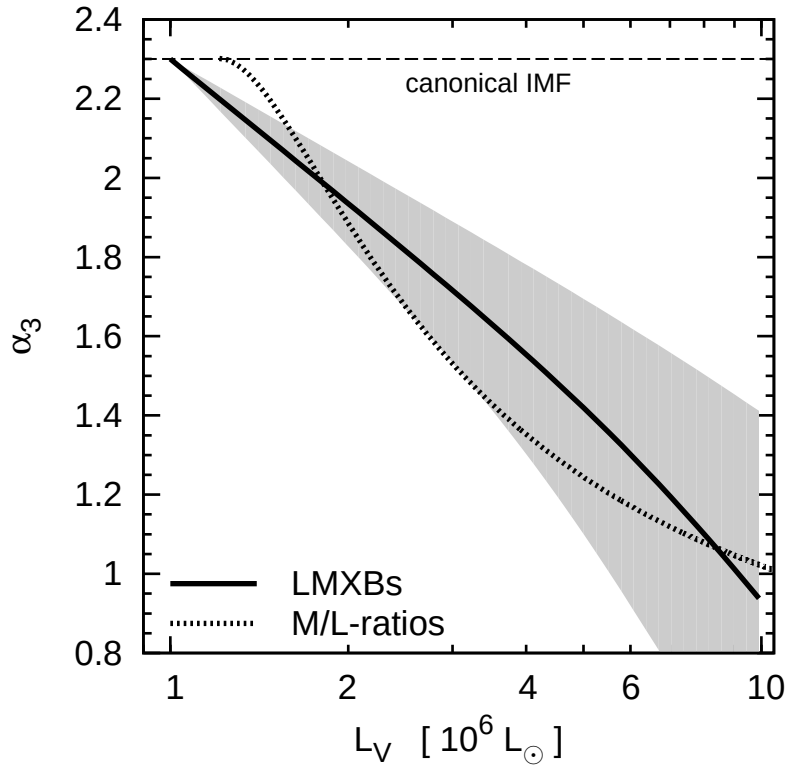

Figure 1.2: The IMF in UCDs. Plotted is the high-mass IMF index, α_3, as a function of the V-band luminosity of the UCDs, L_V, which serves as an indicator for the mass of the UCDs. The solid line shows the best estimate for the high-mass index of the IMF that is required to increase the dark remnant content in UCDs such that the observed LMXB-frequency is matched. The grey shaded area quantifies the likely 3 σ uncertainty on this estimate (see Chapter 5). The horizontal long dashed line marks the canoncial IMF with $\alpha_3 = 2.3$. The dotted line shows the independently calculated high-mass IMF index obtained from the observed mass-to-light ratios of UCDs (see Chapter 3).

1.8 The relation between UCDs and other pressure-supported stellar systems

($\rightarrow$ Chapters 2 and 6)

A much debated issue is the origin and nature of UCDs (e.g. Haşegan et al. 2005). For insights on this matter, it is useful not only to study the internal properties of UCDs, but also to look at the similarities and the differences between UCDs and other pressure-supported stellar systems. The quantities considered for this purpose are the luminosities, the half-light radii and the dynamical masses of the stellar systems, as well as additional physical quantities that can be derived from these parameters.

1.8.1 Half-light radii against luminosity

By displaying the half-light radii of old dynamically hot stellar systems against their mass or luminosity, the following can be seen:

- Nearly all objects belong to one out of two mass-radius sequences. The first sequence

comprises the nEs, the dEs and the dSphs. The second sequence comprises the GCs and the UCDs. Whether a given stellar system is a galaxy or a star cluster can be distinguished by noting to which one of these sequences it belongs.

- The mass-radius sequence of galaxies is flatter below a mass $M \lesssim 10^{10}\ \mathrm{M}_{\odot}$ than it is above this mass limit. This marks the transition between dEs and nEs. The changing slope of the mass-radius sequence suggests that either the dEs are of a different origin than the nEs, or that the dEs have the same origin as the nEs, but evolved differently. It is argued in this thesis that the nEs are primordial galaxies while the dEs are created through the interactions between primordial galaxies, i.e. dEs and nEs have different origins.

- The mass-radius sequence of star clusters is flat below a mass $M \lesssim 10^{6}\ \mathrm{M}_{\odot}$, but not above this mass limit. This marks the transition from GCs to UCDs. The changing slope suggests that either the GCs are of a different origin than the UCDs, or that the GCs have the same origin as the UCDs, but evolved differently. Processes that might be relevant in UCDs but not in GCs are collisions between proto-stars (see Bonnell & Bate 2002) and the capture of radiation within the gas cloud that was the progenitor of a UCD (see Murray 2009). Both processes have been suggested as the cause for a top-heavy IMF, with which the UCDs may have formed according to this thesis. There would then be no fundamental difference between GCs and UCDs, except for their different evolution due to their different masses.

- The UCDs and the nEs lie along a single straight line in mass-radius parameter space. This may indicate that they are shaped by a common physical process, despite the fact that UCDs and nEs are separated by a gap in mass comprising two orders of magnitude. Murray (2009) suggested that the UCDs formed by the monolithic collapse of a gas cloud. If this notion is correct, formation by the monolithic collapse of a gas cloud could be the process that the UCDs and the nEs have in common.

1.8.2 Dynamical mass-to-light ratios against luminosity

By displaying the dynamical mass-to-light ratios of dynamically hot stellar systems against their luminosity, the following can be seen:

- The central dynamical mass-to-light ratios of nEs are in some cases slightly higher than what could be explained by a pure stellar population with the canonical IMF. This is either interpreted as dark matter in nEs (Tortora et al. 2009) or as a varying IMF in nEs (Cappellari M. et al. 2012).

- The dynamical mass-to-light ratios of some dSphs are extremely high. This has been interpreted as dark matter in dSphs (e.g. Strigari et al. 2008), as an indicator for non-Newtonian dynamics in dSphs (e.g. Gentile et al. 2007; McGaugh & Wolf 2010), or as an indication for that the dSphs are not in virial equilibrium (e.g. Casas et al. 2012). Note that the interpretation of the high dynamical mass-to-light ratios of dSphs as a presence of dark matter is problematical, since there is significant evidence that dSphs are dark-matter free galaxies that formed through the collision of other galaxies (e.g. Kroupa P. et al. 2010).

- The dynamical mass-to-light ratios of UCDs are somewhat and systematically higher than would be expected if the UCDs were pure stellar populations that formed with the canonical IMF. It is shown in this thesis that a promising explanation for this finding is that the IMF in UCDs was top-heavy (see Chapters 3, 4 and 5).
- The dynamical mass-to-light ratios of GCs are much lower than would be expected if the GCs were pure stellar populations that formed with the canonical IMF and were subject only to stellar evolution. A possible explanation for this finding is that the GCs formed mass-segregated and lost many faint low-mass stars at the outskirts of the GCs during gas expulsion (Marks et al. 2008, 2012).

1.8.3 Relaxation times

The median relaxation time of a stellar system measures the time at which the motions of the stars in a stellar system have randomized completely due to encounters with other stars in the stellar system. It is shown to be

$$t_{\rm rh} = \frac{0.234}{\log(M/{\rm M}_\odot)} \times \sqrt{\frac{M\ r_{\rm e}^3}{G}}, \tag{1.6}$$

where M is the mass of the stellar system in units of $\mathrm{M}_\odot$, $r_{\rm e}$ is its projected half-light radius in units of pc and $G = 0.0045\ \mathrm{pc}^3\,\mathrm{M}_\odot^{-1}\,\mathrm{Myr}^{-2}$ is the gravitational constant. If a stellar system is much older than $t_{\rm rh}$, it has evolved dynamically. This means that the stellar system has completed a significant part of its lifetime until its evolution driven by encounters between its stars lead to the dissolution of the stellar system.

If the $t_{\rm rh}$ UCDs and GCs are compared to the age of the universe, it turns out that $t_{\rm rh} \lesssim \tau_H$ for GCs and $t_{\rm rh} \gtrsim \tau_H$ for UCDs. Thus, taking $t_{\rm rh} > \tau_{\rm H}$ as the criterion that defines a galaxy (cf. Kroupa 2012), UCDs would be galaxies, while their location in mass-radius parameter space suggests that they are star-clusters (cf. Section 1.8.1).

1.9 Tidal dwarf galaxies as progenitors of dE and dSph galaxies

($\rightarrow$ Chapter 6)

According to the currently prevailing cosmological model, the main contributions to the total energy content of the Universe are dark energy (Λ) and cold dark matter (CDM). For this reason this cosmological model is called the ΛCDM-model.

A prediction by the ΛCDM-model is that two kinds of dwarf galaxies should exist in the Universe, namely primordial dwarf galaxies (PDGs) that formed within haloes of cold dark matter (CDM) and tidal dwarf galaxies (TDGs) that are created by interactions between existing galaxies (Weilbacher et al. 2000; Bournaud & Duc 2006; Kroupa P. et al. 2010). This finding has been termed the 'dual dwarf theorem' by Kroupa (2012).

The PDGs are often identified with the dEs and the dSphs, since the masses derived for dEs and dSphs are in the expected range and the stellar populations of the dEs and the dSphs are old. Moreover, assuming that dSphs are in virial equilibrium and Newtonian dynamics is valid in them, the motions of the stars in dSphs can usually only be explained with dark matter in

dSphs. The TDGs can be identified with young stellar systems that have been observed near galaxies that show traces of a recent interaction. Thus, observations seem consistent with the 'dual dwarf theorem' on first sight.

However, between one and two TDGs that survive on a time-scale of 10^9 years are created per encounter between gas-rich galaxies according to Bournaud & Duc (2006). This raises the question what the young TDG-candidates observed near interacting galaxies would look like after some 10^9 years.

It has been shown in this thesis that the young TDG-candidates would naturally evolve onto the mass-radius sequence constituted by the dEs. Thus, the TDGs would become indistinguishable from dEs as far as their masses and their radii are concerned as soon as the TDGs reach ages that are typical for dEs. It has moreover been shown by Okazaki & Taniguchi (2000) that already a rather low production rate of 1-2 long-lived TDGs per galaxy encounter would be sufficient to account for all dEs in the Universe. Thus, the dEs can be interpreted as old TDGs. This would also explain the anisotropic distribution that has been found for the dSphs (i.e. low-mass dEs) that accompany the Milky Way (Metz et al. 2009; Pawlowski et al. 2012b) and the Andromeda galaxy (Ibata et al. 2013) .

It is however known that TDGs cannot contain significant amounts of dark matter, even if their progenitor galaxies did (Barnes & Hernquist 1992b; Bournaud 2010). As a consequence, an additional population of PDGs that formed within CDM-haloes is expected to be located in a different region in mass-radius parameter space. This is because PDGs and TDGs are expected to evolve differently, if PDGs contain an additional matter component that would, due to its different nature, not behave like baryonic matter.

As far as their location in mass-radius parameter space is concerned, the GCs and the UCDs seem to be good candidates for the PDGs, if the dEs are the TDGs. The slightly elevated mass-to-light ratios of the UCDs are however probably due to a large population of stellar remnants, and not an indicator for CDM-halos around UCDs (see Chapters 3, and 5). Moreover, complexes of star clusters as they are observed in interacting galaxies can evolve into UCDs (Fellhauer & Kroupa 2002a) and like any stellar system of tidal origin, such UCDs would not have their own CDM-halos.

It may seem surprising that the formation of stellar systems that appear to be as different as dEs and UCDs could have been triggered by the same process, namely the interaction between gas-rich galaxies. This notion is however indeed consistent with the numerical calculations by Bournaud et al. (2008), even though it is not understood what exactly would lead to the formation of two distinct kinds of stellar systems from the matter expelled through the interaction of galaxies.

However, if both dEs and UCDs are stellar systems that formed through tidal interactions, there are no candidates for PDGs that formed within CDM-halos. This contradicts the 'dual dwarf theorem' that follows from the ΛCDM-model. Thus, if the above interpretation of the nature of dEs and UCDs is correct, the ΛCDM model needs to be revised significantly, or to be replaced with a new model.

1.10 The satellite galaxies of the Milky Way as CDM-dominated objects

(→ Chapter 7)

One of the predictions of the ΛCDM-model is the existence of many subhaloes within larger CDM-haloes. The mass-function of the subhaloes is well constrained within the ΛCDM-model, so that the expected number of subhaloes within the hypothetical CDM-halo of the Milky Way can be calculated. This number is however much higher than the number of dwarf galaxies that accompany the Milky Way (Moore et al. 1999; Klypin et al. 1999), which implies that most sub-haloes of the CDM-halo of the Milky cannot contain a visible galaxy if the ΛCDM-model is correct. For this reason, models for the removal of baryons from CDM-haloes have been developed. Based on such models, a mass function for luminous CDM-subhaloes can be estimated, which quantifies the mass function of galaxies according to the ΛCDM-model.

In this thesis, the mass function for luminous CDM-subhaloes that is expected for a galaxy like the Milky Way according to Li et al. (2010) is compared to the mass function of satellite galaxies of the Milky Way. Note that the masses of the satellite galaxies of the Milky were computed under the assumptions that the galaxies are in virial equilibrium and that Newtonian dynamics is valid in them.

However, if the masses estimated for the satellite galaxies of the Milky Way are correct, they are not consistent with having been drawn from the mass function of luminous sub-haloes by Li et al. (2010). Given the evidence for the low-mass satellite galaxies of the Milky Way being ancient TDGs instead of PDGs, this inconsistency is not unexpected. A complete absence of PDGs around the Milky Way is however inconsistent with the ΛCDM-model, which implies that this model needs to be revised significantly, or to be replaced with a new model.

Chapter 2

From star clusters to dwarf galaxies: The properties of dynamically hot stellar systems

J. Dabringhausen, M. Hilker, P. Kroupa, 2008, **MNRAS**, 386, 864

Abstract:

Objects with radii of $10\ \mathrm{pc}$ to $100\ \mathrm{pc}$ and masses in the range from $10^6\ \mathrm{M}_\odot$ to $10^8\ \mathrm{M}_\odot$ have been discovered during the past decade. These so-called ultra compact dwarf galaxies (UCDs) constitute a transition between classical star clusters and elliptical galaxies in terms of radii, relaxation times and V-band mass-to-light ratios. Using new data, the increase of typical radii with mass for compact objects more massive than $10^6\,\mathrm{M}_\odot$ can be confirmed. There is a continuous transition to the typical, mass-independent radii of globular clusters (GCs). It can be concluded from the different relations between mass and radius of GCs and UCDs that at least their evolution must have proceeded differently, while the continuous transition could indicate a common formation scenario. The strong increase of the characteristic radii also implies a strong increase of the median two-body relaxation time, t_{rel}, which becomes longer than a Hubble time, τ_{H}, in the mass interval between $10^6\,\mathrm{M}_\odot$ and $10^7\,\mathrm{M}_\odot$. This is also the mass interval where the highest stellar densities are reached. The mass-to-light ratios of UCDs are clearly higher than the ones of GCs, and the departure from mass-to-light ratios typical for GCs happens again at a mass of $\approx 10^6\,\mathrm{M}_\odot$. Dwarf spheroidal galaxies turn out to be total outliers compared to all other dynamically hot stellar systems regarding their dynamical mass-to-light ratios. Stellar population models were consulted in order to compare the mass-to-light ratios of the UCDs with theoretical predictions for dynamically unevolved simple stellar populations (SSPs), which are probably a good approximation to the actual stellar populations in the UCDs. The SSP models also allow to account for the effects of metallicity on the mass-to-light ratio. It is found that the UCDs, if taken as a sample, have a tendency to higher mass-to-light ratios than it would be expected from the SSP models assuming that the initial stellar mass function in the UCDs is the same as in resolved stellar populations. This can be interpreted in several ways: As a failure of state-of-the-art stellar evolution and stellar population modelling, as a presence of dark matter in UCDs or as stellar populations which formed with initial stellar mass functions different to the canonical one for resolved populations. But it is noteworthy that evidence for dark matter emerges only in systems with $t_{\mathrm{rel}} \gtrsim \tau_{\mathrm{H}}$.

2.1 Introduction

Star clusters can be defined as stellar population with a median two-body relaxation time, $t_{\rm rel}$, shorter than a Hubble time, $\tau_{\rm H}$, while galaxies would have $t_{\rm rel} > \tau_{\rm H}$ (Kroupa 1998). The dynamical evolution of the former is well described by pure Newtonian dynamics, while for the successful representation of the latter either a significant amount of dark matter (DM) is required for Newtonian gravity to remain valid, or modified gravity needs to be invoked. By moving from two-body relaxation dominated systems to such where two-body relaxation plays no role, we thus observe the appearance of fundamentally new physics. A transition class of objects between classical star clusters and galaxies may shed insights to the possible nature of the deviant dynamics apparent on galaxy scales.

It has been almost 10 years since Hilker et al. (1999) and Drinkwater et al. (2000) discovered these transition objects in the Fornax galaxy cluster. With apparent V-band magnitudes of $\lesssim 19.5\,\mathrm{mag}$ at that distance, they can in principle be detected without difficulty. However, they cannot be discriminated from point sources with ground-based telescopes, except with the ones with the highest currently available resolutions. Because of this combination of small extension and high brightness they were usually thought to be foreground stars. Only a radial velocity survey of *all* objects with a certain brightness in an area around the central galaxy of the Fornax cluster was able to reveal their membership to that galaxy cluster. Phillipps et al. (2001) were the first ones to call them ultra compact dwarf galaxies (UCDs), a term which is widely in use for this type of objects at the present. Drinkwater et al. (2003) reported that these objects are not only distinct from the globular clusters in the Milky Way (MWGCs) by their higher V-band (L_V) luminosity, but also by their larger radii and higher dynamical V-band mass-to-light (M/L_V) ratios. At the same time, there is no gap in luminosity between globular clusters (GCs) and UCDs (Mieske et al. 2002, 2004). Haşegan et al. (2005) discovered in the Virgo cluster massive compact star clusters with similar properties like the ones in the Fornax cluster, but called them dwarf-globular transition objects (DGTOs). Like Drinkwater et al. (2003), they state that the dynamical M/L_V ratios of some of the objects they discovered are significantly higher than the ones of the MWGCs. Mieske et al. (2006a) concluded from the Hβ indices of UCDs in the Fornax cluster that they are most likely of intermediate age, while Evstigneeva et al. (2007) found the Hβ indices of UCDs in the Virgo cluster most consistent with old ages. Their stellar population has evolved passively for a long time in any case, which makes UCDs similar to most GCs and elliptical galaxies in this respect.

Several formation scenarios that account for the physical properties of the UCDs have been proposed:

1. UCDs are the mergers of many massive young clusters that formed in a star burst triggered by a galaxy-galaxy encounter (e.g. like in the Antennae). After $\simeq 10\,\mathrm{Gyr}$ of dynamical (and stellar) evolution, such an object would resemble a UCD (Kroupa 1998; Fellhauer & Kroupa 2002a).

2. UCDs are the most luminous GCs (Mieske et al. 2002).

3. UCDs are the central parts of nucleated galaxies that were disrupted by tidal forces as they moved in the gravitational field of a larger galaxy. Only the tightly bound cores survived until the present times (Zinnecker et al. 1988; Bassino et al. 1994; Bekki et al. 2003; Goerdt et al. 2008).

4. UCDs are the remnants of the fundamental building blocks in galaxy formation (Drinkwater et al. 2004).

Some bright UCDs in the Fornax cluster and the Virgo cluster have been analysed by Hilker et al. (2007) and Evstigneeva et al. (2007) very recently. They provide detailed high-quality data for 11 UCDs with dynamical masses between $10^7\ \mathrm{M}_\odot$ and $10^8\ \mathrm{M}_\odot$. Similar data have been obtained by Rejkuba et al. (2007) for compact objects in Centaurus A, but mostly with masses between $10^6\ \mathrm{M}_\odot$ and $10^7\ \mathrm{M}_\odot$. They enlarge a sample by Haşegan et al. (2005) in the Virgo cluster by 20 objects in the same mass range. Taken together, these data allow us to analyse the change of the internal parameters of massive compact objects with mass or luminosity in more detail than Drinkwater et al. (2003) or Haşegan et al. (2005). Furthermore, a comparison to other dynamically hot stellar systems (i.e. stellar systems whose stars are on randomised orbits) becomes possible, since samples with similar measured quantities are available as well. The quantities that are considered here include their M/L_V ratio, Υ_V, and their projected (effective) half-light radius, r_e, in dependency of their dynamical mass.

Especially the dynamical M/L_V ratios of the UCDs has caught the attention of astronomers lately. Evstigneeva et al. (2007) find the UCDs in their sample to be consistent with predictions from simple stellar population (SSP) models within the errors. Hilker et al. (2007) note a tendency of the SSP models to under-predict the M/L_V ratios if a stellar population consistent with observations in the solar neighbourhood is assumed. Haşegan et al. (2005) find that some of the stellar systems they discuss have M/L_V ratios that imply extreme stellar populations in these objects. They suggest a presence of DM in these objects, provided that they are in dynamical equilibrium. This contradicts scenario (1), in which UCDs form DM free. Also if UCDs are nothing but very luminous GCs (scenario 2), they would be expected to be DM free, since GCs of usual size are. The simulations by Bekki et al. (2003) on scenario (3) predict DM free UCDs, since the DM halo of the progenitor galaxy of the UCD is found to be disrupted by the tidal interactions with the host galaxy of the UCD. This stands in contrast to the results from similar simulations by Goerdt et al. (2008), who found that a UCD can still be DM dominated if it is the stripped nucleus of a nucleated galaxy. Scenario (iv) also suggests dark matter in UCDs. A detailed analysis of the M/L_V ratios of the UCDs and their comparison to different SSP models may therefore give insights on their origin.

The stellar population of the UCDs obviously plays a decisive role for the M/L_V ratio that has to be expected. The stellar population of each stellar system is determined, aside from an influence by stellar and dynamical evolution, by the stellar initial mass function (IMF), $\xi(m)$,

$$dN \propto \xi(m)\, dm, \tag{2.1}$$

where m is the stellar initial mass and dN the number of stars in the mass interval $[m, m+dm]$. The IMF has to be distinguished from the present day stellar mass function (PDMF) which gives the number density of stars in dependency of stellar masses today. The IMF is a very useful concept, especially for a dynamically unevolved stellar system, because the number of stars that formed in the mass interval $[m, m+dm]$ is conserved with time on the whole domain of the IMF. As a consequence, the PDMF and IMF are very similar for stars still on the main sequence at the present time. It turns out in Section 2.3.2 that UCDs can indeed be considered as dynamically unevolved stellar systems due to their mass and extension and therefore long relaxation time.

In the past, there have been numerous efforts to infer the shape of the IMF from the PDMF as observed in resolvable stellar populations. There is common agreement that these observations

are compatible with the IMF originally proposed by Salpeter (1955) for field stars in the solar neighbourhood: $\xi(m) \propto m^{-\alpha}$ with $\alpha = 2.35$ for $0.4\,\mathrm{M}_\odot \lesssim m \lesssim 10\,\mathrm{M}_\odot$. Later observations indicated that α is constant up to the highest observed stellar masses (which are between $120\,\mathrm{M}_\odot$ and $200\,\mathrm{M}_\odot$, Weidner & Kroupa 2004; Oey & Clarke 2005; Figer 2005), but gets smaller below $0.5\,\mathrm{M}_\odot$ (Kroupa 2001 and references therein). The IMFs we consider for the stellar populations of the UCDs are guided by these results.

With masses between $10^7\,\mathrm{M}_\odot$ and $10^8\,\mathrm{M}_\odot$ and half-light radii mostly below 50 pc, UCDs may have formed containing, within no more than some ten pc, between 10^5 and 10^6 O-stars or an order of magnitude more if the IMF was top-heavy. This is a scale of star formation beyond current theoretical reach, and it is therefore interesting to study the stellar content of these objects to probe the very extreme physics of their formation.

Let us stress the importance of *dynamical* mass estimates for a meaningful discussion of the M/L_V ratios. This puts a hard constraint on the UCDs that can be included in this discussion since it requires high-resolution spectroscopy of faint objects. However, a dynamical mass estimate is independent from the total luminosity of the stellar system. Instead, the mass estimate is based on the surface brightness profile and the width of the spectral lines as described in detail in Hilker et al. (2007). Dynamical mass estimates clearly rely on a number of assumptions that cannot be verified easily, but mass estimates for unresolved stellar populations based on stellar population models do so as well. The true advantage of the dynamical mass estimates for this work is that they allow an independent estimate for the M/L_V ratio that can be compared to theoretical predictions from stellar population models.

This paper is organised as follows. In Section 2.2 a sample of different dynamically hot stellar systems, including UCDs, is introduced. Section 2.3 is dedicated to the dependencies of internal parameters of dynamically hot stellar systems on their mass. The M/L_V ratio of UCDs, GCs and elliptical galaxies is compared to the predictions from simple stellar population models in Section 2.4. While doing this, we take the influence of their metallicity on their luminosity into account. Section 2.5 contains a discussion of the transition from GCs to UCDs. Furthermore the reliability of our results concerning the M/L_V ratio of UCDs is addressed. We conclude with Section 2.6.

2.2 The data

One of the tasks performed in this paper is to compare UCDs to other dynamically hot stellar systems. This requires a set of data which spans over many orders of magnitude in dynamical mass. A homogeneous data sample is unfortunately not available due to the diversity of the objects. We therefore collect data from different sources in the literature, where comparable parameters have been measured or where at least a correlation between the measured data to the ones that are to be compared is known. In the following, we specify the sources for our data and how we derived the quantities we use in this paper from them, if necessary.

2.2.1 Massive Compact Objects

It is convenient in this paper to introduce massive compact objects (MCOs) as a collective term for all stellar systems in the sample discussed here that should neither be denominated as MWGCs nor as elliptical galaxies. This definition of MCOs includes a number of objects that are considered as UCDs in other works. The motivation for the introduction of this term lies

in the fact that the sample of objects discussed here also includes a number of objects which in their entirety seem to mark a transition between GCs and UCDs. This will become apparent below. A clear distinction between GCs and UCDs is thereby problematic here.

We differentiate the MCOs by the way their dynamical masses were estimated:

For the 19 MCOs listed in Tab. 2.1, the mass estimate included the fitting of a density profile to each one of them individually. These 19 objects are 12 MCOs from the Virgo cluster, five UCDs from the Fornax cluster as well as two objects from the Local Group: ω Cen in the Milky Way and G1 in Andromeda. We consider ω Cen as an MCO instead of an MWGC because of its spread in [Fe/H], which sets it apart from every other star cluster in the halo of the Galaxy (e.g. Kayser et al. 2006; Villanova S. et al. 2007) We refer to them as "MCOs with mass distribution modelling".

We also include 20 objects in Centaurus A from Rejkuba et al. (2007) for which measurements of the velocity dispersion and at least one colour index are available. Tab. 2.2 lists their properties. Their mass in $\mathrm{M}_\odot$ is calculated by using a virial mass estimator given in Spitzer (1987):

$$M_\sigma \simeq 10\, G^{-1} r_\mathrm{e} \sigma^2, \tag{2.2}$$

where r_e is the projected half-light radius[1] in pc and σ is the global velocity dispersion in $\mathrm{pc\,Myr^{-1}}$. G is the gravitational constant, which is $0.0045\,\mathrm{pc^3\,M_\odot^{-1}\,Myr^{-2}}$ We refer to them as "MCOs with global mass estimate".

[1]Actually, it is the half-mass radius that enters into eq. (2.2), but we assume that the mass density follows the luminosity density whenever necessary. This allows us to identify the half-mass radius with the half-light radius.

Table 2.1: Properties of MCOs with masses from mass distribution modelling. The contents of the columns are the following. Column 1: The name given to the MCO (the same as in the source papers), Column 2: The projected half-light radius of the MCO, Column 3: The global velocity dispersion of the MCO, Column 4: The central velocity dispersion of the MCO, Column 5: The absolute magnitude of the MCO in the V-band, Column 6: The dynamical mass of the MCO, Column 7: The M/L_V ratio of the MCO, Column 8: References to the papers that are the basis for our data: 1: Evstigneeva et al. (2007), 2: Haşegan et al. (2005), 3: Hilker et al. (2007), 4: Baumgardt et al. (2003), 5: van de Ven et al. (2006), 6: Harris (1996). Some errors are marked with an asterisk; they have not been published so far.

Name	r_e [pc]	σ [$\mathrm{km\,s^{-1}}$]	σ_0 [$\mathrm{km\,s^{-1}}$]	M_V [mag]	M [$10^6\mathrm{M}_\odot$]	M/L_V [$\mathrm{M}_\odot/\mathrm{L}_\odot$]	Ref
VUCD1	11.3 ± 0.7*	32.2 ± 2.4	39.3 ± 2.0	-12.26	28.0 ± 5.0	4.0 ± 0.7	1
VUCD3	18.7 ± 1.8*	35.8 ± 1.5	52.2 ± 2.5	-12.58	50.0 ± 7.0	5.4 ± 0.9	1
VUCD4	22.0 ± 2.7*	21.3 ± 2.0	26.9 ± 2.3	-12.30	24.0 ± 6.0	3.4 ± 0.9	1
VUCD5	17.9 ± 0.8*	26.4 ± 1.6	32.5 ± 2.3	-12.32	29.0 ± 4.0	3.9 ± 0.6	1
VUCD6	14.8 ± 3.1*	22.3 ± 1.8	29.6 ± 2.2	-12.10	18.0 ± 5.0	2.9 ± 0.9	1
VUCD7	96.8 ± 20*	27.2 ± 4.6	45.1 ± 1.5	-13.44	88.0 ± 21.0	4.3 ± 1.1	1
S417	14.36 ± 0.36	26.4 ± 2.7	31.7 ± 1.4	-11.78 ± 0.16	27.0 ± 5.0	6.6 ± 1.5	1,2
UCD1	22.4 ± 1.0	27.1 ± 1.8	41.3 ± 1.0	-12.19	32.1 ± 3.6	4.99 ± 0.60	3,1
UCD2	23.2 ± 1.0	21.6 ± 1.8	31.3 ± 0.6	-12.27	21.8 ± 3.1	3.15 ± 0.49	3,1
UCD3	89.9 ± 6.0	25.0 ± 3.4	29.3 ± 1.2	-13.57	94.5 ± 22.0	4.13 ± 0.98	3,1
UCD4	29.6 ± 2.0	22.8 ± 3.1	37.3 ± 0.6	-12.45	37.3 ± 8.6	4.57 ± 1.11	3,1
UCD5	30.0 ± 2.5	18.7 ± 3.2	28.7 ± 0.8	-11.99	18.0 ± 5.0	3.37 ± 0.85	3,1
S314	3.23 ± 0.19	...	35.3 ± 1.4	-10.91 ± 0.16	5.8 ± 1.0	2.94 ± 0.68	2
S490	3.64 ± 0.36	...	42.5 ± 2.7	-11.00 ± 0.16	8.7 ± 2.1	4.06 ± 1.15	2
S928	23.16 ± 1.37	...	22.4 ± 1.0	-11.58 ± 0.16	21.3 ± 2.9	6.06 ± 1.23	2
S999	20.13 ± 0.98	...	25.6 ± 1.4	-11.08 ± 0.16	21.6 ± 2.9	9.36 ± 1.87	2
H8005	28.69 ± 0.55	...	10.8 ± 2.3	-10.83 ± 0.16	5.5 ± 2.3	2.98 ± 1.35	2
G1	8.21	...	25.1 ± 1.7	-10.94	8.2 ± 0.85	4.10 ± 0.42	4
ω Cen	6.70 ± 0.28	16.0	19.0 ± 1.5	-10.29	2.5 ± 0.1	2.5 ± 0.3	5,6

2.2.2 Globular clusters

We compare the MCOs to the MWGCs for which McLaughlin & van der Marel (2005) calculated dynamical M/L_V ratios (listed in their table 13). Their value for the effective half-mass radius and their estimate of the dynamical M/L_V ratio in the V-band for the King model is used in this work. By using the absolute magnitude in the V-band given in Harris (1996), the cluster mass can be calculated from its M/L_V ratio.

It can hardly be expected that such a limited sample is representative for GCs in general. Nevertheless, this seems to be the case to some extent, as surveys of extragalactic GC systems show (e.g. Larsen et al. 2001; Chandar et al. 2004 and Jordán A. et al. 2005 concerning the radii of GCs, and Richtler 2003 and Jordán A. et al. 2007 concerning the absolute magnitudes of GCs, which indicate their masses if a constant M/L ratio for them is assumed). It therefore seems possible to take the distribution of the radii and the masses of the MWGS as a rough representation of GCs in general. The advantage of the chosen sample is that, as for the MCOs, mass estimates from velocity dispersions are available for them.

2.2.3 Early-type galaxies

We also compare the MCOs to more massive dynamically hot stellar systems by making use of some of the data published by Bender et al. (1992), i.e. their values for the central velocity dispersion, σ_0, the projected half-light radius, r_e and the absolute magnitude in the B-band of elliptical galaxies and bulges of early-type spiral galaxies in their sample. Bender et al. (1992) give a simple formula for estimating the King mass from r_e and σ_0, which we use as well for the objects from their paper:

$$M_{\sigma 0} = 5\, G^{-1} r_\mathrm{e} \sigma_0^2, \tag{2.3}$$

with r_e in pc, σ_0 in $\mathrm{pc\,Myr^{-1}}$ and $G = 0.0045\,\mathrm{pc^3\,M_\odot^{-1}\,Myr^{-2}}$.

If these objects are to be compared to the MCOs, their V-band luminosities have to be estimated from their B-band luminosities, since for the MCOs luminosities in the V-band are measured. It is known that there is a correlation between the luminosity and the colour of elliptical galaxies. However, given the weakness of this dependency, we think that accounting for it (e.g. with the data on colour of the same galaxies from Bender et al. 1993) would probably not pay the effort. This becomes evident, if the uncertainties connected to the mass estimates from eq. (2.3) especially are considered (see Section 2.2.4). Therefore, adopting a uniform $B-V$ colour index of 0.9 seems a reasonable approximation for the purpose of this paper.

To enhance the sample, data on nucleated dwarf elliptical galaxies from Geha et al. (2003) are included.

Data on dwarf spheroidal galaxies (dSphs) are also included. They are taken from Metz & Kroupa (2007), their table 2, because their data on dSphs are more up to date than the ones in Bender et al. (1992). The half-light radii of the dSphs are not listed in that table, but are usually found in the references given there (with the exception of And II, for which the half-light radius is taken from the paper by McConnachie & Irwin 2006).

2.2.4 A note on different dynamical mass estimators

The dynamical mass of each of the objects introduced above was estimated in one of three different ways. While for some objects the mass estimate included the fitting of an individual density profile to them, for other objects the mass was calculated by using one of two global

Table 2.2: Properties of the compact objects in Centaurus A. Here the mass was calculated by using the same mass estimator for all objects, namely eq. (2.2). All data are from Rejkuba et al. (2007). The meaning of the contents of the columns is the following. Column 1: The identification of the object (like in Rejkuba et al. (2007)), Column 2: The effective (projected half light) radius of the MCO, Column 3: The global velocity dispersion, Column 4: The estimated (dynamical) mass, Column 5: The M/L_V ratio.

Name	$r_{\rm e}$ [pc]	σ [km/s]	M_σ [$10^6 {\rm M}_\odot$]	M/L_V [${\rm M}_\odot/{\rm L}_\odot$]
HGHH92-C7	7.5 ± 0.1	$21.6^{+1.0}_{-2.6}$	$7.8^{+0.7}_{-1.9}$	$3.3^{+0.8}_{-1.1}$
HGHH92-C11	7.8 ± 0.1	$19.6^{+0.9}_{-2.3}$	$6.7^{+0.6}_{-1.6}$	$5.7^{+1.4}_{-1.9}$
HHH86-C15	5.3 ± 0.7	$11.1^{+0.7}_{-0.7}$	$1.5^{+0.2}_{-0.5}$	$2.3^{+0.6}_{-0.9}$
HGHH92-C17	5.7 ± 0.1	$20.9^{+1.6}_{-1.6}$	$5.8^{+0.5}_{-1.4}$	$3.8^{+0.9}_{-1.3}$
HGHH92-C21	7.0 ± 0.1	$19.3^{+0.8}_{-2.3}$	$5.8^{+0.5}_{-1.4}$	$4.8^{+1.1}_{-1.6}$
HGHH92-C22	3.8 ± 0.1	$17.9^{+0.1}_{-0.1}$	$2.8^{+0.3}_{-0.7}$	$3.0^{+0.7}_{-1.0}$
HGHH92-C23	3.3 ± 0.1	$31.3^{+1.4}_{-3.9}$	$7.2^{+0.7}_{-1.8}$	$1.8^{+0.5}_{-0.6}$
HGHH92-C29	6.9 ± 0.1	$16.1^{+0.8}_{-0.8}$	$4.1^{+0.4}_{-1.0}$	$4.4^{+1.0}_{-1.4}$
HGHH92-C36	3.6 ± 0.3	$15.7^{+1.9}_{-1.9}$	$2.0^{+0.3}_{-0.6}$	$2.6^{+0.6}_{-0.9}$
HGHH92-C37	2.9 ± 0.3	$12.6^{+0.8}_{-0.8}$	$1.1^{+0.1}_{-0.3}$	$1.5^{+0.4}_{-0.6}$
HHH86-C38	2.8 ± 0.2	$14.2^{+1.1}_{-1.1}$	$1.3^{+0.2}_{-0.4}$	$1.8^{+0.4}_{-0.6}$
HGHH92-C41	4.5 ± 0.1	$11.5^{+1.3}_{-1.3}$	$1.4^{+0.1}_{-0.3}$	$2.2^{+0.5}_{-0.7}$
HGHH92-C44	5.7 ± 0.1	$13.1^{+1.0}_{-1.0}$	$2.3^{+0.2}_{-0.6}$	$3.9^{+0.9}_{-1.3}$
HCH99-2	11.4 ± 1.1	$14.1^{+0.5}_{-0.5}$	$5.3^{+0.7}_{-1.5}$	$4.5^{+1.2}_{-1.6}$
HCH99-15	5.9 ± 0.2	$21.3^{+1.7}_{-1.7}$	$6.2^{+0.6}_{-1.5}$	$3.4^{+0.8}_{-1.1}$
HCH99-16	12.1 ± 0.6	$9.5^{+1.4}_{-1.4}$	$2.5^{+0.3}_{-0.6}$	$2.8^{+0.7}_{-0.9}$
HCH99-18	13.7 ± 0.3	$21.2^{+1.1}_{-1.1}$	$14.3^{+1.3}_{-3.5}$	$4.7^{+1.2}_{-1.6}$
HCH99-21	7.1 ± 2.7	$10.6^{+2.3}_{-2.3}$	$1.9^{+0.7}_{-1.0}$	$1.7^{+0.7}_{-1.0}$
R223	2.6 ± 0.3	$14.4^{+1.5}_{-1.5}$	$1.3^{+0.2}_{-0.4}$	$2.3^{+0.6}_{-0.9}$
R261	1.90 ± 0.4	$14.6^{+0.7}_{-0.7}$	$1.0^{+0.2}_{-0.3}$	$1.1^{+0.3}_{-0.4}$

mass estimators. The choice of the mass estimator depended on whether σ or σ_0 of the a stellar system was measured. This raises the question whether the mass estimates obtained in these different ways are indeed comparable. If they are comparable, two requirements should be fulfilled:

1. There should not be a tendency for one method to over- or underestimate the mass.

2. Applying different mass estimators on the same object should give similar results.

This can be tested on the 19 MCOs in Tab. 2.1 where σ and σ_0 or σ_0 only is available beside the mass estimate using an individual density profile, M, which is probably the most reliable one and therefore is considered as a standard here. Fig. 2.1 shows the masses as determined by using the global mass estimators in comparison to the mass from an individual density profile fit.

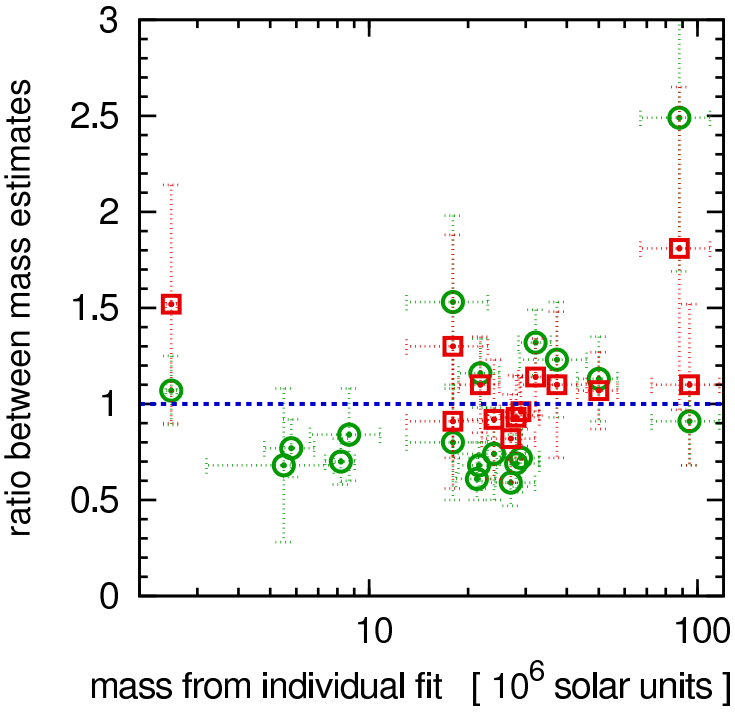

Figure 2.1: Plot of the ratios between global estimates and mass estimates including mass distribution modelling for the 19 MCOs in Tab. 2.1 against the estimate for their mass from an individual fit. Open squares show M_σ/M and circles show $M_{\sigma 0}/M$.

As a measure for the mean deviation of the mass estimated using eq. (2.2), M_σ, and the mass estimated using eq. (2.3), $M_{\sigma 0}$, from M, we calculate $\overline{\Delta M_\sigma} = \frac{1}{N_1}\sum_i^{N_1} |M_i - M_{\sigma\, i}|$ and $\overline{\Delta M_{\sigma 0}} = \frac{1}{N_2}\sum_i^{N_2} |M_i - M_{\sigma 0\, i}|$, where N_1 and N_2 denote the number of objects that are included for that summation. This results in $\overline{\Delta M_\sigma} = 8.5 \times 10^6$ M$_\odot$ for the average deviation of M_σ from M. This value can be compared to the mean value for the mass $\overline{M}$ of the same MCOs, with the masses as they are estimated using individual models for the density profile, which is $\overline{M} = 36.2 \times 10^6$ M$_\odot$. This means that the average deviation of M_σ from $\overline{M}$ is about 23%.

Similarly, the average deviation of $M_{\sigma 0}$ from M can be calculated: $\overline{\Delta M_{\sigma 0}} = 12.5 \times 10^6 M_\odot$. If this is again compared to $\overline{M}$ of the according MCOs, it turns out that the average deviation of $M_{\sigma 0}$ from $\overline{M}$ is about 44%. The larger discrepancies between M and $M_{\sigma 0}$ than between M and M_σ is at least partially due to the uncertainties to the inner density profiles of the MCOs, because the central structure of an MCO strongly influences the value that is determined for its σ_0.

The (relative and absolute) discrepancy between M and M_σ or $M_{\sigma 0}$ is the largest for VUCD7. However, VUCD7 is one of those MCOs that are best fit by a two-component (King+Sersic) density profile, in contrast to most of the other MCOs. It is therefore not surprising that the mass estimators eq. (2.2) and eq. (2.3) fail here, since they assume a King profile. This illustrates the risk connected to assuming a single typical profile for a number of objects. Excluding VUCD7, the average deviation of M_σ from $\overline{M}$ can be lowered to about 10%, and the average deviation of $M_{\sigma 0}$ from $\overline{M}$ can be lowered to about 24%.

In summary, the three ways to estimate the dynamical mass seem to produce comparable results. Note that also Hilker et al. (2007) and Evstigneeva et al. (2007) usually find that the internal parameters derived from global King estimators ($\alpha = 2$) are almost identical to the pa-

rameters derived using mass distribution modelling. We will therefore not discriminate between M_σ, $M_{\sigma 0}$ and M any further, but denote all dynamical masses as M.

2.3 Dependencies on dynamical mass

In this section, the effective radii, median relaxation times, central densities and M/L_V ratios are compared to each other.

2.3.1 Dependency of the effective radius on mass

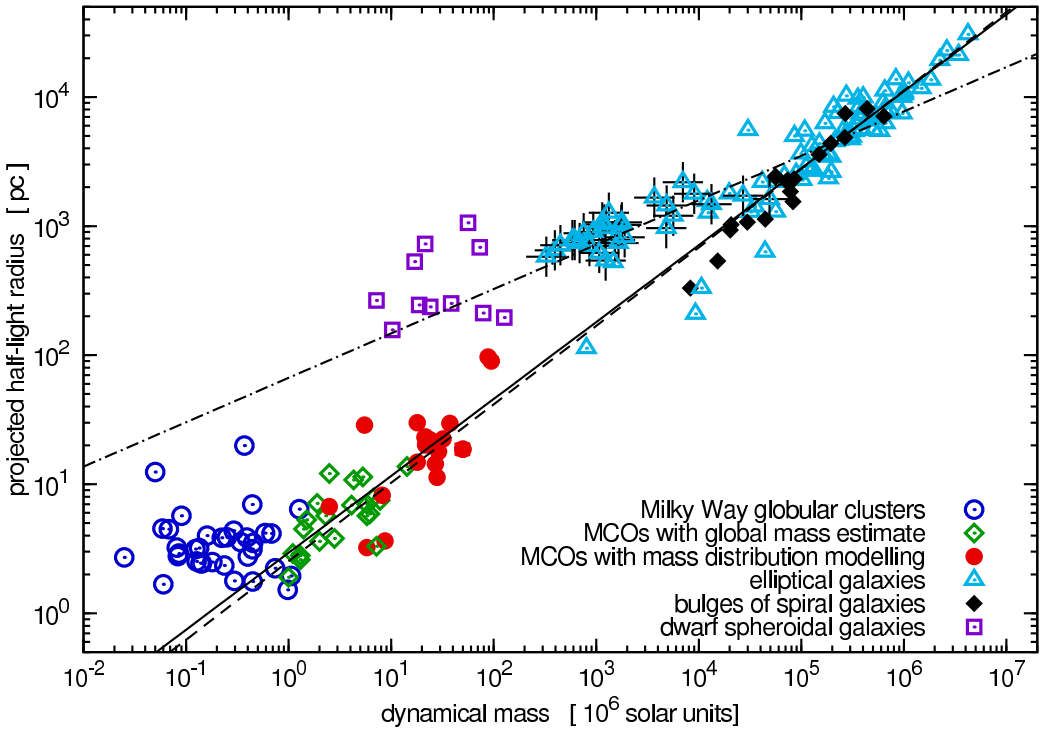

Figure 2.2: Plot of the half-light radius, r_e, against mass, M, for different types of dynamically hot stellar systems. The symbols that are used have the following meaning: Open circles for MWGCs, open diamonds for MCOs with global mass estimate (i.e. calculated from eq. 2.2), filled circles for MCOs with (the probably more reliable) mass estimates from mass distribution modelling (i.e. mass estimates taken from Haşegan et al. 2005, Hilker et al. 2007 and Evstigneeva et al. 2007 as well as the mass estimates for ω Cen and G1), open squares for dSphs, triangles for elliptical galaxies and filled diamonds for bulges of early-type spiral galaxies. Errors are comparable to the symbol sizes. The lines show fits to the data for a relation between mass and radius for bright ellipticals, compact ellipticals and bulges (dashed line), bright ellipticals, compact ellipticals, bulges and MCOs (solid line) and all elliptical galaxies, bulges and dSphs (dashed-dotted line). Most elliptical galaxies with low brightness have been excluded from the first two fits, see text for more details. They are marked with a cross. Note that the underlying assumption for the mass estimates is that the stellar systems are essentially undisturbed by tidal fields, which may be wrong for the dSphs especially (Kroupa 1997).

In Fig. 2.2, the mass dependency of r_e of the MCOs and other dynamically hot stellar systems is plotted. Some well established observations can be identified easily in this plot: The strong correlation between M and r_e for elliptical galaxies (Bender et al. 1992) in the high mass

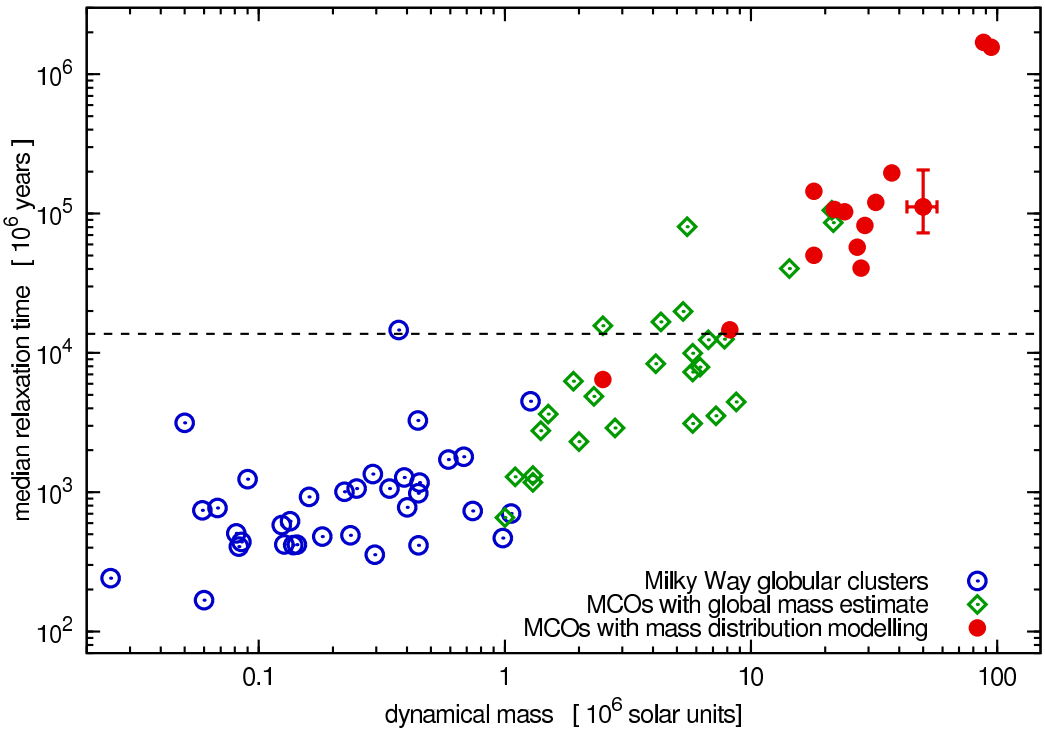

Figure 2.3: The median relaxation time, $t_{\rm rel}$, plotted against dynamical mass, M. Contrary to Fig. 2.2, this figure shows MWGCs and MCOs only. The dashed line marks the current age of the universe. The symbols are as in Fig. 2.2. One MCO is plotted with typical errors.

range and the absence of a dependency of $r_{\rm e}$ on M for GCs (McLaughlin 2000; Jordán A. et al. 2005) at the lowest masses. Remarkable is the large spread of radii at intermediate masses which becomes largest in the mass interval of $10^7\,{\rm M}_\odot \lesssim M \lesssim 10^8\,{\rm M}_\odot$, the mass interval where the rather compact UCDs as well as the (typically about an order of magnitude) more extended dSphs lie. The underlying assumption for this statement is that dSphs are objects in (or close to) virial equilibrium. This has been argued to be the case by e.g. Wu (2007) and Gilmore et al. (2007) for at least those dSphs that are most distant to the Galactic centre, although this would imply extremely high M/L_V ratios in some cases. Gilmore et al. (2007) state that there is a bimodality of the characteristic radii of objects in the mass range $10^7\,{\rm M}_\odot \lesssim M \lesssim 10^8\,{\rm M}_\odot$, i.e. an almost complete absence of objects with $r_{\rm e} \sim 100\,{\rm pc}$. In Fig. 2.2, they are indeed only represented by VUCD7 and UCD3[2] (and M32 at a higher mass). One way to interpret this is to consider UCDs and the dSphs as two kinds of stellar systems that formed under different conditions, as Gilmore et al. (2007) propose.

However, Metz & Kroupa (2007) argue that the formation of dSphs may have been triggered by the tidal forces in an encounter between two galaxies, i.e. they propose in principle the same scenario for the formation of dSphs which Fellhauer & Kroupa (2002a) suggested for the formation of UCDs. The morphological differences can be understood in terms of the influence of the surroundings on the star-forming regions: the dSphs can form from star cluster complexes in a weak tidal field (e.g. the tidal arm of the Tadpole galaxy), while the UCDs form in a strong tidal field (e.g. the Antennae galaxy). This scenario is supported with the observation that the orbital angular momenta of the satellite galaxies of the Milky Way are correlated (Metz et al.

[2]Note that Gilmore et al. (2007) consider a half-light radius of only 22 pc (from Drinkwater et al. (2003)) for UCD3 and omit VUCD7 from their discussion.

2008). It can also offer an explanation for the seemingly high M/L_V ratios of some of the dSphs, if they are largely unbound phase-space structures and therefore cannot be described by simple application of Jeans' equations (Kroupa 1997).

It is surprising that the MCOs lie on the same relation between mass and radius as massive elliptical galaxies with masses $\gtrsim 10^{11}\,\mathrm{M}_\odot$, while elliptical galaxies with lower masses (i.e. objects in the intermediate mass range) mostly lie on a different relation, which points towards the parameter space of dSphs. This could be evidence for the low-mass elliptical galaxies being mostly of tidal origin, as proposed by Okazaki & Taniguchi (2000) (also see fig. 7 in Monreal-Ibero et al. 2007), and as discussed by Metz & Kroupa 2007 for dSphs. The few *compact* low-mass elliptical galaxies can then be interpreted as low-mass counterparts of the elliptical galaxies more massive than $\gtrsim 10^{11}\,\mathrm{M}_\odot$.

Following the above interpretation, some objects are thus excluded for quantifying the relation between mass and radius that MCOs share with massive elliptical galaxies in a least squares fit. These objects are, besides the MWGCs and the dSphs, the dwarf ellipticals from Geha et al. (2003) and the galaxies that Bender et al. (1992) define as "bright dwarf ellipticals"[3]. The exclusion of the latter two groups may seem somewhat arbitrary, but it turns out that they define the apparent turn-off from the relation for the remaining objects (i.e. bright elliptical galaxies, galaxy bulges, compact ellipticals and MCOs) at $\gtrsim 10^{11}\,\mathrm{M}_\odot$ quite well. Assuming a function of the form

$$\frac{r_\mathrm{e}}{\mathrm{pc}} = a\left(\frac{M}{10^6\,\mathrm{M}_\odot}\right)^b \tag{2.4}$$

for the relation between M and r_e, which corresponds to a straight line in Fig. 2.2, leads to

$$\begin{aligned} a &= 2.95^{+0.24}_{-0.22}, \\ b &= 0.596 \pm 0.007, \end{aligned}$$

for the best-fitting parameters. If the MCOs are not used for the fit,

$$\begin{aligned} a &= 2.54^{+0.91}_{-0.67}, \\ b &= 0.608 \pm 0.025, \end{aligned}$$

is obtained, i.e. within the errors the same relation as with the MCOs. The small impact that excluding the MCOs has on the fit is demonstrated in Fig. 2.2 by plotting eq. (2.4) with both sets of values for a and b. This verifies that the MCOs lie along the same relation between M and r_e as massive elliptical galaxies.

For comparison, an analogous fit to *all* elliptical galaxies as well as the dSphs (but without the MCOs) is performed. This corresponds to the hypothesis that these objects are drawn from a homogeneous population, which obeys a single relation between mass and radius. This leads to

$$\begin{aligned} a &= 34.8^{+8.1}_{-6.6}, \\ b &= 0.399 \pm 0.019, \end{aligned}$$

for the best-fitting parameters. However, the distribution of the massive elliptical galaxies is clearly asymmetric around this relation, which suggests that the first two relations are a better fit to them.

[3] i.e. those galaxies which have $M_V > -18.5$ and are not classified as "compact dwarf ellipticals"by Bender et al. (1992)

We note that the larger sample of elliptical galaxies which is used by Graham et al. (2006) shows a very similar distribution of characteristic radii against mass, although Graham et al. (2006) estimated the masses of the galaxies different from the approach chosen here, namely by assuming a stellar population for them and then calculating their total masses from their luminosities (cf. their figure 1b).

The radii of MCOs are thus, unlike the ones of GCs, correlated to their masses. The comparison of the massive MCOs with the MWGCs shows that the characteristic radii of GCs are indeed typically about an order of magnitude smaller than the ones of the massive MCOs. However, Fig. 2.2 also seems to suggest a rather fluent transition between objects that lie on the scaling relation for GCs and objects that lie on the scaling relation for elliptical galaxies at a mass of about $10^6\ \mathrm{M}_\odot$. This confirms the conclusions Haşegan et al. (2005) have drawn based on fewer data.

This change of typical radii cannot be due to an observational bias against small radii for more massive objects, since MCOs are identified by their brightness, their membership to a galaxy cluster and their *compactness*. The data on rather low-mass MCOs from Haşegan et al. (2005) and Rejkuba et al. (2007) (both indicated as open diamonds in Fig. 2.2) indeed include objects with radii on both scales. Consequently, this change of the typical r_e must be connected to a difference in evolution or formation of objects less massive than $\approx\ 10^6\ \mathrm{M}_\odot$ and more massive than $\approx 10^7\ \mathrm{M}_\odot$.

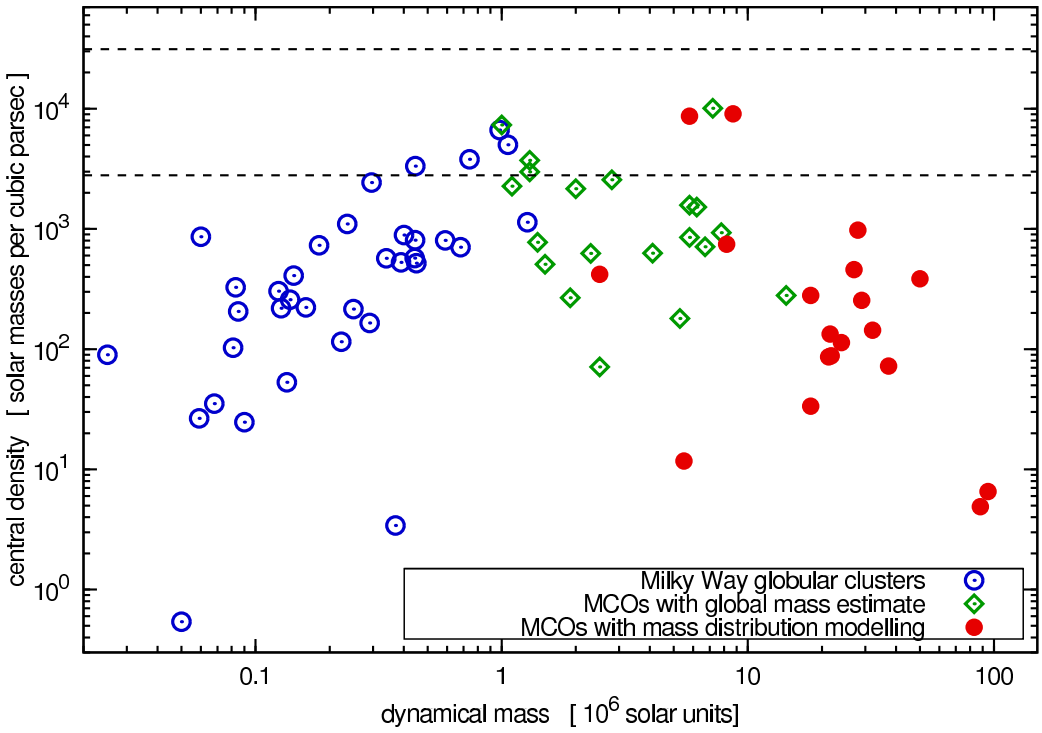

Figure 2.4: The central density of MWGCs and MCOs plotted against dynamical mass. The symbols are as in Fig. 2.3. The dashed lines indicate constant densities: assuming a mean stellar mass of $0.4\ \mathrm{M}_\odot$, the lower dashed line indicates a density where the mean distance between stars is 6000 AU (about 100 times the diameter of the orbit of Neptune), and the upper dashed line indicates where the mean distance between stars is 3000 AU (about 50 times the diameter of the orbit of Neptune).

2.3.2 Dependency of the median two-body relaxation time on mass

The median two-body relaxation time is closely connected with mass and characteristic radius of an object. It is given in Myr in a formula originally found by Spitzer & Hart (1971),

$$t_{\rm rel} = \frac{0.061\,N}{\log(0.4\,N)} \times \sqrt{\frac{r_{\rm h}^3}{GM}}, \tag{2.5}$$

where N is the number stars in the cluster, $r_{\rm h}$ its half-mass radius in pc, M its mass in $\mathrm{M}_\odot$ and G the gravitational constant, which is $0.0045\,\mathrm{pc}^3\,\mathrm{M}_\odot^{-1}\,\mathrm{Myr}^{-2}$. $t_{\rm rel}$ can be considered as a measure for the relaxation time at the half mass-radius. However, eq. (2.5) is only an approximation: It is obtained under the assumption that the stars move in a smooth potential and are only disturbed by two-body encounters (i.e. no binaries), beside the supposition that the cluster is in virial equilibrium.

Eq. (2.5) includes parameters which are not known for most of the MCOs, but it can be transformed into one that only depends on M and the effective half-light radius, $r_{\rm e}$, as free parameters if some assumptions are made. It can then be applied to the data in this paper. This is done by assuming that the mass is distributed as the luminosity and by substituting $r_{\rm e} = 0.75\,r_{\rm h}$ (Spitzer 1987). We further assume a mean stellar mass of $0.4\,\mathrm{M}_\odot$ in concordance with the mean stellar mass in a stellar population with the canonical IMF (see eq. 2.10). This yields

$$t_{\rm rel} = \frac{0.234}{\log(M/\mathrm{M}_\odot)} \times \sqrt{\frac{M r_{\rm e}^3}{G}} \tag{2.6}$$

in the same units as eq. (2.5). An inspection of eq. (2.6) reveals that $r_{\rm e}$ dominates the behaviour of $t_{\rm rel}$ due to its power. Therefore, a plot of $t_{\rm rel}$ against M looks very similar to a plot of $r_{\rm e}$ against M (Fig. 2.2).

In Fig. 2.3, $t_{\rm rel}$ is plotted against M of MWGCs and MCOs only. The stated similarity to Fig. 2.2 in the according mass range is apparent. The new and important piece of information that can be read off Fig. 2.3 is how $t_{\rm rel}$ of the objects compares to a Hubble time. It is clearly below a Hubble time for most MWGCs, while it is clearly above a Hubble time for all MCOs more massive than $10^7\,\mathrm{M}_\odot$. This corresponds to the increase of the typical radii in the mass interval from $10^6\,\mathrm{M}_\odot$ to $10^7\,\mathrm{M}_\odot$. As MWGCs and MCOs are considered to be old objects, this implies that MWGCs can have undergone considerable dynamical evolution since their formation while massive MCOs have not. Consequently, massive MCOs are much less vulnerable to mass loss driven by two-body relaxation.

2.3.3 Dependency of the central density on mass

It is worthwhile to consider the impact of the development of the typical radii with dynamical mass on the central density of the MWGCs and MCOs. The central density is here defined as the mean density within the projected half-light (i.e. half-mass) radius. It is plotted in Fig. 2.4 against mass.

The independence of the MWGC radii on their dynamical mass translates into an increase of the central density with dynamical mass. The increase of the typical radii above a dynamical mass of $10^6\,\mathrm{M}_\odot$, as visible in Fig. 2.2, is strong enough for a slow decrease of the central density to occur. It has already been noted by Burstein et al. (1997) that there is a maximum global luminosity density for early-type galaxies, which is proportional to $M^{-4/3}$. In this light,

the decrease of the densities with mass for the MCOs is only a consequence of the common relation between the MCOs and the massive elliptical galaxies that was found in Section 2.3.1.

2.3.4 Dependency of the M/L_V ratio on mass

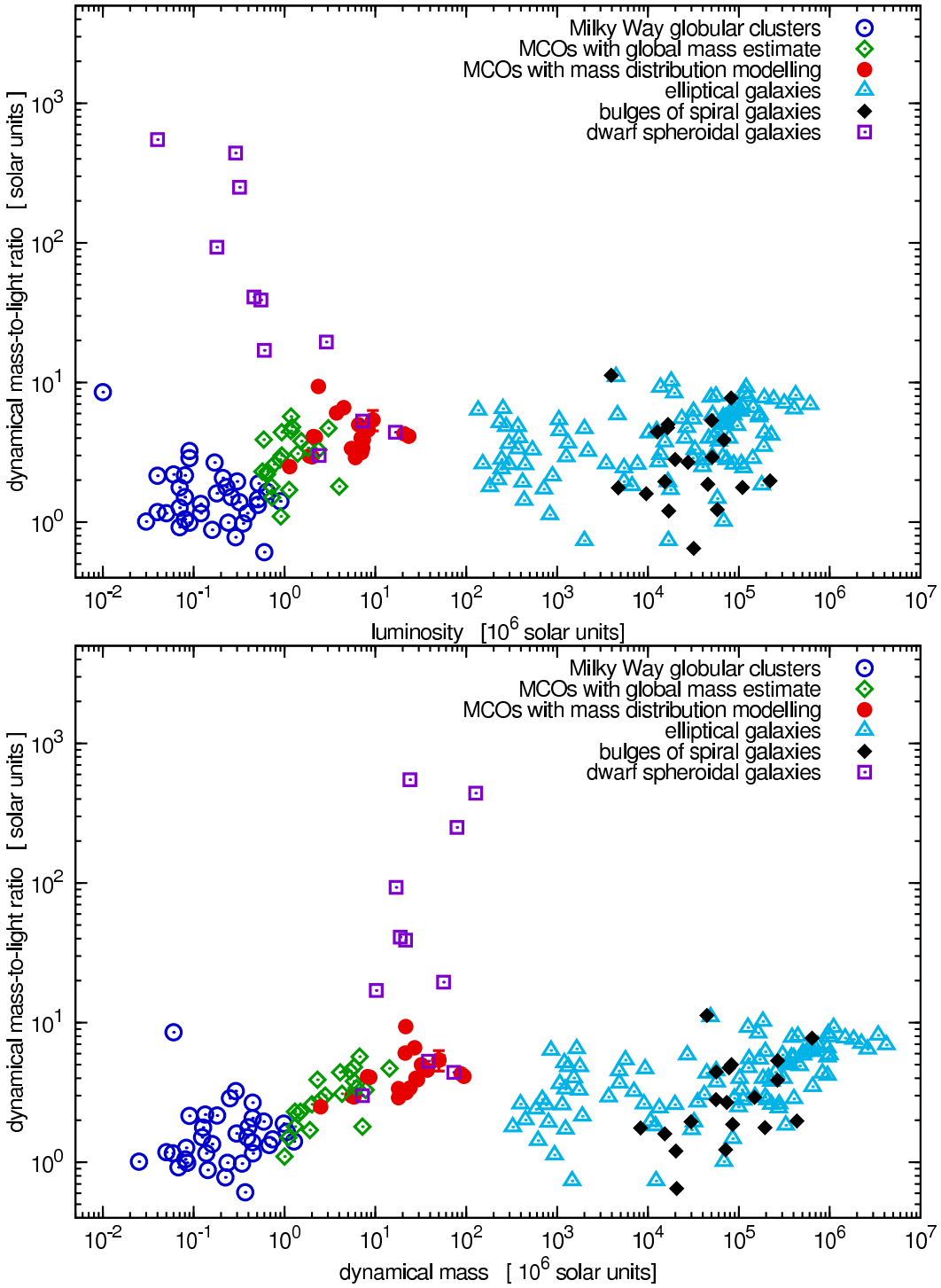

Figure 2.5: Dynamical M/L_V ratio plotted against luminosity in the V-band, L_V (upper panel), and mass, M (lower panel). The symbols are as in Fig. 2.2. The errors to the values of the MCOs are not much larger than the symbol size.

Fig. 2.5 shows the dynamical M/L_V ratios of the sample against the luminosity in the V-band (upper panel) and the dynamical mass (lower panel). It is visible from this figure that the dSphs with the lowest V-band luminosities also have the highest M/L_V ratios, as was already noted in Mateo (1998). Other than that, the general distribution of the data in both panels is almost identical, except for a steeper rise of the M/L_V ratios from the MWGCs to the MCOs when they are plotted against L_V.

It might be tempting to identify the gap in the luminosity sequence at $\approx 10^8$ $\mathrm{L}_\odot$ with the borderline between a star cluster-like population to the left and a galaxy-like population to the right. However, the *homogeneous* sample of faint early-type galaxies in the Fornax cluster observed by Hilker et al. (2003) does not show such a gap in luminosity down to the luminosities of dSphs. The gap visible in Fig. 2.5 is thus most likely an artifact caused by the inhomogeneity of our data sample.

The spread of the M/L_V ratios of the dSphs is very striking in Fig. 2.5. With M/L_V ratios of several 10^2 $\mathrm{M}_\odot/\mathrm{L}_\odot$, some of them are total outliers compared to all other dynamically hot stellar systems. It is especially the spread of their M/L_V ratios that supports the notion that dSphs cannot be treated as objects in dynamical equilibrium. If they were in dynamical equilibrium, DM haloes with very different properties would have to be assumed for objects that are quite similar to each other as far as the properties of their baryonic matter are concerned.

It can be seen for the remaining objects that almost every MCO above a mass of 10^6 $\mathrm{M}_\odot$ has a M/L_V ratio which is manifestly higher than the mean value for MWGCs. As for the radii, the transition from the M/L_V ratios of GCs to the ones of MCOs seems fluent. The objects classified as some kind of elliptical galaxy (including bulges of early-type spiral galaxies) span the whole range of M/L_V ratios that is occupied by GCs *and* MCOs, with bulges and large elliptical galaxies having a larger spread to higher M/L_V ratios.

It should be remembered in this context that the masses of the early-type galaxies that are used to determine their M/L_V-ratios have been calculated with eq. (2.3), i.e. the mass estimates are based on the distribution of the visible matter. If these galaxies are embedded in DM haloes, the mass estimates are too low for the total masses of the galaxies, but are still good approximations for the mass of those parts of the galaxies that are dominated by baryonic matter. It is noteworthy that evidence for DM only emerges in objects with $t_{\mathrm{rel}} > \tau_{\mathrm{H}}$ (also see Fig. 2.10 and 2.12).

The physical reasons for the distribution of M/L_V ratios are a rather complicated issue. It mainly depends on two things: A possible non-baryonic DM content in the objects and the stellar populations of the objects. The M/L_V ratio of a stellar population is influenced by its star formation history, its IMF, the metallicity of the stars and by how much the stellar population was altered by dynamical evolution. Unfortunately, most of the objects in our sample cannot be resolved into stars so far, which makes it impossible to determine their stellar populations directly. Nevertheless, observations of these objects and theoretical considerations can give some clues on their stellar populations. Some of these findings are summarised below.

- MWGCs contain old stellar populations (older than ≈ 10 Gyr, VandenBerg 2000; Salaris & Weiss 2002). The MCOs in the Virgo cluster seem to have similar ages (Evstigneeva et al. 2007), but the MCOs in the Fornax cluster might be a bit younger (Mieske et al. 2006a). The ages of elliptical galaxies are found to range from a few Gyr to $\gtrsim 10\,\mathrm{Gyr}$ (Trager et al. 2000; Annibali et al. 2007).

- MWGCs are known to have low metallicities. The metallicities of the MCOs are, if estimated, consistent with those of metal-rich MWGCs. Elliptical galaxies have about

solar metallicities in their central parts (Trager et al. 2000; Annibali et al. 2007) and a decrease of their metallicities towards their outer regions (Tantalo et al. 1998; Baes et al. 2007).

- Dynamical evolution can lower the M/L_V ratio of a stellar system noticeably, if the time scale for its dynamical evolution is shorter than the time scale for the evolution of its stars (Baumgardt & Makino 2003; Borch et al. 2007).

With this information, the different M/L_V ratios of the objects plotted in Fig. 2.5 become understandable at least qualitatively. The rather low M/L_V ratio of MWGCs can be understood as an effect of their low metallicity and the considerable dynamical evolution that was suggested for them in section 2.3.2. Considering the lifetimes Baumgardt & Makino (2003) expect for a sample of MWGCs (while accounting for the tidal field of the Galaxy) and their results for the development of the M/L ratio as a function of the star cluster lifetime, a decrease of the M/L ratio by about $0.3\ \mathrm{M}_\odot\ \mathrm{L}_\odot^{-1}$ to $0.7\ \mathrm{M}_\odot\ \mathrm{L}_\odot^{-1}$ compared to the M/L ratio of a dynamically unevolved stellar population would seem typical for MWGCs. The massive MCOs and the elliptical galaxies on the other hand are more metal-rich and due to their size and extension dynamically almost unevolved. This might be able to explain higher M/L_V ratios compared to MWGCs even if they do not contain DM. Note however that a DM content in elliptical galaxies has been discussed: quite recently, Cappellari M. et al. (2006) estimated a median DM content of $\approx 30\%$ within the half-light radii of a sample of elliptical galaxies, if an IMF as in the Solar neighbourhood is assumed[4]. The large spread of the M/L_V ratios of ellipticals is not surprising in the light of their large age spread. Also recall the metallicity gradient in elliptical galaxies, which is natural if they are more complex than MWGCs and thus more diverse in their internal properties.

2.4 The observed M/L_V ratios and predictions of stellar population models

For the remainder of this paper, we will compare the observed M/L_V ratios of the objects discussed in the previous sections to predictions from stellar population models, with the focus on the M/L_V ratios of the MCOs.

2.4.1 The MCOs as simple stellar populations

In order to find which stellar population models are appropriate for the MCOs, we recall that most of the objects discussed here are old and note that a super-solar abundance of α-elements seems to be typical for the dynamically hot stellar systems discussed here, see e.g Carney (1996) for MWGCs, Evstigneeva et al. (2007) for MCOs, and Annibali et al. (2007) for elliptical galaxies. Therefore, self-enrichment through the ejecta of type I supernovae (SNI) apparently does not play a major role in these systems, as SNI are important contributors of iron to the

[4]Cappellari M. et al. (2006) do not discuss gas as a possible contributor to the non-luminous matter. However, considering the results by Combes et al. (2007), the mass of the gas is probably indeed negligible for their sample of galaxies. Combes et al. (2007) estimate the mass of the molecular gas for the same sample of galaxies and find masses of the order of some $10^7\ \mathrm{M}_\odot$, which is about 3 to 4 orders of magnitudes less than the results in Cappellari M. et al. (2006) suggest for the total masses of the galaxies.

interstellar medium (Matteucci & Greggio 1986). This can be taken as an indicator for a stellar population with a narrow age spread, if the progenitors of SNI are assumed to be white dwarfs that surpass the Chandrasekhar limit by accretion of additional matter (Whelan & Iben 1973). Matteucci & Recchi (2001) and Greggio (2005) suggest median time scales between some ten Myr and a few Gyr for the evolution of white dwarfs into SN I, depending on the initial conditions for the population. Considering stellar systems with ages of ≈ 10 Gyr, this can be taken as a rather short time scale. The assumption of populations of coeval stars within each stellar system thereby seems a reasonable approximation for at least MWGCs and MCOs.

Besides age and age spread of the stars, a discussion of the M/L_V ratios of stellar systems has to account for the metallicities of their stars, since the metallicity is known to have a influence on the colour and the luminosity of a star with a given mass. Therefore the metallicities of the stars have to be known if one intends to construct a model for a stellar population which accurately describes a real stellar population, including its M/L_V ratio.

In the following, two assumptions for the metal abundances in the stellar populations of the MCOs are made. This is not only for the sake of simplicity but also for the lack of more detailed data in most cases.

Firstly, it is assumed that the metallicity-luminosity dependency of the stellar system can be characterised by the mean metallicity Z of the stellar system. This would certainly be the case if Z was equal to the metallicities of the component stars, i.e. if all stars had the same metallicity. However, this is not necessarily the case for the stars in MCOs, as the examples of ω Cen (e.g. Kayser et al. 2006; Villanova S. et al. 2007) and G1 (Meylan et al. 2001) show. On the other hand, imposing a more complicated metallicity distribution on the stars of the unresolved stellar populations of the other MCOs does not seem reasonable.

Secondly, it is assumed that the mean iron abundance, [Fe/H], allows solid conclusions on Z. This assumption can be motivated with the finding that $[\alpha/\mathrm{Fe}] \simeq 0.3$ seems not only to be true for MWGCs (Carney 1996), but also for most of the MCOs that were analysed by Evstigneeva et al. (2007). This value appears to be very typical for massive, dense star clusters.

The approximations and assumptions that have been made here and in Section 2.3.4 imply in their entirety that the stellar populations in MCOs can be considered as simple stellar populations (SSPs), meaning that all stars and stellar remnants have the same age and the same chemical composition.

2.4.2 The metallicities of the MCOs

Information on the metallicities of MCOs are published in Haşegan et al. (2005), Mieske et al. (2006a), and Evstigneeva et al. (2007). Evstigneeva et al. (2007) give for each of the MCOs they examined an interval in which the actual mean metallicity Z of the MCO lies. We assume that this true value for Z of the MCO lies in the middle of the interval given. Haşegan et al. (2005) and Mieske et al. (2006a) do not give estimates for Z of the objects they discuss, but for [Fe/H]. Based on the observational findings by Carney (1996) and Evstigneeva et al. (2007) and the assumption that the iron abundance characterises the metallicity of the MCOs, we adopt $[\alpha/\mathrm{Fe}] = 0.3$ for each one of them and use the relation

$$[Z/\mathrm{H}] = [\mathrm{Fe/H}] + 0.94\,[\alpha/\mathrm{Fe}] \tag{2.7}$$

found by Thomas et al. (2003) to calculate $[Z/\mathrm{H}]$ from [Fe/H]. The values that are adopted for the element abundances of the MCOs are summarised in Tab. 2.3.

Table 2.3: MCOs with published metallicity estimates. [Fe/H] in Column 3 is taken as the measure for Z of the object. Also $(V-I)$ colour indices are given for some objects whose metallicities were derived from line indices. They provide the opportunity to test the validity of eq. (2.8) on a sample of MCOs (see section 2.5.2). The columns of the table contain the following information: Column 1: The name of the object, Column 2: [Z/H] if given in the reference, Column 3: [Fe/H] either from the reference or calculated using eq. (2.7), Column 4: The $(V-I)$ colour index, Column 5: The reference to the source paper: 1: Evstigneeva et al. (2007), 2: Mieske et al. (2006a), 3: Haşegan et al. (2005), 4: Meylan et al. (2001), 5: Harris (1996).

Name	[Z/H]	[Fe/H]	$(V-I)$	Ref.
VUCD1	$-1.35\ldots-0.33$	$-1.12\ \pm0.51$	0.96	1
VUCD3	$0.00\ldots\ 0.35$	-0.107 ± 0.175	1.27	1
VUCD4	$-1.35\ldots\ 0.33$	$-1.12\ \pm0.51$	0.99	1
VUCD5	$-0.33\ldots\ 0.00$	-0.447 ± 0.165	1.11	1
VUCD6	$-1.35\ldots-0.33$	$-1.12\ \pm0.51$	1.02	1
VUCD7	$-1.35\ldots-0.33$	$-1.12\ \pm0.51$	1.13	1
S417	$-1.35\ldots\ 0.00$	-0.957 ± 0.65		1
UCD1		$-0.38\ \pm0.05$	1.11	2
UCD2		$-0.90\ \pm0.33$	1.12	2
UCD3		$-0.52\ \pm0.11$	1.18	2
UCD4		$-0.85\ \pm0.29$	1.12	2
UCD5		...		
S314		-0.50		3
S490		0.18		3
S928		-1.34		3
S999		-1.38		3
H8005		-1.27		3
G1		$-0.95\ \pm0.09$		4
ω Cen		-1.62		5

For the objects in Centaurus A no metallicities have been published so far, but $(B-V)$ and $(V-I)$ colour indices for them are available in Rejkuba et al. (2007). Observations show that there is a correlation between colour indices and [Fe/H] in GC systems. On this basis, an estimate of [Fe/H] in the objects in Centaurus A can be made by assuming that they follow a relation between colour and metallicity that has been established on another GC system. Barmby et al. (2000) give relations between [Fe/H] and $(V-I)$ as well as [Fe/H] and $(B-V)$ for the GC system of the Milky Way, using the data from Harris (1996):

$$[\mathrm{Fe/H}]_{(V-I)} = (4.22\pm0.39)\times(V-I) - (5.39\pm0.35) \tag{2.8}$$

and

$$[\mathrm{Fe/H}]_{(B-V)} = (5.50\pm0.33)\times(B-V) - (5.26\pm0.23). \tag{2.9}$$

The confidence range of these equations is set by the values $(V-I)$ and [Fe/H] can assume for MWGCs. Their values for [Fe/H] are mostly between -2 and $-0.5\,\mathrm{dex}$.

The advantage of the relations from Barmby et al. (2000) is that they have been established for both colour indices that have been measured for the objects in Centaurus A, i.e. they allow

Table 2.4: Colours and derived [Fe/H] for the Centaurus A objects. The contents of the columns in the table are the following: Column 1: Identification of the object like in Rejkuba et al. (2007), Column 2: The $(V-I)$ colour index, Column 3: The $(B-V)$ colour index, Column 4: [Fe/H] calculated from the $(V-I)$ colour index, Column 5: [Fe/H] calculated from the $(B-V)$ colour index, Column 6: Our final estimate for [Fe/H] with the adopted errors.

Name	$(B-V)$	$(V-I)$	$[\mathrm{Fe/H}]_{(B-V)}$	$[\mathrm{Fe/H}]_{(V-I)}$	[Fe/H]
HGHH92-C7	0.75	0.91	-1.13	-1.55	-1.34 ± 0.30
HGHH92-C11	0.94	1.12	-0.09	-0.66	-0.38 ± 0.39
HHH86-C15	0.89	1.03	-0.36	-1.04	-0.70 ± 0.42
HGHH92-C17	0.77	0.88	-1.02	-1.68	-1.35 ± 0.39
HGHH92-C21	0.78	0.93	-0.97	-1.47	-1.22 ± 0.33
HGHH92-C22	0.79	0.91	-0.91	-1.55	-1.23 ± 0.39
HGHH92-C23	0.76	0.78	-1.08	-2.10	-1.59 ± 0.55
HGHH92-C29	0.89	1.08	-0.36	-0.83	-0.60 ± 0.35
HGHH92-C36	0.73	0.85	-1.24	-1.80	-1.52 ± 0.35
HGHH92-C37	0.84	0.99	-0.64	-1.21	-0.93 ± 0.37
HHH86-C38	0.78	0.91	-0.97	-1.55	-1.26 ± 0.36
HGHH92-C41	0.89	1.09	-0.36	-0.79	-0.58 ± 0.33
HGHH92-C44	0.69	0.85	-1.47	-1.80	-1.63 ± 0.26
HCH99-2	0.74	0.84	-1.19	-1.85	-1.52 ± 0.39
HCH99-15	...	1.06	...	-0.92	-0.62 ± 0.23
HCH99-16	...	0.79	...	-2.06	-1.76 ± 0.23
HCH99-18	0.89	0.89	-0.36	-1.63	-1.00 ± 0.67
HCH99-21	...	0.78	...	-2.10	-1.80 ± 0.23
R223	0.80	0.95	-0.86	-1.38	-1.12 ± 0.35
R261	0.83	0.99	-0.70	-1.21	-0.95 ± 0.35

us to fully benefit from the available data. Their disadvantage is that they do not account for a slight curvature in the relation between [Fe/H] and the colour indices, which is typical for this relation according to Yoon et al. (2006). However, given the apparent weakness of this departure from linearity, it seems justified to neglect it.

We calculate $[\mathrm{Fe/H}]_{(V-I)}$ and $[\mathrm{Fe/H}]_{(B-V)}$ for each cluster in Centaurus A from eq. (2.8) and (2.9) if both colour indices are available. The results from eq. (2.8) turn out to be systematically lower by $\approx 0.6\,\mathrm{dex}$ on average than the results from eq. (2.9), as can be seen in Fig. 2.6. It is obvious that the different results for the iron abundance calculated from different colour indices may indicate a serious problem with those estimates. A discussion on how reliable the results based on these metallicity estimates are will be given Section 2.5. For now, we clearly distinguish between objects with [Fe/H] estimates from colour indices and objects with [Fe/H] estimates from line indices.

The relation between [Fe/H] and $(V-I)$ colour found by Kissler-Patig et al. (1998) by including (beside MWGCs) GCs around NGC 1399 has a slightly flatter slope than eq. (2.8). It yields however similar results in the colour range interesting for the purpose here (deviations would be $\approx 0.2\,\mathrm{dex}$ in the most extreme cases).

As a compromise between the two values that are estimated for the iron abundances of the objects in Centaurus A, we adopt the mean of both values as our final value for [Fe/H]. The

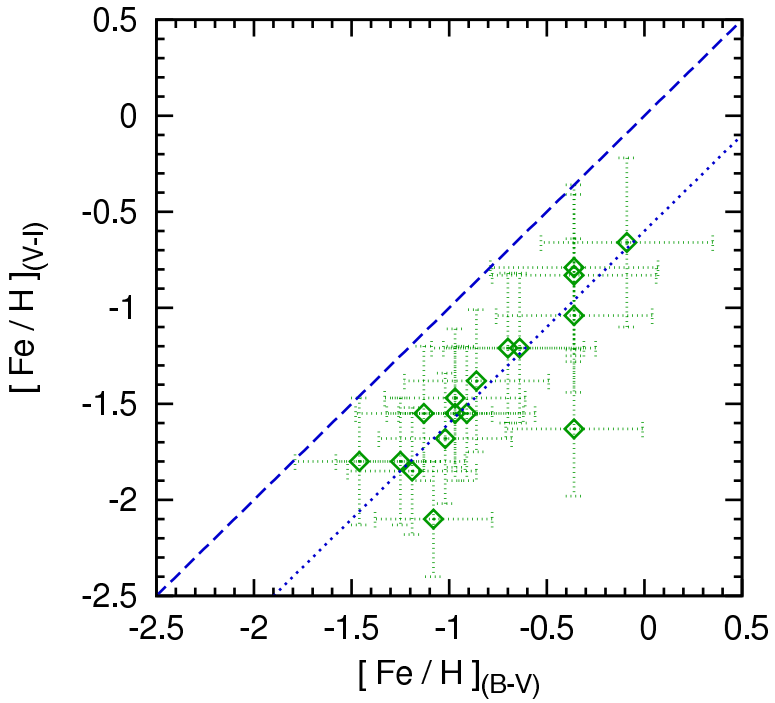

Figure 2.6: Comparison between $[\mathrm{Fe/H}]_{(V-I)}$ and $[\mathrm{Fe/H}]_{(B-V)}$ for the objects in Centaurus A. The numbers have been calculated with eq. (2.8) and eq. (2.9) respectively. The dashed line indicates equality of $[\mathrm{Fe/H}]_{(V-I)}$ and $[\mathrm{Fe/H}]_{(B-V)}$. The dotted line, corresponding to $[\mathrm{Fe/H}]_{(V-I)} = [\mathrm{Fe/H}]_{(B-V)} - 0.6$, is a fit by eye to the actual distribution of the data.

error to this value has two components. The first of them is due to the intrinsic uncertainties to eqs. (2.8) and (2.9). The second component is the uncertainty due to the systematic difference between the results from eqs. (2.8) and (2.9). We estimate this error as half the difference between both estimates for a particular object. For the total error to the estimate of [Fe/H], the square root of the sum of the squares of both errors is assumed.

For three objects only a $(V-I)$ colour index is given. In these cases we simply set $[\mathrm{Fe/H}]_{(V-I)} + 0.3\,\mathrm{dex} = [\mathrm{Fe/H}]$, as $0.3\,\mathrm{dex}$ is the average value by which the $(V-I)$ colour indices of the other objects are changed. For estimating an error to these values for [Fe/H], the scatter of the data for $[\mathrm{Fe/H}]_{(V-I)}$ and $[\mathrm{Fe/H}]_{(B-V)}$ around the relation $[\mathrm{Fe/H}]_{(V-I)} = [\mathrm{Fe/H}]_{(B-V)} - 0.6$ is calculated for the objects in Fig 2.6. The scatter, s, is given by the equation $s^2 = \frac{1}{N-1}\sum_i^N [[\mathrm{Fe/H}]_{(V-I)\,i} - ([\mathrm{Fe/H}]_{(B-V)\,i} - 0.6\,\mathrm{dex})]^2$, where $N = 17$ is the number of objects in Fig. 6. This results in $s = 0.23\,\mathrm{dex}$, which we adopt as the error to the [Fe/H] values of these three objects.

The numbers for the metallicities of the objects in Centaurus A are listed in Tab. 2.4.

Note that Haşegan et al. (2005) obtain the [Fe/H] estimates for their objects also by comparison of the colour indices to the ones of GCs, i.e. in very much the same fashion as is done here for the objects in Centaurus A. The only MCOs with abundance estimates from line indices and thus estimates directly linked to an actual presence of the according elements in the cluster are the objects from Evstigneeva et al. (2007), the objects from Hilker et al. (2007), ω Cen and G1.

Since Figs. 2.2, 2.3, 2.4 and 2.5 suggest a rather fluent transition from the properties of MWGCs to the ones of MCOs, it seems worthwhile to include them in the discussion further on. A comprehensive compilation of the iron abundances of MWGCs is provided by Harris (1996). Based on the results of Carney (1996), we assume $[\alpha/\mathrm{Fe}] = 0.3$ in order to calculate Z

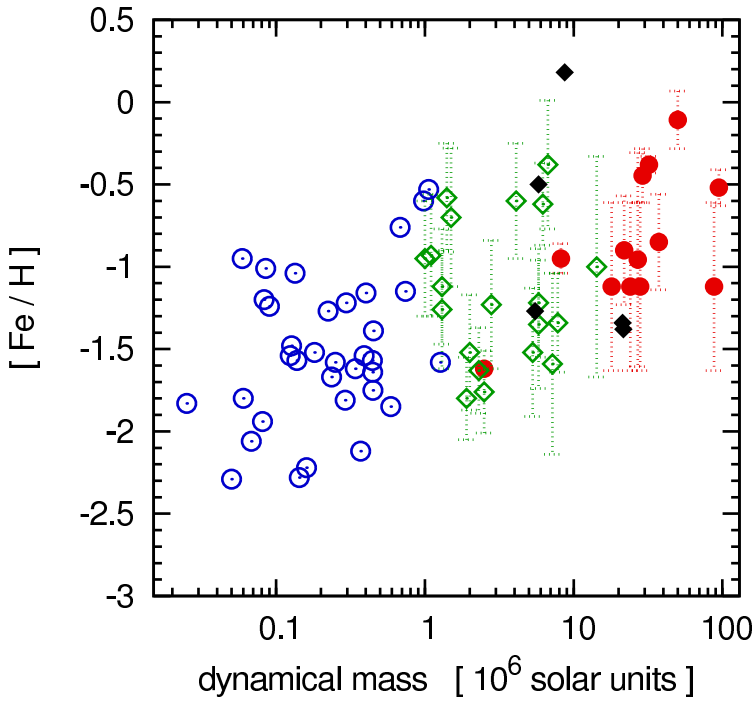

Figure 2.7: The iron abundances adopted for this work plotted against the dynamical mass for the MWGCs and the MCOs. Open circles represent the MWGCs, filled circles the MCOs with abundance estimates from line indices, open diamonds the MCOs in Centaurus A (Rejkuba et al. 2007) and filled diamonds the MCOs in the Virgo cluster from Haşegan et al. (2005). The values for [Fe/H] of the latter two have been calculated from colour indices.

for them, as we did for the MCOs (eq. 2.7).
Like the ones of MCOs, the stellar populations of MWGCs can be considered as old and coeval, but, in contrast to the ones of MCOs, dynamically evolved (i.e. loss of low-mass stars though evaporation driven by two-body relaxation).

The [Fe/H] that are adopted for the MWGCs and the MCOs are plotted in Fig. 2.7. A tendency to higher abundances with higher masses is undeniable. Note however that selection effects might play a role here. There is a bias against metal-rich objects for MWGCs, because they are concentrated towards the bulge of the Galaxy and therefore harder to observe than the metal-poor halo MWGCs (Harris 1976). The GC systems of elliptical galaxies, on the other hand, have a larger fraction of red (probably metal-rich) GCs, which are also somewhat brighter than the blue (probably metal-poor) ones (Harris et al. 2006; Wehner & Harris 2007).

2.4.3 Predictions for M/L_V ratios from SSP models

If information on the dependency of M/L_V ratio of a SSP on Z is combined with the estimates on the metallicity of the MCOs, it can be appraised what differences in Υ_V are *not* due to differences in Z. Theoretical estimates of Υ_V for different Z are taken from Maraston (2005) for SSPs that formed with a canonical IMF or a Salpeter-Massey IMF and from Bruzual & Charlot (2003) for SSPs that formed with a Chabrier IMF.

The canonical IMF is a continuous multi-power law,

$$\xi_{\rm K}(m) \propto m^{-\alpha_i}, \tag{2.10}$$

with $\alpha_1 = 1.3$ for $m < 0.5\ \mathrm{M}_\odot$ and $\alpha_2 = 2.3$ for $m > 0.5\,\mathrm{M}_\odot$. It has been constrained after a decade-long study of various biases and found to be consistent with all resolved stellar populations so far (Kroupa et al. 1993; Kroupa 2001, 2002, 2007). The Chabrier IMF is given for $m < 1\,\mathrm{M}_\odot$ as

$$\xi_{\mathrm{C}}(m) \propto \frac{1}{m}\ \exp\left[-\frac{(\log(m/\mathrm{M}_\odot) - \log 0.08)^2}{0.9522}\right] \tag{2.11}$$

and equals the canonical IMF for $m > 1\ \mathrm{M}_\odot$ up to a normalisation factor. The transition at $1\,\mathrm{M}_\odot$ is continuous (Chabrier 2001, 2003). This IMF cannot be distinguished from the canonical IMF within the observational errors (Fig. 2.8). To simplify matters, we will therefore also refer to the Chabrier IMF as the canonical IMF. The Salpeter-Massey IMF is a single power law with $\alpha = 2.35$ (Salpeter 1955; Massey 1998). The SSP models used here have been obtained under the assumption that the IMFs are defined from $0.1\,\mathrm{M}_\odot$ to $100\,\mathrm{M}_\odot$.

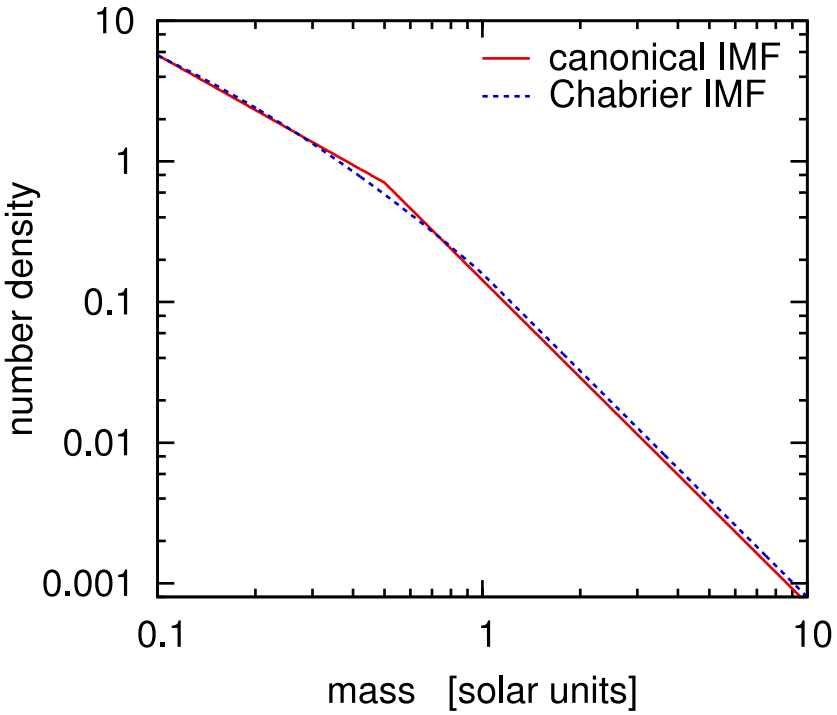

Figure 2.8: A comparison between the canonical IMF and the Chabrier IMF in the interval from $0.1\,\mathrm{M}_\odot$ to $10\,\mathrm{M}_\odot$. Both IMFs are normalised such that $\int_{0.1}^{100} \xi(m) m\, dm = 1$, where m is the mass in solar units. The two IMFs are barely distinguishable on the whole mass interval. They actually are identical above a mass of $1\,\mathrm{M}_\odot$, except for a slightly different normalisation factor.

Note that the upper mass limit of the IMF as suggested by Weidner & Kroupa (2004), Oey & Clarke (2005) and Figer (2005) is higher than $100\ \mathrm{M}_\odot$, but this does not have a mentionable affect on the expected M/L ratios of the SSPs discussed here due to the scarcity of high-mass stars in them.

A lower mass limit of $0.1\,\mathrm{M}_\odot$ for the IMF neglects the existence of brown dwarfs. This is probably unproblematic, if one follows the argumentation by Thies & Kroupa (2007). They suggest that star-like objects and brown dwarf-like objects are different populations and thus their frequencies cannot be described by a single, continuous IMF as e.g. in Kroupa (2001). The combined mass functions for brown dwarfs and stars which they find for star clusters in the Milky Way have many fewer brown dwarfs. Assuming a similar situation in the MCOs, brown

Table 2.5: Fit parameters for the interpolation formula for Υ_V to the data from the SSP models. The SSP models are from: 1: Maraston (2005), 2: Bruzual & Charlot (2003).

Model	a	b	c	Ref.
Salpeter IMF, 9 Gyr	3.33	0.82	2.30	1
Salpeter IMF, 13 Gyr	3.37	1.20	2.84	1
canonical IMF, 9 Gyr	3.42	0.42	1.51	1
canonical IMF, 13 Gyr	3.46	0.79	1.88	1
canonical IMF, 9 Gyr	3.70	0.23	1.23	2
canonical IMF, 13 Gyr	3.48	0.55	1.71	2

dwarfs are not expected to contribute more than a few percent to their total mass (opposed to $\approx 10\%$ for a mass function as in Kroupa 2001).

The ages that are considered here for the SSPs are 9 Gyr and 13 Gyr. Note that Maraston (2005) distinguishes between different horizontal branch morphologies, but this has a negligible impact on the dependency of Υ_V on Z of an old SSP.

The benefit from using both the SSP models from Bruzual & Charlot (2003) and Maraston (2005) although they cover the same ages and use (in principle) the same IMF is that different stellar evolutionary models have been used for constructing them.

In order to make statements on the Υ_V of objects with any Z, an interpolation formula that covers the whole Z-interval is needed. While it should be fairly simple, it should also closely fit the M/L_V ratios that Bruzual & Charlot (2003) and Maraston (2005) find for specific metallicities. A function of the form

$$F_i([Z/\mathrm{H}]) = (a^{[Z/\mathrm{H}]+b} + c)\frac{\mathrm{M}_\odot}{\mathrm{L}_\odot}, \tag{2.12}$$

where the index i distinguishes the different SSP models, fullfils these requirements well enough as Fig. 2.9 visualises. It can therefore safely be assumed that deviant estimates for Υ_V are not due to an inadequate interpolation formula, but due to incorrect assumptions on the stellar population in the MCOs or to a failure of the SSP models. The parameters a, b and c found in least-squares fits are given in Tab. 2.5. Comparing these parameters for different SSP models with the canonical IMF reveals that they do not only depend on the assumed age of the SSP, but also on whether the SSP models come from Bruzual & Charlot (2003) or Maraston (2005). This results in noticeably lower expectations for the M/L_V ratio from the SSP models from Bruzual & Charlot (2003), if compared to an in terms of age and IMF identical model from Maraston (2005). This proves the relevance of different stellar evolutionary models for the predictions from the SSP models.

It should be mentioned that the value of Υ_V for the highest metallicity was left out for the fit of eq. (2.12) to the data from Maraston (2005), because the omitted value was obtained by using a different stellar evolution model than for the other data from Maraston (2005). Moreover, excluding it results into a much closer fit of $F_i([Z/\mathrm{H}])$ to the remaining data, which already cover the metallicity range of the MCOs and the MWGCs.

Note that stellar evolution only raises the M/L_V ratio of a stellar population. The M/L_V ratio of a $13\,\mathrm{Gyr}$ old SSP therefore provides an upper limit for the M/L_V ratio of a stellar population with a certain metallicity and IMF, since stellar populations cannot be much older

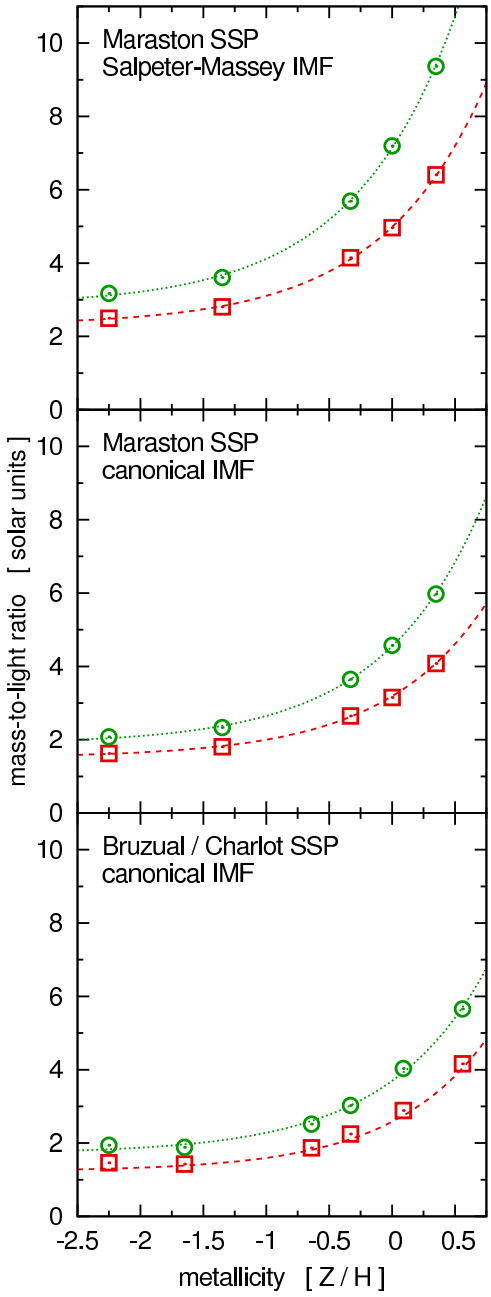

Figure 2.9: The dependency of Υ_V on Z for different SSPs. The origin and the IMF of the SSP model are detailed in in the upper part of each panel. The squares correspond to the models for 9 Gyr old populations and circles correspond to the models for 13 Gyr old SSPs. The lines indicate the interpolation (eq. 2.12) between the data from the SSP models.

according to the current estimates on the age of the universe ($13.73^{+0.16}_{-0.15}\,\mathrm{Gyr}$; Spergel D. N. et al. 2007).

If the stellar population of a star cluster with metallicity Z_1 is similar to one of the modelled SSPs, one would expect Υ_V to be close to the prediction from eq. (2.12) for the M/L_V ratio at Z_1:

$$\Upsilon_V|_{Z_1} \approx F_i|_{Z_1}.$$

If the stellar PDMF and the age of the star cluster is known (or assumed) to be similar to one of

the SSP models that were introduced above and Z_1 has been measured, Υ_V of a cluster which has the metallicity Z_2, but is identical to the first one in all other respects can be estimated:

$$\Upsilon_V|_{Z_2} \approx \frac{F_i|_{Z_2}}{F_i|_{Z_1}} \times \Upsilon_V|_{Z_1}. \tag{2.13}$$

The division by $F_i|_{Z_1}$ is imposed by the condition that the estimate for Υ_V must not be changed for $Z_1 = Z_2$. $\Upsilon_V|_{Z_1}/F_i|_{Z_1}$ is the factor by which the theoretical prediction for the M/L_V ratio of a stellar system differs from the value that is observed. The multiplication of these numbers with $F_i|_{Z_2}$ is not necessary in principle, but it scales them by a constant M/L_V ratio such that the predicted M/L_V ratio from an SSP model with metallicity Z_2 is expected to coincide with an observed value, if the model is appropriate.

In order to eliminate the differences in Υ_V that are caused by differences in metallicity among the MCOs in the sample, we estimate Υ_V for them as it would be if they all had the same metallicity. This can be achieved by setting Z_2 identical for all objects while using the measured Z for Z_1 in eq. (2.13):

$$\Upsilon_{V,\mathrm{n}} = \frac{F_i|_{\mathrm{Z}_\odot}}{F_i|_Z} \times \Upsilon_V, \tag{2.14}$$

where our (arbitrary) choice for Z_2 is the solar metallicity, $\mathrm{Z}_\odot$. We refer to the M/L_V ratios calculated this way as the "normalised M/L_V ratios", $\Upsilon_{V,\mathrm{n}}$. Note that a comparison of a whole sample of values of observed M/L_V ratios to a single prediction for the M/L_V ratio of a SSP (as done in Fig. 2.10) becomes possible that way.

The values for $\Upsilon_{V,\mathrm{n}}$ turn out to be quite insensitive to the actual choice out of the six sets of parameters a, b and c that encode different SSP models. This is due to the fact that the functions describing the dependency of Υ_V on Z are almost identical up to a scale factor for all the model populations that are considered here, i.e. the ratio $F_i|_{Z_2}/F_i|_{Z_1}$ is almost independent of the SSP model chosen. This means that the $\Upsilon_{V,\mathrm{n}}$ that are calculated here are very likely to be a good representation of the M/L ratios the MCOs and MWGCs would have if all their stars had solar composition, even if their PDMFs are different from all mass functions discussed here.

However, the choice of the SSP model certainly *has* an impact on the prediction for the M/L_V ratio of a population that completely fulfils the assumptions made for the model: For different models, the predictions on such a population would be different by about a factor of $F_i([Z/\mathrm{H}])/F_j([Z/\mathrm{H}])$.

2.4.4 The normalised M/L_V ratios of the MCOs and the MWGCs

The results for $\Upsilon_{V,\mathrm{n}}$ of the MCOs and the MWGCs assuming different SSPs are presented in Fig. 2.10.

The general distribution of the plotted points in all six panels of Fig. 2.10 still closely resembles the distribution of the points in Fig. 2.5, which represent the same objects but with their observed M/L_V ratios. However, the increase of the M/L_V ratios from the MWGCs to the MCOs is less pronounced once the effect of the metallicity on the luminosity has been accounted for, since the metallicities of the MCOs are usually somewhat higher than the ones of MWGCs (Fig. 2.7).

There is a large spectrum of values for the $\Upsilon_{V,\mathrm{n}}$ of the MCOs, ranging from $\approx 2\,\mathrm{M}_\odot\,\mathrm{L}_{\odot,V}^{-1}$ to $\approx 15\,\mathrm{M}_\odot\,\mathrm{L}_{\odot,V}^{-1}$. However, most of them lie between $\approx 3\,\mathrm{M}_\odot\,\mathrm{L}_{\odot,V}^{-1}$ and $\approx 7\,\mathrm{M}_{\odot,V}\,\mathrm{L}_{\odot,V}^{-1}$.

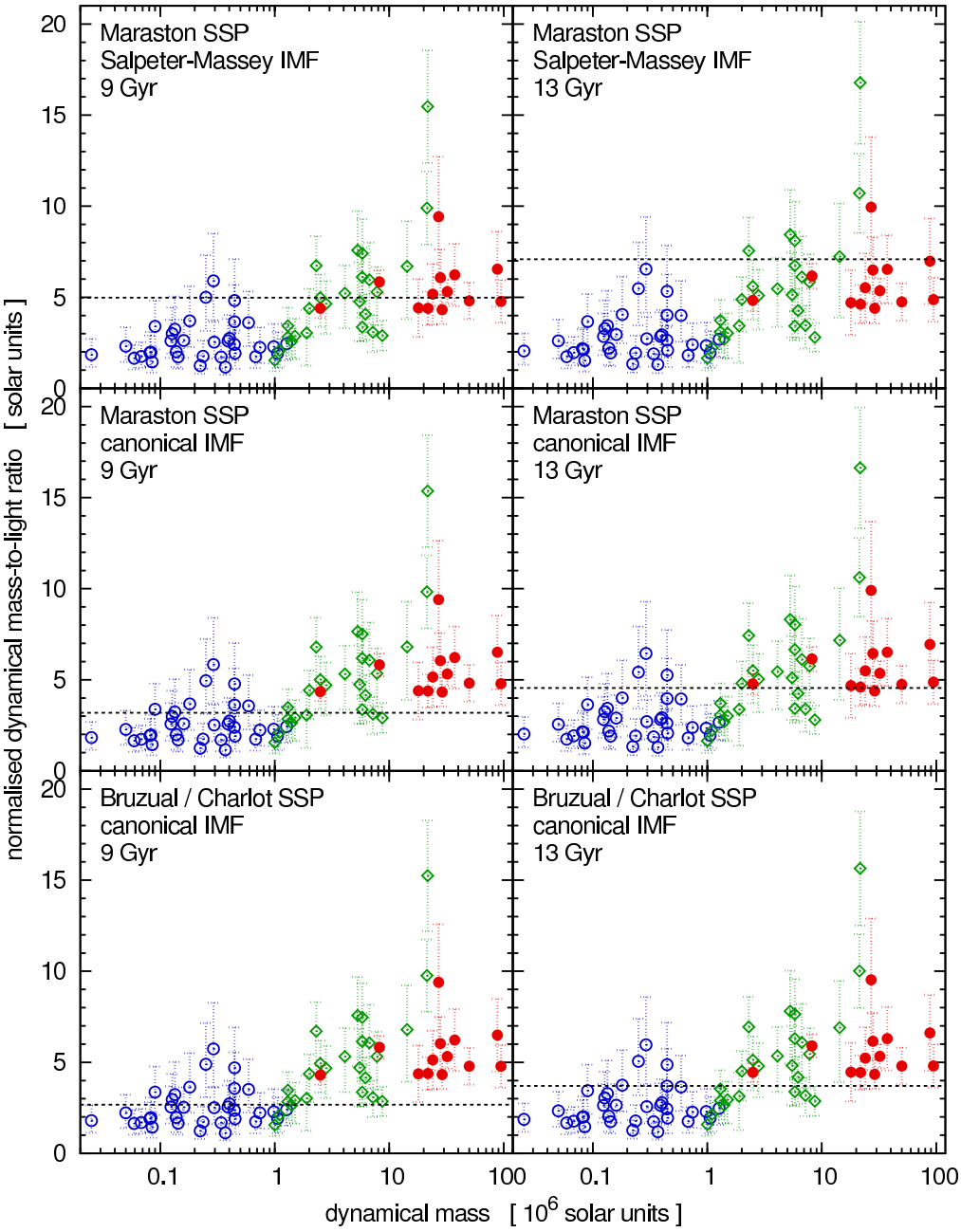

Figure 2.10: Normalised mass-to-light ratio, $\Upsilon_{V,\mathrm{n}}$, against mass for the MWGCs and MCOs based on the assumption that their stellar population can be described with SSP models. The origin of the SSP model, the assumed IMF and the assumed age of the SSP are given in the captions in each panel. The filled circles represent $\Upsilon_{V,\mathrm{n}}$ of MCOs with measured Z, the open diamonds represent objects for which Z was estimated from colour indices and open circles represent MWGCs. The dashed line indicates $F_i|_{\mathrm{Z}_\odot}$, i.e. the M/L_V ratio that the interpolation formula for the dependency of Υ_V on Z predicts for $\mathrm{Z}_\odot$, our reference metallicity. All points below that line have a lower Υ_V than the model predicts at their metallicity, all points above it exceed the model prediction. Naturally $F_i|_{\mathrm{Z}_\odot}$ is very similar to the M/L_V ratios at $\mathrm{Z}_\odot$ given in the actual models, where such a direct comparison is possible. (Maraston (2005) have data on Υ_V for $\mathrm{Z}_\odot$, Bruzual & Charlot (2003) use different grid points).

This still covers a large range of values, but taking into account that the $\Upsilon_{V,\mathrm{n}}$ of individiual MCOs typically also are uncertain within a range of $\approx 2\ \mathrm{M}_\odot\ \mathrm{L}_{\odot,V}^{-1}$ to $\approx 4\ \mathrm{M}_\odot\ \mathrm{L}_{\odot,V}^{-1}$, it is not

necessary to discuss physical reasons that could provide this scatter. However, two extreme outliers deserve more attention.

The first one of them is the faint MWGC NGC 6535, which has $\Upsilon_{V,\mathrm{n}} \approx 15\ \mathrm{M}_\odot\ \mathrm{L}_{\odot,V}^{-1}$ with large errors. As it is not only faint, but also fairly close to the galactic centre (the position is $l = 27^\circ\,18'$, $b = 10^\circ\,44'$ in Galactic coordinates), an accurate determination of its radius and velocity dispersion may be difficult due to the contamination with foreground stars. Moreover, its velocity dispersion has been derived from unpublished measurements. We therefore exclude it from Fig. 2.10.

The second outlier is the MCO S999 in the Virgo cluster (Haşegan et al. 2005), which is the object with the largest $\Upsilon_{V,\mathrm{n}}$ in all panels of Fig. 2.10. If this rather high value is not due to a flawed measurement, a scenario proposed by Fellhauer & Kroupa (2006) might offer an explanation. They proposed an enhancement of the M/L_V ratio of MCOs by tidal interaction with the host galaxy. If this is indeed the case for S999, a faint envelope of stars may be detectable around it. It is noteworthy that this model can only provide an explanation for the $\Upsilon_{V,\mathrm{n}}$ for a few MCOs out of a larger sample, as it requires quite specific orbital parameters.

A comparison of the predictions of the SSP models with solar metallicity with the values for calculated $\Upsilon_{V,\mathrm{n}}$ shows that the bulk of MWGCs and MCOs with masses $\lesssim 2 \times 10^6 \mathrm{M}_\odot$ has lower $\Upsilon_{V,\mathrm{n}}$ than it would be expected based on the assumed SSP models. Fig. 2.3 immediately reveals that these star clusters have relaxation times well below a Hubble time, which means that they are dynamically evolved due to their age. This result is therefore in (at least qualitative) agreement with the prediction by Baumgardt & Makino (2003) and Borch et al. (2007), who expect, based on their numerical simulations, the M/L_V ratio of a star cluster in a tidal field to be lowered by dynamical evolution for most of its lifetime.

The MCOs however have a strong tendency to *higher* M/L_V ratios compared to the theoretical prediction for a SSP with the canonical IMF, even for a 13 Gyr old population. There is only one SSP model, where in most of the cases the model expectation for $\Upsilon_{V,\mathrm{n}}$ is higher than the actual $\Upsilon_{V,\mathrm{n}}$ of the massive MCOs. This is the model with a 13 Gyr old stellar population which formed with a Salpeter-Massey IMF. For a 9 Gyr old population which formed with a Salpeter-Massey IMF, there seems to be agreement between the model prediction for Υ_V and the actual Υ_V. However, assuming that the IMF is truly universal and recalling that the stellar PDMFs of MCOs should still reflect their stellar IMFs as their dynamical evolution is slow, it can be concluded that the stellar population of the MCOs should be well described by a SSP formed with the canonical IMF. The Salpeter-Massey IMF deviates in the low-mass part strongly from the canonical IMF and can thus be ruled out if the above assumptions hold.

It should be noted that the finding of observed M/L_V ratios being higher than the theoretical prediction from a SSP model does not mean that the mass function of the chosen SSP model is inappropriate. Likewise, an agreement between the observed M/L_V ratios and the prediction from the SSP model does not mean that the assumed IMF is correct. Consider for instance the presence of non-stellar black holes or non-baryonic DM in the MCOs, that lead to a rise of the M/L_V ratio unaccounted for by any SSP model. However, in case the SSP model systematically overestimates the M/L_V ratios of a sample of clusters, the model is certainly not a good description for the stellar population of the clusters.

Even if it is assumed that the MCOs only contain stars and stellar remnants, the significance of the tendency for higher $\Upsilon_{V,\mathrm{n}}$ of the MCOs compared to SSPs whose IMFs agree with the canonical IMF should still be discussed. The case of a 13 Gyr old SSP with the canonical IMF from Maraston (2005) is of special interest and will therefore be treated in detail, because this is the model where the deviation of the $\Upsilon_{V,\mathrm{n}}$ calculated for the MCOs from the theoretical

expectation is the least pronounced. The values for $\Upsilon_{V,\mathrm{n}}$ agree in fact with the prediction from the appropriate SSP model within the error for a large fraction of the MCOs, as can be seen in the middle right panel of Fig. 2.10. On the other hand, if taken as a sample, the MCOs which are more massive than $2 \times 10^6\,\mathrm{M}_\odot$ still have a clear tendency for higher normalised M/L_V ratios than one would expect from the SSP model.

A possibility to test whether a tendency is a significant deviation from an expectation is Pearson's test for the goodness of fit, as it is found in Bhattacharyya & Johnson (1977) (see Appendix A.1.1). We apply this test on the MCOs more massive than $2 \times 10^6\,\mathrm{M}_\odot$ under the assumption that their values for $\Upsilon_{V,\mathrm{n}}$ would scatter just as much to higher values as to lower values compared to the prediction for $\Upsilon_{V,\mathrm{n}}$ from an appropriate model.

The result of the test is then that the probability for the found (or an even more one-sided) distribution of the values for $\Upsilon_{V,\mathrm{n}}$ of the MCOs more massive than $2 \times 10^6\ \mathrm{M}_\odot$ around the expected value for a 13 Gyr old SSP with a canonical IMF from Maraston (2005) is $\ll 0.005$. The hypothesis that this SSP model can fully describe the properties of the MCOs can therefore be excluded according to this test.

The reliability of this result can be doubted, because it is not entirely clear whether the sample of the 31 objects, for which $M \geq 2 \times 10^6\ \mathrm{M}_\odot$ is fulfilled, is large enough to apply Pearson's test for the goodness of fit. Moreover, the objects with the more uncertain metallicity estimates from colour indices are included in this sample.

We therefore also apply the sign test, as described in Bhattacharyya & Johnson (1977) (see Appendix A.1.2), on the 13 MCOs with metallicity estimates from line indices. The hypothesis to be tested is that there is no significant difference between their values for $\Upsilon_{V,\mathrm{n}}$ and the theoretical expectation assuming a 13 Gyr old SSP with a canonical IMF from Maraston (2005). The probability that the $\Upsilon_{V,\mathrm{n}}$ are larger than the theoretical expectation in 12 or more cases is 0.002 according to this test, i.e. it is highly improbable that the hypothesis is correct.

Both statistical tests thus suggest that stellar population models cannot explain the M/L_V ratios as long as a canonical IMF is assumed, even for the maximum age the stellar population could have in order to be consistent with the age of the universe according to cosmological models. Note that Mieske et al. (2006a) suggest intermediate ages for the MCOs in the Fornax cluster. The actual discrepancy between the true values for M/L_V ratios and the SSP models with the canonical IMF would then be larger than in the case discussed above. *This means that as long as the SSP models do not fail to describe real stellar populations, the MCOs either contain additional non-luminous matter, or their PDMFs must be different from what one would expect for a stellar system formed with the canonical IMF.*

2.4.5 The normalised M/L_V ratios of elliptical galaxies

We now compare the M/L_V ratio of elliptical galaxies and galactic bulges with the prediction for the M/L_V ratio of a 13 Gyr old SSP with the canonical IMF according to the models from Maraston (2005).

The metallicity estimate that enters the calculation of the normalised M/L_V ratio of the elliptical galaxies and galactic bulges is based on results on the metallicities of galaxies from the Sloan Digital Sky Survey obtained by Gallazzi et al. (2005). It is apparent from their data that the metallicities of galaxies in a given total-stellar-mass bin are distributed over a range of possible values (their figure 8 and table 2). In the present paper, the median of this distribution is taken as a representative value for the metallicities of the galaxies in that mass bin. The metallicities of the elliptical galaxies and galactic bulges in our sample as a function of their

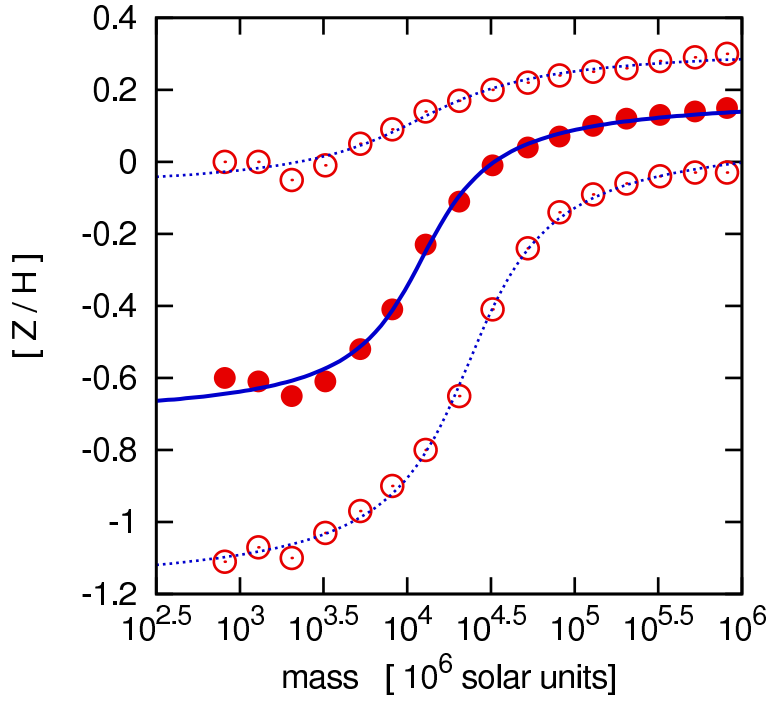

Figure 2.11: The 16th percentiles (lower open circles), the median values (filled circles) and the 84th percentiles (upper open circles) of the distributions of the metallicities of galaxies in different total-stellar-mass bins (Gallazzi et al. 2005). The lower dotted line, the solid line and the upper dotted line are our fits of eq. (2.15) to the 16th percentiles, the median values and the 84th percentiles, respectively.

Table 2.6: Best-fitting parameters of eq. (2.15) if fitted to the medians (50th percentiles) of the distributions of the metallicities of galaxies in different mass bins, as well as to the 16th and 84th percentiles of these distributions. The required data on the metallicity distributions is taken from Gallazzi et al. (2005), their table 2.

Percentile	a	b	c	d
Median (P50)	0.29	3.06	−4.09	−0.267
P16	0.41	2.72	−4.37	−0.555
P84	0.13	1.78	−4.07	0.118

mass are calculated using the function

$$[Z/\mathrm{H}](M) = a \arctan\left(b\left[\log\left(\frac{M}{10^6\,\mathrm{M}_\odot}\right) + c\right]\right) + d \tag{2.15}$$

with parameters a, b, c and d found in a least-squares fit to the median metallicities of galaxies in total-stellar-mass bins between $\approx 10^9\,\mathrm{M}_\odot$ and $\approx 10^{12}\,\mathrm{M}_\odot$, as given by Gallazzi et al. (2005). The data from Gallazzi et al. (2005) as well as the fit to them is shown in Fig. 2.11. The best-fitting parameters a, b, c and d are noted in Tab. 2.6.

For the abundances of dSphs, it is assumed that their values for [Fe/H] can be identified with their values for $[Z/\mathrm{H}]$. Iron abundances for most dSphs discussed here are given in Mateo (1998), except for And II (McConnachie et al. 2005), And XI (McConnachie et al. 2005) and UMa I (Simon & Geha 2007).

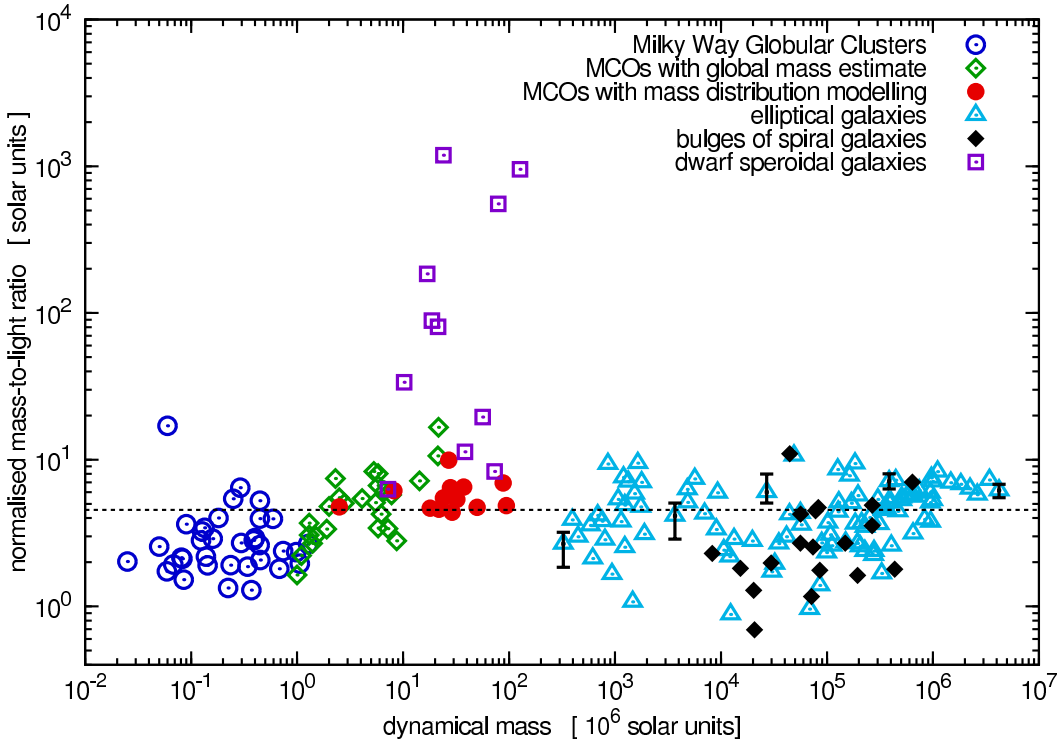

Figure 2.12: The normalised M/L_V ratios of all objects plotted in Fig. 2.5. The symbols are as in Fig. 2. The stellar population model assumed for calculating the normalised M/L_V ratios is the one from Maraston (2005) for a 13 Gyr old SSP (i.e. the same SSP model as for the middle right panel of Fig. 2.10). Black bars indicate for five of the elliptical galaxies the range of normalised M/L_V ratios they would assume if their metallicity would vary between the adopted values for the 16th percentile and the 84th percentile of the distribution of the metallicities of galaxies with that mass. The dashed line corresponds to the normalised M/L_V ratio expected according to the SSP model assumed for the objects in this figure.

The normalised M/L ratios which are implied by the adopted metallicities for the elliptical galaxies, the galactic bulges and dSphs introduced in Section 2.2 are plotted together with the normalised M/L_V ratios of MCOs and MWGCs in Fig. 2.12.

Gallazzi et al. (2005) find especially for low-mass galaxies a large spread for the distribution of their metallicities. To quantify the uncertainties that arise for the adopted normalised M/L_V ratios from the range of likely actual metallicities of galaxies, eq. (2.15) is also fitted to the values from Gallazzi et al. (2005) for the 16th and 84th percentiles of the distributions of metallicities of galaxies in different mass bins. The best fitting parameters a, b, c and d can be found in Tab. 2.6. Using these parameters, likely values for a high and a low metallicity in a given galaxy can be estimated depending on its mass and the according normalised M/L_V ratio can then be calculated. In Fig. 2.12, the possible range of normalised M/L_V ratios suggested by the lower and the upper estimate of its metallicity is indicated for five sample objects with black bars.

It thereby becomes apparent in Fig. 2.12 that the spread of the normalised M/L_V ratios of elliptical galaxies and galactic bulges cannot be explained by different metallicities alone, but that at least one more parameter (e.g. the mean age of their stellar populations) must vary among them as well.

Consider the elliptical galaxies and galactic bulges with the highest normalised M/L_V ra-

tios. Given the adopted range for their likely metallicities, the range of M/L_V ratios possible for them is inconsistent with the prediction for their normalised M/L_V ratio from a model for a 13 Gyr old SSP from Maraston (2005); especially for the objects with high dynamical masses. This suggests, as for the MCOs, an IMF different from the canonical IMF for their stellar populations or the presence of additional (gaseous or non-baryonic) matter in them.

2.5 Discussion

2.5.1 How reliable are the SSP models?

The results that have been obtained in Section 2.4.1 are strongly based on the reliability of SSP models which are in turn based on the reliability of evolutionary stellar models. However, the reliability of these models cannot be taken for granted, as the differences between the models from Bruzual & Charlot (2003) and Maraston (2005) already indicate.

Another issue that may hint at difficulties with the SSP models is the relation between the iron abundance and the colour indices they suggest. This becomes apparent when using them to predict [Fe/H] of the MCOs in Centaurus A from their colours. This can be done by setting up alternative equations to eqs. (2.8) and (2.9) by fitting interpolation functions to the $(V-I)$-[Fe/H] value pairs and the $(B-V)$-[Fe/H] value pairs given by the SSP models (i.e. as in Section 2.4.3 for a relation between the metallicity and the M/L_V ratio). Fig. 2.13 shows that a good fit between the data and the interpolation can be achieved with functions of the form

$$[\mathrm{Fe/H}]_{(V-I),\mathrm{SSP}} = a\,(V-I) + b(V-I)^{0.5} + c \tag{2.16}$$

for the $(V-I)$ colour index and analogous for the $(B-V)$ colour index. The subscribt SSP in eq. (2.16) is supposed to indicate that these estimates for [Fe/H] from colour indices are based on SSP models, in contrast to the estimates for [Fe/H] from eqs. (2.8) and (2.9), which are based on observations of the MWGCs.

In Fig. 2.14, $[\mathrm{Fe/H}]_{(V-I),\mathrm{SSP}}$ is plotted against $[\mathrm{Fe/H}]_{(B-V),\mathrm{SSP}}$ for the objects in Centaurus A. Each panel represents a choice of the SSP model which is assumed to represent the stellar population of the objects in Centaurus A best. There are two features of the distribution of the data, which are remarkably little affected by that choice. The first one is the undeniable tendency for $[\mathrm{Fe/H}]_{(V-I),\mathrm{SSP}} < [\mathrm{Fe/H}]_{(B-V),\mathrm{SSP}}$. The second one is that the spread of the values for $[\mathrm{Fe/H}]_{(V-I),\mathrm{SSP}}$ is larger than the spread of the values for $[\mathrm{Fe/H}]_{(B-V),\mathrm{SSP}}$. However, if one of the SSP models is an adequate description for the actual SSPs in Centaurus A, no systematic difference between the two estimates for [Fe/H] from this SSP model would be expected.

One could therefore come to the conclusion that none of the SSP models considered in this paper reflects the actual stellar populations of the objects in Centaurus A. Note however that neither assuming an age of $5\,\mathrm{Gyr}$ nor considering a different horizontal branch morphology for the models from Maraston (2005) can enhance the concordance between $[\mathrm{Fe/H}]_{(B-V),\mathrm{SSP}}$ and $[\mathrm{Fe/H}]_{(V-I),\mathrm{SSP}}$ for the objects in Centaurus A. This could be evidence of the standard SSP models failing to give a detailed and accurate description of real stellar populations in principle. Xin et al. (2007) claim that this might indeed be the case as long as SSP models are only based on the evolution of single stars but neglect the existence of blue stragglers, which are thought to be products of stellar interactions. Given the complex abundance patterns in resolved massive star clusters, it also seems well possible that the observed (integrated) $(B-V)$ and $(V-I)$ color indices of the objects in Centaurus A can only be reproduced by stellar population models which account for an age and metallicity spread of the stars.

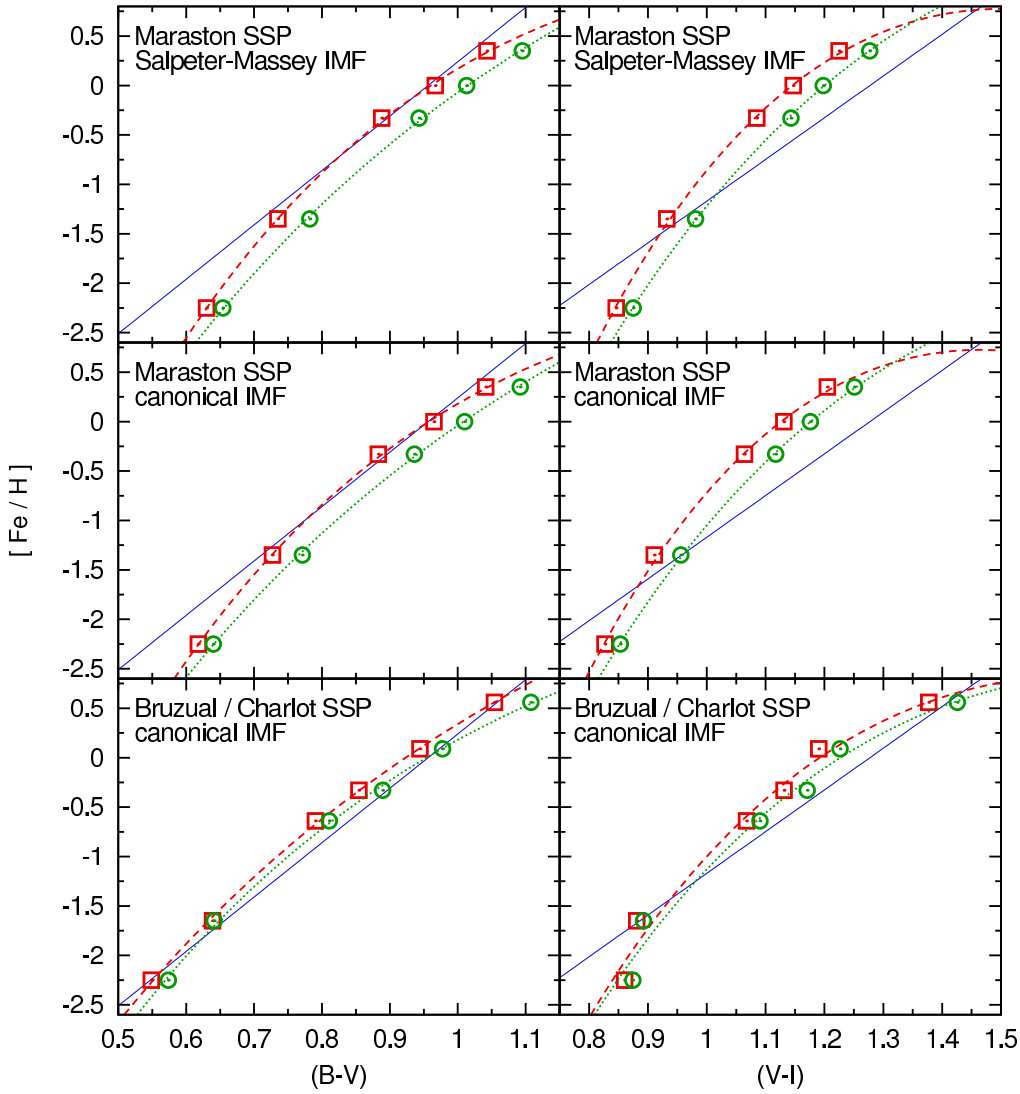

Figure 2.13: The relation between colour indices and [Fe/H] according to SSP models. The right panels show [Fe/H] against the $(V-I)$ colour index while the left panels show [Fe/H] against the $(B-V)$ colour index. Squares show the data for 9 Gyr old populations. The dashed line is the fit to them. Circles show the data for 13 Gyr old populations. The dotted line is the fit to them. The thin solid lines represent the relations that have been established for MWGCs by Barmby et al. (2000). Out of the SSP models by Maraston (2005), the case of a red horizontal branch is shown in this figure. This morphology is said to reflect the horizontal branches in most of the metal-rich GCs and therefore seems to be an appropriate choice for the MCOs, which show similar metallicities if measured.

An alternative explanation for the inconsistency between $[\mathrm{Fe/H}]_{(B-V),\mathrm{SSP}}$ and $[\mathrm{Fe/H}]_{(V-I),\mathrm{SSP}}$ could be a so far unidentified observational bias in the colour observations of the objects in Centaurus A. This notion is made attractive by the finding that applying the observed relations eqs. (2.8) and (2.9) for the estimation of [Fe/H] leads to $[\mathrm{Fe/H}]_{(V-I),\mathrm{SSP}} < [\mathrm{Fe/H}]_{(B-V),\mathrm{SSP}}$ for the MCOs in Centaurus A as well (Fig. 2.6). If the difference between the metallicity estimates from eqs. (2.8) and (2.9) was, for instance, caused by a systematic error to the $(B-V)$ colour indices, their offset from the true $(B-V)$ colour indices would be ≈ 0.1 dex.

Considering both the inconsistency of the iron abundances derived from the different colour indices by using the SSP models and the noticeably different predictions of different SSP models

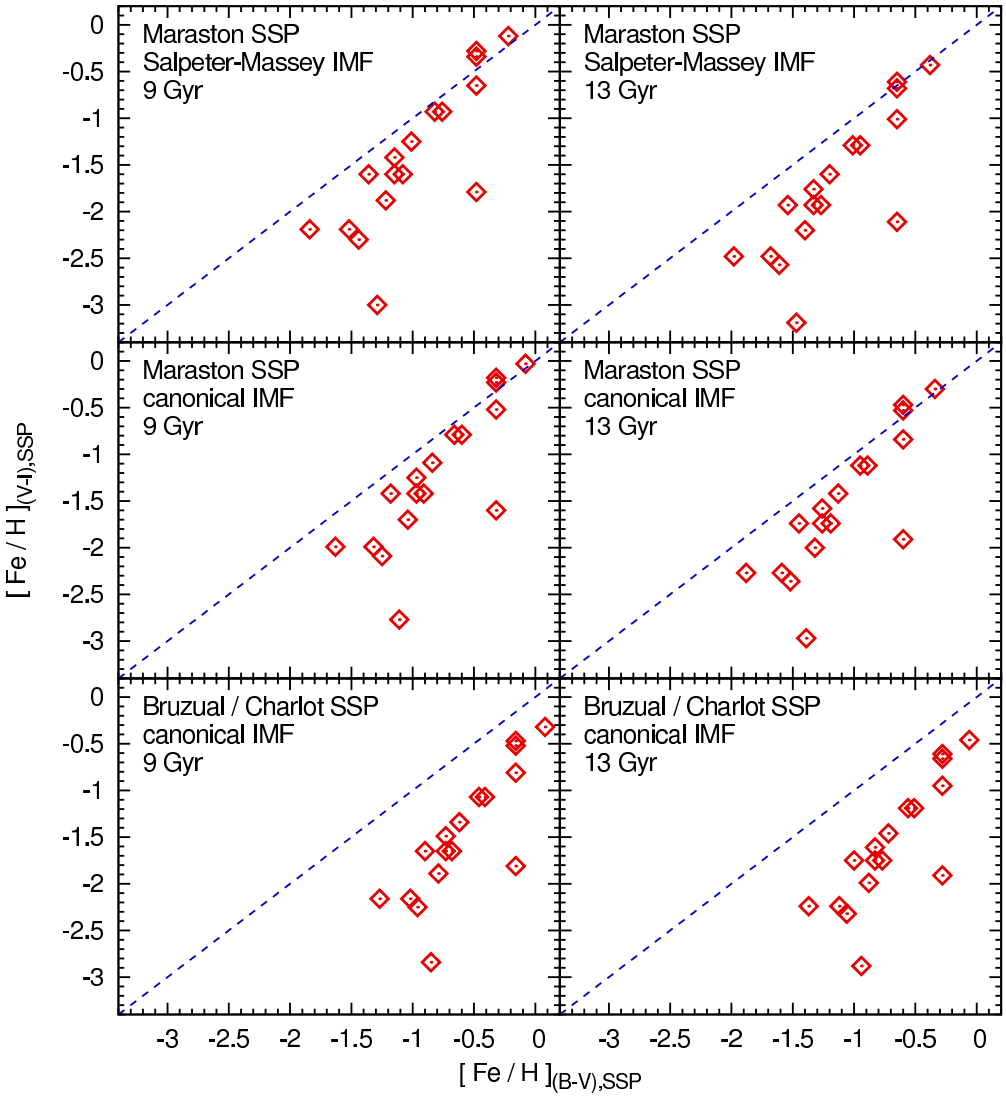

Figure 2.14: A comparison between $[\mathrm{Fe/H}]_{(B-V),\mathrm{SSP}}$ and $[\mathrm{Fe/H}]_{(V-I),\mathrm{SSP}}$ for the objects in Centaurus A (Tab. 2.2 and Tab. 2.4). The values are estimated by using the fits to the data from the SSP models plotted in Fig. 2.13. The dashed line indicates equality of both estimates for the iron abundances. If there was no systematic difference between them when applied to the objects in Centaurus A, the distribution of the data would follow these lines. Errors to the plotted points are not shown. They are probably governed by the errors to the colour measurements (which are unknown to us) and by a mismatch between the SSP models and the real stellar populations of MCOs (which is to be shown by this figure), but not by the errors to the interpolations plotted in Fig. 2.13. For the SSP models from Maraston (2005), a red horizontal branch is assumed. However, this does not have a strong impact on the distribution of the data in the according panels of this figure.

on the M/L_V ratio of the same population, it still seems possible that the enhancement of the M/L ratios of the MCOs compared to the theoretical predictions for SSPs with the canonical IMF is due to a failure of the SSP models.

2.5.2 How reliable is an estimate of [Fe/H] from colour based on observations?

The alternative to estimating [Fe/H] from colour indices based on a SSP model is the approach chosen for this paper, namely using a relation between [Fe/H] and colour indices that has been established on a sample of observed star clusters, such as eqs. (2.8) and (2.9). But just like the estimate of [Fe/H] by using SSP models, this approach is not unproblematic, as will be discussed here.

It is helpful to define two terms for the further discussion: We call the sample of objects for which the relation between [Fe/H] and colour was established the "calibration sample". The sample for which only colour indices are measured and where the relation between [Fe/H] and colour is used for a metallicity estimate is called the "target sample". In our specific case, the MCOs in Centaurus A are the target sample and applying eqs. (2.8) and (2.9) on them makes the MWGCs the calibration sample.

There are two problems, that are generally attached to an estimate of the iron abundances from the colours of objects in a target sample based on observations of an calibration sample. Firstly, it has to be assumed that the objects in both samples have at least typically the same PDMFs for shining stars and the same ages. If this is not the case, this method is likely to fail because colours depend on these parameters as well as on metallicity.

Secondly, relations such as eqs. (2.8) and (2.9) are only *fitting formulae* to a data sample with scatter. However, if these relations are applied to the objects in the calibration sample, the resulting estimates for [Fe/H] lie in the same parameter space as the values for [Fe/H] from line indices. The same is true if the calibration sample and the target sample are indeed comparable.

As a test whether the MWGCs are a good choice for the calibration sample for the MCOs in Centaurus A, the values for $[\mathrm{Fe/H}]_{(V-I)}$ from eq. (2.8) are compared to the values for the estimates of the iron abundances from line indices (and thus directly linked to a observed iron content in the star clusters), $[\mathrm{Fe/H}]_{\mathrm{obs}}$. The published data (see Tab. 2.3) allow such a comparison for the ten objects plotted in Fig. 2.15.

There is no significant trend for $[\mathrm{Fe/H}]_{(V-I)}$ to be larger or smaller than $[\mathrm{Fe/H}]_{\mathrm{obs}}$, as the application of the sign test (Bhattacharyya & Johnson 1977, Appendix A.1.2) shows. Under the hypothesis that there is no significant difference between the two values, the probability for having only four or less out of ten with $[\mathrm{Fe/H}]_{\mathrm{obs}} > [\mathrm{Fe/H}]_{(V-I)}$ is 0.377. A result as the one plotted in Fig. 2.15 is therefore quite probable. From this point of view it seems justifiable to apply eq. (2.8) on the MCOs, although it was originally fitted to the MWGCs.

Recall however that $[\mathrm{Fe/H}]_{(B-V)}$ is systematically higher than $[\mathrm{Fe/H}]_{(V-I)}$ for the objects in Centaurus A (Fig. 2.6). Since we adopt the mean of $[\mathrm{Fe/H}]_{(V-I)}$ and $[\mathrm{Fe/H}]_{(B-V)}$, [Fe/H] of the clusters in Centaurus A will be overestimated if $[\mathrm{Fe/H}]_{(V-I)}$ reflects their true abundances well. This is a conservative choice in our case, because a higher estimate for [Fe/H] leads to a lower estimate for $\Upsilon_{V,\mathrm{n}}$. We arrived at the result that a SSP model with the canonical IMF underpredicts the M/L_V ratios of the MCOs nevertheless, this therefore being a robust conclusion.

2.5.3 The impact of a wrong estimate of [Fe/H] on the comparison of the dynamical M/L_V ratios with the SSP models

As the metallicities of the MCOs may be subject to systematic errors, it makes sense to discuss the impact of a wrong metallicity estimate on our claim that the M/L_V ratios of the MCOs are

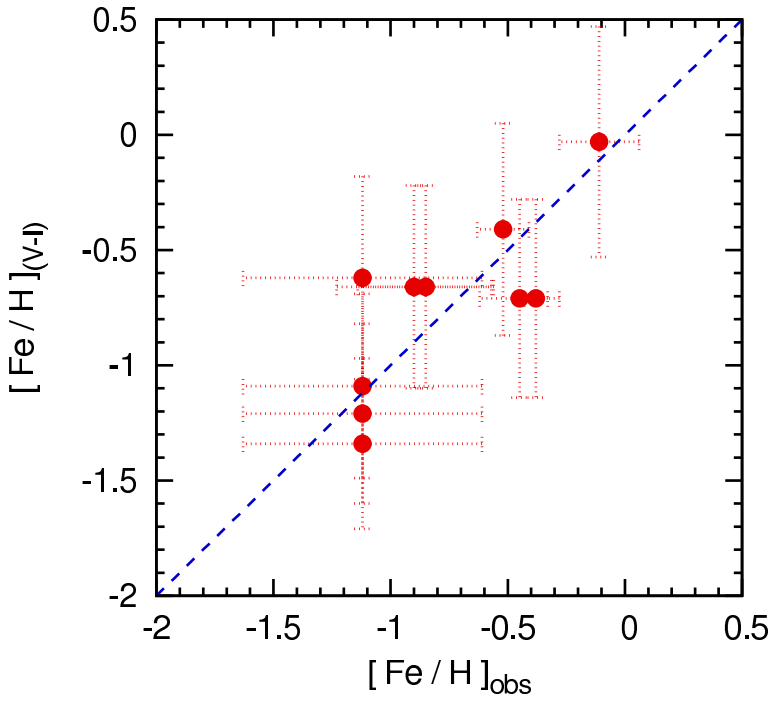

Figure 2.15: $[\mathrm{Fe/H}]_{(V-I)}$ calculated from eq. 2.8 plotted against the iron abundance estimate from line indices, $[\mathrm{Fe/H}]_{\mathrm{obs}}$, for the objects whose $(V-I)$ colours are given in Tab. 2.3. The dashed line indicates equality between observed and calculated values. Apparently there is no clear tendency for the points to be located only on one side of the line. This indicates that there is no systematic difference between $[\mathrm{Fe/H}]_{(V-I)}$ and $[\mathrm{Fe/H}]_{\mathrm{obs}}$.

inconsistent with the predictions from SSP models with the canonical IMF. We discuss one case in detail in order to give an impression how this affects our results.

Suppose the objects in the calibration sample are well described by a SSP with the same mass function, but that the target sample is younger than the calibration sample. The colour of the objects in the target sample is then bluer than it would be if they were of the same age as the objects in the calibration sample.

When relations like eqs. (2.8) and (2.9) are applied in order to estimate the iron abundance, it is implicitly assumed that the stellar populations of the objects in the target sample are the same as the ones in the calibration sample. The estimates for the iron abundances are therefore too low if the target sample is younger than the calibration sample, because of the age-metallicity degeneracy (Worthey 1994). As a consequence, the $\Upsilon_{V,\mathrm{n}}$ calculated from eq. (2.14) is too high, since the denominator on the right side of eq. (2.14) only decreases with decreasing Z due to the exponential nature of eq. (2.12).

However, the prediction for $\Upsilon_{V,\mathrm{n}}$ made by a SSP model increases with the assumed age of the SSP. The expectation for the $\Upsilon_{V,\mathrm{n}}$ of the objects in the target sample is therefore also too high, if they are compared to an SSP model which is, concerning the assumed age of the objects, more appropriate for the objects in the calibration sample. Thus, the error that is made in the estimation of the values for $[Z/\mathrm{H}]$ of the objects in the target sample by assuming a common age for all objects tends to balance the error that is made when all objects are compared to the same SSP model.

An analogous argument can be found if the objects in the target sample are depleted in low-mass stars compared to the objects in the calibration sample. In this case, it is the scarcity

of low-mass stars that makes the objects in the target sample bluer and thereby leads to a too low metallicity estimate for them. The resulting too high estimate for $\Upsilon_{V,\mathrm{n}}$ for these objects is compensated if they are compared to a SSP model with a full population of low-mass stars (which are faint and therefore enhance the M/L_V ratio of the stellar population).

The reverse argumentation can be applied to objects with a higher age or more low-mass stars than the objects in the calibration sample.

It thereby seems that, also for objects with metallicity estimates from colour indices, finding the values for $\Upsilon_{V,\mathrm{n}}$ above the expectation from the SSP model really is an indicator for additional non-luminous matter in the object.

2.5.4 Implications of a high M/L_V-ratio in the MCOs

Two explanations for the systematic enhancement of the M/L_V ratios of the MCOs more massive than $2 \times 10^6\,\mathrm{M}_\odot$ compared to the predictions from SSP models with the canonical IMF are possible.

The first possibility is that the massive MCOs are embedded in DM haloes, as proposed by Haşegan et al. (2005). However, for MCOs with small effective radii and high M/L_V ratios, the mean density of the DM within five half-light radii would have to be between $1\,\mathrm{M}_\odot\,\mathrm{pc}^{-3}$ and $10\,\mathrm{M}_\odot\,\mathrm{pc}^{-3}$ in order to have the observed impact on their dynamics. Adopting the universal DM density profiles as they are predicted by standard $\Lambda\,\mathrm{CDM}$ cosmology (Navarro et al. 1997), only DM haloes with masses of $10^{12}\,\mathrm{M}_\odot$ or more could accumulate enough DM in their central parts.

The alternative to suggesting non-baryonic DM in the MCOs is to give up the notion of a universal IMF for all stellar populations. Such an alternative IMF would either be over-abundant in low-mass stars with high M/L_V ratios (bottom-heavy IMF), see Mieske et al. (2007), or over-abundant in massive stars (top-heavy IMF). The latter possibility would imply a high number of dark stellar remnants in an old stellar population. Especially a top-heavy IMF seems attractive, since it is also suggested by models for galaxy evolution (e.g. Baugh et al. 2005; Nagashima et al. 2005; van Dokkum 2008) or GC evolution (e.g. D'Antona & Caloi 2004; Prantzos & Charbonnel 2006). These issues will be examined in more detail in a forthcoming paper (see Chapter 3).

2.5.5 On the nature of MCOs

Apart from the finding that the MCOs more massive than $2 \times 10^6\ \mathrm{M}_\odot$ are in disagreement with the expectations for their M/L_V ratios according to SSP models with the canonical IMF, the increase of typical radii at about the same mass is probably the most intriguing observation. This raises the question whether the massive MCOs (mostly classified as UCDs in the literature) constitute a population different to other populations of stellar systems as far as their origin is concerned. This question is of special interest for the relation between massive MCOs and GCs, since the seemingly *continuous* rise of the mean radius above $10^6\,\mathrm{M}_\odot$ makes the notion of a single population of objects attractive (single population in the sense of a common scenario that leads to their formation). In this case, the evolution of such an object must be different at very high masses in order to account for the increase of radius with mass. A possible reason for this could be a dependency of star formation on gas density (which increases with mass for objects with the same extension, consider e.g. the MWGCs in Fig. 2.4). If this dependency would lead to a greater mass loss during the lifetime of the cluster, it could explain the greater

extensions because mass loss enlarges a star cluster. A possible example would be a top-heavy IMF in very dense star forming regions, which would cause a stronger mass loss by type II supernovae.

On the other hand, there have been efforts to design models that can specifically reproduce the parameters of UCDs. One of these models is the scenario by Fellhauer & Kroupa (2002a) that UCDs are the merger of massive cluster complexes as are seen to be forming in massively interacting galaxies. Another one is the scenario by Bekki et al. (2003) and Goerdt et al. (2008) that UCDs are the cores of nucleated galaxies[5]. Under the condition that GCs form in the collapse of a single molecular cloud, objects that were formed in one of the above scenarios would indeed be of a different origin. This would offer natural explanations for the masses and the radii of those objects to be larger than for typical GCs. In this case, UCDs and GCs are two different populations that mix in the mass interval from $10^6\ \mathrm{M}_\odot$ to $10^7\ \mathrm{M}_\odot$ because both kinds of objects formed in intense starbursts that converted a similar amount of gas into stars.

A question connected to the issues discussed here is whether it is expedient to discriminate the MCOs into UCDs and GCs. We think that this distinction can be justified. It clearly makes sense if UCDs really formed in a different way than GCs. But it also makes sense in the case that GCs and UCDs were initially formed in the same way, thus are in principle to be considered as the same class of objects as far as their origin is concerned. In this case, "UCD"would be a useful term to emphasise the peculiarities, for example the higher relaxation times, which very massive clusters usually show in comparison with their low-mass counterparts. Thus, UCDs could be *defined* as those compact stellar systems, which have relaxation times longer than a Hubble time and thereby are (almost) collisionless systems on this time scale. This definition is the same as the one proposed by Kroupa (1998) for a distinction between star clusters and galaxies, i.e. UCDs are galaxies in that sense.

Also G1 and ω Cen are classified as MCOs instead of GCs in this paper, because of the spread that their stars show in [Fe/H] (ω Cen certainly and G1 presumably). Peculiarities in element abundances can in principle be another way to discriminate UCDs from GCs by observational parameters. However, the MCOs in other galaxy clusters cannot be resolved into stars with the current instrumentation. A similar pattern of the chemical composition of their stars as in the MCOs in the Local Group can for this reason only be presumed so far, but not be proven in the near future.

2.6 Conclusions

In this paper, a sample of compact stellar systems covering the transition from globular clusters (GCs) to ultra compact dwarf galaxies (UCDs) and referred to as massive compact objects (MCOs) in this work, is compared to other dynamically hot stellar systems. Moreover, the M/L_V ratios of the MCOs and the Milky Way GCs are compared to predictions from models for stellar populations. Our main conclusions are as follows.

Departing from radii typical for GCs, which are constant with mass, greater extensions are correlated with higher masses for dense stellar systems more massive than $10^6\,\mathrm{M}_\odot$. A strong increase of the median two-body relaxation time with mass is the natural consequence. We also find that stellar densities peak at a mass near $10^6\ \mathrm{M}_\odot$.

[5]Note that the scenario Bekki et al. (2003) proposes is inconsistent with ΛCDM-theory, because it has to assume that the DM haloes of the progenitors of the UCDs are cored instead of cusped.

Dwarf spheroidal galaxies (dSphs) take on a special position among dynamically hot stellar systems. This is especially apparent from their dynamical M/L_V ratios, which are in some cases higher by one to two orders of magnitude than for any other dynamically hot stellar system. Also note the large spread of the M/L_V ratios of the dSphs, which would imply very different DM densities in the visible parts of different dSphs, if the dSphs were in dynamical equilibrium. It therefore seems improbable that the masses of dSphs can be determined by simple application of Jeans' equations.

The fact that compact stellar systems with $t_{rel} < \tau_H$ mostly have a much lower M/L ratio than systems with $t_{rel} > \tau_H$ appears to be qualitatively consistent with Baumgardt & Makino (2003) and Borch et al. (2007). They state that dynamical evolution lowers the M/L ratio of star clusters in tidal fields compared to dynamically unevolved clusters for most of their lifetime. Dynamical evolution is slow for UCDs, as their high relaxation times indicate, and consequently the decrease of the M/L_V ratio by this process is slow as well. Moreover, the slow dynamical evolution leads to the stellar present-day mass function being almost identical with the stellar initial mass function for main sequence stars. We also found that the assumption of a population of old coeval stars in each massive MCO probably constitutes a good approximation to their real stellar populations.

Taken together, the lack of dynamical evolution and the narrow age spread of the stellar populations make a comparison between the MCOs and theoretical predictions from SSP models with widely used IMFs reasonable. The SSP models also allow to account for the differences due to the different metallicities of the MCOs. The limiting factor here is, if the reliability of the SSP models is taken for granted, the only rough knowledge of the element abundances in the MCOs. It turns out that the dynamical M/L_V ratios of the MCOs more massive than $2\times10^6\,\mathrm{M}_\odot$ have a significant tendency to be even higher than the predictions of models for very old stellar populations, provided the IMF is chosen in agreement to the observations of stellar populations, where at present times low-mass main-sequence stars can be resolved (i.e. populations in the Milky Way and in objects in its immediate surroundings, such as the Magellanic Clouds).

It was shown however, that the SSP models that were used for the estimate of the expected M/L_V ratio of the MCOs cannot produce consistent [Fe/H] estimates for the objects in Centaurus A from the different colour indices measured for them. This poses the question whether the SSP models in their current state (e.g. without binary evolution) are truly reliable. On the other hand, if the predictions for the M/L_V ratios from the SSP models are correct, the discrepancy between them and the dynamical M/L_V ratios observed in the MCOs suggests that the more massive MCOs contain DM or that the stellar IMF in some stellar systems is different to the ones of resolved stellar populations. Both possibilities will be studied in follow-up papers.

Summarising, $\approx 10^6\,\mathrm{M}_\odot$ is a critical mass-scale at which the system length-scale begins to increase, the highest stellar density is reached, the relaxation time becomes comparable to a Hubble time and evidence for dark matter appears.

Acknowlegdements

JD aknowledges support through DFG grant KR1635/13 and ESO funding for a one-week stay in Garching, where some of the ideas presented in this paper have been discussed. We thank M. Rejkuba for kindly making her data on the objects in Centaurus A available to us before their publication. Fig. 2.8 has been prepared by J. Pflamm-Altenburg using a numerical routine described in the Appendix of Pflamm-Altenburg & Kroupa (2006).

Chapter 3

A top-heavy stellar initial mass function in starbursts as an explanation for the high mass-to-light ratios of ultra compact dwarf galaxies

J. Dabringhausen, P. Kroupa, H. Baumgardt, 2009, **MNRAS**, 394, 1529

Abstract:

It has been shown recently that the dynamical V-band mass-to-light ratios of compact stellar systems with masses from 10^6 $\mathrm{M}_\odot$ to 10^8 $\mathrm{M}_\odot$ are not consistent with the predictions from simple stellar population (SSP) models. Top-heavy stellar initial mass functions (IMFs) in these so-called ultra compact dwarf galaxies (UCDs) offer an attractive explanation for this finding, the stellar remnants and retained stellar envelopes providing the unseen mass. We therefore construct a model which quantifies by how much the IMFs of UCDs would have to deviate in the intermediate-mass and high-mass range from the canonical IMF in order to account for the enhanced M/L_V ratio of the UCDs. The deduced high-mass IMF in the UCDs depends on the age of the UCDs and the number of faint products of stellar evolution retained by them. Assuming that the IMF in the UCDs is a three-part power-law equal to the canonical IMF in the low-mass range and taking 20 per cent as a plausible choice for the fraction of the remnants of high-mass stars retained by UCDs, the model suggests the exponent of the high-mass IMF to be ≈ 1.6 if the UCDs are 13 Gyr old (i.e. almost as old as the Universe) or ≈ 1.0 if the UCDs are 7 Gyr old, in contrast to 2.3 for the Salpeter-Massey IMF. If the IMF was as top-heavy as suggested here, the stability of the UCDs might have been threatened by heavy mass loss induced by the radiation and evolution of massive stars. The central densities of UCDs must have been in the range 10^6-10^7 $\mathrm{M}_\odot\,\mathrm{pc}^{-3}$ when they formed with star formation rates of 10-100 $\mathrm{M}_\odot\,\mathrm{yr}^{-1}$.

3.1 Introduction

Ultra compact dwarf galaxies (UCDs) are stellar systems in which 10^6 $\mathrm{M}_\odot$ to 10^8 $\mathrm{M}_\odot$ of gas were converted into stars within a volume of some ten pc in diameter (Hilker et al. 1999; Drinkwater et al. 2000, 2003; Phillipps et al. 2001; Haşegan et al. 2005). If UCDs are essentially the massive end of the globular cluster sequence (Mieske et al. 2002, 2004; Forbes et al. 2008), then this must have happened within a few Myr, so that the star formation rate would have been 10-100 $\mathrm{M}_\odot\,\mathrm{yr}^{-1}$. Indeed, the enhancement in α-elements, that Evstigneeva et al. (2007) found in most of the UCDs they examined, suggests a short time scale for the formation of their stellar populations. Taken together, these properties indicate that UCDs once were among the most extreme star-forming regions in the universe.

A fundamental function underlying star formation is the stellar initial mass function (IMF), $\xi(m)$,

$$dN \propto \xi(m)\, dm, \tag{3.1}$$

where dN is the number of stars with initial masses between m and $m + dm$. The IMF is the parent distribution for the mass functions of stars in star clusters (Kroupa & Weidner 2003). These mass functions are subject to statistical scatter (Elmegreen 1997; Kroupa 2001) and have an upper mass limit determined by the mass of the gas cloud out of which the star cluster formed (Weidner & Kroupa 2006).

One of the most debated questions concerning the IMF is whether it is universal, i.e. independent on the conditions under which star formation takes place. This is not expected from a theoretical point of view. Adams & Fatuzzo (1996) and Larson (1998) suggest an increase of the characteristic masses of pre-stellar cloud cores with increasing ambient temperature. Murray & Lin (1996) discuss interactions of pre-stellar clumps leading to mergers as a process in star formation. Their model predicts an increase of the mean stellar mass with the density of the star-forming region. At the transition from massive globular clusters (GCs) to UCDs (i.e. in the mass range between 10^6 and 10^7 $\mathrm{M}_\odot$), encounters between pre-stellar clumps must have been particularly important. Only about 100 times the diameter of the orbit of Neptune is available for the mean distance between stars in the central parts of some of these high-mass GCs or low-mass UCDs (see fig. 4 in Dabringhausen et al. 2008). If expansion due to mass-loss through gas expulsion and stellar evolution played a role during their youth, then the densities of UCDs would have been even higher at their birth.

On the other hand, all observed *resolved* stellar populations are consistent with having formed with the same IMF. This *canonical* IMF can be formulated as a two-part power law,

$$\xi_\mathrm{c}(m) = k_i m^{-\alpha_i}, \tag{3.2}$$

with

$$\alpha_1 = 1.3, \qquad 0.1 \lesssim \frac{m}{\mathrm{M}_\odot} < 0.5,$$
$$\alpha_2 = 2.3, \qquad 0.5 \leq \frac{m}{\mathrm{M}_\odot} \leq m_\mathrm{max},$$

where m_max is a function of the natal stellar mass of an embedded star cluster at the time when star formation is over and $\xi_\mathrm{c} = 0$ for $m > m_\mathrm{max}$ (Kroupa 2001, 2008). The factors k_i ensure that the IMF is continuous where the power changes.

During the past years suggestions for the IMF not being universal, but over-abundant in high-mass stars (top-heavy) under extreme conditions, have accumulated for different types of

stellar systems. These include galaxies (e.g. Baugh et al. 2005, Nagashima et al. 2005 and van Dokkum 2008), the Galactic bulge and centre (e.g. Ballero et al. 2007 and et al. 2007) and Galactic globular clusters (e.g. D'Antona & Caloi 2004 and Prantzos & Charbonnel 2006).

Especially Milky Way globular clusters (MWGCs) have been examined closely. Their stellar mass functions might have been altered strongly by early residual gas expulsion (Marks et al. 2008) and stellar and dynamical evolution Baumgardt & Makino 2003; Borch et al. 2007; Kruijssen 2008; Kruijssen & Lamers 2008), but the observation of individual stars in the MWGCs can still give clues on their IMFs; namely by interpreting the complex patterns of the element abundances in MWGC stars (e.g. the Na-O anti-correlation, see Gratton et al. 2004 for a review on the composition of MWGC stars). These peculiarities are usually taken as evidence for self-enrichment, meaning that the last stars that formed in a particular MWGC contain material that has been processed by stars that formed earlier in the same cluster.

Different theories on how exactly the process of self-enrichment took place have been brought forward: the metal-enrichment in subsequent stellar generations could be caused by the ejecta of massive asymptotic-giant-branch stars, as suggested e.g. by D'Antona & Caloi (2004) and D'Antona et al. (2007), or by the winds from very massive stars, as suggested e.g. by Prantzos & Charbonnel (2006) and Decressin et al. (2007). Yet both approaches require a top-heavy IMF, although residual gas expulsion from mass-segregated clusters alleviates this need (Decressin et al. 2008).

It was shown e.g. in Dabringhausen et al. (2008) and Forbes et al. (2008) that GCs and UCDs do not constitute two clearly distinguishable populations, if a sample that covers the whole mass interval from GCs to massive UCDs is considered. This suggests a close relation between GCs and UCDs. It therefore seems well possible that the peculiarities in the element abundances that are found for stars in massive MWGCs could as well be present in the even more massive UCDs. But the only nearby objects that may be considered as UCDs and can (like the MWGCs) be resolved into individual stars are ω Cen and (at least to some extent) G1 in M31. Such observations indeed show the stellar content of these most massive star clusters (or low-mass UCDs) to have a spread of metallicities and ages (e.g. Meylan et al. 2001, Kayser et al. 2006 and Villanova S. et al. 2007).

However, there is an alternative way to set constrains on the IMFs of the UCDs, namely by the comparison with simple stellar population (SSP) models. Various authors thereby found that the UCDs tend to have higher dynamical V-band mass-to-light (M/L_V) ratios than expected for any possible stellar population that formed with the canonical IMF (Haşegan et al. 2005; Hilker et al. 2007; Rejkuba et al. 2007; Dabringhausen et al. 2008; Mieske et al. 2008)).

This result could indicate the presence of non-baryonic dark matter (Haşegan et al. 2005; Baumgardt & Mieske 2008). However, Murray (2009) argues that both numerical simulations and observations of dwarf spheroidal galaxies hint to dark matter densities that are far too low to influence the dynamics of UCDs. This strengthens the notion that the high M/L_V ratios of the UCDs are the consequence of an IMF different from the canonical one. Mieske & Kroupa (2008) discuss an over-abundance of low-mass stars (i.e. stars with high M/L_V ratios) as a possible cause for the high M/L_V ratios of the UCDs. They make testable predictions based on the CO-index (Kroupa & Gilmore 1994). Complementary to their approach, this contribution is dedicated to top-heavy IMFs as an explanation for the high M/L_V ratio of the UCDs, which is in this scenario the consequence of a large number of remnants from burnt-out stars in them. The possible need for a top-heavy IMF also in the context of the element anti-correlations in massive GCs, as outlined above, makes this approach particularly attractive.

This paper is organised as follows. In Section 3.2, the data sample used in this work is intro-

duced. Section 3.3 describes the model that is constructed for the stellar populations in UCDs. The results suggested by this model for the IMF of intermediate-mass and high-mass stars are presented in Section 3.4. Some implications of these results are discussed in Section 3.5. We summarise and conclude in Section 3.6.

3.2 The data sample

The present paper is based on the data of GCs and UCDs compiled in Mieske et al. (2008), their table 5, because the chosen sample fulfils two requirements necessary for what is done in the present paper:

1. Estimates for the *dynamical mass* have to be available for the objects.

2. Estimates of the global metallicity of the objects have to be possible.

This sample is currently the largest and most updated sample of its kind. We note however that the results in Dabringhausen et al. (2008) are qualitatively unchanged, although the present sample has been revised and enhanced compared to the sample they use.

The term 'dynamical mass' refers to a mass estimate that is based on the velocity dispersion of the stars in the stellar system (derived from spectral line widths) and the spatial structure of the stellar system (see Hilker et al. 2007 for details). The mass estimates are therefore independent from the observed total luminosities of the stellar systems.

The metallicities of the stellar systems are of importance for the present paper because of their influence on the luminosity of stellar populations. Knowing them is therefore essential for creating models of stellar populations with a certain M/L_V ratio, which is the focus of the present paper.

Besides newly estimated quantities, table 5 in Mieske et al. (2008) also comprises numbers that are taken from the previous literature, as documented in their paper for the masses but not for the metallicities. Details on the origin of the metallicity estimates for objects with masses $\geq 2 \times 10^6$ $\mathrm{M}_\odot$ are given in Tab. 3.2 of our paper. When Mieske et al. (2008) make their own metallicity estimate from the $(V-I)$ colours of the stellar systems they use the relation

$$[\mathrm{Fe/H}] = 3.27(V-I) - 4.50 \tag{3.3}$$

(eq. 4 in Kissler-Patig et al. 1998). This has been done for all objects in their sample with masses $< 2 \times 10^6$ $\mathrm{M}_\odot$, unless the stellar systems are MWGCs for which the metallicities are taken from Harris (1996) (private communication with S. Mieske).

Following Mieske et al. (2008), we take an estimated mass of $\geq 2 \times 10^6$ $\mathrm{M}_\odot$ as an easy-to-handle criterion to categorise a compact stellar system as a UCD instead of a GC. This mass marks quite well the transition from objects with GC-like properties to objects with UCD-like properties (Maraston 2005; Mieske et al. 2008; Dabringhausen et al. 2008), including the on average distinctively higher M/L_V ratios of the more massive objects. Note that the two-body relaxation time exceeds a Hubble time for systems larger than 2×10^6 $\mathrm{M}_\odot$ (Mieske et al. 2008), which has been proposed as the defining property to distinguish galaxies from star clusters (Kroupa 1998; Dabringhausen et al. 2008).

3.3 A model for the stellar populations of the UCDs

We now construct a model for the stellar populations of the UCDs under the assumption that the deviations of their M/L_V ratios from the theoretical expectation for the M/L_V ratio of a stellar population with the canonical IMF are caused by an IMF that varies for intermediate-mass and high-mass stars. The actual shape of the IMF in the UCDs cannot be specified from resolved stellar populations so far. The purpose of the following can therefore only be to give an idea by how much the IMF must deviate from the canonical IMF in order to account for the mismatch between observations and theoretical expectations for the M/L_V ratio of the UCDs.

3.3.1 The model ingredients

The problem of modelling a stellar population with a M/L_V ratio equal to an observed value can be formulated as

$$\frac{M_{\rm m}}{L_{\rm m}} - \Upsilon_V = 0, \tag{3.4}$$

where $M_{\rm m}$ is the total mass of the model population, $L_{\rm m}$ is its luminosity in the V-band and Υ_V is the observed M/L_V ratio of a stellar system. $M_{\rm m}$ and $L_{\rm m}$ depend on various parameters, such as the assumed age of the population, the shape of its IMF and the chosen model for stellar and cluster evolution. $L_{\rm m}$ additionally depends on the metallicity. These dependencies will be formulated below, along with the assumptions that are made for the model presented here.

The IMF

The IMFs of the UCDs are connected to their present-day mass functions in the simplest way possible, because of their median two-body relaxation times, $t_{\rm rh}$, which are of the order of a Hubble time or larger (Dabringhausen et al. 2008; Mieske et al. 2008). The timescale on which a stellar system dissolves depends on the tidal field strength, but can be expected to be many $t_{\rm rh}$, so that the stellar populations of UCDs are practically unaltered by dynamical evolution. This stands in contrast to GCs, whose $t_{\rm rh}$ are much shorter and therefore can have experienced significant dynamical evolution since their formation (also see Section 3.4.2).

We introduce a family of IMFs for the model stellar populations of the UCDs:

$$\xi_{\rm pl}(m) = k_i m^{-\alpha_i}, \tag{3.5}$$

with

$$\begin{aligned} \alpha_1 &= 1.3, & 0.1 \leq \frac{m}{\rm M_\odot} < 0.5, \\ \alpha_2 &= 2.3, & 0.5 \leq \frac{m}{\rm M_\odot} < 1, \\ \alpha_3 &\in \mathbb{R}, & 1 \leq \frac{m}{\rm M_\odot} \leq m_{\rm max}, \end{aligned}$$

where $m_{\rm max}$ is the upper mass limit for stars. These IMFs will be referred to as the 'three-part power-law IMFs'. They are equal to the canonical IMF except for their slope above $1\ {\rm M_\odot}$. We assume that the UCDs have formed with a three-part power-law IMF.

Upper mass limits of $100\ {\rm M_\odot}$ and $150\ {\rm M_\odot}$ are considered. The upper mass limit of $100\ {\rm M_\odot}$ equals the upper mass limit assumed in the simple stellar population (SSP) models which are

used in this paper (see Section 3.3.1). These are the same stellar population models Dabringhausen et al. (2008) took as a reference when they found that the M/L_V ratios of a significant majority of the UCDs tends to be higher than model predictions for the canonical IMF. This mass limit is however not in agreement with the upper mass limit for stars in very massive star clusters given by Weidner & Kroupa (2004), Oey & Clarke (2005) and Figer (2005), which is close to $150\ \mathrm{M}_\odot$. Therefore this more realistic upper mass limit is considered as well. It turns out that the results are affected surprisingly little by the upper mass limit of the IMF (Figs. 3.2 and 3.4 below).

Note that the lower mass limit of the IMF neglects the existence of brown dwarfs. This is probably unproblematic, since Thies & Kroupa (2007) showed that a combined mass function of brown dwarfs and stars shows a discontinuity. In the case that the low-mass IMFs of the UCDs are comparable to the ones in Galactic open star clusters (as assumed to be the case here), their results suggest that brown dwarfs contribute only a few percent to the total mass of the UCDs.

The formulation of the IMF in UCDs given in eq. 3.5 attributes a possibly enhanced M/L_V ratio of a UCD solely to a top-heavy IMF, i.e. to a large population of stellar remnants that would have to be expected in such a case. Note however that the assumption of a bottom-heavy, Salpeter-Massey-like IMF in UCDs is currently an equally valid approach to explain their M/L_V ratios (cf. figure 10 in Dabringhausen et al. 2008). Observations to test the hypothesis of a bottom-heavy IMF in UCDs using a method proposed in Mieske & Kroupa (2008) are underway.

Simple stellar population models

A simple stellar population (SSP) is defined as a population of stars of the same age and metallicity. Various authors have set up grids of models of such populations, e.g. Bruzual & Charlot (2003) and Maraston (2005). The alteration of the stellar mass function due to dynamical evolution is not considered in these grids; only stellar evolution changes the mass spectrum of the stars in the model populations.

The most closely examined object in the sample of UCDs used here, ω Cen, is known to have several stellar sub-populations of different ages and metallicities, i.e. ω Cen is not a SSP (e.g. Hilker & Richtler 2000; Hilker et al. 2004; Villanova S. et al. 2007). Still, the sub-populations in ω Cen can all be characterised as old and metal-poor. Taking ω Cen in this sense as representative for the UCDs, we assume that their stellar populations are composed of different sub-populations, but that these sub-populations are *similar* enough to describe each UCD as a single SSP for the purpose of this paper. Also note that stellar-encounter-driven dynamical evolution is negligible in the UCDs (Dabringhausen et al. 2008). A disagreement between the SSP models and the observations can in this light be interpreted as being caused by assuming the wrong IMF.

The SSP models of Bruzual & Charlot (2003) and Maraston (2005) differ by the stellar evolutionary models used to calculate the luminosity of the modelled population as well as the total mass assumed for this population. Bruzual & Charlot (2003) assume a somewhat higher mass-loss rate for the stellar populations (Maraston 2005, in particular her figure 22), while the luminosities they get from the stellar models they use are lower. In effect, the estimates for the M/L ratios by Bruzual & Charlot (2003) are similar to the ones by Maraston (2005, her figure 24). However, considering the predictions for the M/L_V ratios of old populations, the estimates by Bruzual & Charlot (2003) are about 20 per cent lower than the ones by Maraston

(2005). Note that this cannot be accounted for by the different formulations for the canonical IMF these authors use since they turn out to be nearly identical (figure 8 in Dabringhausen et al. 2008). In fact, Bruzual & Charlot (2003) find that the stellar mass of a 10 Gyr old population is 52 per cent of the initial stellar mass for the canonical IMF they use, while it would have been 54 per cent if they had used the same formulation of the IMF as Maraston (2005) does. The reminder of the difference in the M/L_V ratio of an old stellar population must thus be the consequence of the different stellar evolutionary models used and different assumptions regarding the remnant masses (also see Dabringhausen et al. 2008 and Mieske et al. 2008). As a compromise between the two sets of SSP models, we follow the approach by Mieske et al. (2008) and take the mean of the predictions from Bruzual & Charlot (2003) and Maraston (2005) as the reference for a comparison to the observations in UCDs.

We consider ages of 7 Gyr and 13 Gyr for the UCDs, since these values are at the limits of the ages expected for them. An age of 7 Gyr would be consistent with the intermediate age for the Fornax UCDs suggested in Mieske et al. (2006a) and Mieske et al. (2008). Note that assuming even younger ages would increase the discrepancy between the observed M/L_V ratio and the model predictions. Ages higher than 13 Gyr are excluded by the estimates for the age of the universe ($13.73^{+0.16}_{-0.15}$ Gyr; Spergel D. N. et al. 2007).

The turn-off mass from the main sequence for a population of coeval stars, $m_{\rm to}$, marks quite well the stellar mass above which stars of that population have already evolved into stellar remnants. It is $\approx 1\,{\rm M}_\odot$ for a ≈ 10 Gyr stellar population. Since stellar evolution is slow for old stars, $m_{\rm to} = 1\ {\rm M}_\odot$ is a reasonably good approximation for a 7 Gyr old SSP as well as for a 13 Gyr old SSP.

The contribution of the stellar remnants to the V-band luminosity of the UCDs is small and therefore neglected in this paper. The luminosity, $L_{\rm m}$, of a modelled stellar population is thus insensitive to the degree of top-heaviness of the IMF, since the IMF is only allowed to vary in a mass range where the stars have evolved after ≈ 10 Gyr. The masses of the stars that have not evolved yet are assumed to be distributed in concordance with the canonical IMF. Thus, $L_{\rm m}$ can be determined using the SSP models from Bruzual & Charlot (2003) and Maraston (2005) with the canonical IMF.

We note that by this approach the influence of binary systems on stellar evolution is neglected.

The initial-to-final-mass relation for stars

In order to find an explicit formulation of $M_{\rm m}$ in eq. (3.4), a formulation of the masses of evolved stars as a function of their initial masses is needed. This function, called the initial-to-final-mass relation, $m_{\rm rem}(m)$, allows to calculate the total mass of an evolved SSP from its IMF for a given age. Using the three-part power-law IMFs from Section 3.3.1, the integral that has to be solved in this calculation reads

$$M_{\rm m} = \int_{0.1}^{m_{\rm max}} m_{\rm rem}(m)\xi_{\rm pl}(m)\,dm, \tag{3.6}$$

where m is the stellar initial mass in ${\rm M}_\odot$. The limits of the integration are set by the lower and the upper initial mass limit for stars.

The initial-to-final-mass relation used in this paper is specified in the following.

For stars with initial masses $m < m_{\rm to}$, $m_{\rm rem} = m$ is assumed, i.e. the mass loss of main-sequence stars is neglected.

Stars with initial masses of $m_{\rm to} < m < 8\,{\rm M}_\odot$ are assumed to have evolved into white dwarfs (WDs), in concordance with the mass limit given by Koester & Reimers (1996). Kalirai et al. (2008) find, performing a weighted least-squares fit of a linear function to data based on observations of WDs in star clusters,

$$m_{\rm rem} = (0.109 \pm 0.007)\frac{m}{{\rm M}_\odot} + (0.394 \pm 0.025), \tag{3.7}$$

for a relation between the mass of WDs and the initial mass of their progenitors, where m is the stellar initial mass in ${\rm M}_\odot$. This relation is adopted in this paper.

Stars initially more massive than $8\ {\rm M}_\odot$ but less massive than $\approx 25\ {\rm M}_\odot$ are predicted to evolve into neutron stars (NSs) with a remarkably narrow mass spread (cf. figures 12 and 16 in Woosley et al. 2002). This is observationally supported by Thorsett & Chakrabarty (1999), who find the mass-distribution of pulsars (i.e. observable NSs) in their data sample to be consistent with a Gaussian distribution with a mean of $1.35\ {\rm M}_\odot$ and a width of $0.04\ {\rm M}_\odot$. Thus, in this paper $1.35{\rm M}_\odot$ is adopted for the masses of all stellar remnants with initial masses between $8\,{\rm M}_\odot$ and $25\,{\rm M}_\odot$.

Stars with initial masses above $25\,{\rm M}_\odot$ are generally thought to be the progenitors of stellar-mass black holes (BHs). However, the theoretical predictions for the masses of their remnants are not only strongly dependent on metallicity, but also on the assumptions on how the evolution of such stars proceeds (see figures 12 and 16 in Woosley et al. 2002). Figure 12 in Woosley et al. (2002) might suggest that the case of the higher remnant masses is the more appropriate choice for low-metallicity environments such as GCs and UCDs. However, the masses of observationally confirmed BHs lie all in a range that is covered by assuming that the remnants of very high-mass stars only have 10 per cent of the initial mass of their progenitors (Casares 2007). In our paper, we thus assume that stars with $m > 25\ {\rm M}_\odot$ evolve into BHs that have either 10 per cent or 50 per cent of the mass of their progenitor stars, but the emphasis is on the case with the less massive BHs because of the observational support for their existence.

Note that BHs formed through single-star evolution differ from NSs in mass, but not in the processes that precede their creation. NSs and BHs are both compact remnants that emerge from the core collapse and SN explosion of a massive star.

To summarise, the complete initial-to-final-mass function, $m_{\rm rem}$ used here is

$$m_{\rm rem} = \begin{cases} \frac{m}{{\rm M}_\odot}, & \frac{m}{{\rm M}_\odot} < \frac{m_{\rm to}}{{\rm M}_\odot}, \\ 0.109\,\frac{m}{{\rm M}_\odot} + 0.394, & \frac{m_{\rm to}}{{\rm M}_\odot} \leq \frac{m}{{\rm M}_\odot} < 8, \\ 1.35, & 8 \leq \frac{m}{{\rm M}_\odot} < 25, \\ 0.1\frac{m}{{\rm M}_\odot} \text{ or } 0.5\frac{m}{{\rm M}_\odot}, & 25 \leq \frac{m}{{\rm M}_\odot} \leq m_{\rm max}, \end{cases} \tag{3.8}$$

where $m_{\rm to}$ denotes the turn-off mass and $m_{\rm max}$ the upper initial mass limit for stars (eqs. 3.2 and 3.5). Inserting eq. (3.8) into eq. (3.6) and carrying out the integration on the right hand side of eq. (3.6) yields the mass of all stars and stellar remnants as a function of only the high-mass IMF-slope, α_3, if $m_{\rm to}$ (i.e. age) and $m_{\rm max}$ are specified. The terms resulting from this integration for initial stellar masses above $m_{\rm to}$ are written down explicitly in Appendix A.2.

Normalised mass-to-light ratios

The metallicities estimated for the UCDs usually do not coincide with the grid points of the SSP models by Bruzual & Charlot (2003) and Maraston (2005). It is therefore necessary to

Table 3.1: Fit parameters for the metallicity-dependent interpolation formula for Υ_V to the data from SSP models with the canonical IMF. BC indicates SSP models from Bruzual & Charlot (2003) and M SSP models from Maraston (2005).

Model	a	b	c
BC, 7 Gyr	3.29	0.12	1.05
M, 7 Gyr	3.26	0.22	1.24
BC, 13 Gyr	3.48	0.55	1.71
M, 13 Gyr	3.46	0.79	1.88

find interpolation formulae that describe the metallicity dependency of the M/L_V ratio in the models (which actually is a dependency of the luminosity on metallicity). This can be done by fitting exponential functions of the form

$$F|_Z = F([Z/\mathrm{H}]) = \left(a^{[Z/\mathrm{H}]+b} + c\right) \frac{\mathrm{M}_\odot}{\mathrm{L}_\odot}, \tag{3.9}$$

to the data from Bruzual & Charlot (2003) and Maraston (2005), where $[Z/\mathrm{H}]$ is the metallicity. The best-fitting parameters a, b and c found in a least-squares fit to the models used in this paper are listed in Table 3.1. The excellent agreement of this type of function to the models from Bruzual & Charlot (2003) and Maraston (2005) is demonstrated in fig. 9 in Dabringhausen et al. (2008).

The reference relation that is taken to describe the metallicity dependency of the M/L_V ratio for a SSP with a certain age and with the canonical IMF is the mean of the corresponding relations derived from the SSP models from Bruzual & Charlot (2003) and Maraston (2005) (cf. Mieske et al. 2008). The ratio between the observed M/L_V ratio for a UCD and the result from the reference relation at the appropriate metallicity is a measure for the discrepancy between the observed value and the theoretical prediction. It is convenient for the purpose here to multiply these values by the prediction of the reference relation for the M/L_V ratio at Solar metallicity. These quantities will be referred to as normalised M/L_V ratios, $\Upsilon_{V,\mathrm{n}}$,

$$\Upsilon_{V,\mathrm{n}} = \frac{\Upsilon_V}{F_{BC}|_Z + F_M|_Z} \times (F_{BC}|_{\mathrm{Z}_\odot} + F_M|_{\mathrm{Z}_\odot}), \tag{3.10}$$

where a subscript BC indicates that the parameters a, b and c correspond to a SSP model from Bruzual & Charlot (2003) and the subscript M indicates that the parameters a, b and c correspond to a SSP model from Maraston (2005) (for the same age).

Using these values for $\Upsilon_{V,\mathrm{n}}$, eq. (3.4) can be rewritten as

$$\frac{M_\mathrm{m}}{L_\mathrm{m}|_{\mathrm{Z}_\odot}} - \Upsilon_{V,\mathrm{n}} = 0. \tag{3.11}$$

$L_\mathrm{m}|_{\mathrm{Z}_\odot}$ is thereby no longer a metallicity-dependent variable, but is fixed to the value the reference relation predicts for Solar metallicity and thereby only depends on the age assumed in the model and the amplitude of the factors k_i in the IMF. The metallicity dependency is shifted into the transformation from the observed M/L_V ratio of the UCD to $\Upsilon_{V,\mathrm{n}}$. The $\Upsilon_{V,\mathrm{n}}$ values are noted in Tab. 3.2 and shown in Fig. 3.1. Their uncertainties have been propagated from the errors of the observed dynamical M/L_V ratios and the errors of the metallicity estimates.

The numerical value of L_m is calculated from the secondary condition that the prediction for $\Upsilon_{V,\mathrm{n}}$ from the SSP models should correspond to a stellar population with the canonical IMF with $m_{\mathrm{max}} = 100\ \mathrm{M}_{\odot}$ and a full population of remnants (i.e. a stellar population as in the SSP models). For this, m_{rem} as given in eq. (3.8) is used, adopting the case that the black hole masses, m_{BH}, are 10 per cent the stellar initial masses ($m_{\mathrm{BH}} = 0.1m$).

There is evidence that GCs usually have α-enrichments, $[\alpha/\mathrm{Fe}]$, of $0.3\,\mathrm{dex}$ (Carney 1996). Evstigneeva et al. (2007) find that the same $[\alpha/\mathrm{Fe}]$ is also typical for the UCDs in the Virgo cluster they examine. On the other hand, Mieske et al. (2007) find that a number of UCD candidates is consistent with having Solar $[\alpha/\mathrm{Fe}]$, which is why Mieske et al. (2008) adopt Solar $[\alpha/\mathrm{Fe}]$ for all stellar systems in their study. However, assuming a super Solar $[\alpha/\mathrm{Fe}]$ is the more careful choice in the context of the present paper, since it attributes more of a possibly enhanced M/L_V ratio in UCDs to metallicity effects. As in Dabringhausen et al. (2008), we therefore adopt $[\alpha/\mathrm{Fe}] = 0.3\,\mathrm{dex}$ for all GCs and UCDs and estimate their metallicities, $[Z/\mathrm{H}]$, from their iron abundances, [Fe/H]. This is done using the relation

$$[Z/\mathrm{H}] = [\mathrm{Fe/H}] + 0.94\,[\alpha/\mathrm{Fe}] \tag{3.12}$$

taken from Thomas et al. (2003). Consequently, the $[Z/\mathrm{H}]$ used for calculating the $\Upsilon_{V,\mathrm{n}}$ are $0.28\,\mathrm{dex}$ higher than the [Fe/H] and the $\Upsilon_{V,\mathrm{n}}$ in this paper are thereby slightly lower than the ones in Mieske et al. (2008).

The assumed age turns out to be almost irrelevant for the $\Upsilon_{V,\mathrm{n}}$ calculated for the individual stellar systems. However, the assumed age does have a strong impact on the $\Upsilon_{V,\mathrm{n}}$ predicted by the SSP-models (see also Dabringhausen2008).

The fate of the processed material and the stellar remnants in the UCDs

In order to have an influence on the dynamics of a stellar system, the stellar remnants that form in it have to remain bound to it. This can be assumed to be the case for the WDs in the UCDs, since WDs inherit the peculiar velocities of their progenitor stars and two-body encounter driven mass loss is negligible for the UCDs (see Section 3.3.1).

Unlike the case with WDs, stellar evolution has a direct impact on the velocity distribution of NSs. It is well established that many pulsars move with high peculiar velocities, which they must have obtained somehow in their formation out of their progenitor stars (Woosley 1987; Lyne & Lorimer 1994). Lyne & Lorimer (1994) give the mean pulsar birth velocity as $450 \pm 90\ \mathrm{km\,s^{-1}}$. Since the processes that lead to the formation of BHs through single-star evolution are the same as the ones that precede the formation of NSs, the BHs should also receive kicks.

The UCDs have velocity dispersions of $\lesssim 50\mathrm{km\,s^{-1}}$, which suggests escape velocities of the order of $\lesssim 100\mathrm{km\ s^{-1}}$. Thus, the peculiar velocities of most NSs and BHs should be high enough to leave the UCDs. On the other hand, NSs are known to populate GCs, which suggests that also the UCDs are able to retain some fraction of these objects.

Most of the matter processed in intermediate-mass and high-mass stars is reinserted as gas and dust into the interstellar medium during stellar evolution. Its fate is therefore crucial for the developement and consequently the M/L_V ratio of a stellar system.

There are in general three possibilities for what can happen to this material. If it remains inside the cluster, it can (at least in principle) simply accumulate (and thereby emit almost no radiation in the V-band) or it can be used up in the formation of subsequent stellar populations.

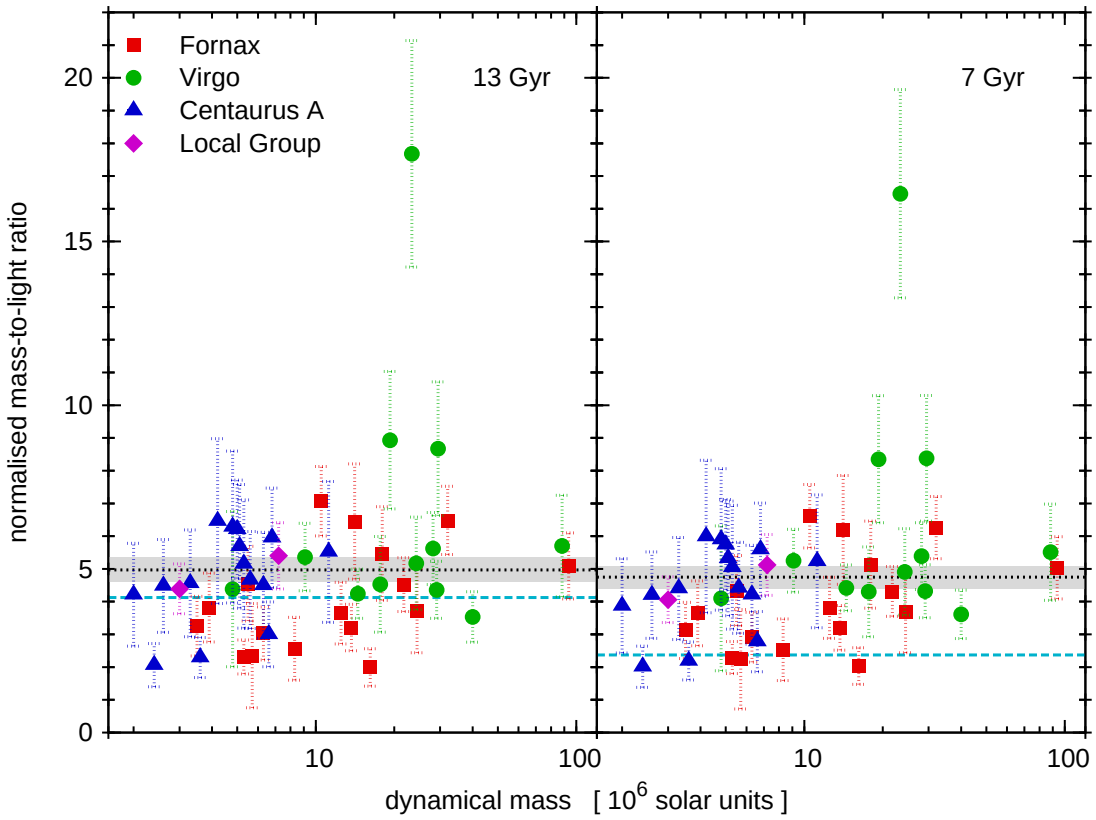

Figure 3.1: Normalised M/L_V ratios, $\Upsilon_{V,\mathrm{n}}$, of the stellar systems collected in table 5 in Mieske et al. (2008), provided their dynamical mass is estimated to be 2×10^6 $\mathrm{M}_\odot$ or more. Thus, the figure only shows objects that are UCDs according to the definition used in this paper. The ages assumed for them are either 13 Gyr (left panel) or 7 Gyr (right panel). The dashed horizontal lines indicate $\Upsilon_{V,\mathrm{n}}$ for a SSP that formed with the canonical IMF and is of the age that is assumed for the UCDs in the according panels. The dotted horizontal lines correspond to the mean of the $\Upsilon_{V,\mathrm{n}}$ of all UCDs in the sample and the shaded areas indicate the uncertainty given to this value. These numbers are used to estimate the high mass-slope of the UCDs (see Section 3.4.2).

Alternatively, the gas can be driven out of the UCDs, e.g. by type I SNe or by the ram pressure caused by the movement of the UCD through the intergalactic medium.

Gas and dust originating from intermediate-mass stars has a good chance to stay inside the UCDs, since these stars form in their final stage planetary nebulae that expand with moderate velocities ($\approx 20\,\mathrm{km\,s^{-1}}$; see e.g. Gesicki et al. 2003). These velocities are too low for the matter to leave a star cluster with a deep potential well immediately. This makes massive AGB stars attractive progenitors for a second generation of stars, as proposed in D'Antona & Caloi (2004) and D'Antona et al. (2007).

However, massive stars evolve into SN and thereby release $\approx 10^{50}$ erg per Solar unit of initial mass of the progenitor star (cf. fig. 1 in Nomoto et al. 2006). This clearly exceeds the binding energy of a star to a UCD. Material originating from these stars will therefore easily escape from the stellar system, unless the kinetic energy of the gas from the SN explosion is dissipated (e.g. by the interaction with primordial gas or the collision of expanding gas envelopes from different SNe with one another). The gas density and the holding time inside the UCDs might become long enough for the gas to cool and to collapse, as discussed in Tenorio-Tagle et al. (2007).

Note however that neither self-enrichment by massive AGB stars nor self-enrichment with SN ejecta can explain the multiple stellar populations in ω Cen, since both scenarios act on a time scale of $\lesssim 200$ Myr, whereas the age difference between the different stellar populations in ω Cen is a few Gyr (Hilker & Richtler 2000; Hilker et al. 2004; Villanova S. et al. 2007).

The essence of this is that the current knowledge on the evolution of the UCDs does not allow solid conclusions on the composition of the UCDs. We therefore consider six different compositions of the UCDs for which we estimate the high-mass IMF-slope:

1. Out of all material from burnt out stars, only WDs are retained by the UCDs. This can be taken as the lower limit for the amount of matter that stays inside the UCDs since the UCDs are nearly unaffected by dynamical evolution (cf. Section 3.3.1).

2. 20 per cent of the compact remnants from stars initially more massive than $8\ \mathrm{M}_\odot$ are retained by the UCDs. The remnant masses of stars with $m > 25\ \mathrm{M}_\odot$, $m_{\rm BH}$, are assumed to be 10 per cent of the initial mass of their progenitors, $m_{\rm BH} = 0.1m$. The NS and BH retention rate of 20 per cent is an arbitrarily chosen value, but this scenario might still be close to a realistic one. On the one hand it allows for some NSs in the UCDs as observed for GCs, but on the other hand it also takes into account that the observed velocity dispersion of pulsars is high by estimating the fraction of retained NSs to be low.

3. As scenario (ii), but with $m_{\rm BH} = 0.5m$.

4. All stellar remnants are retained by the UCDs and $m_{\rm BH} = 0.1m$. Such a population, where all stars and stellar remnants, but not the ejecta from stars are considered, is assumed in the SSP models.

5. As scenario (iv), but with $m_{\rm BH} = 0.5m$.

6. The UCDs were gas-free after star-formation ceased in them, but all material that was processed in burnt-out stars is retained by the UCDs and star formation with the gaseous component of this matter is somehow inhibited. Of all the models considered here, this is the one where stars contribute the least to the total mass of the UCD (consisting of stars, remnants and possibly gas). Note however that the hydrodynamic calculations by Tenorio-Tagle et al. (2007) suggest that such a scenario is unlikely because the gas accumulating in the UCDs due to stellar evolution will more likely either leave the UCDs or collapse into new stars.

Interstellar gas and all remnants in the UCDs are considered not to contribute to the light of the UCDs. In other words, the very high M/L_V ratios of these components of the UCDs are taken to be infinity.

3.4 Results

The value for the high-mass IMF slope, α_3, implied by a given normalised M/L_V ratio, $\Upsilon_{V,\mathrm{n}}$, for the assumptions on the stellar populations in the UCDs specified in Section 3.3 can be calculated from eq. (3.11) using the Newton-Raphson root-finding method.

There is a lower limit for the $\Upsilon_{V,\mathrm{n}}$ that leads to a solution for eq. (3.11), because the lowest $\Upsilon_{V,\mathrm{n}}$ that can be realised within the model is the one for a stellar population whose IMF is cut

off at $1\,\mathrm{M}_\odot$ (i.e. $\alpha_3 = \infty$). If the age of the UCDs is assumed to be 13 Gyr, the individual $\Upsilon_{V,\mathrm{n}}$ of a number of UCDs is actually below that limit.

Close to that lower limit, α_3 increases rapidly with decreasing $\Upsilon_{V,\mathrm{n}}$, implying a steep high-mass IMF (Fig. 3.2). In this range, the solutions to eq. (3.11) become degenerate for the different assumptions on how much mass is retained by the UCDs. That is because a steep high-mass IMF means few high-mass stars and it is therefore not decisive for the $\Upsilon_{V,\mathrm{n}}$ of an old stellar system how much matter from those stars is retained.

The α_3 of the canonical IMF is in the regime where the relation between $\Upsilon_{V,\mathrm{n}}$ and α_3 is already close to being degenerate for different assumptions on the NS and BH retention rate. Only assuming all matter processed in burnt-out stars remains inside the UCDs without forming new stars would lead to a distinctively higher $\Upsilon_{V,\mathrm{n}}$ for $\alpha_3 = 2.3$. In other words, the predictions of the models from Bruzual & Charlot (2003) and Maraston (2005) for the $\Upsilon_{V,\mathrm{n}}$ for a SSP with the canonical IMF (shown as the horizontal dashed line in Fig. 3.1 and as the vertical dashed line in Fig. 3.2) depend, except for extreme cases, only weakly on the fate assumed for the material processed in massive stars.

Table 3.2: Normalised M/L_V ratios, $\Upsilon_{V,\mathrm{n}}$, of the UCDs for assumed ages of 7 Gyr and 13 Gyr, and the high-mass slopes, α_3, these $\Upsilon_{V,\mathrm{n}}$ suggest if 20 per cent of the remnants of massive stars are retained by the UCDs, BHs have 10 per cent of the initial mass of their progenitor stars and the upper mass limit of the IMF is $m_{\max} = 100\,\mathrm{M}_\odot$. The contents of the columns are the following: Column 1: The object identification (as in Mieske et al. 2008, table 5), Column 2: The projected half-light radius of the UCD, Column 3: The estimate for the iron-abundance, Column 4: The mass of the UCD, Column 5: Its $\Upsilon_{V,\mathrm{n}}$ based on the models by Bruzual & Charlot (2003) and Maraston (2005) for a 7 Gyr old SSP with the canonical IMF, Column 6: The estimate for α_3 based on the value for $\Upsilon_{V,\mathrm{n}}$ in Column 5, Columns 7 and 8: As Columns 5 and 6 respectively, but for an assumed age of the UCD of 13 Gyr. The superscript numbers in Column 3 indicate the origin of the [Fe/H] estimate: 1: Mieske et al. (2008), 2: Haşegan et al. (2005), 3: Meylan et al. (2001), 4: Harris (1996). A superscript * indicates that [Fe/H] was not obtained from colour indices, but from line indices or the properties of the resolved stellar population of the stellar object (private communication with S. Mieske). $\Upsilon_{V,\mathrm{n}}$ is estimated using $[Z/\mathrm{H}]$, which is ≈ 0.3 dex higher than the corresponding [Fe/H] due to the assumed α-enhancement of the stellar systems (see Section 3.3.1). Dots in Columns 5 and 8 indicate where no solution for eq. (3.11) is found under the given assumptions. The canonical IMF would have $\alpha_2 = \alpha_3 = 2.3$ (Salpeter-Massey index, eq. 3.2).

Name	M	r_e	[Fe/H]	$\Upsilon_{V,\mathrm{n}}$ (7 Gyr)	α_3 (7 Gyr)	$\Upsilon_{V,\mathrm{n}}$ (13 Gyr)	α_3 (13 Gyr)
	$[10^6\,\mathrm{M}_\odot]$	[pc]		$[\mathrm{M}_\odot\,\mathrm{L}_{\odot,V}^{-1}]$		$[\mathrm{M}_\odot\,\mathrm{L}_{\odot,V}^{-1}]$	
F-7	10.5	14.9	-1.3^1	6.61 ± 0.97	$0.86^{+0.08}_{-0.06}$	7.07 ± 1.06	$1.15^{+0.15}_{-0.10}$
UCD1	32.1	22.4	-0.7^1	6.26 ± 0.95	$0.88^{+0.09}_{-0.07}$	6.48 ± 1.04	$1.23^{+0.20}_{-0.12}$
F-9	14.1	9.1	-0.8^1	6.19 ± 1.66	$0.89^{+0.18}_{-0.11}$	6.45 ± 1.76	$1.23^{+0.46}_{-0.19}$
UCD5	18.0	31.2	-1.2^1	5.13 ± 1.33	$0.99^{+0.22}_{-0.12}$	5.47 ± 1.43	$1.42^{+0.82}_{-0.25}$
F-19	93.6	89.7	-0.4^{1*}	5.03 ± 0.95	$1.00^{+0.15}_{-0.10}$	5.09 ± 1.01	$1.53^{+0.65}_{-0.24}$
F-34	5.5	4.9	-0.9^1	4.34 ± 1.07	$1.10^{+0.27}_{-0.14}$	4.55 ± 1.14	$1.77^{+\ldots}_{-0.40}$
UCD2	21.8	32.1	-0.9^{1*}	4.31 ± 0.76	$1.11^{+0.17}_{-0.11}$	4.52 ± 0.82	$1.79^{+1.22}_{-0.34}$
F-6	12.5	7.3	0.2^{1*}	3.81 ± 0.93	$1.21^{+0.35}_{-0.17}$	3.82 ± 1.05	$2.65^{+\ldots}_{-1.03}$
F-24	24.5	29.5	-0.4^{1*}	3.69 ± 1.25	$1.24^{+0.76}_{-0.22}$	3.73 ± 1.29	$2.91^{+\ldots}_{-1.35}$
F-53	3.9	4.4	-0.9^1	3.64 ± 0.99	$1.25^{+0.49}_{-0.19}$	3.65 ± 0.94	$3.22^{+\ldots}_{-1.47}$
F-5	13.7	5.0	-0.3^1	3.20 ± 0.68	$1.39^{+0.49}_{-0.20}$	3.25 ± 0.91	...

F-51	3.5	4.2	-0.8^{1}	3.12 ± 0.86	$1.43^{+0.98}_{-0.26}$	3.21 ± 0.71	...
F-17	6.3	3.3	-0.8^{1}	2.91 ± 0.76	$1.54^{+1.33}_{-0.30}$	3.03 ± 0.81	...
F-12	8.3	10.3	-0.4^{1*}	2.53 ± 0.94	$1.87^{+...}_{-0.57}$	2.56 ± 0.96	...
F-22	5.3	10.0	-0.4^{1*}	2.29 ± 0.49	$2.32^{+...}_{-0.69}$	2.35 ± 1.59	...
F-11	5.7	3.6	-0.9^{1}	2.24 ± 1.52	$2.47^{+...}_{-1.25}$	2.31 ± 0.52	...
F-1	16.2	23.1	0.0^{1*}	2.03 ± 0.56	$3.95^{+...}_{-2.15}$	1.99 ± 0.57	...
S999	23.4	19.1	-1.4^{2}	16.46 ± 3.18	$0.51^{+0.07}_{-0.06}$	17.68 ± 3.46	$0.67^{+0.09}_{-0.07}$
S417	29.5	14.4	-0.7^{2}	8.38 ± 1.92	$0.75^{+0.12}_{-0.08}$	8.93 ± 2.10	$0.99^{+0.19}_{-0.11}$
S928	19.3	21.8	-1.3^{2}	8.35 ± 1.94	$0.75^{+0.12}_{-0.08}$	8.67 ± 2.04	$1.01^{+0.20}_{-0.12}$
VUCD7	88.3	96.8	-0.7^{1*}	5.51 ± 1.47	$0.95^{+0.21}_{-0.12}$	5.70 ± 1.55	$1.37^{+0.73}_{-0.23}$
VUCD1	28.2	11.3	-0.8^{1*}	5.39 ± 1.02	$0.96^{+0.13}_{-0.09}$	5.62 ± 1.10	$1.38^{+0.41}_{-0.19}$
S314	9.1	3.2	-0.5^{2}	5.25 ± 0.96	$0.98^{+0.13}_{-0.09}$	5.36 ± 1.03	$1.45^{+0.48}_{-0.21}$
VUCD4	24.3	22.0	-1.0^{1*}	4.91 ± 1.32	$1.02^{+0.24}_{-0.13}$	5.17 ± 1.41	$1.50^{+1.31}_{-0.29}$
S490	14.5	3.6	0.2^{2}	4.42 ± 0.70	$1.09^{+0.14}_{-0.10}$	4.53 ± 1.46	$1.78^{+...}_{-0.48}$
VUCD5	29.1	17.9	-0.4^{1*}	4.32 ± 0.81	$1.10^{+0.18}_{-0.11}$	4.36 ± 0.87	$1.90^{+...}_{-0.42}$
VUCD6	17.7	14.8	-1.0^{1*}	4.30 ± 1.37	$1.11^{+0.42}_{-0.17}$	4.24 ± 0.75	$2.01^{+...}_{-0.44}$
H8005	4.8	28.1	-1.3^{2}	4.10 ± 2.21	$1.14^{+...}_{-0.27}$	4.38 ± 2.37	$1.89^{+...}_{-0.70}$
VUCD3	40.0	18.7	0.0^{2}	3.61 ± 0.74	$1.26^{+0.31}_{-0.16}$	3.53 ± 0.77	$3.98^{+...}_{-2.02}$
HCH99-2	4.2	11.4	-1.5^{1}	5.99 ± 2.33	$0.91^{+0.34}_{-0.15}$	6.46 ± 2.52	$1.23^{+1.16}_{-0.24}$
HGHH92-C21	4.8	7.0	-1.2^{1}	5.90 ± 2.16	$0.91^{+0.31}_{-0.15}$	6.28 ± 2.32	$1.26^{+1.10}_{-0.24}$
VHH81-C5	5.0	10.0	-1.6^{1}	5.74 ± 1.38	$0.93^{+0.17}_{-0.11}$	6.21 ± 1.50	$1.27^{+0.42}_{-0.18}$
HGHH92-C1	6.8	24.0	-1.2^{1}	5.59 ± 1.42	$0.94^{+0.19}_{-0.11}$	5.95 ± 1.52	$1.31^{+0.54}_{-0.21}$
HGHH92-C17	5.1	5.7	-1.3^{1}	5.32 ± 1.75	$0.97^{+0.30}_{-0.15}$	5.69 ± 1.89	$1.37^{+1.33}_{-0.27}$
HCH99-18	11.2	13.7	-1.0^{1}	5.23 ± 2.03	$0.98^{+0.41}_{-0.17}$	5.52 ± 2.15	$1.41^{+...}_{-0.32}$
HGHH92-C11	5.3	7.8	-0.5^{1}	5.05 ± 1.89	$1.00^{+0.41}_{-0.17}$	5.15 ± 1.96	$1.51^{+...}_{-0.36}$
HCH99-15	5.6	5.9	-1.0^{1}	4.42 ± 1.39	$1.09^{+0.38}_{-0.17}$	4.66 ± 1.48	$1.71^{+...}_{-0.43}$
HGHH92-C29	3.3	6.9	-0.7^{1}	4.40 ± 1.56	$1.09^{+0.49}_{-0.18}$	4.56 ± 1.63	$1.77^{+...}_{-0.49}$
HGHH92-C7	6.3	7.5	-1.3^{1}	4.21 ± 1.51	$1.12^{+0.57}_{-0.19}$	4.50 ± 1.62	$1.80^{+...}_{-0.52}$
HGHH92-C22	2.6	3.8	-1.2^{1}	4.20 ± 1.32	$1.13^{+0.43}_{-0.18}$	4.48 ± 1.42	$1.82^{+...}_{-0.49}$
HCH99-16	2.0	12.1	-1.9^{1}	3.87 ± 1.44	$1.19^{+0.82}_{-0.22}$	4.21 ± 1.57	$2.04^{+...}_{-0.69}$
HGHH92-C23	6.6	3.3	-1.5^{1}	2.78 ± 0.92	$1.63^{+...}_{-0.39}$	3.00 ± 0.99	...
HGHH92-C6	3.6	4.4	-0.9^{1}	2.19 ± 0.58	$2.67^{+...}_{-1.03}$	2.29 ± 0.61	...
VHH81-C3	2.4	4.4	-0.6^{1}	2.01 ± 0.63	$4.28^{+...}_{-2.53}$	2.06 ± 0.66	...
G1	7.2	3.0	-1.0^{3}	5.12 ± 0.93	$0.99^{+0.14}_{-0.09}$	5.40 ± 1.01	$1.44^{+0.44}_{-0.20}$
ω Cen	3.0	8.0	-1.6^{4}	4.06 ± 0.70	$1.15^{+0.18}_{-0.11}$	4.39 ± 0.76	$1.88^{+1.44}_{-0.37}$

Comparing solutions of eq. (3.11) for the same $\Upsilon_{V,\mathrm{n}}$ and remnant retention rate, but for upper mass limits of $100\ \mathrm{M}_{\odot}$ and $150\ \mathrm{M}_{\odot}$, reveals that the remnants of very massive stars do not play a decisive role for the α_3 that are obtained, as illustrated in Figs. 3.2 and 3.4. This finding may be surprising, since the total mass of the remnants of high-mass stars is a function of the exponent α_3 (see Appendix A.2). This mass must therefore increase dramatically with increasing α_3 above some critical value for α_3.

The results of solving eq. (3.11) if a remnant retention rate of 20 per cent and $m_{\mathrm{BH}} = 0.1m$ is assumed are noted in Table 3.2. However, for many individual UCDs solutions do not exist

if a high age is assumed for them (i.e. their $\Upsilon_{V,\mathrm{n}}$ is clearly below the prediction from the SSP models for a canonical IMF), and the uncertainties are large in any case. On the other hand, application of the Pearson test for the goodness of fit (cf. Bhattacharyya & Johnson 1977 and Dabringhausen et al. 2008) on the 46 UCDs from Mieske et al. (2008) shows that the actual distribution of the $\Upsilon_{V,\mathrm{n}}$ of the UCDs in the sample is highly unlikely if their individual $\Upsilon_{V,\mathrm{n}}$ scatters equally to both sides of the prediction for the $\Upsilon_{V,\mathrm{n}}$ of a SSP with the canonical IMF (less than 1 per cent if the age of the UCDs is assumed to be at its maximum, 13 Gyr, and much less than 0.5 per cent if the age of the UCDs is assumed to be 7 Gyr). The properties of the *sec342* of UCDs therefore imply an IMF that deviates from the canonical IMF (provided that they do not contain non-baryonic DM), such as a three-part power-law IMF with $\alpha_3 < 2.3$.

The emphasis in this paper is therefore on constraining likely values for the high-mass IMF slopes of the UCDs from the properties of the whole sample of UCDs and different subsamples thereof. It is decisive for this to know whether the $\Upsilon_{V,\mathrm{n}}$ of the UCDs are correlated with their mass, M, and to quantify this correlation if there is one (Section 3.4.1). If such a dependency is found, the dependency of α_3 on $\Upsilon_{V,\mathrm{n}}$ can be translated into a dependency of α_3 on M.

3.4.1 Does α_3 depend on mass?

At present, it is unclear whether UCDs are the most massive GCs (e.g. Mieske et al. 2002, 2004; Forbes et al. 2008) or whether UCDs and GCs are different populations (e.g. Drinkwater et al. 2004; Goerdt et al. 2008). However, the answer to this question has implications on how a dependency of $\Upsilon_{V,\mathrm{n}}$ on M, $\Upsilon_{V,\mathrm{n}}(M)$, has to be formulated for GCs and UCDs. An appropriate formulation of $\Upsilon_{V,\mathrm{n}}(M)$ as a representation for the typical $\Upsilon_{V,\mathrm{n}}$ of objects with a given mass would be a single, continuous function in the first case, but different functions for GCs and UCDs in the second case.

The MWGCs, which make up most of the GCs in the sample used here (tab. 5 in Mieske et al. 2008), show no evidence for a bulk-dependency of Υ_V with M (McLaughlin 2000). Therefore, the mean $\Upsilon_{V,\mathrm{n}}$ of the GCs in the data sample, $\overline{\Upsilon_{\mathrm{GC}}}$, is adopted for $\Upsilon_{V,\mathrm{n}}(M)$ in this mass range. Thus, for $M < 2 \times 10^6$ $\mathrm{M}_\odot$, $\Upsilon_{V,\mathrm{n}}(M) = 2.43 \pm 0.16$ $\mathrm{M}_\odot\,\mathrm{L}_{\odot,V}^{-1}$ if the assumed age is 7 Gyr and $\Upsilon_{V,\mathrm{n}}(M) = 2.61 \pm 0.18$ $\mathrm{M}_\odot\,\mathrm{L}_{\odot,V}^{-1}$ if the assumed age is 13 Gyr (uncertainties are one-sigma values).

The uncertainties of the data for the UCDs leaves many options for an appropriate formulation of $\Upsilon_{V,\mathrm{n}}(M)$ for them. We choose

$$\Upsilon_{V,\mathrm{n}}(M) = \left(A \left[\log_{10}\left(\frac{M}{\mathrm{M}_\odot} \right) - \log_{10}(2 \times 10^6) \right] + B \right) \frac{\mathrm{M}_\odot}{\mathrm{L}_\odot} \tag{3.13}$$

for $M > 2 \times 10^6$ $\mathrm{M}_\odot$, where M is in Solar units and A and B are parameters which are either fixed by a secondary condition or determined by a least-squares fit. Note that weighting the uncertainties when fitting is not advisable in this case, as it would cause an unwanted bias. This becomes evident by considering two stellar systems with the same mass and uncertainty of the mass, but different luminosities. The uncertainty of a luminosity measurement is negligible compared to the uncertainty of a mass estimate. The uncertainty of the M/L ratio is thus higher for the stellar system with the higher M/L ratio, even if the parameter that induces this uncertainty is the same for both systems. The parameters A and B are therefore determined with equal weight to every measurement and the uncertainties of A and B are estimated only from the scatter of the data.

In order to constrain $\Upsilon_{V\mathrm{n}}(M)$ for the UCDs in the case that UCDs and GCs are two distinct populations, A and B in eq. (3.13) are left as free parameters for the fit. The best-fitting parameters are $A = 1.84 \pm 0.89$ and $B = 3.71 \pm 0.70$ if the UCDs are assumed to be 7 Gyr old and $A = 1.87 \pm 0.81$ and $B = 3.47 \pm 0.64$ if the UCDs are assumed to be 13 Gyr old. This may hint at a systematic increase of the $\Upsilon_{V,\mathrm{n}}$ of the UCDs with M, but the significance of this result ($\approx 2\sigma$) is not high enough to allow definite conclusions[1]. This finding is consistent with Mieske et al. (2008), who performed a similar test but only for the UCDs in Fornax.

If UCDs are the most massive GCs, $\Upsilon_{V,\mathrm{n}}(M)$ is expected to be continuous at $M = 2 \times 10^6\,\mathrm{M}_\odot$, which in this paper is taken to be the mass that separates GCs and UCDs (see Section 3.2). For this case, $\Upsilon_{V,\mathrm{n}}(M)$ of the UCDs is therefore estimated by setting B in eq. (3.13) to the numerical value of $\overline{\Upsilon_{\mathrm{GC}}}$ in Solar units and leaving only A as a free parameter to be determined in the fit. The result is $A = 3.00 \pm 0.42$ if the UCDs are assumed to be 7 Gyr old and $A = 3.04 \pm 0.46$ if the UCDs are assumed to be 13 Gyr old. In this case, the increase of the $\Upsilon_{V,\mathrm{n}}$ of the UCDs with their mass is highly significant.

$\Upsilon_{V,\mathrm{n}}(M)$ is plotted in Fig. 3.3 together with the data for the GCs and the UCDs.

3.4.2 Constraining α_3 from the whole sample of UCDs

UCDs and GCs as independent populations

[1] We mention that weighting the UCDs by the uncertainties leads qualitatively to the same results, although the best-fitting values for A and B and their uncertainties are slightly lower.

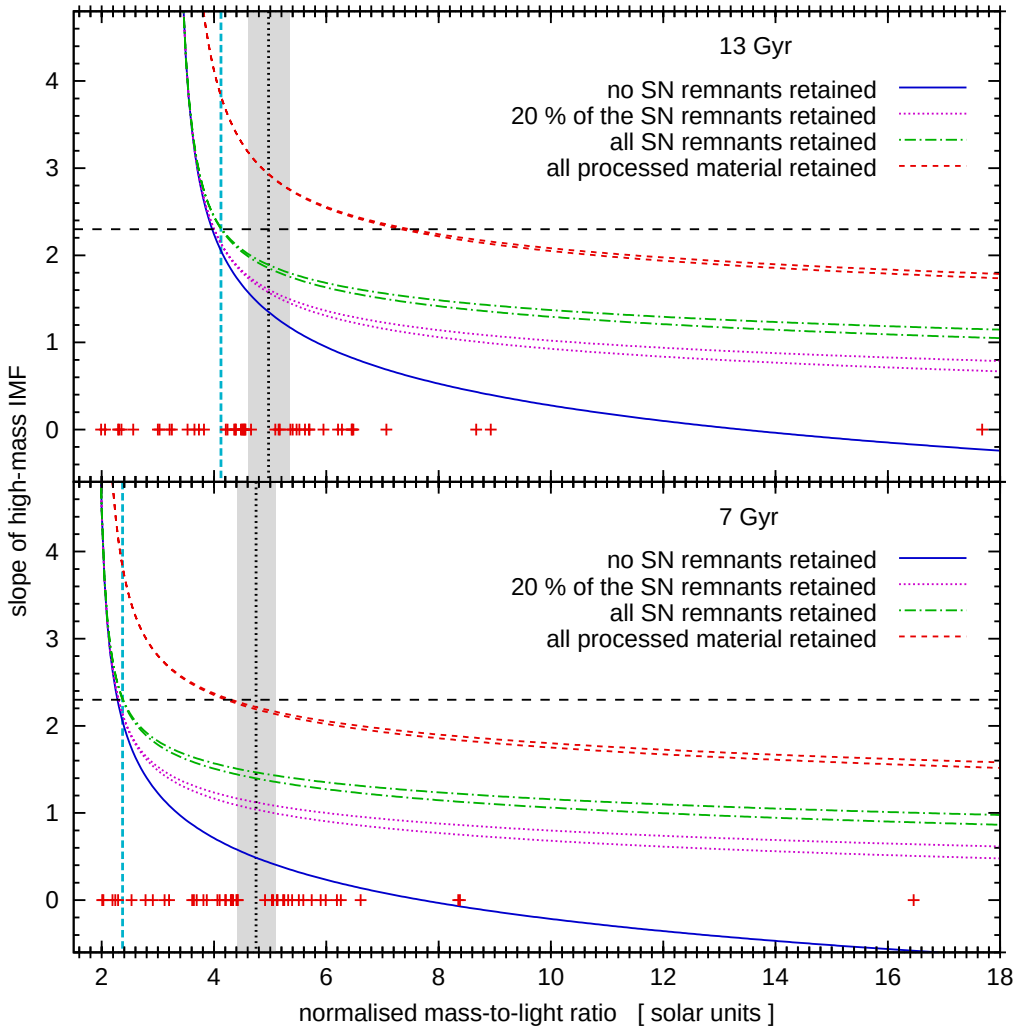

Figure 3.2: The high-mass slope, α_3, against the normalised mass-to-light ratio, $\Upsilon_{V,n}$, as implied by solving eq. (3.11) for a three-part power-law IMF (see eq. 3.5 and the equations in the appendix). The curves are for a 13 Gyr old SSP (upper panel) and for a 7 Gyr old SSP (lower panel). The different styles of the curves correspond to different assumptions on how much processed matter (with extremely high M/L_V ratio) besides WDs is retained by the UCDs (from the bottom to the top curves in each panel): no remnants of massive stars; 20 per cent of the remnants of massive stars; all remnants of massive stars; all material processed by burnt-out stars. Two curves of the same style indicate different assumptions for the upper mass limit of the IMF for the same assumption on the matter retained in the UCDs: $100\ \mathrm{M}_\odot$ (lower curve) and $150\ \mathrm{M}_\odot$ (upper curve). The dashed horizontal lines indicate in each panel the canonical high-mass IMF index, $\alpha_3 = 2.3$. Its intersections with the curves show the $\Upsilon_{V,\mathrm{n}}$ which the canonical IMF would imply for a particular remnant population. The $\Upsilon_{V,\mathrm{n}}$ of the individual UCDs are shown as crosses at the bottom of each panel. The dashed vertical lines indicate $\Upsilon_{V,\mathrm{n}}$ for a SSP that formed with the canonical IMF and is of the age that is assumed for the UCDs in the according panels. The dotted vertical lines correspond to the mean of the $\Upsilon_{V,\mathrm{n}}$ of all UCDs in the sample and the shaded areas indicate the uncertainty given to this value (see Section 3.4.2). The intersections of a vertical line with the curves show that α_3 corresponding to a particular $\Upsilon_{V,\mathrm{n}}$ for the different assumptions on the retained remnant population. In this Figure, the remnants of stars with $m > 25\ \mathrm{M}_\odot$ are assumed to have masses of 10 per cent of the initial mass of their progenitors whereever this is relevant.

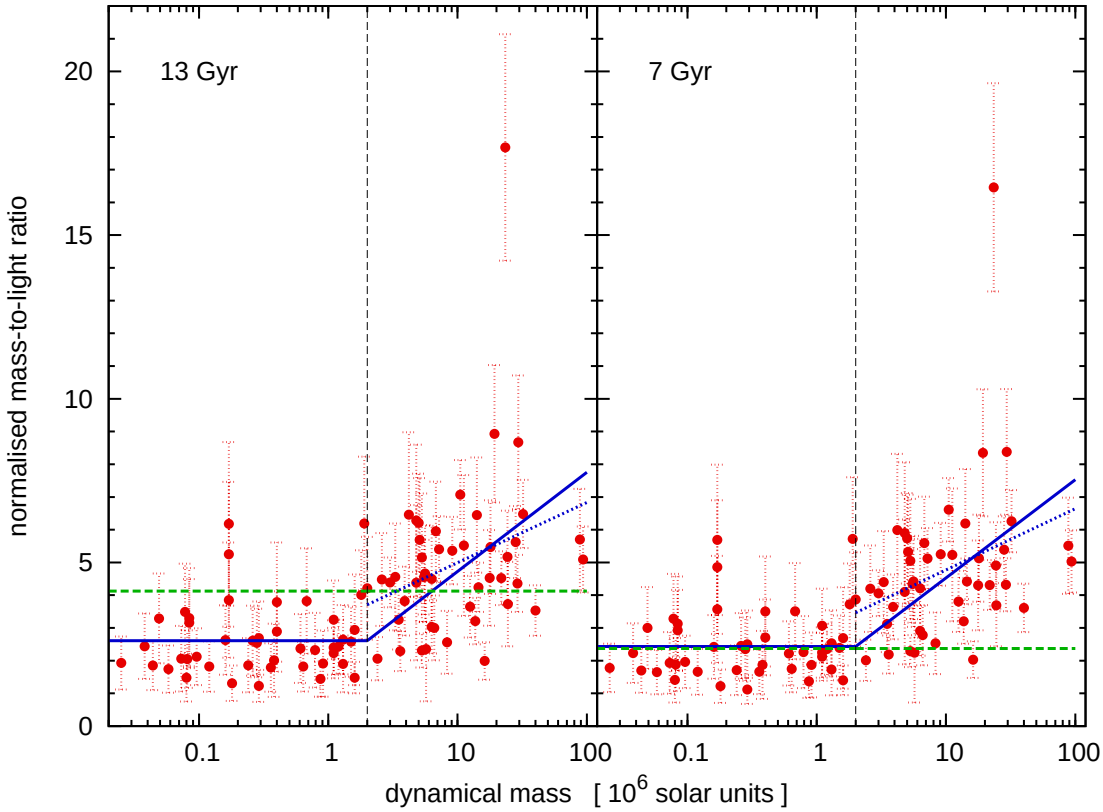

Figure 3.3: Normalised M/L_V ratios, $\Upsilon_{V,\mathrm{n}}$, of all objects listed in table 5 in Mieske et al. (2008). The assumed ages for them are either 13 Gyr (left panel) or 7 Gyr (right panel). Contrary to Fig. 3.1, this figure also shows stellar systems with dynamical masses less than 2×10^6 $\mathrm{M}_\odot$, i.e. stellar systems that are not UCDs but GCs according to the definition used in this paper. Objects considered as GCs are seperated from objects considered as UCDs by the thin, dashed vertical line in each panel. The solid line indicates $\Upsilon_{V,\mathrm{n}}(M)$, a function that describes the systematic increase of the average $\Upsilon_{V,\mathrm{n}}$ with mass for the case that GCs and UCDs are a single population. If GCs and UCDs are separate populations, $\Upsilon_{V,\mathrm{n}}(M)$ of the UCDs is represented by the dotted line that starts at 2×10^6 $\mathrm{M}_\odot$. Note that in this case the uncertainty to the slope is very high and is therefore not significant. The dashed horizontal line indicates the prediction for $\Upsilon_{V,\mathrm{n}}$ of an SSP with the canonical IMF.

Table 3.3: Estimates for the most likely values of α_3 for different assumptions concerning age and remnant population of the UCDs, as detailed in Section 3.4.2. The first column specifies the supposed remnant population of the UCDs ($m_{\rm max} = 100\ {\rm M}_\odot$). For the stars more massive than $25\,{\rm M}_\odot$, the cases of them forming BHs with 10 per cent their initial mass, $m_{\rm BH} = 0.1m$, or 50 per cent their initial mass, $m_{\rm BH} = 0.5m$, are considered whereever this makes a difference. The second column displays the α_3 corresponding to the mean of the $\Upsilon_{V,{\rm n}}$ of the UCDs and the uncertainties to α_3 calculated from the uncertainties to the mean $\Upsilon_{V,{\rm n}}$. This can be taken as a convenient number to quantify the high-mass IMF slope of the UCDs as a class of objects. The numbers in Columns 3 to 5 have the same meaning as the numbers in Column 2, but for different subsamples of UCDs. The subsamples are chosen by the larger structures the UCDs are bound to, namely the Fornax Cluster (Column 3), the Virgo Cluster with S999 (Column 4) and without S999 (Column 5) and Centaurus A (Column 6).

	All	Fornax	Virgo (with S999)	Virgo (without S999)	Centaurus A
Model	$\overline{\alpha_3}$	$\overline{\alpha_3}$	$\overline{\alpha_3}$	$\overline{\alpha_3}$	$\overline{\alpha_3}$
assumed age of 13 Gyr					
no SN remnants	$1.35^{+0.23}_{-0.17}$	$2.10^{+0.90}_{-0.42}$	$0.81^{+0.37}_{-0.23}$	$1.11^{+0.25}_{-0.18}$	$1.49^{+0.29}_{-0.21}$
20 per cent of the SN remnants, $m_{\rm BH} = 0.1m$	$1.57^{+0.17}_{-0.12}$	$2.17^{+0.84}_{-0.35}$	$1.22^{+0.23}_{-0.13}$	$1.41^{+0.17}_{-0.12}$	$1.68^{+0.23}_{-0.15}$
20 per cent of the SN remnants, $m_{\rm BH} = 0.5m$	$1.78^{+0.13}_{-0.09}$	$2.26^{+0.76}_{-0.29}$	$1.50^{+0.19}_{-0.11}$	$1.65^{+0.14}_{-0.09}$	$1.86^{+0.18}_{-0.12}$
all SN remnants, $m_{\rm BH} = 0.1m$	$1.85^{+0.14}_{-0.10}$	$2.33^{+0.73}_{-0.29}$	$1.56^{+0.20}_{-0.12}$	$1.72^{+0.14}_{-0.10}$	$1.94^{+0.18}_{-0.12}$
all SN remnants, $m_{\rm BH} = 0.5m$	$2.11^{+0.11}_{-0.08}$	$2.50^{+0.61}_{-0.23}$	$1.86^{+0.18}_{-0.10}$	$2.00^{+0.12}_{-0.08}$	$2.18^{+0.15}_{-0.10}$
all processed material	$2.93^{+0.26}_{-0.18}$	$3.90^{+1.55}_{-0.59}$	$2.43^{+0.32}_{-0.18}$	$2.69^{+0.25}_{-0.16}$	$3.08^{+0.36}_{-0.22}$
assumed age of 7 Gyr					
no SN remnants	$0.49^{+0.09}_{-0.08}$	$0.73^{+0.15}_{-0.12}$	$0.19^{+0.20}_{-0.15}$	$0.36^{+0.11}_{-0.10}$	$0.56^{+0.11}_{-0.09}$
20 per cent of the SN remnants, $m_{\rm BH} = 0.1m$	$1.04^{+0.05}_{-0.04}$	$1.17^{+0.09}_{-0.07}$	$0.88^{+0.10}_{-0.08}$	$0.97^{+0.07}_{-0.05}$	$1.09^{+0.06}_{-0.05}$
20 per cent of the SN remnants, $m_{\rm BH} = 0.5m$	$1.34^{+0.04}_{-0.04}$	$1.46^{+0.07}_{-0.06}$	$1.21^{+0.09}_{-0.07}$	$1.28^{+0.05}_{-0.04}$	$1.38^{+0.04}_{-0.04}$
all SN remnants, $m_{\rm BH} = 0.1m$	$1.40^{+0.05}_{-0.04}$	$1.52^{+0.08}_{-0.06}$	$1.25^{+0.10}_{-0.07}$	$1.33^{+0.06}_{-0.05}$	$1.43^{+0.05}_{-0.05}$
all SN remnants, $m_{\rm BH} = 0.5m$	$1.72^{+0.04}_{-0.04}$	$1.82^{+0.07}_{-0.05}$	$1.59^{+0.09}_{-0.06}$	$1.66^{+0.05}_{-0.04}$	$1.75^{+0.05}_{-0.04}$
all processed material	$2.19^{+0.07}_{-0.05}$	$2.36^{+0.12}_{-0.09}$	$2.00^{+0.13}_{-0.09}$	$2.10^{+0.08}_{-0.06}$	$2.25^{+0.08}_{-0.07}$

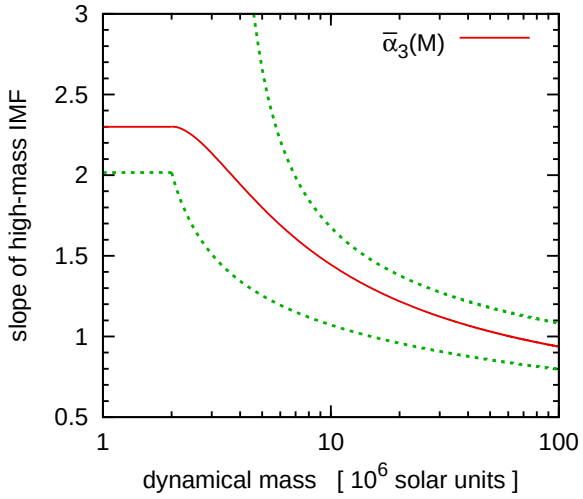

Figure 3.4: The high-mass slope, α_3, in dependency of mass M, as implied by solving eq. (3.11) for the values of $\Upsilon_{V,\mathrm{n}}(M)$ at the according M and for a three-part power-law IMF (see eq. 3.5 and the equations in the Appendix). The curves are for a 13 Gyr old SSP (upper panel) and for a 7 Gyr old SSP (lower panel). The different styles of the curves correspond to different assumptions on how much processed matter (with very high M/L_V ratio) besides WDs is retained by the UCDs (from the bottom to the top curves in each panel): no remnants of massive stars; 20 per cent of the remnants of massive stars; all remnants of massive stars; all material processed by burnt-out stars. Two lines of the same style indicate different assumptions for the upper mass limit of the IMF for the same assumption on the matter retained in the UCDs: $100\ \mathrm{M}_\odot$ (lower line) and $150\ \mathrm{M}_\odot$ (upper line). The dashed horizontal lines indicate in each panel the canonical high-mass IMF index, $\alpha_3 = 2.3$. In this Figure, the remnants of stars with $m > 25\,\mathrm{M}_\odot$ are assumed to have masses of 10 per cent of the initial mass of their progenitors whereever this is relevant.

It was shown in Section 3.4.1 that there is no hard evidence for a correlation of the $\Upsilon_{V,\mathrm{n}}$ of the UCDs with their mass if UCDs and GCs are separate populations. For this case, it is therefore a useful and good assumption that all UCDs have the same $\Upsilon_{V,\mathrm{n}}$ and that deviations from it are due to statistical scatter. Thus, we estimate the $\Upsilon_{V,\mathrm{n}}$ of the UCDs and the uncertainty of this value by performing a least-squares fit of eq. (3.13) with $A = 0$ to the $\Upsilon_{V,\mathrm{n}}$ of the UCDs. The best-fitting parameter B then equals to the numerical value of the mean of the $\Upsilon_{V,\mathrm{n}}$ of the individual UCDs, $\overline{\Upsilon_{\mathrm{UCD}}}$, and is $(4.75 \pm 0.34)\ \mathrm{M}_\odot\,\mathrm{L}_{\odot,V}^{-1}$ if the age of the UCDs is assumed to be 7 Gyr and $(4.97 \pm 0.37)\ \mathrm{M}_\odot\,\mathrm{L}_{\odot,V}^{-1}$ if the age of the UCDs is assumed to be 13 Gyr. $\overline{\Upsilon_{\mathrm{UCD}}}$ is shown as the horizontal dotted line in Fig. 3.1 and as the vertical dotted line in Fig. 3.2. The uncertainties of $\overline{\Upsilon_{\mathrm{UCD}}}$ are indicated as shaded areas in these figures.

A given value for $\overline{\Upsilon_{\mathrm{UCD}}}$ is taken to depend only on α_3. This implies that all UCDs have formed with the same (top-heavy) IMF, which can be considered as characteristic for very dense star-forming regions. Note however that even if this assumption is consistent with the available data, it is a simplification because the $\Upsilon_{V,\mathrm{n}}$ of the UCDs are *expected* to scatter due to age differences. Furthermore, the suggestion that the IMF is top-heavy in UCDs in comparison to less massive stellar systems is based on the notion that the process of star formation (and thus the IMF) depends on the physical conditions under which it takes place. This implies that there can be as many IMFs as physical conditions under which star formation takes place.

$\overline{\Upsilon_{\mathrm{UCD}}}$ can be translated into different expected values for α_3, depending on the assumed remnant population in the UCDs. The upper limit to the expected α_3 can be obtained from the lower bound of the uncertainty of $\overline{\Upsilon_{\mathrm{UCD}}}$, and the lower limit to the expected α_3 can be obtained

from the upper bound of the uncertainty of $\overline{\Upsilon_{\rm UCD}}$. The values for α_3 are listed in Tab. 3.3.

Mieske et al. (2006a) found that the UCDs in Fornax and the ones in Virgo are (despite their similarity) distinct in their properties, which could indicate a different origin or age for the two groups. Among these distinctive properties is the average $\Upsilon_{V,\rm n}$ of the UCDs, which is clearly higher for the ones in the Virgo Cluster. It is therefore worthwhile to relax the assumption of a common $\Upsilon_{V,\rm n}$ for all UCDs and assume a common $\Upsilon_{V,\rm n}$ only for the UCDs that are bound to the same larger structure (i.e. the Fornax Cluster, the Virgo Cluster or Centaurus A), although the smaller size of the subsamples decreases their statistical significance. Estimates for α_3 for the UCDs in the different subsamples can then be obtained in the same way as for the whole sample. The results are given in Tab. 3.3.

Note that the values obtained for α_3 for the UCDs in Fornax have large uncertainties if they are assumed to be 13 Gyr old. This is because in that case $\overline{\Upsilon_{\rm UCD}}$ for them is quite close to the $\Upsilon_{V,\rm n}$ where α_3 asympotically approaches infinity. Consequently α_3 is obtained from an interval in $\Upsilon_{V,\rm n}$ where small variations of $\Upsilon_{V,\rm n}$ imply large changes in α_3. This applies in particular to the upper limit to α_3. Thus, the numbers in question are only of use for giving lower bounds for the high-mass IMF slope, which are obtained at a $\Upsilon_{V,\rm n}$ where the dependency of α_3 on $\Upsilon_{V,\rm n}$ is more moderate.

Also note the strong impact of S999 with its extreme $\Upsilon_{V,\rm n}$ (upper-most data-point in Figs. 3.1 and 3.3)on the α_3 derived for the UCDs in the Virgo Cluster. The relevance of this particular cluster is evidently much smaller if the whole sample of UCDs is considered. The main results presented in this paper are therefore either not or only mildly affected by this stellar system. In particular, S999 plays no role for deciding whether there is a significant correlation between the $\Upsilon_{V,\rm n}$ of the UCDs and their mass. Such an outlier may be due to recently induced tidal effects (Fellhauer & Kroupa 2006).

GCs and UCDs as a single population

Contrary to the case that UCDs and GCs constitute different populations, the slope A is highly significant if UCDs and GCs are a single population. A relation between α_3 and mass, $\alpha_3(M)$, can be established by solving eq. (3.11) for the different $\Upsilon_{V,\rm n}(M)$ corresponding to different masses. The results for this are plotted in Fig. 3.4. The fact that in the mass range of GCs, $\Upsilon_{V,\rm n}(M)$ almost coincides with the model predictions for a SSP with the canonical IMF for an assumed age of 7 Gyr is purely coincidental. Independent estimates on the ages of MWGCs (which are the bulk of the GCs in the sample used here) are closer to 13 Gyr than to 7 Gyr for most of them (VandenBerg 2000; Salaris & Weiss 2002). However, if an age of 13 Gyr is assumed for the GCs and UCDs, $\alpha_3(M)$ is not defined for $M \lesssim 3 \times 10^6$ $\rm M_\odot$ because in this mass range $\Upsilon_{V,\rm n}(M)$ is below the minimum value for which eq. (3.11) is solvable.

This finding implies that the present-day stellar mass function of the corresponding stellar systems has to be poorer in very low-mass stars than the canonical IMF, since their $\Upsilon_{V,\rm n}$ cannot be realised in any case if the mass function of their main sequence stars equals the canonical IMF. There are different processes which tend to drive very low-mass stars out of a star-cluster. One of them is dynamical evolution (cf. Kruijssen 2008 and Kruijssen & Lamers 2008). It acts faster the less massive a star cluster is. However, the expected effect on the M/L_V ratio is only small according to Baumgardt & Makino (2003), their figure 14 and Borch et al. (2007). More relevant would be gas expulsion if the GCs were initially mass-segregated (Marks et al. 2008). In other words, if GCs have formed with the canonical IMF, their stellar mass functions must have changed with time (see also Dabringhausen et al. 2008 and Mieske et al. 2008). The

dependency of the stellar mass function on the cluster concentration (De Marchi et al. 2007) indeed suggests this to be the case. Consequently, the assumption of a stellar population only altered by stellar evolution would only be valid for stellar systems with $M \gtrsim 3 \times 10^6\,\mathrm{M}_\odot$.

For a parametrisation of α_3 as a function of the mass of a stellar system we suggest

$$\overline{\alpha_3}(M) = \left[\log_{10}\left(\frac{0.85(10^{-6}\,M/\mathrm{M}_\odot)^2}{(10^{-6}\,M/\mathrm{M}_\odot)-1}\right)\right]^{-1} + 0.42, \tag{3.14}$$

for $M \geq 2 \times 10^6\,\mathrm{M}_\odot$, and $\overline{\alpha_3}(M) = 2.3$ for $M < 2 \times 10^6\,\mathrm{M}_\odot$, where M is measured in $\mathrm{M}_\odot$. $\overline{\alpha_3}(M)$ thus returns the canonical IMF for GCs, which is motivated with the invariance of the IMF in resolved stellar populations (Kroupa 2001, 2008; Marks et al. 2008). In the range of massive UCDs, which are the least vulnerable to dynamical evolution, $\overline{\alpha_3}(M)$ is chosen to be roughly the mean of $\alpha_3(M)$ for assumed ages of 7 Gyr and 13 Gyr at a NS and BH retention rate of 20 per cent. Note that the change of $\alpha_3(M)$ in this mass range is only moderate for the two extreme assumptions on the age of the UCDs. In the intermediate mass range from $2 \times 10^6\,\mathrm{M}_\odot$ to $\approx 10^7\,\mathrm{M}_\odot$, $\overline{\alpha_3}(M)$ is an (in principle arbitrary) interpolation from the low-mass regime to the very high-mass regime. $\overline{\alpha_3}(M)$ is plotted in Fig. 3.5.

3.5 Discussion

3.5.1 Stability of the UCDs

Baumgardt et al. (2008) show that for a star cluster with the canonical IMF the combined energy input from all SNe exceeds the binding energy of star clusters with initial masses up to $\approx 10^7\,\mathrm{M}_\odot$ (cf. their fig. 3)[2]. This implies that star clusters loose not only most of the matter bound in massive stars, but also their primordial gas in less than $40\,\mathrm{Myr}$ ($\approx 40\,\mathrm{Myr}$ is the time it takes until all massive stars in a SSP have evolved, cf. the grids by Schaller et al. 1992). Although many UCDs certainly had initial masses higher than $10^7\,\mathrm{M}_\odot$, they also had many more massive stars that evolved into SNe if they formed with IMFs as top-heavy as suggested in this paper. In this case, they would loose an even larger fraction of their initial mass during their early evolution than less massive stellar systems, because of the large mass-faction bound in massive stars. For instance, 23.0 per cent of the total initial stellar mass of a star cluster is in stars more massive than $8\,\mathrm{M}_\odot$ if $\alpha_3 = 2.3$. This value rises to 73.0 per cent for $\alpha_3 = 1.57$ (which is the high-mass IMF slope suggested in Tab. 3.3 for 13 Gyr old UCDs that retain 20 per cent of their NSs and BHs with $m_{\mathrm{BH}} = 0.1m$) and to 93.3 per cent for $\alpha_3 = 1.04$ (which is the corresponding value for 7 Gyr old UCDs).

Observations of star-forming regions in the Milky Way show that only a fraction of available gas is actually converted into stars (e.g. Lada & Lada 2003). Assuming that this left-over gas is swept out of young star clusters by the radiation and evolution of massive stars, the total mass-loss of the stellar system until the end of massive-star evolution can be written as

$$M_{\mathrm{init}} - M_{\mathrm{final}} = M_{\mathrm{init}}[1 - \mathrm{SFE}(1-x)], \tag{3.15}$$

where M_{init} and M_{final} are the initial mass of the stellar system and the final mass of the stellar system respectively (stars and gas), SFE is star formation efficiency of the stellar system and x

[2]Star clusters less massive than $10^7\,\mathrm{M}_\odot$ can survive this energy input because the energy from the SNe is not distributed uniformly on all matter in the cluster.

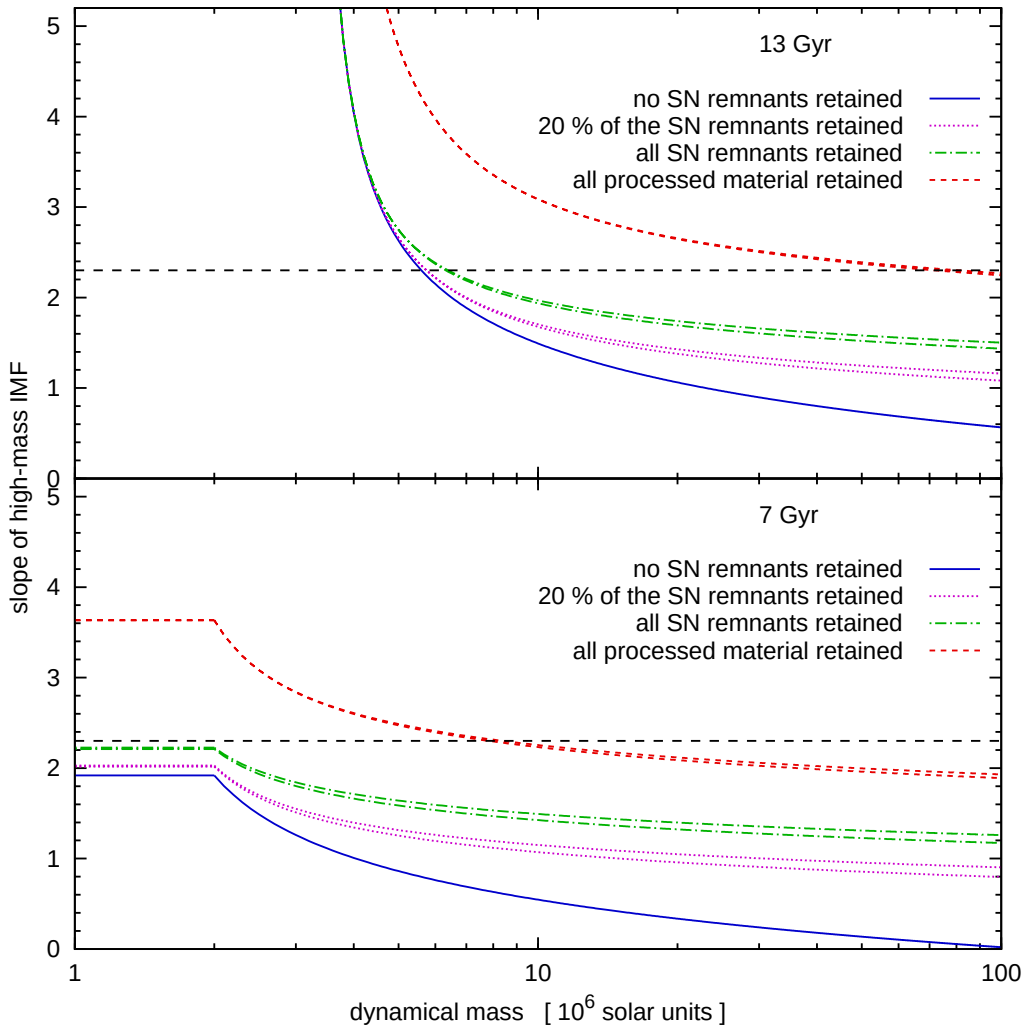

Figure 3.5: The parametrisation of the high mass IMF slope, α_3, as a function of the mass of a stellar system, M, as given by eq. (3.14). It is indicated by the solid line. Also shown are $\alpha_3(M)$ as found from eq. (3.11) using eq. (3.13) assuming a NS and BH retention rate of 20 per cent and BHs having 10 per cent of the initial mass of their progenitor stars. The upper dashed line corresponds to an estimated age of 13 Gyr and the lower dashed line to an estimated age of 7 Gyr for the UCDs.

the mass-fraction of stars with $m > 8\,\mathrm{M}_\odot$. It is thereby assumed in eq. (3.15) that the total mass of the remnants remaining in the stellar system is negligible compared to the total initial mass of all stars with $m > 8\,\mathrm{M}_\odot$. This approximation is well fulfilled for all cases where the mass of the remnants of massive stars is rather small or only a few of them remain inside the stellar system. (These cases correspond to our models 1, 2, 3 and 4 for the composition of the UCDs; see Section 3.3.1. That is why the IMFs estimated for the UCDs turn out to be so flat if one of these models is assumed for their composition, even if the difference between the predicted M/L ratio and the observed M/L ratio is not very large.) Assuming that the star formation efficiency in a UCD is 0.4, the mass-loss within the first $40\,\mathrm{Myr}$ is, according to eq. 3.15, 69.2 per cent of the total initial mass (stellar and gas) if the high-mass IMF slope of the UCD was $\alpha_3 = 2.3$ (canonical IMF), but 89.2 per cent for $\alpha_3 = 1.57$ and 97.3 per cent for $\alpha_3 = 1.04$. (Note that a SFE of 0.4 would be a high value for an open cluster, but not necessarily for a UCD, cf. Murray 2009. Note also that we ignore the probably significant loss of stars from the

UCD due to the unbinding effect from gas expulsion. We return to this in a follow-up paper.)

The behaviour of a stellar system that loses a large fraction of its initial mass very much depends on the rate of the mass-loss. This behaviour can be characterised by two limiting cases:

- Rapid mass-loss (i.e. the mass-loss takes place on a timescale shorter or comparable to the crossing time): Arguing with the virial theorem, Hills (1980) finds from analytic estimates that a star cluster dissolves if it loses more than 50 per cent of its initial mass instantaneously. Using N-body integrations, Boily & Kroupa (2003) and Fellhauer & Kroupa (2005b) show that the survival of a star cluster is also dependent on the density profile of the star cluster and the velocity distribution of its stars, but a sudden loss of more than 67 per cent of its initial mass is critical in any case.

- Adiabatic mass-loss (i.e. the mass-loss is slow enough for the stellar system to stay near virial equilibrium at all times): Adiabatic mass-loss does not unbind the remainder of the star cluster, but inflates it. The change in radius is

$$\frac{r_{\rm final}}{r_{\rm init}} = \frac{M_{\rm init}}{M_{\rm final}}, \tag{3.16}$$

  where $r_{\rm init}$ and $M_{\rm init}$ are the radius and mass, respectively, of the stellar system at the beginning of mass-loss and $r_{\rm final}$ and $M_{\rm final}$ the according parameters at the end of mass-loss (Kroupa 2008).

Important numbers for deciding whether the mass-loss from UCDs is rapid or adiabatic are their crossing times, $t_{\rm cr}$, which is defined as $t_{\rm cr} = 2r_h/\sigma$, with r_h being the 3D half-mass radius and σ being the 3D velocity dispersion of the stellar system (Kroupa 2008). Furthermore the ratios between half-mass radius and tidal radius, $r_{\rm h}/r_{\rm t}$, decide upon survival of the stellar system. The data published in Evstigneeva et al. (2007) and Hilker et al. (2007) for the properties of UCDs as they are observed today imply $r_{\rm h}/r_{\rm t}$ well below 0.1 for most of them (sometimes as low as 0.01) and $t_{\rm cr}$ of the order of 1 Myr. This suggests a timespan of the order of $40\ t_{\rm cr}$ for the timescale for SN-driven mass-loss.

In the grid of N-body simulations performed by Baumgardt & Kroupa (2007), star-clusters are predicted to dissolve if they loose 95 per cent of their initial mass, even for the most moderate tidal fields ($r_{\rm h}/r_{\rm t} = 0.01$) and longest duration for mass-loss (10 $t_{\rm cr}$) they consider. However, if the stellar system looses only 90 per cent of its initial mass on that timescale, the stellar system may not completely dissolve as long as the tidal field is weak. The mass fraction of the remnant of the star cluster that continues to be gravitationally bound after it has returned to virial equilibrium is then 0.65 for $r_{\rm h}/r_{\rm t} = 0.01$ and 0.35 for $r_{\rm h}/r_{\rm t} = 0.033$, while the half-mass radius increases to approximately ten times its initial value in both cases. This implies that the stellar density in those systems decreases to less than 10^{-3} times its initial value. If also the gas leaving intermediate mass stars as they evolve into WDs is driven out of the UCDs (e.g. through type I SNe), the mass of the UCDs is decreased further to 0.57 of its original value for $\alpha_3 = 1.57$ and to 0.40 of its original value for $\alpha_3 = 1.04$. Since this mass-loss would be adiabatic, the according change in radius can be calculated using eq. (3.16) and is a factor of 1.75 for $\alpha_3 = 1.57$ and a factor of 2.48 for $\alpha_3 = 1.04$. The density would thus be further decreased by a factor $\lesssim 10$. At present, the UCDs typically have mean central densities from 10^2 to $10^3\,{\rm M}_\odot\,{\rm pc}^{-3}$ (fig. 4 in Dabringhausen2008). A mass-loss of 90 per cent of the initial

mass (stellar and gas) over the first $\approx 40\ t_{\rm cr}$ and subsequent adiabatic mass-loss through the evolution of intermediate-mass stars would therefore suggest initial central densities of at least 10^6 to $10^7\ {\rm M}_\odot\,{\rm pc}^{-3}$. This corresponds to 3.9×10^5 to 3.9×10^6 stars per ${\rm pc}^3$ for $\alpha_3 = 1.57$ and 8.4×10^4 to 8.4×10^5 stars per ${\rm pc}^3$ for $\alpha_3 = 1.04$, the fraction of stars more massive than $8\ {\rm M}_\odot$ among them being 5.5 per cent for $\alpha_3 = 1.57$ and 23.7 per cent for $\alpha_3 = 1.04$. Such systems would thus have had extensions similar to GCs (i.e. $r_{\rm h}$ of a few pc). Typical total initial stellar masses would be some $10^7\ {\rm M}_\odot$, implying a population of $\approx 10^6$ stars with $m \geq 8\ {\rm M}_\odot$ for $\alpha_3 = 1.57$ as well as for $\alpha_3 = 1.04$.

These numbers underline the extreme nature of UCDs. Their stability seems questionable if they would have formed with a top-heavy IMF and their contemporary structural parameters. However, the smaller extensions and higher masses the UCDs must have had before evolutionary processes set in imply that the conditions for adiabatic mass-loss were fulfilled much better at that time. However, also if mass-loss from a UCD with a top-heavy IMF was adiabatic at all times, and its stability was therefore not threatened, eq. 3.15 still implies an enormous inflation and decrease of density for it.

The observation of UCDs today therefore does not contradict a formation scenario with a very top-heavy IMF for them. A more detailed, numerical study of this issue will be provided in a follow-up paper.

3.5.2 The Star formation rate in UCDs at their formation

The notion that UCDs might be the most massive star clusters implies that they formed from a collapsing molecular cloud. Star formation within the cloud is thought to set in as soon as a certain density is reached, which is according to Kawamura et al. (1998) at a column density in excess of $1.6\times10^{21}\,N(H_2)\,{\rm cm}^{-2}$. Defining the size, R, of a cloud as $(S/\pi)^{0.5}$ where S is the total cloud surface area, gives typical sizes of $3\,{\rm pc}$ for the clouds in the sample of Kawamura et al. (1998). This corresponds to a mean density, $\overline{\rho}$, of $\approx 4\,{\rm M}_\odot\,{\rm pc}^{-3}$ as the criterion for the onset of star formation. It then proceeds rapidly and is completed within a timescale of the order of a free fall time (Elmegreen 2000; Hartmann et al. 2001). For spherically symmetric matter distributions, the free fall time, $t_{\rm ff}$, is given as $t_{\rm ff} = (3\pi/32G\overline{\rho})^{0.5}$, where G is the gravitational constant. Note the independence of $t_{\rm ff}$ on the total mass. The assumption of spherical symmetry for star-forming gas clouds thus leads to a time scale of 4 Myr on which star formation takes place, whereby the bulk of the stars may form on an even shorter time scale (for instance, 80 per cent within 1 Myr in the Orion Nebula Cluster, Prosser et al. 1994). If applied to the UCDs, this suggests that their stellar populations formed with star formation rates of $\approx 10\ {\rm M}_\odot\,{\rm yr}^{-1}$ to $\approx 100\ {\rm M}_\odot\,{\rm yr}^{-1}$, depending on the mass of the UCD. Given that most if not all stars are formed in star clusters (Lada & Lada 2003) and that the time scale for star cluster formation appears to be independent of the mass of the cluster, these star formation rates would be the highest ever to be found in a single star formation event.

3.6 Summary and Conclusions

It was shown in previous papers that the dynamical M/L_V ratios, Υ_V, of compact stellar systems more massive than $2\times10^6\ {\rm M}_\odot$ are not consistent with the predictions from simple stellar population models, if the canonical IMF is assumed for star formation in them. Out of the possible explanations for this result (top-heavy IMF, bottom-heavy IMF, dark matter, inaccu-

racy of the SSP models), the notion of a top-heavy initial stellar mass function (IMF) in dense star-forming regions seems especially attractive.

With this motivation, we quantify by how much the IMF in a sample of massive compact stellar systems (referred to as UCDs) has to deviate from the canonical IMF in the intermediate and high mass part for the modelled Υ_V to agree with the observed ones. The model constructed for this accounts for the different metallicities of the UCDs. Several combinations of assumptions concerning age (7 Gyr or 13 Gyr) and the amount of processed material with very high Υ_V retained by the UCDs besides white dwarfs (no remnants of massive stars; 20 per cent of the remnants of massive stars; all remnants of massive stars; all material processed by burnt-out stars) are considered. The IMF of the UCDs is taken to be a three-part power-law that equals the canonical IMF below an initial stellar mass of $1\,\mathrm{M}_\odot$. The exact upper mass limit of the IMF ($m_{\mathrm{max}} = 100\,\mathrm{M}_\odot$ or $m_{\mathrm{max}} = 150\,\mathrm{M}_\odot$) turns out to have a negligible impact on the results.

Assuming that all UCDs have the same normalised M/L ratio (which is justifiable considering the uncertainties of their Υ_V) and that the processed material retained by the UCDs are all white dwarfs and 20 per cent of the remnants of massive stars, our model suggests a high-mass IMF slope, α_3, of ≈ 1.6 if the UCDs are 13 Gyr old (i.e. almost as old as the Universe) or ≈ 1.0 if the UCDs are 7 Gyr old. If the UCDs were assumed to have formed with the canonical IMF, their Υ_V would only be explainable if they contain significant amounts of non-baryonic dark matter or dense interstellar gas. Note that there would need to be some mechanism that inhibits on-going star formation in this case.

The Υ_V of the UCDs in the Fornax cluster tend to be lower than the ones of the other UCDs. If the Fornax UCDs are assumed to be 13 Gyr old they have a normal Υ_V and consequently not at a top-heavy IMF. Assuming that the discrepancy between the prediction of SSP models with the canonical IMF and the observed M/L_V ratios of the Fornax UCDs as high as for the Virgo UCDs suggests an ages around 7 Gyr for the Fornax UCDs if the Virgo UCDs are taken to be 13 Gyr old (Mieske et al. 2008).

The dependency of α_3 on the normalised M/L_V ratio, $\Upsilon_{V,\mathrm{n}}$, established in eq. (3.11), can be translated into a dependency of α_3 on the mass of the stellar system, M. This is done using the increase of $\Upsilon_{V,\mathrm{n}}$ with M formulated in eq. 3.13 and shown in Fig. 3.3. A possible parametrisation of this dependency is given in eq. (3.14) and plotted in Fig. 3.5.

The mass-loss due to the evolution of massive stars may reach 90 per cent of the initial stellar mass of a star cluster for very top-heavy IMFs, even if primordial gas expulsion is not considered. The survival of the UCDs seems not to be threatened by the mass loss implied by the evolution of the stars alone, as this mass loss would be adiabatic. However, the radiation and evolution of massive stars also drives the expulsion of the primordial gas. The timescale on which this process takes place is critical for the survival of the UCD. This is an issue deserving further study. In any case, the results in Sections 3.5.1 and 3.5.2 suggest that UCDs formed with likely central stellar densities of 10^6 to $10^7\,\mathrm{M}_\odot\,\mathrm{pc}^{-3}$ and possible star formation rates of $\approx 10\,\mathrm{M}_\odot\,\mathrm{yr}^{-1}$ to $\approx 100\,\mathrm{M}_\odot\,\mathrm{yr}^{-1}$. These are among the most extreme sites of star formation.

Acknowledgements

JD acknowledges support through DFG grant KR1635/13.

Chapter 4

Mass loss and expansion of ultra compact dwarf galaxies through gas expulsion and stellar evolution for top-heavy stellar initial mass functions

J. Dabringhausen, M. Fellhauer, P. Kroupa, 2010, **MNRAS**, 403, 1054

Abstract:

The dynamical V-band mass-to-light ratios of ultra compact dwarf galaxies (UCDs) are higher than predicted by simple stellar population models with the canonical stellar initial mass function (IMF). One way to explain this finding is a top-heavy IMF, so that the unseen mass is provided by additional remnants of high-mass stars. A possible explanation for why the IMF in UCDs could be top-heavy while this is not the case in less massive stellar systems is that encounters between proto-stars and stars become probable in forming massive systems. However, the required number of additional stellar remnants proves to be rather high, which raises the question of how their progenitors would affect the early evolution of a UCD. We have therefore calculated the first 200 Myr of the evolution of the UCDs, using the particle-mesh code Superbox. It is assumed that the stellar populations of UCDs were created in an initial starburst, which implies heavy mass loss during the following ≈ 40 Myr due to primordial gas expulsion and supernova explosions. This mass loss is modelled by reducing the mass of the particles according to tabulated mass loss histories which account for different IMFs, star formation efficiencies (SFEs), heating efficiencies (HEs), initial masses and initial extensions of the computed UCDs. For each combination of SFE and HE we find objects that roughly resemble UCDs at the end of the simulation. For low SFEs, the IMF would have to be steeper than in the case of very high SFEs for the models not to expand too much. However, the main conclusion is that the existence of UCDs does not contradict the notion that their stellar populations formed rapidly and with a top-heavy IMF. We find tentative evidence that the UCDs may have had densities as high as $10^8 \mathrm{M}_\odot\ \mathrm{pc}^{-3}$ at birth. This will have to be confirmed by follow-up modelling.

4.1 Introduction

Ultra compact dwarf galaxies (UCDs) are stellar systems with total stellar masses between 10^6 and $10^8 \mathrm{M}_\odot$ and projected half-light radii of $\lesssim 50$ pc (Hilker et al. 1999; Drinkwater et al. 2000, 2003; Phillipps et al. 2001; Haşegan et al. 2005). They can be considered to be galaxies because of their high median two-body relaxation times, $t_{\rm rh}$, which are at least of the order of a Hubble time, $\tau_{\rm H}$, while star clusters, including globular clusters (GCs), have $t_{\rm rh} < \tau_{\rm H}$ (Kroupa 1998; Dabringhausen et al. 2008).

One of the most intriguing properties of UCDs are their generally high dynamical M/L_V ratios (Dabringhausen et al. 2008; Mieske et al. 2008). Different explanations have been suggested for this finding, such as the presence of non-baryonic cold dark matter (CDM) in them (e.g. Haşegan et al. 2005 and Goerdt et al. 2008) or the disturbance of UCDs by the tidal field of a massive galaxy (Fellhauer & Kroupa 2006). However, if dwarf spheroidal galaxies (dSphs) are indeed DM dominated[1] and if UCDs are located at the centre of the same type of haloes as dSphs, the DM-density in UCDs would be two orders of magnitude too low to explain their elevated M/L_V ratios, although adiabatic contraction (Blumenthal et al. 1986) may alleviate this problem (Murray 2009). Tidal distortion can explain the high M/L_V ratios of only a few UCDs out of a larger sample, as it requires quite specific orbital parameters in order to have an observable effect. On the other hand, the massive star cluster W3 in the merger remnant galaxy NGC 7252 has a mass and a projected half-light radius typical for a UCD, while its age suggests that it formed during the merger of the progenitors of NGC 7252 (Maraston et al. 2004). Fellhauer & Kroupa (2005a) have shown that star cluster complexes as observed in interacting systems like the Antennae (NGC 4038 and NGC 4039) are likely to evolve into an object similar to W3 on the required time-scale, but stellar systems originating from tidal interactions would essentially be CDM-free (Barnes & Hernquist 1992b). In summary, an unusual stellar initial mass function (IMF) appears to be an attractive and physically plausible alternative for explaining the M/L ratios of UCDs.

The IMF is a function defining the mass spectrum of stars born in a single star-formation event. If age, metallicity and IMF of a stellar population are known, its M/L_V ratio can be calculated. For a given metallicity and a high enough age, a high M/L_V ratio of a stellar population would either indicate an IMF with very many low-mass stars (bottom-heavy IMF) or an IMF with very many high-mass stars (top-heavy IMF). In the case of a top-heavy IMF, the high M/L_V of the stellar population is the consequence of a high number of stellar remnants, which contribute mass, but almost no V-band luminosity. As an explanation for the M/L_V ratios in UCDs, a bottom-heavy IMF has been discussed in Mieske & Kroupa (2008), while a top-heavy IMF has been discussed in Murray (2009) and Dabringhausen et al. (2009).

Proposing a variability of the IMF might seem daring at first sight, because so far surveys of stars have failed in providing supportive evidence for this notion (Kroupa 2001, 2002; Kumar et al. 2008). This finding implies an invariant, universal IMF, which is referred to as the

[1] There is an ongoing debate on the origin of the dSphs around the Milky Way. Their disk-like distribution has a natural explanation if the dSphs are ancient tidal dwarf galaxies instead of DM-dominated primordial galaxies (Metz et al. 2009 and references therein). The high M/L ratios derived for them would in this scenario either be the consequence of the assumption of virial equilibrium not holding for them (Kroupa 1997) or would imply that Newtonian gravity cannot be applied in the limit of very weak fields. A tidal origin of dSphs may suggest the same for dwarf elliptical galaxies, since Kormendy (1985) argues that these two populations may actually be the same type of galaxies.

canonical IMF. It can be written as

$$\xi_{\rm c}(m_*) = k k_i m_*^{-\alpha_i}, \tag{4.1}$$

with

$$\begin{array}{llll} \alpha_1 = 1.3, & k_1 = 1, & 0.1 \leq \frac{m_*}{\rm M_\odot} < 0.5, & \\ \alpha_2 = 2.3, & k_2 = k_1\, 0.5^{\alpha_2-\alpha_1} = 0.5, & 0.5 \leq \frac{m_*}{\rm M_\odot} \leq m_{\rm max}, & \end{array}$$ where m_* is the initial stellar mass,

$m_{\rm max}$ is the upper mass limit of the IMF, the factors k_i ensure that the IMF is continuous where the power changes and k is a normalisation constant (Kroupa 2008). The subscript c identifies the canonical IMF. $\xi_{\rm c}(m_*)$ equals 0 if $m_* < 0.1\,{\rm M_\odot}$ or $m_* > m_{\rm max}$. For stellar systems as massive as the UCDs, $m_{\rm max}$ is equal to the maximum mass for stars, which is close to $150\,{\rm M_\odot}$ (Weidner & Kroupa 2004; Oey & Clarke 2005; Figer 2005). For any IMF, $dN = \xi(m_*)dm_*$ is the number of born stars in the mass interval $[m_*, m_* + dm_*]$. In the present paper, the constant k is chosen such that

$$\int_{0.1}^{m_{\rm max}} \xi(m_*) m_*\, dm_* = 1\,{\rm M_\odot}. \tag{4.2}$$

Using this normalisation,

$$N = \int_{0.1}^{m_{\rm max}} \xi(m_*)\, dm_* \tag{4.3}$$

is formally the number of stars whose total mass is $1\,{\rm M_\odot}$. Multiplying equation 4.3 by the factor $M_{*,0}/{\rm M_\odot}$ therefore equals the initial number of stars in a star cluster with an initial stellar mass of $M_{*,0}$ and the mean stellar mass, $\overline{m}$, equals equation (4.2) divided by equation (4.3).

Note that there are limitations to the determination of the IMF from star counts. For instance, massive stars are short-lived, which is why this approach can only give the high-mass IMF for recent star formation events. Low-mass stars on the other hand can be almost as old as the Universe, but they can only be detected very locally.

The existence of a universal law for the stellar mass spectrum would indeed be surprising from a theoretical point of view, since models for star-formation predict that the stellar mass spectrum depends on the conditions under which star formation takes place (e.g. Adams & Fatuzzo 1996, Murray & Lin 1996, Larson 1998 and Clark et al. 2007). Moreover, a top-heavy IMF is in fact required in a number of astrophysical models. This includes, besides the model proposed in Dabringhausen et al. (2009) for the UCDs, also models for globular clusters (GCs) (D'Antona & Caloi 2004; Prantzos & Charbonnel 2006; Decressin et al. 2007)[2], distant galaxies (Baugh et al. 2005; Nagashima et al. 2005; van Dokkum 2008; Chary 2008) and the Galactic centre (et al. 2007). The motivations for the top-heaviness of the IMF in these models include a higher ambient temperature at the time when the observed population formed and violent star formation in particularly dense gas. These conditions were likely to be given in the young UCDs, since the universe was much younger when they formed (i.e. the temperature of the cosmic microwave background was higher). Furthermore, the α-enrichment found by Evstigneeva et al. (2007) in most of the Virgo-UCDs suggests rapid star-formation.

However, if stellar remnants are to account for the unseen mass in the UCDs, the top-heaviness of the IMF would have to be very pronounced. Introducing an IMF that equals the

[2]If UCDs are indeed the most massive GCs, as proposed for instance in Mieske et al. (2002), Mieske et al. (2004) and Forbes et al. (2008), it is evident that a top-heavy IMF in GCs suggests the same for UCDs. Note however that residual gas expulsion from mass-segregated clusters alleviates the need of a top-heavy IMF in GCs (Decressin et al. 2008).

canonical IMF below $1\,\mathrm{M}_\odot$ but has a different slope, α, for $m > 1\,\mathrm{M}_\odot$, Dabringhausen et al. (2009) suggest $1.0 < \alpha < 1.6$, depending on the age of the UCDs. These high-mass IMF slopes imply that the clear majority of the total initial stellar mass was locked up in stars more massive than $8\,\mathrm{M}_\odot$, in contrast to the case with the canonical IMF. These stars have a very high luminosity and evolve rapidly, which makes their abundance a key issue for the evolution of a stellar system.

Table 4.1: The initial parameters and some derived quantities for the UCD-models. The last two lines show the models for newly formed ONC-type star clusters from Kroupa et al. (2001) for comparison. The columns denote the identification number of the model, the initial Plummer-radius $R_{\rm pl,0}$, its *total* initial mass $M_{\rm pl,0}$, its *stellar* initial mass $M_{*,0}$, the star formation efficiency (SFE$= M_{0,*}/M_{\rm pl,0}$), the heating efficiency, the initial characteristic crossing-time $T_{\rm cr}$, the initial characteristic three-dimensional velocity dispersion $\sigma_{\rm 3D,0}$, the initial central mass density and an estimate for the time-scale on which a given proto-star encounters a star during the formation of the UCD (see Section 4.2.1).

model	$R_{\rm pl,0}$ [pc]	$M_{\rm pl,0}$ [$\rm M_\odot$]	$M_{*,0}$ [$\rm M_\odot$]	SFE	HE	$T_{\rm cr}$ [Myr]	$\sigma_{\rm 3D,0}$ [$\rm km\,s^{-1}$]	$\rho_{\rm pl,0,c}$ [$10^6 \rm M_\odot\,pc^{-3}$]	$t_{\rm enc}$ Myr
m7_r3_s1_h1	3.0	1.0×10^7	1.0×10^7	1.0	1.0	0.153	65.0	0.088	0.23
m7_r5_s1_h1	5.0	1.0×10^7	1.0×10^7	1.0	1.0	0.330	50.3	0.019	1.4
m8_r5_s1_h1	5.0	1.0×10^8	1.0×10^8	1.0	1.0	0.104	159.0	0.191	0.043
m7_r3_s04_h1	3.0	2.5×10^7	1.0×10^7	0.4	1.0	0.097	102.8	0.221	0.15
m7_r5_s04_h1	5.0	2.5×10^7	1.0×10^7	0.4	1.0	0.209	79.6	0.048	0.87
m8_r5_s04_h1	5.0	2.5×10^8	1.0×10^8	0.4	1.0	0.066	251.6	0.477	0.027
m7_r3_s04_h003	3.0	2.5×10^7	1.0×10^7	0.4	0.03	0.097	102.8	0.221	0.15
m7_r5_s04_h003	5.0	2.5×10^7	1.0×10^7	0.4	0.03	0.209	79.6	0.048	0.87
m8_r5_s04_h003	5.0	2.5×10^8	1.0×10^8	0.4	0.03	0.066	251.6	0.477	0.027
ONC A	0.345	1.12×10^4	3.75×10^3	0.33	–	0.23	6.8	0.065	9.4
ONC B	0.158	1.25×10^4	4.17×10^3	0.33	–	0.066	10.8	0.759	0.52

If UCDs indeed are the most massive star clusters, their stellar populations would essentially have formed in a single burst over a time-span of $\approx 1\,\mathrm{Myr}$ (cf. Elmegreen 2000; Hartmann et al. 2001), meaning that their stars evolve almost simultaneously. Considering the high energies involved in massive star evolution, this implies that UCDs with very top-heavy IMFs (with high-mass IMF-slopes $1.0 < \alpha < 1.6$, see Dabringhausen et al. (2009)) could have lost 90 per cent of their initial stellar mass over a time span of ≈ 40 Myr (which is the lifetime of the least massive stars that evolve into SNe, cf. the stellar evolutionary grid by Schaller et al. 1992). If there was residual gas (i.e. gas that was not used up in star formation) in them, which was swept out during this phase of violent star cluster evolution, the mass loss would have been even more pronounced. Such an extensive mass loss shapes the later appearance of a stellar system and may even be critical for its survival, if it happens on a short enough time scale (Boily & Kroupa 2003; Fellhauer & Kroupa 2005a). However, Dabringhausen et al. (2009) argued from structural parameters that mass loss on a time scale of 40 Myr for UCDs is probably in the adiabatic regime and therefore inflates them, but does not threaten to dissolve them. It is clear that a numerical study of this issue, including a more detailed treatment of mass loss through stellar evolution and residual gas expulsion, is necessary to confirm these arguments. It is provided in this paper.

4.2 Setup

4.2.1 Initial conditions

In the present paper, UCDs are assumed to have formed in the monolithic collapse of a fragmenting gas cloud, and thus in contrast to the model for UCD-formation proposed in Fellhauer & Kroupa (2002a) and Fellhauer & Kroupa (2005b), i.e. the merger of a star cluster complex into a single object (see also Kroupa 1998). This is not to say that the merging of star clusters is completely irrelevant for UCD formation. For instance, the densest part at the centre a proto-UCD could undergo monolithic collapse, while in the outskirts of the proto-UCD a multitude of star clusters is formed, which eventually merge. However, the apparent universality of the IMF in star clusters below the mass-scale of a UCD suggests that a UCD could not have a different IMF, if it is exclusively build up from such systems.

The adopted formation scenario for UCDs thus suggests that they are the most massive star clusters, which implies that their stellar population formed rapidly in $\approx 1\,\mathrm{Myr}$ (cf. Elmegreen 2000; Hartmann et al. 2001). The α-enrichment of the UCDs in Virgo reported by Evstigneeva et al. (2007) indeed suggests a short time scale for star formation, although for UCDs in other environments, this α-enrichment is less pronounced or even absent (cf. fig. 8 in Mieske et al. 2007). For simplicity, we assume that the stellar populations of UCDs have formed instantaneously instead of over a very short time-span. This is a conservative assumption for the present study, since it focusses on the stability of UCDs. A stellar population that is built up over an extended time-span also releases the total energy it produces (through stellar processes) over a longer time-span. In consequence, the mass loss from UCDs, which is powered by the energy produced by the stellar population, will be slower and therefore less threatening for the stability of the UCD.

Structural parameters

The UCD-models are set up with their mass distributed according to the Plummer-model (Plummer 1911). The Plummer-model is the simplest plausible and self-consistent model for a star cluster (Binney & Tremaine 1987; Heggie & Hut 2003). The advantage of using Plummer-models is that all major quantities are analytically accessible.

We choose nine different combinations of initial stellar mass, $M_{*,0}$, initial Plummer-radius, $R_{\rm pl,0}$, star formations efficiencies (SFEs) and heating efficiencies (HEs) for the UCD-models. The choices of the mentioned parameters are detailed below and the considered combinations of them are listed in Table 4.1, together with some major quantities derived from them.

$M_{*,0}$ is chosen such in the models that a stellar mass of the order of 10^6 to $10^7\,{\rm M}_\odot$ remains after the evolution of the massive stars has come to an end. This is the range in which the stellar masses of the observed UCDs lie. The chosen values for $R_{\rm pl,0}$ are either 3 pc or 5 pc and thus similar to the observed radii of GCs (eg. McLaughlin 2000 or Jordán A. et al. 2005). This leads to initial central densities, $\rho_{\rm pl,0,c}$, ranging from $1.9\times10^4{\rm M}_\odot\,{\rm pc}^{-3}$ to $4.8\times10^5{\rm M}_\odot\,{\rm pc}^{-3}$ (Table 4.1). These values for $\rho_{\rm pl,0,c}$ are similar to the ones that have been calculated for Galactic open clusters, such as the Orion Nebula Cluster (ONC), whose initial parameters are discussed in Kroupa et al. (2001). They consider models with $\rho_{\rm pl,0,c}=6.5\times10^4{\rm M}_\odot\,{\rm pc}^{-3}$ or $\rho_{\rm pl,0,c}=7.6\times10^5{\rm M}_\odot\,{\rm pc}^{-3}$ for that star cluster, as can be calculated from the initial masses and half-light radii given in their table 1. The models discussed here are thus not extreme because of the densities in their central regions, but because of the extension of this central region. This may account for the proposed top-heaviness of the IMF in UCDs, see Section 4.2.1.

Embedded star clusters in the Milky way are thus less extended than the models discussed in this paper (also see Lada & Lada 2003, their table 1). Note that also GCs were initially less extended than the UCD-models discussed in this paper, unless they lost very little mass since their formation. The reason why smaller $R_{\rm pl,i}$ are not considered here are the extreme initial central densities they would imply for the objects (for instance of the order of $10^7\,{\rm M}_\odot\,{\rm pc}^{-3}$ for $R_{\rm pl,0}=1\,{\rm pc}$; also see Fig. 4.14). Besides, the very small crossing times of such objects would make computations of the evolution very time-consuming while mass loss from them would approach the adiabatic regime, where the behaviour of the cluster can be calculated analytically with equation (4.17) below.

The actual values of the SFE and the HE are hard to quantify. In order to get an idea of how these parameters would influence the early evolution of a UCD, vastly different and in some cases extreme values for them are considered in this paper.

The SFE is defined as the fraction of the primordial gas that is converted into stars during a star-forming event within the cluster- or UCD-forming cloud core region. In the UCD-models, it is taken to be 1 or 0.4, the latter value being approximately the upper limit of the SFEs reported for open star clusters (Lada & Lada 2003). These high choices for the SFEs in UCDs are motivated by the fact that it would be more difficult to expel the primordial gas from UCDs than from open clusters because of the deep potential wells of UCDs (see also Elmegreen & Efremov 1997). It has even been suggested (e.g. in Elmegreen 1999 or Murray 2009) that all available gas is turned into stars, if the forming stellar system is dense and massive enough. If indeed all star clusters and UCDs form on the same time scale, the star formation rate must be higher in UCDs than in any of the less massive stellar systems. Taking 1 Myr as the characteristic time scale for star formation in these systems, the average star formation rate in UCDs would be 10-100 ${\rm M}_\odot\,{\rm yr}^{-1}$ (Dabringhausen et al. 2009). Assuming UCDs are essentially star clusters and that star formation is the more rapid the denser the primordial gas is, this could be understood

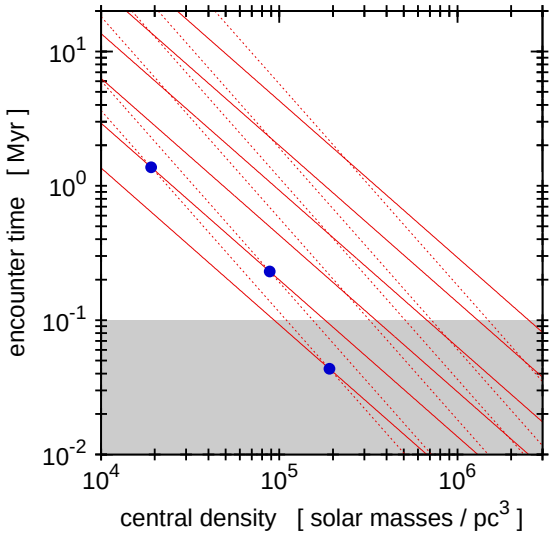

Figure 4.1: The expected time until a proto-star collides with a star, $t_{\rm enc}$, in a forming UCD, assuming that half of its total stellar population has already been formed (see Section 4.2.1 for details). The estimated $t_{\rm enc}$ for the UCD-models, in which all gas is eventually converted into stars, are indicated by the three (blue) points. The grey shaded area is where $t_{\rm enc}$ is below the approximate life-time of a proto-star, which is assumed to be 10^5 years. The solid lines show the $t_{\rm enc}$ as a function of $\rho_{\rm pl,0,c}$ for different constant $M_{\rm pl,0}$, starting from 10^3 $\mathrm{M}_\odot$ and increasing by a factor of 10 downwards. The dotted lines show the $t_{\rm enc}$ as a function of $\rho_{\rm pl,0,c}$ for different constant $R_{\rm pl,0}$, with $R_{\rm pl,0}$ being 0.1, 0.3, 0.5, 1, 3 and 5 pc from top to bottom.

if the primordial gas cloud forming a UCD is, compared to open star clusters, compressed to a higher density during its collapse.

The HE is defined as the fraction of the energy released by stellar processes that actually drives gas out of a star-forming region instead of being radiated away. That is, the HE is the ratio between the kinetic energy of the interstellar medium (ISM) expelled from the stellar system to the total energy inserted into its ISM. The HEs in starbursts have been argued to be near 1 in some studies (e.g. Chevalier & Clegg 1985), while others suggest that only a few percent of the energy inserted into the ISM is turned in kinetic energy of gas leaving the stellar system (e.g. Recchi et al. 2001; also see Melioli & de Gouveia Dal Pino 2004). For the present paper, HEs of 1 and 0.03 are considered.

A major improvement compared to the rather arbitrary choice of SFEs and HEs made here would clearly be to estimate these parameters in self-consistent modelling of a collapsing gas cloud large enough to form a UCD. This would also clarify how long it would actually take the stellar population to form in such a system, but is currently not a computable option.

A possible influence of encounters on the IMF

If UCDs indeed formed with the initial conditions proposed here, the likeliness for close encounters between members of their emerging stellar populations (stars and proto-stars) would be what sets them apart from ONC-like star clusters. This motivates why the IMF in UCDs might be top-heavy, while this is not observed in star clusters like the ONC.

The case of a proto-star encountering a star is of particular interest. A proto-star exists over a time of $\approx 10^5$ yr until most of its mass has accreted onto the central core (Wuchterl & Tscharnuter 2003) and is thus short-lived, compared to the characterisic time-scale for star-

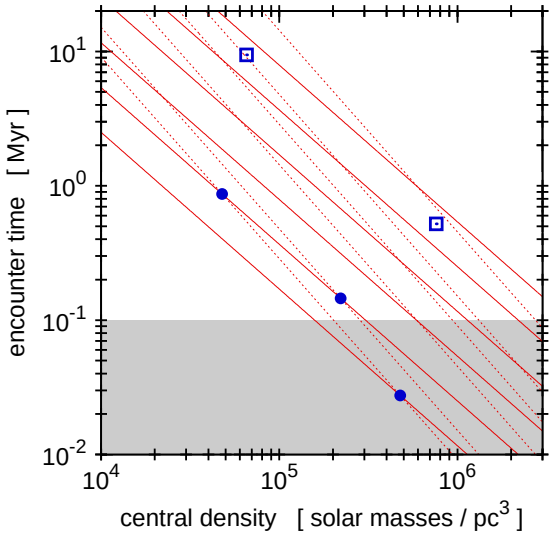

Figure 4.2: As Fig. (4.1), but for the UCD-models, where a star formation efficiency of 0.4 instead of 1 is assumed. While UCD-models shown here are assumed to have the same *stellar* masses as the ones shown in Fig. (4.1) their *total* masses are higher, leading to higher velocity dispersions and thus shorter $t_{\rm enc}$ at the same stellar density. The meaning of the solid and the dotted lines is the same as in Fig. (4.1), but the lowest constant value for $M_{\rm pl,0}$ chosen here is $2.5 \times 10^3\,{\rm M}_\odot$ and increasing by a factor of 10 downwards with every solid line. The open squares show models A and B for the initial states of ONC-type star clusters from Kroupa et al. (2001), which have, compared to the UCD-models in this figure, a slightly lower SFE of 0.33.

formation in a star cluster (≈ 1 Myr). It has however a radius, $r_{\rm proto}$, of the order of 100 AU for essentially all stellar masses, since the dependency of $r_{\rm proto}$ on the mass of the proto-star is only weak (cf. equation 4 in Goodwin et al. 2007). This makes an encounter of a proto-star with a star quite likely, as soon as a considerable stellar population is already present.

To estimate a characteristic time-scale for such an encounter for the UCD-models listed in Table 4.1, consider Plummer-spheres with the initial parameters from that table. Their density-profiles are given as

$$\rho(R) = \frac{3M_{\rm pl,0}}{4\pi R_{\rm pl,0}^3}\left[1+\left(\frac{R}{R_{\rm pl,0}}\right)^2\right]^{-\frac{5}{2}} \tag{4.4}$$

(equation 8.51 in Kroupa 2008), and thus their central *stellar* densities at the time when half of their stellar populations have formed can be estimated as

$$\rho_{\rm pl,*,c} = \frac{3M_{*,0}}{8\pi R_{\rm pl,0}^3}. \tag{4.5}$$

This density implies a volume that contains one star on average, V_*. It can be written as

$$V_* = \frac{\overline{m}}{\rho_{\rm pl,*,c}}, \tag{4.6}$$

where $\overline{m}$ is the average stellar mass. The time-dependent volume through which a proto-star in the central region has travelled due to its motion can be written as

$$V(t) = \pi r_{\rm proto}^2\,\sigma_{\rm 3D,0,c}\,t, \tag{4.7}$$

where $\sigma_{\rm 3D,0,c}$ is the *central* 3D velocity dispersion, which is

$$\sigma_{\rm 3D,0,c} = \sqrt{\frac{GM_{\rm pl,0}}{2R_{\rm pl,0}}}, \tag{4.8}$$

where G is the gravitational constant (cf. equation 8.59 in Kroupa 2008). The values calculated from equation (4.8) for the UCD-models in this paper are an order of magnitude higher than in the models for the initial states of ONC-type star clusters from Kroupa et al. (2001), while their central densities are essentially the same (see Table 4.1). The time $t = t_{\rm enc}$ by which a proto-star is to be expected to have encountered a star can be calculated be setting $V(t) = V_*$ and solving for t. Thus,

$$t_{\rm enc} = \frac{\overline{m}}{\pi r_{\rm proto}^2 \, \rho_{\rm pl,*,c} \, \sigma_{\rm 3D,0,c}}. \tag{4.9}$$

Assuming that a top-heavy IMF results from an canonical IMF by the collisions of proto-stars with stars, $\overline{m} = 0.65 \, {\rm M}_\odot$ (which is the average stellar mass for a canonical IMF, see Table 4.2), and $r_{\rm proto} = 100 \, {\rm AU} = 4.85 \times 10^{-4} \, {\rm pc}$ are reasonable choices for emerging open star clusters and emerging UCDs alike. This implies that the IMF would be canonical until it is altered under the influence of encounters between the members of an emerging stellar population and would stay canonical in stellar systems where such encounters are rare at all times.

Note that the derivation of equation (4.9) implicitly assumes that the cross section for an encounter of a proto-star with a star is the geometrical cross section, $A_{\rm geo} = \pi r_{\rm proto}^2$, whereas the actual cross section for such an encounter is higher due to the influence of gravity. If both the proto-star and the star have the same mass, $\overline{m}$, this actual cross section is given as

$$A = \pi r_{\rm proto}^2 (1 + \Theta) \tag{4.10}$$

at the centre of the emerging UCD, where Θ is the Safronov number,

$$\Theta = \frac{2G \, \overline{m}}{\sigma_{\rm 3D,0,c}^2 \, r_{\rm proto}} \tag{4.11}$$

(Murray & Lin 1996). However, assuming $r_{\rm proto} = 100$ AU and $\overline{m} = 0.65 {\rm M}_\odot$ leads to $\Theta = 0.26$ in the less compact model for the initial states of ONC-type star clusters (ONC A in Table 4.1). Using the same assumptions, Θ is lower for all other models in Table 4.1 due to their higher velocity dispersions. In the case of the UCD-models from this paper, the difference between the actual cross section and the geometric cross section is less than 1 per cent. Thus, gravitational focussing of stars onto the proto-star plays a minor role for the models in Table 4.1, which justifies the approximation.

The values for $t_{\rm enc}$ resulting from equation (4.9) are noted in Table 4.1 and plotted in Figs. 4.1 and 4.2. Comparing these values with the characteristic life-time of a proto-star, $t_{\rm proto} \approx 10^5$ years, it can be seen that $t_{\rm enc} < t_{\rm proto}$ for the UCD-models with $M_{*,0} = 10^8 \, {\rm M}_\odot$. For the UCD-models with $M_{*,0} = 10^7 \, {\rm M}_\odot$ and $R_{\rm pl,0} = 3 \, {\rm pc}$, $t_{\rm enc}$ is only slightly larger than $t_{\rm proto}$. However, for the UCD-models with $M_{*,0} = 10^7 \, {\rm M}_\odot$ and $R_{\rm pl,0} = 5 \, {\rm pc}$, $t_{\rm enc}$ exceeds $t_{\rm proto}$ by about an order of magnitude. This suggests that the encounters between proto-stars and stars would influence star-formation in the models with $M_{*,0} = 10^8 \, {\rm M}_\odot$ and also, to a much lesser extent, in the more compact UCD-models with $M_{*,0} = 10^7 \, {\rm M}_\odot$, but not in the UCD-models with $M_{*,0} = 10^7 \, {\rm M}_\odot$ and $R_{\rm pl,0} = 5 \, {\rm pc}$. The UCD-models with $M_{*,0} = 10^7 \, {\rm M}_\odot$ and $R_{\rm pl,0} = 5 \, {\rm pc}$ are in this respect similar to models A and B for the initial states of ONC-type

star clusters from Kroupa et al. (2001) (see Fig. 4.2). This implies, invoking the universality of the IMF in open star clusters, that the IMF in those UCD-models should also be given by equation (4.1), if deviations from the canonical IMF are caused by encounters between proto-stars and stars. According to the calculations in this paper, the UCD-models with $M_{*,0} = 10^7\,\mathrm{M}_\odot$ and $R_{\mathrm{pl},0} = 5\,\mathrm{pc}$ would indeed only evolve into objects similar to an observed UCD if their mass loss is as implied by the canonical IMF. The IMF in the other UCD-models would however have to be top-heavy to some extent for this (see Section 4.3). The UCD-models in this paper are thus self-consistent in that sense.

We note that equation (4.9) reveals the particular importance of encounters between proto-stars and stars. For a collision between two stars, r_{proto} has to be substituted by a value $\ll 1\,\mathrm{AU}$, which leads to $t_{\mathrm{enc}} \gg 10^5$ years. Thus, collisions between stars only as a mechanism that changes the shape of the IMF (Bonnell et al. 1998; Bonnell & Bate 2002) requires even higher densities. For the encounter between two proto-stars, the density of stars at a given time has to be substituted by the density of proto-stars at that time. Taking 1 Myr as the characteristic time-scale on which star-formation takes place and 10^5 years as the life-time of a proto-star suggests that the density of proto-stars is $\approx 0.1\rho_{\mathrm{pl},*,\mathrm{c}}$, which is five times less than the density of stars at the time when half of the total stellar population of the UCD has formed.

A caveat to the above discussion is that it is not specified what the consequence of a collision between a proto-star and a star is. This is a merger if the encounter is slow enough. If the encounter is fast enough for the star to only pass through the proto-star, the star transfers some of its kinetic energy on the proto-star and thereby disperses some of the matter that would otherwise accrete on the proto-star. For deciding which of these processes would dominate for a given velocity dispersion, as well as for answering the question of how and to what extent they would alter the IMF, detailed modelling of the collisions would be required. However, the discussion here implies that any process resulting from an encounter between stars and proto-stars should only be relevant for the denser UCD-models in Tab. 4.1, in contrast to the models for ONC-type star clusters, where most proto-stars should be unaffected by encounters.

We revisit the matter of a possible influence of encounters on the IMF in UCDs in Section 4.3.4.

The IMF of the UCD-models

For each of the nine sets of models listed in Table 4.1, six IMFs are considered. They are either canonical or top-heavy to a different degree and have upper mass limits, m_{max}, of either $100\,\mathrm{M}_\odot$ or $150\,\mathrm{M}_\odot$. However, all of them agree with the canonical IMF (equation 4.1) for $m < 1\,\mathrm{M}_\odot$. Studies on m_{max} suggest that $m_{\mathrm{max}} = 150\,\mathrm{M}_\odot$ is more realistic than $m_{\mathrm{max}} = 100\,\mathrm{M}_\odot$ for very massive star clusters and therefore also for UCDs (e.g. Massey & Hunter 1998, Figer et al. 1998, Figer 2004). However, the treatment of stellar evolution and its effect on the mass loss from UCDs in this paper (see Section 4.2.2) is based on stellar models that only range up to a $120\,\mathrm{M}_\odot$ star. Assuming $m_{\mathrm{max}} = 150\,\mathrm{M}_\odot$ for our models therefore requires extrapolating from the given data, which may be problematic due to the strong dependencies of stellar properties on stellar mass. The emphasis in this paper is therefore on IMFs with $m_{\mathrm{max}} = 100\,\mathrm{M}_\odot$ (which is also a common choice in simple stellar population models). The impact of the higher $m_{\mathrm{max}} = 150\,\mathrm{M}_\odot$ is only tested for the canonical IMF and the most top-heavy IMF.

Table 4.2: The IMFs considered for UCDs. The content of columns is the following: Column 1: the identification number of the IMF, Column 2: the slope of the high-mass end of the IMF, α (where 2.3 is the Salpeter slope), Column 3: the upper stellar mass limit, $m_{\rm max}$, Column 4: the ratio between the total inital mass of stars more massive than $8\ {\rm M}_\odot$ and the total initial mass of all stars, Column 5: the ratio between the inital number of stars more massive than $8\ {\rm M}_\odot$ and the initial number of all stars, Column 6: the initial mean mass of stars.

IMF	α	$m_{\rm max}$ $[{\rm M}_\odot]$	$M_{\rm hms,0}/M_{*,0}$	$N_{\rm hms,0}/N_{*,0}$	$\overline{m}$ $[{\rm M}_\odot]$
1	1.1	150	0.921	0.2031	10.02
2	1.1	100	0.886	0.1830	7.16
3	1.5	100	0.719	0.0632	2.49
4	1.9	100	0.453	0.0210	1.07
5	2.3	150	0.230	0.0072	0.65
6	2.3	100	0.213	0.0071	0.64

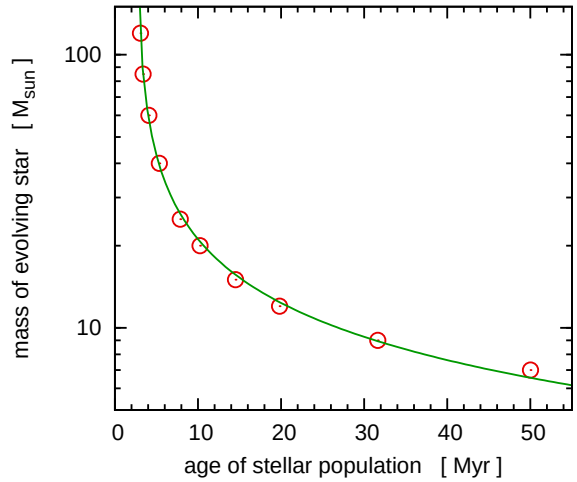

Figure 4.3: The data from Schaller et al. (1992) on the lifetimes of stars with different initial masses from 7 to $120\,{\rm M}_\odot$ (open circles) and an interpolation function to them (solid line), which is given by equation (4.12). It is apparent that the stars with the highest masses evolve over an extremely short time span. This increases the significance of the upper mass limit of the IMF for the dynamical evolution of a star cluster or UCD.

4.2.2 Generating the mass loss Tables

The interstellar medium (ISM) of a new-born star cluster or UCD is massively heated by the radiation from massive stars, which leads to a mass loss from it until the ISM is depleted. The eventual evolution of the massive stars into supernovae (SNe) heats the ISM as well, but also replenishes the ISM. The rate at which mass is lost from the star cluster or UCD due to this interaction between the massive stars and the ISM is the driving force for its early evolution. This is why the mass loss rate has to be quantified for our models. It is recorded in look-up tables, listing how much the mass of the UCD-models has to be reduced for each time-step in the calculation.

Evidently, knowing the lifetimes of massive stars is essential for generating the mass loss tables. A very good proxy for the time at which the life of the star ends is the time at which carbon burning has finished. The time that has elapsed until this evolutionary stage is reached is

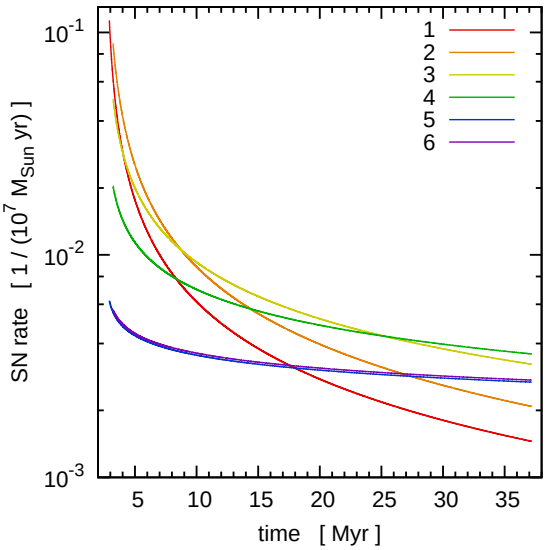

Figure 4.4: The SN rates with time for the modelled UCDs with initial total stellar mass $M_{*,0} = 10^7 \mathrm{M}_\odot$. The different curves are for the different IMFs listed in Tab. 4.2. The numbers refer to the labels given to the IMFs in Tab. 4.2. Note that the choice of the upper mass limit of the IMF determines the time when the first SN explodes, but turns out to be almost irrelevant for the SN rates. For the models with $M_{*,0} = 10^8$ M$_\odot$, the SN rates are higher by a factor of 10. The SN rates are propotional to the energy input by the SN, because all SN are assumed to release the same amount of energy (10^{51}erg).

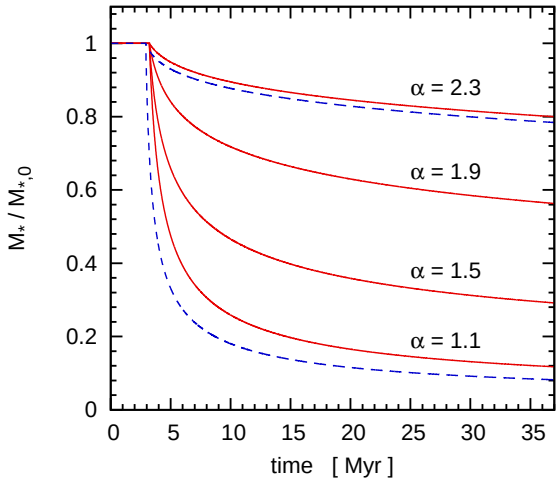

Figure 4.5: The evolution of the stellar mass of the UCD, M_*, with time due to stellar evolution. M_* is plotted in units of the initial stellar mass of the UCD, $M_{*,0}$. The different lines in this figure represent M_* for the different IMFs listed in Table 4.2. The high-mass slope of the IMF is noted above the curves. Solid (red) lines are for IMFs with an upper mass limit of 100 M$_\odot$ and dashed (blue) lines are for an upper mass limit of 150 M$_\odot$. The choice of the upper mass limit has only a minor impact for the canonical IMF ($\alpha = 2.3$), but is more significant for the most top-heavy IMF we consider ($\alpha = 1.1$). For models with SFE=1 and HE=1 these curves show the total mass loss as well.

taken from the stellar evolutionary grid by Schaller et al. (1992) for massive stars with various initial masses. This time-span is identified with the lifetime of a star in this paper. A good fit to the lifetimes of stars with high mass ($m_* \geq 7$ M$_\odot$) and low metallicity ($Z = 0.001$ and

$[Z/\mathrm{H}] = -1.3$ respectively) is the function

$$m_* = a(t_* - b)^c, \tag{4.12}$$

with

$$a = 74.6, \quad b = 2.59, \quad c = -0.63.$$

where the initial mass of the star, m_*, is measured in $\mathrm{M}_\odot$ and the lifetime of the star, t_*, is measured in Myr (Fig. 4.3). It thus covers the whole range of stellar initial masses of stars that undergo SN explosions at the end of their evolution, which is $m_* \gtrsim 8\ \mathrm{M}_\odot$ (Koester & Reimers 1996). The parameters a, b and c have been found by a least-squares fit. The models for low-metallicity stars were preferred over models for stars with Solar metallicity because of the mostly sub-solar metallicities of the UCDs (Mieske et al. 2006a; Evstigneeva et al. 2007). This choice has however only a minor impact on the best-fitting parameters a, b and c. Note that since all stars in the UCD-models are assumed to have formed at once in this paper, it is possible to substitute the stellar lifetime, t_*, in equation (4.12) with the age of the UCD-model, t, in order to find the initial mass of the stars that undergo SNe at that time.

Now consider the increase of the age of the UCD-model by the time step $t_\mathrm{i} \rightarrow t_{\mathrm{i}+1}$. During this time, ΔN_* stars with a total mass ΔM_* will complete their evolution. These quantities can be written as

$$\Delta N_{*,\mathrm{i}} = \frac{M_{*,0}}{\mathrm{M}_\odot} \int_{m_{*,\mathrm{i}+1}}^{m_{*,\mathrm{i}}} \xi(m_*)\, dm_*, \tag{4.13}$$

and

$$\Delta M_{*,\mathrm{i}} = \frac{M_{*,0}}{\mathrm{M}_\odot} \int_{m_{*,\mathrm{i}+1}}^{m_{*,\mathrm{i}}} \xi(m_*) m_*\, dm_*, \tag{4.14}$$

where $\xi(m_*)$ is the IMF, $m_{*,\mathrm{i}}$ is the initial mass of stars that evolve at $t = t_\mathrm{i}$ and $m_{*,\mathrm{i}+1}$ is the initial mass of stars that evolve at $t = t_{\mathrm{i}+1}$. $M_{*,0}$ is the total initial stellar mass of the UCD-model. Given the normalisation chosen for the IMF (see equations 4.1 and 4.2), the purpose of the factors $M_{*,0}/\mathrm{M}_\odot$ is to scale equations 4.13, 4.14 and 4.15 to a UCD-model with the initial mass of $M_{*,0}$. ΔN_* is equivalent to the number of SNe during the time step $t_\mathrm{i} \rightarrow t_{\mathrm{i}+1}$; i.e. the SN-rate in the limit of $t_{\mathrm{i}+1} - t_\mathrm{i} \rightarrow 0$. At the time when the most massive stars evolve, this SN-rate is, for instance, ≈ 1 SN per 10 years for the UCD-models with $M_{*,0} = 10^7\ \mathrm{M}_\odot$ and a high-mass IMF slope of $\alpha = 1.1$, while it is a few SN per 10^3 years for the UCD-models with $M_{*,0} = 10^7\ \mathrm{M}_\odot$ and $\alpha = 2.3$. The influence of the top-heaviness of the IMF on the SN-rates decreases as time proceeds. The SN-rates for the UCD-models with $M_{*,0} = 10^7\ \mathrm{M}_\odot$ and the IMFs from Table 4.2 are shown in Fig. 4.4. The SN-rates for the UCD-models with $M_{*,0} = 10^8\ \mathrm{M}_\odot$ are higher by a factor of 10 compared to the ones shown in this figure, but the same otherwise.

Fig. 4.5 depicts the change of the stellar mass of the UCD-model with time, i.e. $M_{*,\mathrm{i}} = M_{*,0}$ for $t_\mathrm{i} \leq t_\mathrm{SN}$ and $M_{*,\mathrm{i}} = M_{*,0} - \sum_{n=1}^{i} \Delta M_{*,\mathrm{n}}$ for $t_\mathrm{i} > t_\mathrm{SN}$, where $M_{*,0}$ is the total initial stellar mass and t_SN is the time when the first stars become SNe.

The total energy deposited by stars into their surroundings by radiation and stellar winds at the time $t = t_i$, $L_{*,\mathrm{i}}$, is given as

$$L_{*,\mathrm{i}} = \frac{M_{*,0}}{\mathrm{M}_\odot} \int_{0.1}^{m_{\mathrm{max,i}}} \xi(m_*) l(m_*)\, dm_*, \tag{4.15}$$

with $m_{\rm max,i}$ being the mass of the most massive star that has not evolved into a SN at that time. $l(m_*)$ is the energy deposition rate of stars into the ISM through radiation and stellar winds as a function of their initial mass. It is estimated as

$$l(m_*) = 2.16 \times 10^{47} \left(\frac{m_*}{\rm M_\odot}\right)^{1.72} \frac{\rm erg}{\rm Myr}, \tag{4.16}$$

which is identical to equation (12) in Baumgardt et al. (2008). As in Baumgardt et al. (2008), equation (4.16) is applied to stars of all masses, even though it was obtained in a fit to high-mass stars. Note that the positive exponent in equation (4.16) and the negative exponent in the IMF cancel out more or less in equation (4.15). The contribution of low- and intermediate-mass stars to the total energy deposition into the ISM is therefore small at first, because the masses of high-mass stars are distributed over a much wider range.

The algorithm

The integrations in equations (4.13) to (4.15) are done numerically for the IMFs listed in Table (4.2). The used program is structured as outlined below.

Start at $t = 0$ with a set of initial parameters taken from Table 4.1 and an IMF taken from Table 4.2. Let Δt be the time step from $t_{\rm i}$ to $t_{\rm i+1}$ and $t_{\rm SN}$ the time when the first stars become SNe.

1. If $t_{\rm i} > t_{\rm SN}$, calculate which stars evolve from $t = t_{\rm i}$ to $t = t_{\rm i} + \Delta t$ using equation (4.12) and then which total mass these stars have, $\Delta M_{*,\rm i}$ (equation 4.14). This mass is added to the total mass of the interstellar medium, $M_{\rm ISM,i}$. This includes the possibility that the UCD-model had no ISM left at the end of the previous time step. In this case, $M_{\rm ISM,i} = \Delta M_{*,\rm i}$.

2. The rate at which the stars and the SNe deposit energy into the ISM during the time step is calculated, $L_{\rm i}$. $L_{\rm i}$ is approximated by $L_{\rm i} = L_{*,\rm i+1} + L_{\rm SN,i}$, where $L_{*,\rm i+1}$ is the rate at which the stars deposit energy into the ISM at $t = t_{\rm i+1}$ (equation 4.15) and $L_{\rm SN,i}$ is the energy that the SNe deposit into the ISM from $t = t_{\rm i}$ to $t = t_{\rm i} + \Delta t$ (which is in the limit of $\Delta t \rightarrow 0$ an energy deposition *rate* as well). Using the number of stars that evolve during the time step $\Delta N_{*,\rm i}$, (equation 4.13), $L_{\rm SN,i}$ can be estimated by assuming that each SN releases a characteristic amount of kinetic and electromagnetic energy, which are the forms of energy that are relevant for driving matter out of the UCD-model. Estimating this quantity as $10^{51}\,\rm erg$ per SN (e.g. Carroll & Ostlie 1996) leads to $L_{\rm SN,i} = 10^{51} \Delta N_{*,\rm i}\,\rm erg\,Myr^{-1}$. The total luminosity is multiplied by the HE to obtain $L_{\rm kin,i}$, which is the luminosity that is not radiated away through thermal emission of the ISM, but is converted into kinetic energy of the gas leaving the UCD.

3. The time $\tau_{\rm i}$ it would take until all gas is expelled from the UCD-model is estimated, assuming that $L_{\rm kin,i}$ does not change during that time. This is done using the equation $\tau_{\rm i} L_{\rm kin,i} = |E_{\rm pot,i} - E_{\rm pot*,i}|$, where $E_{\rm pot,i}$ is the total binding energy of the UCD-model at $t = t_i$ and $E_{\rm pot*,i}$ is the binding energy the UCD would have if it would lose all gas at that time. Note that the UCD-model inflates as it loses mass and $E_{\rm pot*,i}$ should therefore be calculated using the Plummer-radius the UCD-model has after all gas is expelled. We estimate it using the relation between initial radius and final radius of a stellar system

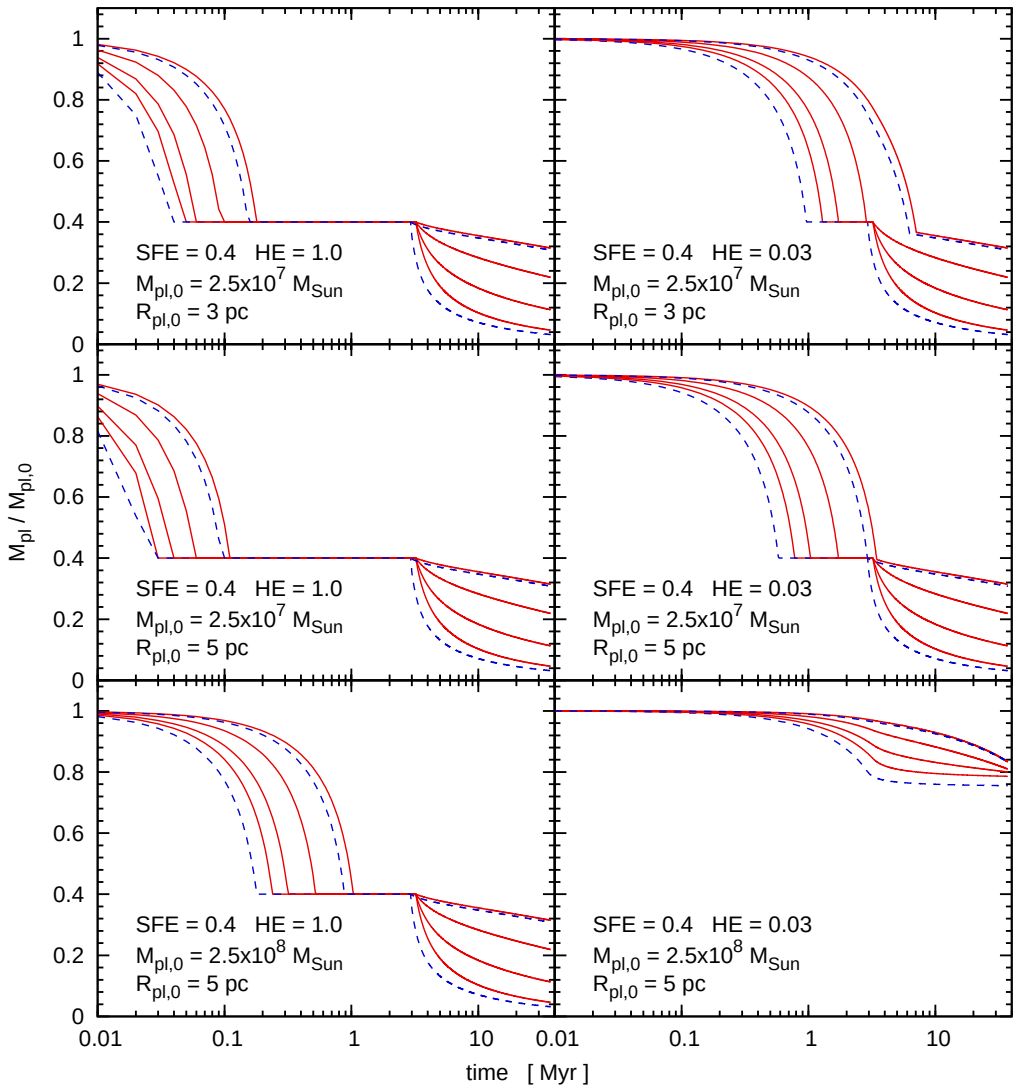

Figure 4.6: The change of the total mass of the UCD-model, $M_{\rm pl}$, with time due to stellar radiation and evolution for our models with $\mathrm{SFE} = 0.4$ and $\mathrm{HE} = 1.0$ or $\mathrm{HE} = 0.03$ relative to the total initial mass of the UCD-model, $M_{\rm pl,0}$. The assumptions regarding SFE, HE, initial mass of the UCD-model and inital Plummer-radius of the UCD-model for the mass loss histories shown are indicated in the corresponding panel. The different lines in this figure represent $M_{\rm pl}$ for the different IMFs listed in Table 4.2. The mass loss increases with the top-heaviness of the assumed IMF: for the topmost curves $\alpha = 2.3$ and for the lowermost curves $\alpha = 1.1$. Solid (red) lines are for IMFs with an upper mass limit of $100\,\mathrm{M}_\odot$ and dashed (blue) lines are for an upper mass limit of $150\,\mathrm{M}_\odot$. The choice of the upper mass limit has only a minor impact for the canonical IMF ($\alpha = 2.3$), but is much more significant for the most top-heavy IMF that are considered ($\alpha = 1.1$). Note that for $t \gtrsim 3\,\mathrm{Myr}$ the mass loss histories shown in this figure are equal to the change in stellar mass shown in Fig. 4.5 if the primordial gas is expelled before the first star has evolved completely. However, contrary to Fig. 4.5 the time-axis is scaled logarithmically here, in order to show the sometimes very rapid expulsion of the primordial gas.

for adiabatic mass loss, even though the mass loss is in our case sometimes clearly not adiabatic. This relation is given by

$$\frac{r_{\rm final}}{r_{\rm init}} = \frac{M_{\rm init}}{M_{\rm final}}, \tag{4.17}$$

where $r_{\rm init}$ and $M_{\rm init}$ are radius and mass of the stellar system at the beginning of mass loss, respectively, and $r_{\rm final}$ and $M_{\rm final}$ the are radius and mass of the stellar system at the end of mass loss, respectively (Kroupa 2008 and references therein). Equation (4.17) underestimates the expansion of the UCD-models at times of non-adiabatic mass loss (cf. equation 8.20 in Kroupa 2008). Therefore, if the UCDs have experienced extended non-adiabatic mass loss, the mass loss rates calculated here are too low, because a more pronounced expansion implies that the potential well becomes shallower and the remaining gas requires less energy to escape from it. This is even more important for a more top-heavy IMF.

4. If $\tau_{\rm i} < \Delta t$, set $\tau_{\rm i} = \Delta t$. The mass loss of the UCD-model during the time step is assumed to be
$$\delta M = M_{\rm ISM,i} \frac{\Delta t}{\tau_{\rm i}}. \tag{4.18}$$

5. Calculate the new parameters of the UCD-model after it has lost the mass δM: The new total stellar mass is decreased by $\Delta M_{*\rm i}$ and the new Plummer-radius is estimated using equation (4.17).

6. If $t_{\rm i+1} = t_{\rm i} + \Delta t$ is less than it takes a star with $m_* = 8\ {\rm M}_\odot$ to evolve into a SN according to equation (4.12), repeat steps (i) through (vi), but for $t_{\rm i+1}$ instead of $t_{\rm i}$.

The underlying assumption in the chosen approach is that the material expelled from a SN does not *immediately* escape the UCD, but that its kinetic energy is thermalised, as it is assumed for massive star clusters in, e.g., Tenorio-Tagle et al. (2007). This can happen either through interaction with the surrounding ISM or through the collision of the expanding envelopes of different SNe. The latter becomes more relevant with increasing top-heaviness of the IMF. The notion of the thermalisation of the SN ejecta is flawed if there is no ISM left and if the SNe are too few for their envelopes to interact with one another. However, in this case also very low HEs are sufficient to keep the UCD-models gas-free.

The mass loss histories calculated by using the above routine are shown in Fig. (4.6) for the models with SFE=0.4 and HE=1 or HE=0.03. For the the models with SFE=1 and HE=1, the evolution of the stellar mass of the UCD-models shown in Fig. 4.5 also illustrates their mass loss history, since the UCD-models are gas-free at all times in this case.

The role of compact stellar remnants

A simplification that is made in the creation of the mass loss histories is that the whole mass of the evolved stars is added to the ISM, including the mass of their compact remnants. For testing under which conditions this approximation is reasonable, the total mass of all compact remnants of stars with initial masses $m_* > 8\ {\rm M}_\odot$, $M_{\rm rem}$, needs to be compared to the total mass of their progenitors, $M_{\rm hms,0}$. If an IMF is given, calculating $M_{\rm rem}$ requires a relation between the initial masses of stars and the masses of their compact remnants. Such an initial-to-final mass relation is, e.g., formulated in equation (8) of Dabringhausen et al. (2009). Their equation is also used here. Thus, stars with initial masses of $8\ {\rm M}_\odot \leq {\rm m}_* < 25\ {\rm M}_\odot$ are thought to evolve into neutron stars (NSs) with a mass of $1.35\ {\rm M}_\odot$, which is the mass Thorsett & Chakrabarty (1999) have found for pulsars, i.e. a sample of neutron stars that can easily be detected. Stars with even higher initial masses are believed to evolve into black holes, but the actual masses of these black holes (BHs) are poorly constrained (cf. figs. 12 and 16 in Woosley et al. 2002).

Table 4.3: The total masses of all stars more massive than $8\ \mathrm{M}_\odot$ ($M_{\mathrm{hms},0}$, Column 2) and the total masses of their compact remnants (M_{rem}, Columns 3 and 4) for the IMFs in Table 4.2. The masses are in units of the total mass of all stars that were formed initially, $M_{*,0}$. The two different values for M_{rem} for a given IMF reflect that the mass of the remnants of very massive stars is poorly known. While the mass of the compact remnants of stars with initial masses of $8\ \mathrm{M}_\odot \leq \mathrm{m}_* < 25\ \mathrm{M}_\odot$ is $1.35\ \mathrm{M}_\odot$ in both estimates, the mass of the compact remnants of stars with $m_* > 25\ \mathrm{M}_\odot$ is assumed to be either $0.1m_*$ (Column 3) or $0.5m_*$ (Column 4).

IMF	$M_{\mathrm{hms},0}/M_{*,0}$	$M_{\mathrm{rem}}/M_{*,0}$ $m_{\mathrm{BH}} = 0.1m_*$	$M_{\mathrm{rem}}/M_{*,0}$ $m_{\mathrm{BH}} = 0.5m_*$
1	0.921	0.0910	0.409
2	0.886	0.0871	0.369
3	0.719	0.0709	0.271
4	0.453	0.0452	0.150
5	0.230	0.0234	0.0698
6	0.213	0.0218	0.0605

Therefore, two cases are considered for the masses of BHs, namely the case that they all have 10 per cent of the initial mass of their progenitors ($m_{\mathrm{BH}} = 0.1m_*$) and the case that they have 50 per cent of the initial mass of their progenitors ($m_{\mathrm{BH}} = 0.5m_*$) are considered. The resulting values are noted in Table 4.3.

It is apparent from these numbers that for $m_{\mathrm{BH}} = 0.1m_*$ the mass locked up in compact remnants is indeed negligible, while this is not the case for $m_{\mathrm{BH}} = 0.5m_*$. However, the masses of observationally confirmed stellar-mass BHs (see Casares 2007) seem to favour the case of $m_{\mathrm{BH}} = 0.1m_*$, leading to BH masses $\lesssim 10\ \mathrm{M}_\odot$. Apart from that, Lyne & Lorimer (1994) report a mean birth velocity of $450 \pm 90\,\mathrm{km\,s^{-1}}$ for pulsars (i.e. neutron stars) and the processes that precede the birth of a stellar mass BH are essentially the same as the ones that precede the birth of a neutron star (Woosley et al. 2002). This suggests that a large fraction of the compact remnants (BHs as well as neutron stars) are born with velocities well above the escape velocity of the UCD-models in Tab. 1, which for a Plummer sphere is about twice the velocity dispersion (compare equations 8.59 and 8.61 in Kroupa 2008). Thus, in a realistic scenario, the total mass of the compact remnants *remaining* in the UCD is likely to be small compared to the total mass of the progenitors of *all* compact remnants. Moreover, the mass-loss histories created by the algorithm described in Section 4.2.2 suggest that the UCDs are gas-free at the end of the evolution of massive stars, with the exception of the models with high initial mass and low heating efficiency. The latter models suggest however that the UCDs consist mainly of gas at that time, which seems unlikely (see Section 4.3.3). As a conclusion, UCDs are likely to have lost most of the mass that was locked in massive stars at the time when massive stars have evolved, if they formed as is assumed here (i.e. as very massive star clusters). This mass loss proceeds however not only by the escape of the gaseous components of the SN-remnants from the UCD (i.e. a process modelled by the algorithm in Section 4.2.2), but also by the ejection of the compact remnants. This latter process would play a substantial role for the total mass loss of the UCD if $m_{\mathrm{BH}} = 0.5m_*$, but not if $m_{\mathrm{BH}} = 0.1m_*$.

Note that the expectation of a large difference between the total mass of the compact remnants left in UCDs and the total mass of their progenitors is also the reason why the IMFs of the UCDs have to be so extremely top-heavy, if the enhanced M/L_V ratios of the UCDs are to be explained by an over-abundance of stellar remnants. This is what motivated the sometimes

extreme choices for the IMF in the UCD-models in the first place.

In essence, neglecting the remnant masses seems justifiable in the context of the present study, as it also helps to avoid a number of very speculative assumptions. This includes the precise mass of the remnants, which fraction of them remains in the UCDs and how much of the kinetic energy available from the SNe is transferred to them. As a result, the mass loss is over-estimated in the UCD-models, but probably not by much more than 10 per cent. Consequently, their expansion is over-estimated as well by about the same amount, if the heating is sufficient to expel all gas from them. This bias is thus opposed to the bias induced by the assumption of adiabatic mass loss at all times in the calculation of the mass loss histories.

We note that also the treatment of the energy input from SNe (each of them contributes $10^{51}\,\mathrm{erg}$) and the energy input from stars (equation 4.15 using equation 4.16) is only approximate, but can hardly be done with greater precision with current knowledge.

4.2.3 Time evolution of the UCDs

The UCD-models are set up to be in virial equilibrium before the onset of mass loss. This is motivated by the fact that star-formation in a star cluster takes place on a time-scale of ≈ 1 Myr, while the crossing times in the UCD-models are about an order of magnitude lower (see Table 4.1) and the time-scale for violent relaxation is a few crossing times (Binney & Tremaine 1987). Thus, the time-scale for the UCD-model to settle into a state near virial equilibrium is shorter than the time-scale for the formation of its stellar population. Note that the assumption of virial equilibrium is crucial for the validity of the results in this paper, since UCDs would evolve completely different if they were not in virial equilibrium at the onset of gas expulsion, see Goodwin (2009). But it is also argued there that very massive star clusters are much more likely to be in virial equilibrium at that time.

To calculate the evolution of the UCDs in the first few Myr the particle-mesh code Superbox (Fellhauer et al. 2000) is used. Each UCD is represented by 1 million particles and is integrated forward in time until 200 Myr using a small time-step of 0.01 Myr for the models with HE=1 and SFE=1 and a time-step of 0.005 Myr for all models with SFE=0.4. The smaller time-step for the models with SFE=0.4 is necessary because of their shorter crossing times due to their higher initial masses for our assumed stellar masses, see Table 4.1. The code is altered to allow for the mass loss due to gas expulsion and rapid stellar evolution in the first tens of Myr. To mimick this mass loss we implemented the look-up tables whose generation is described in Section 4.2.2. They give the total mass of the UCD at each time-step. The mass of each particle and henceforth the total mass of the modelled UCD is reduced accordingly.

The UCDs are modelled in isolation, i.e. in the absence of a tidal field, even though UCDs are found in the vicinity of massive elliptical galaxies. But regarding the short time span of our computations of 200 Myr (compared to their orbital times of a Gyr or longer) and the fact that e.g. at a distance of 80 kpc and adopting the potential of M 82 the tidal radii would be 600 pc for the models with $M_{\mathrm{pl},0} = 10^7\,\mathrm{M}_\odot$ and 1400 pc for the models with $M_{\mathrm{pl},0} = 10^8\,\mathrm{M}_\odot$, the effect of the tidal fields can be neglected. (See also table 6 in Hilker et al. 2007 and table 8 in Evstigneeva et al. 2007 for a comparison between half-light radii and tidal radii of UCDs.)

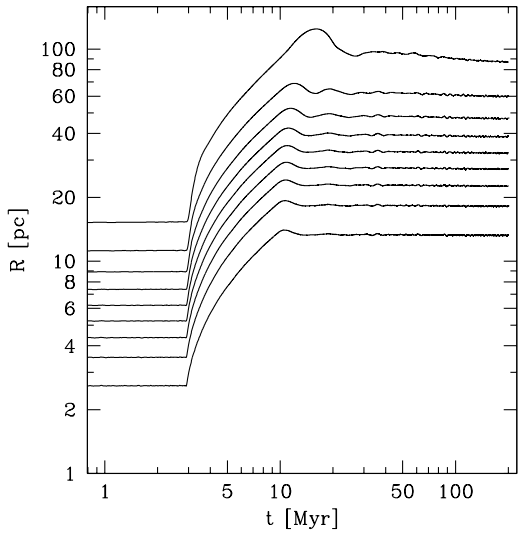

Figure 4.7: Change of the Lagrangian radii (10, 20, ... 90 per cent mass) with time for model m8_r5_s1_h1 with IMF 1 ($m_{\rm max} = 150\,{\rm M}_\odot$, $\alpha = 1.1$).

4.3 Results

We calculated a suite of 56 models, combining each of the sets of UCD parameters given in Table 4.1 with each IMF given in Table 4.2. The results are discussed separately for the different assumptions regarding the SFE and the HE in the following, see also Tables 4.4, 4.5 and 4.6.

4.3.1 SFE=1

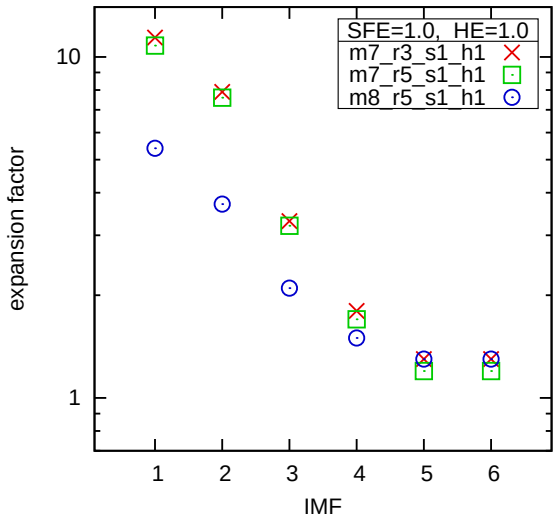

Figure 4.8: Expansion factors $f_{\rm e}$ of our models for a star formation efficiency of 1 and a heating efficiency of 1 plotted against the number given to the assumed IMF (as in Table 4.2). The symbols show the different initial structural parameters of the UCD-models: (red) crosses for $R_{\rm pl,0} = 3\,{\rm pc}$ and $M_{\rm pl,0} = 10^7\,{\rm M}_\odot$, (green) squares for $R_{\rm pl,0} = 5\,{\rm pc}$ and $M_{\rm pl,0} = 10^7\,{\rm M}_\odot$ and (blue) circles for $R_{\rm pl,0} = 5\,{\rm pc}$ and $M_{\rm pl,0} = 10^7\,{\rm M}_\odot$.

Table 4.4: Final results of the calculations for a SFE of 1 and a HE of 1. The models whose final parameters match the observed parameters of UCDs best are marked with a (+) before the first column. The information given in the columns is the following: Column 1: the name of the model as given in Table 4.1, Column 2: the IMF as given in Table 4.2, Column 3: the total mass of stars that have not evolved at the end of massive-star evolution (i.e. stars with $m < 8\,\mathrm{M}_\odot$) in units of the initial total mass of all stars, Column 4: the total mass of stars that remain bound to the cluster in units of the total mass of all stars less massive than $8\,\mathrm{M}_\odot$ (i.e. no stars become unbound if the entry in this column is 1), Column 5: the mass of the cluster at the end of the calculation, Column 6: the final half-mass radius, Columns 7 and 8: the final Plummer-radius $R_{\rm pl,f}$ and its 1-σ error, Column 9: the expansion factor $f_{\rm e}$, Columns 10 and 11: the central surface density $\Sigma_{0,\rm f}$ with its error, Columns 12 and 13: and the central line-of-sight velocity dispersion $\sigma_{0,\rm f}$ with its error. $\Sigma_{0,\rm f}$ and $\sigma_{0,\rm f}$ are derived by fitting Plummer-profiles to the data at $t = 200$ Myr, using a non-linear least-squares Marquardt-Levenberg algorithm. Both the fits to $\Sigma_{0,\rm f}$ and to $\sigma_{0,\rm f}$ also deliver estimates for $R_{\rm pl,f}$. The quoted value for $R_{\rm pl,f}$ is the one obtained from the fit to $\Sigma_{0,\rm f}$, but the one obtained from the fit to $\sigma_{0,\rm f}$ is not much different.

	model	IMF	$M_{*,\rm f}/M_{*,0}$	$M_{*\rm b,f}/M_{*,f}$	$M_{\rm f}$ [$10^6\mathrm{M}_\odot$]	$R_{50,\rm f}$ [pc]	$R_{\rm pl,f}$ [pc]	error	$f_{\rm e}$	$\Sigma_{0,\rm f}$ [$\mathrm{M}_\odot\,\mathrm{pc}^{-2}$]	error	$\sigma_{0,\rm f}$ [$\mathrm{km\,s}^{-1}$]	error
	m7_r3_s1_h1	1	0.079	0.952	0.75	30.6	34.1	0.2	11.4	241	1	4.19	0.02
	m7_r5_s1_h1	1	0.079	0.850	0.67	52.2	53.9	0.9	10.8	17	0	3.02	0.02
	m8_r5_s1_h1	1	0.079	0.998	7.8	26.2	27.1	0.1	5.4	3869	2	21.65	0.07
	m7_r3_s1_h1	2	0.114	0.973	1.11	22.3	23.7	0.1	7.9	736	2	6.09	0.02
	m7_r5_s1_h1	2	0.114	0.953	1.09	37.4	38.0	0.2	7.6	280	1	4.77	0.02
(+)	m8_r5_s1_h1	2	0.114	1.000	11.4	18.4	18.6	0.1	3.7	12069	22	31.36	0.07
	m7_r3_s1_h1	3	0.281	0.999	2.81	9.6	10.0	0.0	3.3	10324	11	14.52	0.06
	m7_r5_s1_h1	3	0.281	0.998	2.80	16.1	16.0	0.1	3.2	4131	8	11.60	0.04
(+)	m8_r5_s1_h1	3	0.281	1.000	28.1	10.8	10.7	0.0	2.1	90300	120	55.20	0.30
(+)	m7_r3_s1_h1	4	0.547	1.000	5.47	5.1	5.3	0.0	1.8	70370	170	27.50	0.02
(+)	m7_r5_s1_h1	4	0.547	1.000	5.47	8.6	8.5	0.0	1.7	28286	27	21.90	0.30
	m8_r5_s1_h1	4	0.547	1.000	54.7	7.4	7.4	0.0	1.5	363990	310	82.50	0.80
	m7_r3_s1_h1	5	0.770	1.000	7.70	3.8	3.9	0.0	1.3	181300	800	37.60	0.50
(+)	m7_r5_s1_h1	5	0.770	1.000	7.70	6.3	6.2	0.0	1.2	73630	140	30.20	0.30
	m8_r5_s1_h1	5	0.770	1.000	77.0	6.3	6.4	0.0	1.3	678800	1400	98.30	1.10
	m7_r3_s1_h1	6	0.787	1.000	7.87	3.7	3.8	0.0	1.3	191560	960	38.40	0.20
(+)	m7_r5_s1_h1	6	0.787	1.000	7.87	6.2	6.1	0.0	1.2	78050	440	30.70	0.30
	m8_r5_s1_h1	6	0.787	1.000	78.7	6.3	6.3	0.0	1.3	713800	1100	100.30	1.20

The assumptions SFE=1 and HE=1 stand for the case of highly efficient star-formation and heating. There is no expulsion of primordial gas in this case, but the mass loss through the evolution of massive stars can still be quite severe (as the UCD is cleared easily from the products of stellar evolution with such a high HE). It amounts to up to about 90 per cent of the initial mass for the UCDs with the most top-heavy IMFs. However, this mass loss is slow compared to the short crossing-times of the initially very massive and compact models. This makes sure that the calculated UCDs always survive this period of mass loss. In Fig. 4.7, the time evolution of the Lagrangian radii of one of the models is shown. It can be seen clearly that after an interval of rapid expansion due to the mass loss the UCD-model finally settles back into a new equilibrium. The expansion factor $f_{\rm e}$ of the models is measured by comparing the final ($R_{\rm pl,f}$) with the initial ($R_{\rm pl,0}$) Plummer-radius,

$$f_{\rm e} \quad = \quad \frac{R_{\rm pl,f}}{R_{\rm pl,0}}. \tag{4.19}$$

The Plummer-radii are found by fitting Plummer-models to the surface density profiles of the UCDs, using a non-linear least-squares Marquardt-Levenberg algorithm. The Plummer-radius is also identical to the projected half-light radius for the models (see equation 8.57 in Kroupa 2008). Fig. 4.8 shows the expansion factors for all UCD-models with SFE=1 and HE=1. It is visible that among the clusters with top-heavy IMFs (IMFs 1 to 4) the UCD-models with the highest mass expand the least. This is because the more massive UCD-models have shorter crossing times and are therefore closer to the regime of adiabatic mass loss.

Table 4.4 shows the final quantities for the models with SFE=1 and HE=1. The models that are the best representations of present-day UCDs at the end of the calculation are marked with a '(+)' in front of the first column. Note that some, but not all of these have the canonical high-mass IMF slope.

We note that assuming HE=1 is not decisive for most of the UCD-models with SFE=1. For instance, if HE=0.03 is assumed for the UCD-models with an initial stellar mass, $M_{*,0}$, of 10^7 $\mathrm{M}_\odot$ and SFE=1, the mass-loss histories of such models are the same as in the case of HE=1. The same is true for UCD-models with 10^8 $\mathrm{M}_\odot$ SFE=1 and HE=0.03 if their IMF is the canonical one. On the other hand, for the two most top-heavy IMFs in Tab. 4.2 (IMFs 1 and 2, $\alpha = 1.1$), the UCD-models with 10^8 $\mathrm{M}_\odot$ and SFE=1 retain most of the gas released by the evolution of massive if HE=0.03, while they are gas-free at all times if HE=1. In the case of H=0.03, these models are very similar to the UCD-models with 10^8 $\mathrm{M}_\odot$, SFE=0.4 and HE=0.03, which are discussed in Section 4.3.3.

Thus, it is UCD-models with the most top-heavy IMFs that retain gas the easiest. This is because by assuming that the amount of energy released by a SN does not depend on the mass of the progenitor star (as done in this paper), the total mass set free by the SNe increases more quickly than the total energy provided by the SNe. Also, the luminosity of the stellar population of the UCD, which is the other energy source that powers its mass loss, decreases more rapidly with time for more top-heavy IMFs.

4.3.2 SFE=0.4 and HE=1

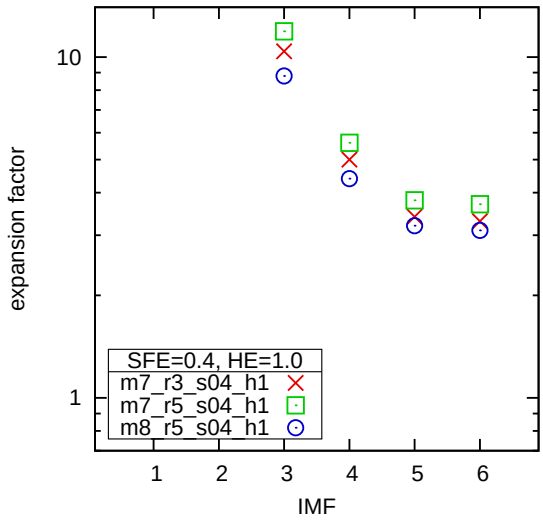

Figure 4.9: Expansion factors $f_{\rm e}$ of the models with a star formation efficiency of 0.4 and a heating efficiency of 1 plotted against the number assigned to the assumed IMF (as in Table 4.2). The symbols show the different inital structural parameters of the UCD-models: (red) crosses for $R_{\rm pl,0} = 3$ pc and $M_{\rm pl,0} = 2.5 \times 10^7$ M$_\odot$, (green) squares for $R_{\rm pl,0} = 5$ pc and $M_{\rm pl,0} = 2.5 \times 10^7$ M$_\odot$ and (blue) circles for $R_{\rm pl,0} = 5$ pc and $M_{\rm pl,0} = 2.5 \times 10^7$ M$_\odot$. The modelled UCDs with IMFs 1 and 2 dissolve completely due to their heavy mass loss.

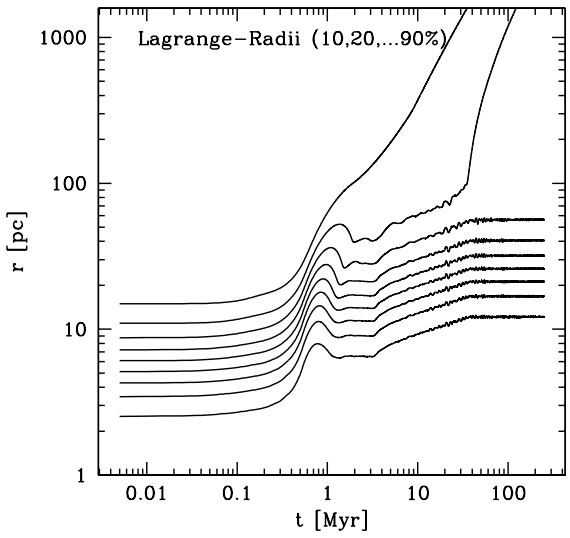

Figure 4.10: As Fig. 4.7, but for model m8_r5_s04_h1 with IMF 4 ($m_{\rm max} = 100$ M$_\odot$, $\alpha = 1.9$).

Table 4.5: As Table 4.4, but for a SFE of 0.4 and a HE of 1. These models predict the complete dissolution of the UCD if IMF 1 or IMF 2 are assumed (the ones with high-mass slope $\alpha = 1.1$).

	model	IMF	$M_{*,\mathrm{f}}/M_{*,0}$	$M_{*\mathrm{b,f}}/M_{*,f}$	M_{f} [$10^6\mathrm{M}_\odot$]	$R_{50,\mathrm{f}}$ [pc]	$R_{\mathrm{pl,f}}$ [pc]	error	f_{e}	$\Sigma_{0,\mathrm{f}}$ [$\mathrm{M}_\odot\,\mathrm{pc}^{-2}$]	error	$\sigma_{0,\mathrm{f}}$ [$\mathrm{km\,s}^{-1}$]	error
	m7_r3_s04_h1	1	0.079	UCD dissolves completely									
	m7_r5_s04_h1	1	0.079	UCD dissolves completely									
	m8_r5_s04_h1	1	0.079	UCD dissolves completely									
	m7_r3_s04_h1	2	0.114	UCD dissolves completely									
	m7_r5_s04_h1	2	0.114	UCD dissolves completely									
	m8_r5_s04_h1	2	0.114	UCD dissolves completely									
	m7_r3_s04_h1	3	0.281	0.236	0.66	30.3	33.4	0.5	10.4	298	2	8.27	0.16
	m7_r5_s04_h1	3	0.281	0.125	0.35	51.3	60.8	1.9	11.9	53	1	4.49	0.06
	m8_r5_s04_h1	3	0.281	0.482	13.5	42.9	46.7	0.6	8.8	3115	16	30.95	0.30
	m7_r3_s04_h1	4	0.547	0.460	2.52	19.0	16.0	0.1	5.0	3615	11	19.89	0.47
	m7_r5_s04_h1	4	0.547	0.234	1.28	28.8	28.6	0.4	5.6	672	4	11.41	0.22
(+)	m8_r5_s04_h1	4	0.547	0.784	26.4	25.6	23.3	0.1	4.4	32182	33	70.43	0.88
	m7_r3_s04_h1	5	0.770	0.626	4.82	13.6	10.9	0.1	3.4	14495	35	33.46	0.50
(+)	m7_r5_s04_h1	5	0.770	0.300	2.31	21.4	19.2	0.1	3.8	2429	8	18.22	0.51
	m8_r5_s04_h1	5	0.770	0.896	69.0	19.2	16.7	0.0	3.2	96070	120	102.64	1.87
	m7_r3_s04_h1	6	0.787	0.671	5.28	13.2	10.5	0.0	3.3	16898	32	35.52	1.44
(+)	m7_r5_s04_h1	6	0.787	0.322	2.53	21.3	19.0	0.2	3.7	2723	11	18.97	0.54
	m8_r5_s04_h1	6	0.787	0.911	71.7	18.9	16.4	0.0	3.1	103396	80	105.38	1.94

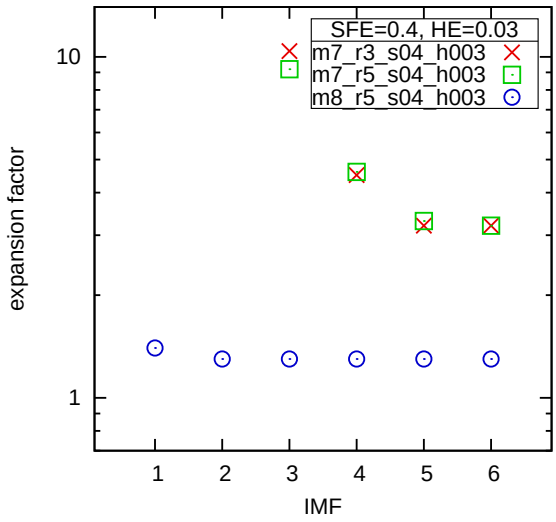

Figure 4.11: As Fig. 4.9, but for a heating efficiency of 0.03 instead of 1. The modelled UCDs with $M_{*,0} = 10^7$ $M_\odot$ and IMFs 1 or 2 dissolve completely due to their heavy mass loss and are therefore not shown here.

The assumptions SFE=0.4 and HE=1 imply an even more dramatic mass loss than the case of SFE=1 and HE=1 (Section 4.3.1). The energy input of massive stars is high enough to clear the UCD-models of the primordial gas either well before or at the time the first stars end their evolution on the main-sequence. The mass loss is in fact so rapid that a significant fraction of the stars of the UCD-models become unbound, even if an IMF with the canonical high-mass slope ($\alpha = 2.3$, IMFs 5 and 6) is assumed. The calculated UCD-models dissolve completely if the IMFs with the flattest high-mass IMF-slopes ($\alpha = 1.1$, IMFs 1 and 2) are assumed. Note that they are dissolved by the *combination* of the very rapid expulsion of the primordial gas and the more gentle mass loss though stellar evolution, since an instantaneous loss of 60 per cent of the initial mass would still leave a bound remnant (Boily & Kroupa 2003), as would the mass loss through stellar evolution alone (cf. Section 4.3.1).

Analogous to Section 4.3.1, the expansion of the UCD-models is measured by the ratio between their final Plummer-radii and their initial Plummer-radii and the results are plotted in Fig. 4.9. It turns out that in this set of models, the UCDs that expand the most are always the ones with the longest crossing times while the UCDs that expand the least are always the ones with the highest initial mass.

Table 4.5 shows the final quantities for the models with SFE=0.4 and HE=1. Model m8_r5_s04_h1 with IMF 4 ($\alpha = 1.9$) is the only one of them with a top-heavy IMF and with a good agreement between its final parameters and the parameters observed in UCDs. The evolution of its Lagrange-radii is shown in Fig. 4.10.

4.3.3 SFE=0.4 and HE=0.03

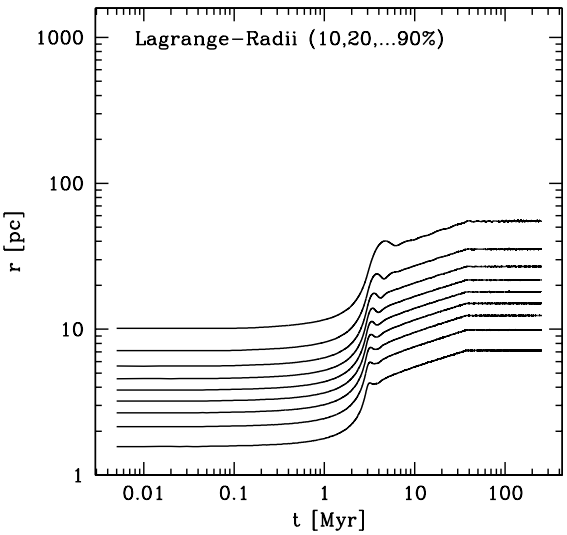

Figure 4.12: As Fig. 4.7, but for model m7_r3_s04_h003 with IMF 4 ($m_{\max} = 100\,\mathrm{M}_\odot$, $\alpha = 1.9$).

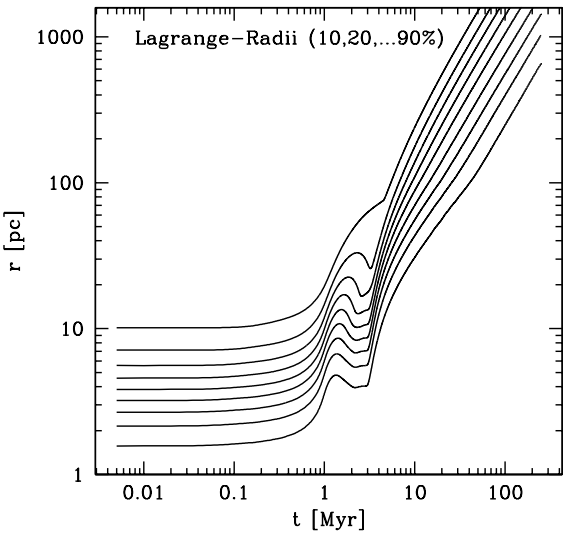

Figure 4.13: Change of the Lagrangian radii (10, 20, ... 90 per cent mass) with time for model m7_r3_s04_h003 with IMF 1 ($m_{\max} = 150\,\mathrm{M}_\odot$, $\alpha = 1.1$). Here the UCD is disrupted by its mass loss, unlike the models shown in Figures. 4.7, 4.10 and 4.12.

Table 4.6: As table 4.4, but for a SFE of 0.4 and a HE of 0.03. These models predict the complete dissolution of the UCD if IMF 1 or IMF 2 and an initial total mass of 2.5×10^7 $M_\odot$ are assumed. The models with an initial total mass of 2.5×10^8 $M_\odot$ on the other hand keep most of their primordial gas and therefore their evolution is completely different.

	model	IMF	$M_{*,\mathrm{f}}/M_{*,0}$	$M_{*\mathrm{b,f}}/M_{*,f}$	M_f [$10^6 M_\odot$]	$R_{50,\mathrm{f}}$ [pc]	$R_{\mathrm{pl,f}}$ [pc]	error	f_e	$\Sigma_{0,\mathrm{f}}$ [$M_\odot$ pc^{-2}]	error	$\sigma_{0,\mathrm{f}}$ [km s^{-1}]	error
	m7_r3_s04_h003	1	0.079	UCD dissolves completely									
	m7_r5_s04_h003	1	0.079	UCD dissolves completely									
	m8_r5_s04_h003	1	0.079	0.997	188.8	8.8	7.2	0.0	1.4	55622	65	271.1	20.9
	m7_r3_s04_h003	2	0.114	UCD dissolves completely									
	m7_r5_s04_h003	2	0.114	UCD dissolves completely									
	m8_r5_s04_h003	2	0.114	0.997	196.5	8.5	7.0	0.0	1.3	86030	150	282.80	23.80
	m7_r3_s04_h003	3	0.281	0.742	2.09	29.0	28.1	0.2	10.4	1164	3	14.64	0.17
	m7_r5_s04_h003	3	0.281	0.469	1.32	42.5	46.8	0.6	9.2	308	1	9.69	0.11
	m8_r5_s04_h003	3	0.281	0.997	200.0	8.4	6.9	0.0	1.3	215810	340	287.40	24.70
(+)	m7_r3_s04_h003	4	0.547	0.944	5.16	17.2	14.5	0.0	4.5	9278	9	29.66	0.43
	m7_r5_s04_h003	4	0.547	0.835	4.57	25.9	23.3	0.0	4.6	3376	6	22.73	0.30
	m8_r5_s04_h003	4	0.547	0.996	202.4	8.4	6.8	0.0	1.3	424440	500	290.70	25.60
(+)	m7_r3_s04_h003	5	0.770	0.978	7.53	12.4	10.3	0.0	3.2	26578	18	42.36	0.79
(+)	m7_r5_s04_h003	5	0.770	0.906	6.98	18.9	16.6	0.0	3.3	9973	140	33.06	0.58
	m8_r5_s04_h003	5	0.770	0.996	208.4	8.2	6.7	0.0	1.3	623290	640	299.50	27.70
(+)	m7_r3_s04_h003	6	0.787	0.980	7.71	12.2	10.1	0.0	3.2	28116	25	43.33	0.82
(+)	m7_r5_s04_h003	6	0.787	0.919	7.23	18.7	16.2	0.0	3.2	10697	17	33.76	0.58
	m8_r5_s04_h003	6	0.787	0.996	208.4	8.2	6.7	0.0	1.3	633900	16	298.90	27.00

In the case of a moderately high star formation efficiency (SFE=0.4) and and low heating efficiency (HE=0.03), the UCD-models with $M_{\rm pl,0} = 2.5 \times 10^7$ M$_\odot$ are gas-free at the end of the computation (as are all models with HE=1). In contrast to that, the models with $M_{\rm pl,0} = 2.5 \times 10^8$ M$_\odot$ keep most of the gas at such a low HE, so that these UCD-models are predicted to expand barely and to consist mainly of gas at the end of the integration, implying very high M/L_V ratios. (In the two most extreme cases, where the high-mass IMF slope is $\alpha = 1.1$, approximately 5 per cent of the total mass of the UCD-model is stars at that time, while the rest is gas.) This is a very implausible situation. It is more likely that if the heating efficiency is too low to drive the gas out of the cluster, the star formation efficiency would become higher through new star formation episodes, until eventually all matter is locked up in low-mass stars and thereby a SFE of 1 is approached.

However, the half-mass radius of a UCD would hardly change with time in this case, since it keeps most of its initial mass (cf. equation 4.17), while the initial half-mass radii of UCDs suggested in this paper are clearly smaller than the half-mass radii of observed present-day UCDs (cf. table 5 in Mieske et al. 2008). This means that, if a UCD indeed retains most of its mass, it must be born with an initial half-mass radius close to the observed values. By calculating mass-loss histories of UCD-models with $M_{\rm pl,0} = 2.5 \times 10^8$ M$_\odot$, SFE=0.4 and HE=0.03 for different initial Plummer radii (by the method described in Section 4.2.2), it turns out that the energy input from massive stars is sufficient to remove all gas from these UCD-models at an initial projected half-mass radius (i.e. Plummer radius) of 12 pc instead of 5 pc, even if the UCD-models have the canonical IMF. In contrast to that, the most massive observed UCDs, with masses of $\approx 10^8$ M$_\odot$, are reported to have half-mass radii of ≈ 100 pc. Thus, adopting a major star burst as the scenario for the birth of a UCD (as done in this paper), an object that is able to keep gas after the star burst would be too compact to evolve into an UCD. On the other hand, if the object has an initial half-mass radius that allows it to evolve into a UCD, it would loose its gas on a time scale of a few Myr. This excludes the above scenario where a UCD forms a substantial part of its stellar population over a longer period of time after the initial star burst.

Fig. 4.11 depicts the expansion rates of the UCDs with SFE=0.4 and HE=0.03 and shows a strong difference between the modelled UCDs with $M_{\rm pl,0} = 2.5 \times 10^8$ M$_\odot$ and the ones with $M_{\rm pl,0} = 2.5 \times 10^7$ M$_\odot$. While the less massive UCD-models expand almost as much as in the case of HE=1 (see Sections 4.3.1 and 4.3.2), the extension of the more massive UCD-models hardly changes.

The final quantities found for the models with SFE=0.4 and HE=0.03 are shown in Table 4.6. Except for models with IMFs that have the canonical high-mass slope, only model m7_r3_s04_h003 with IMF 4 ($\alpha = 1.9$) is a good representation of a UCD. The time-evolution of its Lagrange-radii is shown in Fig. 4.12. Fig. 4.13 on the other hand illustrates the evolution of a UCD that dissolves completely because of extreme mass loss due to its very top-heavy IMF. The only difference to the model shown in Fig. 4.12 is that IMF 1($\alpha = 1.1$) instead of IMF 4 was assumed.

4.3.4 Implications on the initial parameters of UCDs

Based on the fraction of the mass that is lost from the modeled stellar systems and the factors by which they expand due to mass loss, initial conditions that would lead to UCD-like objects can be estimated. The results of such estimates are shown in Fig. 4.14. Thus, UCDs may have been born from extremely compact configurations with densities ranging up to $10^8 \mathrm{M}_\odot\,\mathrm{pc}^{-3}$. These

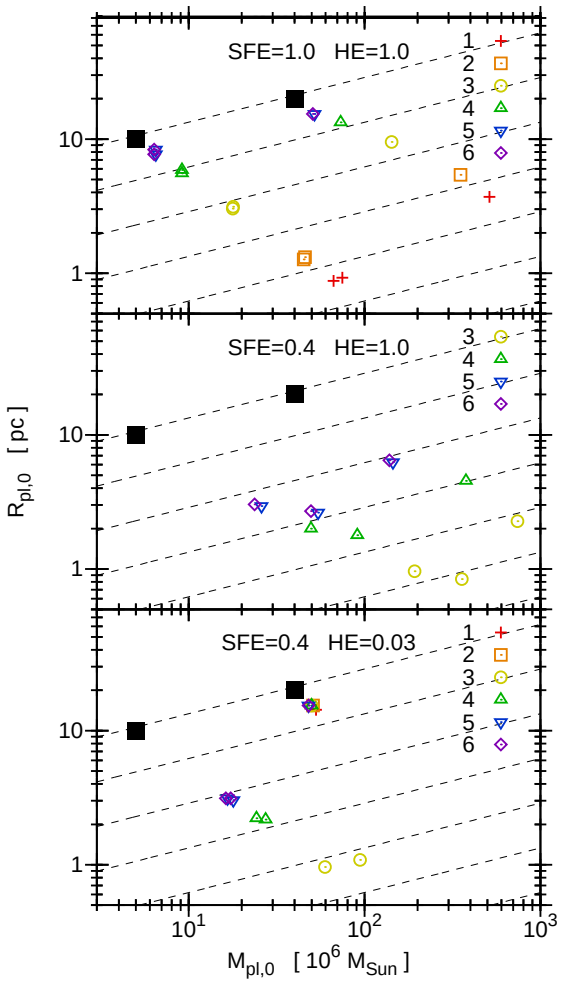

Figure 4.14: Estimated initial masses and Plummer-radii that would lead to representative, UCD-type objects. The black square to the left represents in each panel an observed typical small UCD with a mass of 5×10^6 $M_\odot$ and a Plummer radius of 10 pc, whereas the black square to the right represents an observed typical large UCD with a mass of 40×10^6 $M_\odot$ and a Plummer radius of 20 pc. The remaining symbols show estimated initial masses and Plummer-radii, that would lead to one of these two representative UCDs with the IMFs from Table 4.2, identified here by the number assigned to them in that table. The assumed star formation efficiency and heating efficiency are indicated at the top of each panel. For the more massive UCD-like object, the estimated initial parameters are based on the total mass loss (through stellar and dynamical evolution) and expansion factors of the models starting with a total stellar initial mass $M_{*,0} = 10^8$ $M_\odot$ (Table 4.1), while the estimates for the less massive UCD-like object are based on the models with $M_{*,0} = 10^7$ $M_\odot$ (Table 4.1). The dashed lines in each panel show constant central densities, starting from 10^3 $M_\odot\,pc^{-3}$ and increasing by a factor of ten downward with each line. Note that the initial conditions resulting in the more massive representative UCD in the lowermost panel (SFE=0.4 and HE=0.03) are based on models where hardly any gas is lost from the UCD-model while no more stars are formed from this material, which is a unrealistic scenario (see Section 4.3.3).

numbers have admittedly to be taken with caution, since the expansion factors and the total mass loss of the objects have been derived for stellar systems with different initial parameters, using mass loss histories through stellar processes that were specifically created for them. Note however the similarity between the expansion factors of models with the same initial mass and IMF, but different initial radii (Figs. 4.8, 4.9 and 4.11). Analogous calculations to the ones

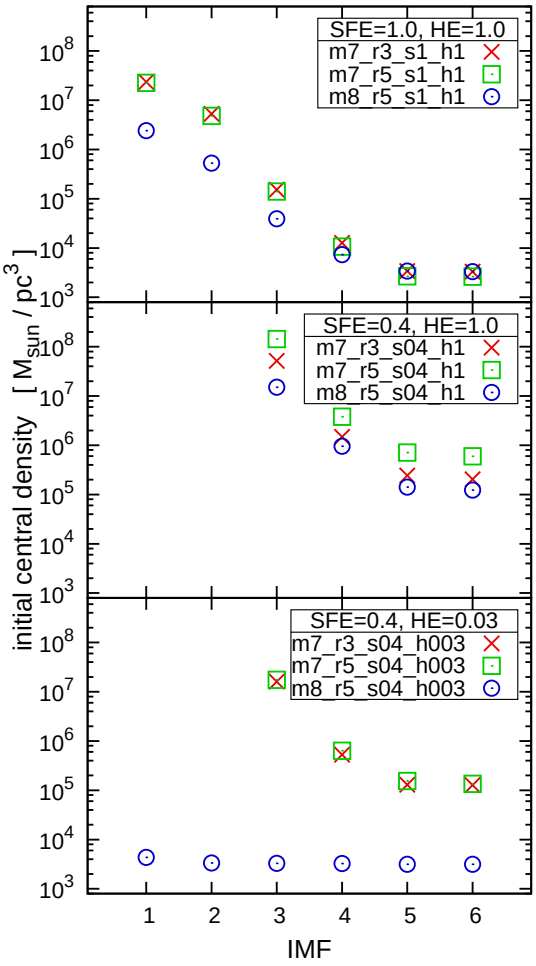

Figure 4.15: The initial central densities that would lead to the representative UCD-type objects shown as black squares in Fig. 4.14, given the mass losses and expansion factors of the UCD-models calculated in this paper for the IMFs listed in Table 4.2. It is assumed (as in Fig. 4.14) that the mass loss and the expansion experienced by an object that evolves into the more massive representative UCD (with a mass of 40×10^6 $M_\odot$ and a Plummer radius of 20 pc) is given by the mass losses and expansions calculated for the UCD-models that start with an initial total stellar mass of 10^8 $M_\odot$ (Table 4.1). The evolution of the less massive representative UCD (with a mass of 5×10^6 $M_\odot$ and a Plummer radius of 10 pc) from its initial state is thought to be consistent with the mass losses and expansion factors found for the UCD-models starting with an initial total stellar mass of 10^7 $M_\odot$ (Table 4.1). The central densities of the initial states of UCDs in this figure are thus given by the initial masses and Plummer radii assigned to them in Fig. (4.14), using equation (4.4) with $R = 0$.

performed here, but with the initial parameters plotted in Fig. 4.14 are therefore likely to lead to final parameters that represent the actual parameters of UCDs better, but this needs to be studied in follow-up work.

The initial central densities following from the pairs of initial masses and initial Plummer-radii plotted in Fig. 4.14 are shown in Fig. 4.15. The initial parameters that would lead to UCD-type objects according to Figs. 4.14 and 4.15 can be compared to the initial parameters of the UCD-models listed in Tab 4.1, whose early evolution was calculated in this paper. It thereby becomes apparent that the initial conditions resulting in UCDs may be even more extreme than the ones that are specified in Table 4.1. Thus, encounters of proto-stars with stars, as discussed

in Section 4.2.1, may be even more relevant for the star formation in actual UCDs than for the UCD-models calculated in this paper. The UCDs may even have been dense enough for frequent collisions between stars, so that this process could also have shaped their IMF (cf. Bonnell et al. 1998).

Note the similarity of Figs. (4.8) (4.9) and (4.11) with the corresponding panels of Fig. (4.15), except for the different scaling. This is because the expansion factor enters with the third power into the calculation of the initial density for a given final mass and final Plummer-radius according to equation (4.4), while the dependency on the lost mass is only linear.

Also note that the negligence of compact remnants induces a bias on the estimated initial parameters: Remnants kept by the UCD-model diminish the mass that leaves the UCD-model and thereby also reduce its expansion. For arriving at the mass and the Plummer radius of the representative UCD-type objects plotted in Fig. 4.14, a UCD-model that keeps some of the mass of the massive stars in the form of remnants would thus need a larger initial radius and a smaller initial mass than a UCD-model that looses all remnants from massive stars. Consequently, the initial density of the UCD-model that keeps some remnants would also be smaller. The total mass of the remnants remaining in the UCDs has however been argued unlikely to be much larger than 10 per cent of the total mass of their progenitor stars (Section 4.2.2) and the bias on the initial parameters shown in Fig. 4.14 would be of the same order. The large implied mass-loss through the evolution of massive stars does not contradict the high M/L_V ratios of UCDs, if the number of massive stars was sufficient in them, i.e. their IMF was top-heavy enough (cf. Dabringhausen et al. 2009).

The bias caused by the the negligence of compact remnants may however be alleviated by an opposed bias. This opposed bias comes from the fact that non-adiabatic behaviour of the UCD-models was taken into account in the actual calculation of their dynamical behaviour, but not in the modelling of the mass loss driving the early evolution of the UCD-models (see Section 4.2.2).

4.4 Summary and conclusions

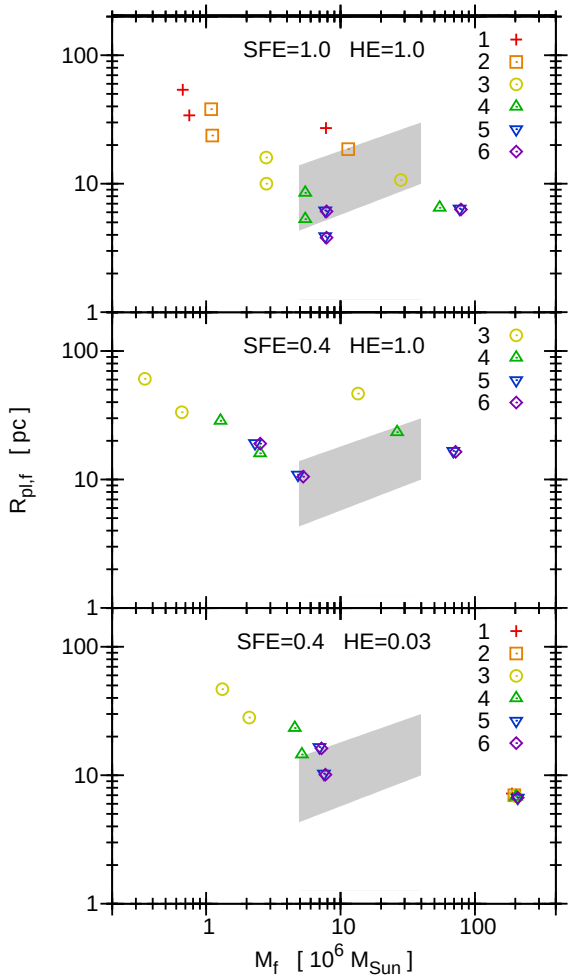

Figure 4.16: The final Plummer-radii against their final masses of all models that have not dissolved at the end of the integration. Different symbols encode different IMFs, identified by the numbers assigned to them in Tab 4.2. The assumed star formation efficiency and heating efficiency is given at the top of each panel. The shaded regions indicate the parameter space occupied by real UCDs.

Table 4.7: Consistency-check between the models for the remnant populations of the UCDs discussed in Dabringhausen et al. (2009) based on their dynamical M/L_V ratios with the models discussed here for their early dynamical evolution, assuming SFE=1 and HE=1 (for other SFEs and HEs see Section 4.4). Dabringhausen et al. (2009) consider two different ages for the UCDs. The first column specifies various remnant populations of the UCDs, as found in Dabringhausen et al. (2009). They differ by the mass of the SN remnants and which fraction of them remains bound to its host UCD. Concerning the kind of compact remnant a SN leaves, it is assumed that stars with initial masses between $8\ \mathrm{M}_\odot$ and $25\ \mathrm{M}_\odot$ become neutron stars with a mass of $1.35\ \mathrm{M}_\odot$. Stars with initial masses above $25\ \mathrm{M}_\odot$ become black holes with either 10 or 50 per cent of the initial mass of their progenitors ($m_{\mathrm{BH}} = 0.1\mathrm{or}\ 0.5\mathrm{m}_*$). The upper mass limit of the IMF is $100\ \mathrm{M}_\odot$ in all models. The second column displays the high-mass IMF slopes, $\overline{\alpha}$, which correspond to these remnant populations, given the mean dynamical M/L_V ratio of the UCDs (see Dabringhausen et al. (2009) for details). The uncertainties on $\overline{\alpha}$ are calculated from the uncertainties on the mean M/L_V ratios. Columns 3 to 5 indicate how consistent the models discussed in Dabringhausen et al. (2009) are with the ones discussed here. In this context, a '+' means that $\overline{\alpha} \pm 0.1$ agrees with the high-mass IMF slope in one of the UCD-models marked with a '(+)' in Table 4.4, i.e. $|\overline{\alpha} - \alpha| < 0.1$, where α is the high-mass slope of the IMF whose number according to Table 4.2 is given in brackets. A '$\bigcirc$' has an analogous meaning, but it is only required that $|\overline{\alpha} - \alpha| < 0.2$. A '$-$' indicates that a model with these initial condidtions can only reproduce final parameters as observed in UCDs with an IMF with $|\overline{\alpha} - \alpha| > 0.2$.

remnant population	$\overline{\alpha}$	m7_r3_h1_s1	m7_r5_h1_s1	m8_r5_h1_s1
	assumed age of 13 Gyr			
no SN remnants retained	$1.35^{+0.23}_{-0.17}$	$-$	$-$	$\bigcirc\ (3)$
20 per cent of the SN remnants retained, $m_{\mathrm{BH}} = 0.1m_*$	$1.57^{+0.17}_{-0.12}$	$-$	$-$	$+\ (3)$
20 per cent of the SN remnants retained, $m_{\mathrm{BH}} = 0.5m_*$	$1.78^{+0.13}_{-0.09}$	$\bigcirc\ (4)$	$\bigcirc\ (4)$	$-$
all SN remnants retained, $m_{\mathrm{BH}} = 0.1m_*$	$1.85^{+0.14}_{-0.10}$	$+\ (4)$	$+\ (4)$	$-$
	assumed age of 7 Gyr			
no SN remnants retained	$0.49^{+0.09}_{-0.08}$	$-$	$-$	$-$
20 per cent of the SN remnants retained, $m_{\mathrm{BH}} = 0.1m_*$	$1.04^{+0.05}_{-0.04}$	$-$	$-$	$+\ (2)$
20 per cent of the SN remnants retained, $m_{\mathrm{BH}} = 0.5m_*$	$1.34^{+0.04}_{-0.04}$	$-$	$-$	$\bigcirc\ (3)$
all SN remnants retained, $m_{\mathrm{BH}} = 0.1m_*$	$1.40^{+0.05}_{-0.04}$	$-$	$-$	$\bigcirc\ (3)$

We calculate the early evolution of extremely massive star clusters, using the particle-mesh code Superbox. Their initial radii are chosen in concordance with typical values for globular clusters (GCs), while their initial masses reflect the masses of ultra compact dwarf galaxies (UCDs). The early evolution of a star cluster is driven by mass loss through gas expulsion and stellar evolution. This mass loss is treated by reducing the mass of each particle in accordance with previously tabulated mass loss histories, so that the total mass of all particles agrees with the total mass of the UCDs as given in those tables. The rate and the magnitude of the mass loss depends in particular on the stellar initial mass function (IMF). Since it was suggested that UCDs may have formed with a top-heavy IMF (Dabringhausen et al. 2009), the integrations use mass loss tables not only for the canonical IMF but also with different top-heavy IMFs. A possible explanation for why the IMF in UCDs could be top-heavy is encounters between proto-stars and stars. If UCDs indeed formed as the most massive star clusters, as suggested in this paper, such encounters would be quite likely in emerging UCDs. In contrast, such encounters are not very probable in stellar systems that evolve into star clusters like the Orion nebula cluster. This implies that star formation in UCDs may be influenced by processes that do not play a significant role in less massive stellar systems. The final masses and Plummer-radii resulting from the calculations in this paper are shown in Fig. 4.16.

The possible initial conditions we uncover here (Figs. 4.14 and 4.15) include densities as high as $10^8\ \mathrm{M}_\odot\,\mathrm{pc}^{-3}$ for the forming UCDs with top-heavy IMFs ($\alpha \leq 1.9$). The supernova rates are at times as high as one per year in the UCD-models with with an initial stellar mass of $10^7\ \mathrm{M}_\odot$ and the most top-heavy IMFs (Fig. 4.4) and higher by a factor of 10 in the UCD-models with an initial stellar mass of $10^8\ \mathrm{M}_\odot$.

Starting from our initial conditions (Table 4.1), we seek those final models that represent UCDs in terms of their radii, masses and M/L_V-ratios in the following.

- If the UCDs form as star clusters with a high star-formation efficiency and a high heating efficiency (as discussed with the case SFE=1 and HE=1; see Section 4.3.1), the properties of present-day UCDs are reproduced from models with all IMFs in Table 4.2 except IMF 1, i.e. with stellar populations with high-mass IMFs in the whole range from $\alpha = 2.3$ (canonical IMF) to $\alpha = 1.1$ (see Table 4.4 and Fig. 4.16). The different models imply however different ages and different stellar remnant populations for the UCDs, because they are constrained by the average M/L_V ratio that is observed for UCDs (cf. table 3 in Dabringhausen et al. 2009). A consistency check between the models in this paper and the models in Dabringhausen et al. (2009) is provided in Table 4.7.Note that the model from Dabringhausen et al. (2009) where stars with an initial mass larger than $25\,\mathrm{M}_\odot$ are assumed to evolve into black holes that have 50 per cent of the mass of their progenitors and all compact remnants are thought to be retained by the UCD is not listed in Table 4.7. This is because it is not consistent with the assumption that UCDs loose most of the mass that was initially locked up in their massive stars. However, it seems likely that UCDs loose indeed most of this mass (see Section 4.2.2. The model from Dabringhausen et al. (2009) where all matter is kept within the UCDs is also omitted from Table 4.7, even though it would seem consistent with the UCD-models with initial stellar mass of $10^8\ \mathrm{M}_\odot$, a SFE of 0.4 and a HE of 0.03. These initial parameters lead however to a unrealistic situation at the end of the calculation, because the UCD-models that can evolve this way stay too compact for being consistent with real UCDs (see Section 4.3.3).

  As a result of the comparison shown in Table 4.7, the models with IMFs 5 and 6 (canonical high-mass IMF slope) can be excluded as formation scenarios for the UCDs as a class of

objects. This is because these models suggest that the M/L_V ratio is consistent with the ones predicted by simple stellar population models, which is not the case for UCDs (Dabringhausen et al. 2008; Mieske et al. 2008). The models with IMFs 5 and 6 would however be consistent with the UCDs in the Fornax Cluster if they are very old, because their average M/L_V ratio is somewhat lower than the ones of UCDs in general (Mieske et al. 2008).

- If the UCDs form as star clusters with a moderate star-formation efficiency and high heating efficiency (as discussed with the case SFE=0.4 and HE=1; see Section 4.3.2), extremely top-heavy IMFs ($\alpha = 1.1$) can be excluded because they would lead to the complete dissolution of the cluster. Model m8_r5_h1_s04 with IMF 4 ($\alpha = 1.9$) resembles a massive present-day UCD at the end of the integration. A comparison with table 3 in Dabringhausen et al. (2009) shows that this model is consistent with two cases listed there. The first of them is the case of the UCDs being 13 Gyr old, keeping 20 per cent of the SN remnants and black holes, which retain 50 per cent of the mass of their progenitor stars. The second is the case of the UCDs being 13 Gyr old, keeping all SN remnants and black holes having 10 per cent of the mass of their progenitor stars. These would be the only cases where a table analogous to Table 4.7 would indicate consistency between the UCD-models here and the ones in Dabringhausen et al. (2009). As in the case of SFE=1 and HE=1, the models with IMFs 5 and 6 (canonical high-mass IMF slope) can be excluded as formation scenarios for the UCDs as a class of objects, because of their too-low M/L_V ratio (Dabringhausen et al. 2008; Mieske et al. 2008).

- If the UCDs form as star clusters with a moderate star-formation efficiency and low heating efficiency (as discussed with the case SFE=0.4 and HE=0.03; see Section 4.3.3), the models with an initial mass of 2.5×10^8 $\mathrm{M}_\odot$ lead to the unrealistic case that gas of the order of 10^8 $\mathrm{M}_\odot$ is confined on a very small volume at the end of our calculations. Models starting with an initial mass of 2.5×10^7 $\mathrm{M}_\odot$ on the other hand dissolve for the two most top-heavy IMFs, like in the case of SFE=0.4 and HE=1. Model m7_r3_s04_h003 with IMF 4 ($\alpha = 1.9$) is similar to a small present-day UCD at the end of the calculation. A comparison with table 3 in Dabringhausen et al. (2009) shows that this model is consistent with two cases listed there. The first of them is the case of the UCDs being 13 Gyr old, keeping 20 per cent of the SN remnants and black holes, which retain 50 per cent of the mass of their progenitor stars. The second is the case of the UCDs being 13 Gyr old, keeping all SN remnants and black holes having 10 per cent of the mass of their progenitor stars. These would be the only cases where a table analogous to Table 4.7 would indicate consistency between the UCD-models here and the ones in Dabringhausen et al. (2009).

  Note the difference to the UCD-models with moderate SFE and high HE. In the case of a moderate SFE and high HE, consistency between the UCD-models from this paper and the models for the remnant populations of UCDs from Dabringhausen et al. (2009) is reached for a UCD-model starting with an initial stellar mass of 10^8 $\mathrm{M}_\odot$, whereas in the case of a moderate SFE and a low HE consistency is reached for a UCD-model starting with an initial stellar mass of 10^7 $\mathrm{M}_\odot$. The UCD-models from this paper are however in both cases consistent with the same models for the remnant populations of UCDs in Dabringhausen et al. (2009). As in the case SFE=1 and HE=1, the models with IMFs 5 and 6 (canonical high-mass IMF slope) can be excluded as formation scenarios for the

UCDs as a class of objects, because of their too-low M/L_V ratio (Dabringhausen et al. 2008; Mieske et al. 2008).

Thus, in summary, the preferred solution of the initial conditions problem for a SFE of 0.4 are a proto-UCD with a stellar initial mass of 10^8 $\mathrm{M}_\odot$ and a projected half-mass radius of 5 pc (HE=1) or a proto-UCD with a stellar initial mass of 10^7 $\mathrm{M}_\odot$ and a projected half-mass radius of 3 pc (HE=0.03). UCD-models with SFE=1 are discussed in Section 4.3.1 and for SFE=1 and HE=1, the preferred solutions are presented in Table 4.7.

The comparison between the final parameters of our models and observed parameters of present-day UCDs contain some uncertainties for initial parameters that lead to the formation of UCDs because of a number of approximations and simplifying assumptions (also see Section 4.2 for this matter). For instance, the density profiles of UCDs are usually better fitted by a King profile (King 1966) than by a Plummer profile. Also, the calculations performed here stop at 250 Myr, whereas UCDs are ≈ 10 Gyr old. Thus UCDs will have suffered from adiabatic mass loss through the evolution of intermediate-mass stars, if the material expelled by them is not used up in the formation of subsequent stellar populations. Finally, the tidal field of the host galaxy of the UCD may play a role for its evolution on a Gyr time-scale. The performed comparison demonstrates however that also the more rapid early mass loss triggered by an over-abundance of massive stars does not necessarily lead to complete dissolution of massive, dense stellar systems, but can result in objects similar to a UCD. The existence of UCDs is therefore not in contradiction with their formation with a top-heavy IMF. In a number of cases, a top-heavy IMF leads to a strong inflation of the modelled UCDs, but does not completely disintegrate them.

Acknowledgements

JD acknowledges support through DFG grant KR1635/13. MF was supported through GEMINI project no. 32070002.

Chapter 5

Low-mass X-ray binaries indicate a top-heavy stellar initial mass function in ultra compact dwarf galaxies

J. Dabringhausen, P. Kroupa, J. Pflamm-Altenburg, S. Mieske, 2012, **ApJ**, 747, 72

Abstract:

It has been shown before that the high mass-to-light ratios of ultra compact dwarf galaxies (UCDs) can be explained if their stellar initial mass function (IMF) was top-heavy, i.e. that the IMF was skewed towards high mass stars. In this case, neutron stars and black holes would provide unseen mass in the UCDs. In order to test this scenario with an independent method, we use data on which fraction of UCDs has a bright X-ray source. These X-ray sources are interpreted as low-mass X-ray binaries (LMXBs), i.e. binaries where a neutron star accretes matter from an evolving low-mass star. We find that LMXBs are indeed up to 10 times more frequent in UCDs than expected if the IMF was invariant. The top-heavy IMF required to account for this overabundance is the same as needed to explain the unusually high mass-to-light ratios of UCDs and a top-heavy IMF appears to be the only simultaneous explanation for both findings. Furthermore, we show that the high rate of type II supernovae (SNII) in the star-burst galaxy Arp 220 suggests a top-heavy IMF in that system. This finding is consistent with the notion that star-burst galaxies are sites where UCDs are likely to be formed and that the IMF of UCDs is top-heavy. It is estimated that the IMF becomes top-heavy whenever the star formation rate per volume surpasses $0.1\,\mathrm{M}_\odot\,\mathrm{yr}^{-1}\,\mathrm{pc}^{-3}$ in pc-scale regions.

5.1 Introduction

The stellar initial mass function (IMF) quantifies the distribution of stellar masses in a newly born stellar population. Together with the dependency of stellar evolution on stellar mass and metallicity, as well as the rate at which stars are formed in the Universe, the shape of the IMF determines the chemical evolution of the Universe and how its stellar content changes with time. The shape of the IMF also has important implications for the evolution of star clusters. Thus, knowing the shape of the IMF is crucial for a broad variety of astrophysical problems.

Resolved stellar populations in the Milky Way and its satellites support the notion that the IMF does not depend on the conditions under which star formation takes place, but that the stellar masses are distributed according to a single IMF known as the *canonical* IMF (Kroupa 2001, 2002; Kumar et al. 2008; Bastian et al. 2010). Ultra compact dwarf galaxies (UCDs) on the other hand provide evidence for the opposite notion, namely that the IMF varies and is top-heavy.

These UCDs are stellar systems that have first been discovered in the Fornax galaxy cluster (Hilker et al. 1999). They have V-band luminosities between 10^6 and some 10^7 $\mathrm{L}_\odot$, but half-light radii of only about 50 pc or less (Drinkwater et al. 2003; Mieske et al. 2008). The confirmed UCDs are at distances where they cannot be resolved into stars with current telescopes, but constrains on their stellar populations can be set by quantities derived from their integrated spectra. One such quantity are the dynamical mass-to-light (M/L) ratios of UCDs, i.e mass estimates based on the density profile and the internal velocity dispersion of the UCDs (Haşegan et al. 2005; Hilker et al. 2007; Evstigneeva et al. 2007; Mieske et al. 2008). For a clear majority of the UCDs, the M/L ratios derived from their dynamics are higher than it would be expected if they were pure stellar populations that formed with the canonical IMF (Haşegan et al. 2005; Dabringhausen et al. 2008; Mieske et al. 2008). This has been taken as evidence for an IMF skewed towards high-mass stars (Dabringhausen et al. 2009), i.e. a top-heavy IMF. The elevated M/L ratios of UCDs would then be explained by a large population of neutron stars and black holes (hereafter called dark remnants), because the age of the UCDs (Evstigneeva et al. 2007; Chilingarian et al. 2008) implies that all massive stars in them have completed their evolution.

It is plausible that the IMF in UCDs is skewed towards high-mass stars. Molecular clouds massive enough to be the progenitors of UCDs become impenetrable for far-infrared radiation while they collapse and become a UCD-type star-cluster. Internal heating of the molecular cloud leads to a higher Jeans-mass in them preferring the formation of high-mass stars (Murray 2009). A molecular cloud can also be heated by an external flux of highly energetic cosmic rays originating from a local overabundance of type II supernovae increasing the local Jeans-mass (Papadopoulos 2010). With the young UCDs being very compact, also crowding of proto-stellar cores and their subsequent merging in young UCDs may lead to an overabundance of high-mass stars in them (Dabringhausen et al. 2010; Weidner et al. 2011).

However, the high M/L ratios of UCDs could in principle also be due to non-baryonic dark matter (DM), as was suggested by Goerdt et al. (2008) and Baumgardt & Mieske (2008). This is because dark remnants and non-baryonic DM would have the same effect on the M/L ratios of the UCDs, provided that a large enough amount of non-baryonic DM can gather within the UCDs. Note that that non-baryonic DM is an unlikely cause for the high M/L ratios of UCDs, since non-baryonic DM is predicted to gather on rather large scales while UCDs are very compact (Gilmore et al. 2007; Murray 2009). However, in order to exclude this possibility completely, the presence of a sufficient number of dark remnants has to be confirmed indepen-

dently by a method that does not rely on the fact that dark remnants are non-luminous matter like non-baryonic DM.

Such a method is searching for low-mass X-ray binaries (LMXBs) in UCDs. In these binary systems, a dark remnant and an evolving low-mass star are orbiting around each other. The expanding outer atmosphere of the low-mass companion is accreted by the dark remnant. This matter produces a characteristic X-ray signature. The number of LMXBs depends on the number of NSs and stellar-mass black holes (BHs) and thus on the IMF (Verbunt & Hut 1987; Verbunt 2003). This implies that stellar systems with a top-heavy IMF can be distinguished from stellar systems with the canonical IMF by an excess of LMXBs.

The formulation of the IMF that is used throughout this paper is introduced in Sec. (5.2). In Sec. (5.3), the LMXB-abundance in globular clusters (GCs) and UCDs in dependency of the IMF and this model is compared to observations. The type-II supernova rate in star-bursting galaxies in dependency of the top-heaviness of the IMF is discussed in Sec. (5.4). It is found in Sec. (5.3) and Sec. (5.4), respectively, that the UCDs and the star-bursting galaxy Arp 220 show indications for a top-heavy IMF. This suggests that the star formation rate per volume is perhaps the parameter that determines whether the IMF in that volume becomes top-heavy, as is argued in Sec. (5.5). Conclusions are given in Sec. (5.6).

5.2 The initial stellar mass function

A varying IMF can be formulated as

$$\xi(m) = k\, k_i\, m^{-\alpha_i}, \tag{5.1}$$

with

$$\begin{aligned} \alpha_1 &= 1.3, & 0.1 \leq \frac{m}{\mathrm{M}_\odot} &< 0.5, \\ \alpha_2 &= 2.3, & 0.5 \leq \frac{m}{\mathrm{M}_\odot} &< m_{\mathrm{tr}}, \\ \alpha_3 &\in \mathbb{R}, & m_{\mathrm{tr}} \leq \frac{m}{\mathrm{M}_\odot} &\leq m_{\mathrm{max}}, \end{aligned}$$

where m is the initial stellar mass, the factors k_i ensure that the IMF is continuous where the power changes and k is a normalization constant. $\xi(m)$ equals 0 if $m < 0.1\,\mathrm{M}_\odot$ or $m > m_{\mathrm{max}}$, where m_{max} is a function of the star-cluster mass (Weidner & Kroupa 2006; Weidner et al. 2010) and m_{tr} is the stellar mass at which the IMF begins to deviate from the canonical IMF. For $m_{\mathrm{tr}} = 1\,\mathrm{M}_\odot$, the formulation of the IMF used here is identical with the one used in Dabringhausen et al. (2009), so that results found here for this choice of m_{tr} can be compared to results in Dabringhausen et al. (2009). For $\alpha_3 = \alpha_2 = 2.3$, Equation (5.1) is the canonical IMF (Kroupa 2001, 2002). For $\alpha_3 < 2.3$, the IMF is top-heavy, implying more intermediate-mass stars and in particular more high-mass stars.

In the mass range of UCDs, m_{max} is not set by the mass of the stellar system, but by the observed mass limit for stars, $m_{\mathrm{max}*}$. Thus, $m_{\mathrm{max}} = m_{\mathrm{max}*}$ for all UCDs. The actual value of $m_{\mathrm{max}*}$ is, however, rather uncertain: Estimates range from the canonical value $m_{\mathrm{max}*} \approx 150\,\mathrm{M}_\odot$ (Weidner & Kroupa 2004; Oey & Clarke 2005) to $m_{\mathrm{max}*} \approx 300\,\mathrm{M}_\odot$ (Crowther et al. 2010, but see Banerjee et al. 2012). In this paper, $m_{\mathrm{max}*} = 150\,\mathrm{M}_\odot$ is assumed, but note that assuming $m_{\mathrm{max}*} = 300\,\mathrm{M}_\odot$ instead would have little effect on the results reported here (see Section 5.3.3 and Figure 5.7).

In the case of GCs and UCDs with LMXBs (see Section 5.3), the observed luminosity, L, is known to originate from stars with masses $m \lesssim 1\ \mathrm{M}_\odot$. This is because their stellar populations are old (Evstigneeva et al. 2007; Chilingarian et al. 2008) and the more massive stars have already completed their evolution. Being fixed by observations, L should however not be changed when the IMF is varied. For the IMF given by Equation (5.1), this can be achieved by finding k from the condition

$$\int_{0.1\ \mathrm{M}_\odot}^{m_{\mathrm{max}*}} \xi_{\mathrm{can}}(m) m\, dm = 1\,\mathrm{M}_\odot, \tag{5.2}$$

where ξ_{can} is the canonical IMF, i.e. $\alpha_3 = 2.3$. With this normalization, the number density of stars with $m < 1\ \mathrm{M}_\odot$ is the same for all values of α_3, since the normalization is set by the canonical IMF and is therefore not affected by variations of α_3.

In the case of the SN-rate of Arp 220 (see Section 5.4), the light used to estimate the star formation rate (SFR), i.e. the mass of the material converted into stars per time-unit, originates from stars over the whole range of stellar masses. With the SFR thereby given, we then normalize the IMF such that the SFR remains constant when the IMF is varied. For the IMF given by Equation (5.1), this can be achieved by finding k from the condition

$$\int_{0.1\ \mathrm{M}_\odot}^{m_{\mathrm{max}*}} \xi(m) m\, dm = 1\,\mathrm{M}_\odot. \tag{5.3}$$

With this normalization, the number density of stars with $m < 1\ \mathrm{M}_\odot$ decreases with decreasing values of α_3, i.e. with increasing top-heaviness of the IMF.

Stellar evolution and dynamical evolution turn the IMF of a star cluster into a (time-dependent) mass function of stars and stellar remnants; the star and stellar remnant mass function, SRMF. For a single-age stellar population, the connection between the IMF and the SRMF can be quantified by an initial-to-final mass relation for stars, m_{rem}, which can be written as

$$m_{\mathrm{rem}} = \begin{cases} \dfrac{m}{\mathrm{M}_\odot}, & \dfrac{m}{\mathrm{M}_\odot} < \dfrac{m_{\mathrm{to}}}{\mathrm{M}_\odot}, \\ 0.109\,\dfrac{m}{\mathrm{M}_\odot} + 0.394, & \dfrac{m_{\mathrm{to}}}{\mathrm{M}_\odot} \leq \dfrac{m}{\mathrm{M}_\odot} < 8, \\ 1.35, & 8 \leq \dfrac{m}{\mathrm{M}_\odot} < 25, \\ 0.1\dfrac{m}{\mathrm{M}_\odot}, & 25 \leq \dfrac{m}{\mathrm{M}_\odot} \leq m_{\mathrm{max}*}, \end{cases} \tag{5.4}$$

where m_{to} is the mass at which stars evolve away from the main sequence at a given age (Dabringhausen et al. 2009). UCDs typically have ages of ≈ 10 Gyr (Evstigneeva et al. 2007; Chilingarian et al. 2008), which implies $m_{\mathrm{to}} \approx 1\ \mathrm{M}_\odot$ for them. In the present paper, Equation (5.4) is used to calculate how the mass of a modeled UCD depends on the variation of its IMF (see Section 5.3.2).

Note that Equation (5.4) reflects the evolution of single stars. In a binary system, the initial mass of a star that evolves into a black hole is expected to be higher, so that stars with masses up to 40 $\mathrm{M}_\odot$ may become NSs instead of BHs (cf. Brown et al. 2001). It is however of minor importance in this paper whether a massive remnant is a NS or a BH. Both kinds of objects can become bright X-ray sources by accreting matter from a companion star and BHs in such binary

systems are actually detected by excluding that they are NSs due to their mass (Casares 2007). Also the total mass of a GC or UCD is not strongly affected by the mass-limit between NSs and BHs. Using Equation (refeq54) with $m_{\rm tr} = 1\ {\rm M}_\odot$ and Equation (5.4) with $m_{to} = 1\ {\rm M}_\odot$, the total mass of NSs and BHs is 4.2 per cent of the total mass of the stellar system for $\alpha_3 = 2.3$ (canonical IMF) and 79.9 per cent for $\alpha_3 = 1$. These numbers are altered to 3.8 per cent of the total mass of the stellar system for $\alpha_3 = 2.3$ and 75.0 per cent for $\alpha_3 = 1$ if the transition from NSs to BHs is shifted from $25\ {\rm M}_\odot$ to $40\ {\rm M}_\odot$.

5.3 The LMXB-abundance in GCs and UCDs

5.3.1 Some properties of GCs and UCDs

For a number of GCs and UCDs, data (Mieske et al. 2008) on V-band luminosity (L_V), dynamical mass ($M_{\rm dyn}$) and effective half-light radius ($r_{\rm h}$) are available. These data suggest a transition at $L_V \approx 10^6\ {\rm L}_\odot$, since the $r_{\rm h}$ and dynamical M/L ratios of objects with $L_V < 10^6\ {\rm L}_\odot$ appear to be independent of L_V, in contrast to objects with $L_V > 10^6\ {\rm L}_\odot$ (see Figures 5.1 and 5.2). This motivates to consider the objects with $L_V < 10^6\ {\rm L}_\odot$ as GCs and those with $L_V \geq 10^6\ {\rm L}_\odot$ as UCDs, even though stellar systems close to this transition could be assigned to either one of these classes (Mieske et al. 2008).

Knowing $r_{\rm h}$ and $M_{\rm dyn}$ of a stellar system allows to estimate its median two-body relaxation time (Spitzer 1987), using

$$t_{\rm rh} = \frac{0.234}{\log_{10}(M_{\rm dyn}/{\rm M}_\odot)} \times \sqrt{\frac{M_{\rm dyn}\, r_{\rm h}^3}{G}}, \tag{5.5}$$

where G is the gravitational constant (Dabringhausen et al. 2008). The significance of $t_{\rm rh}$ lies in the fact that it sets the time-scale on which the structure of a self-bound stellar system is changed by the process of energy equipartition. If $\tau \gtrsim t_{\rm rh}$ holds for a stellar system with τ being its age, it can be considered nearly unaffected by dynamical evolution and is thus only subject to stellar evolution. This is the case for UCDs, as $t_{\rm rh} \gtrsim \tau_{\rm H}$ is valid for them, where $\tau_{\rm H}$ is the age of the Universe suggested by the ΛCDM-model (see Figure 5.3). Thus, the properties of UCDs can be calculated from their IMF while considering the effects of stellar evolution, but without accounting for the effects of dynamical evolution. This means in particular that the SRMF of UCDs can be calculated from their IMF and Equation (5.4). Note that GCs, on the other hand, *are* subject to dynamical evolution, since their ages, $\tau_{\rm GC}$ are also similar to $\tau_{\rm H}$ and thus $\tau_{\rm GC} > t_{\rm rh}$.

The data (Mieske et al. 2008) on L_V and $r_{\rm h}$ of individual GCs in the MW and in Centaurus A and UCDs in the Virgo-cluster are also useful for estimating an average $r_{\rm h}$, $\overline{r}_{\rm h}$, as a function of L_V. GCs over the luminosity range from $10^4\ {\rm L}_\odot$ to $10^6\ {\rm L}_\odot$ do not show a luminosity-radius trend (McLaughlin 2000; Jordán A. et al. 2005). The logarithmic average $r_{\rm h}$ of GC is

$$\log_{10}\left(\frac{\overline{r}_{\rm h}}{\rm pc}\right) = 0.4314 \tag{5.6}$$

(Jordán A. et al. 2005). Performing a linear least-squares fit to data in Mieske et al. (2008) on UCDs in the Virgo cluster leads to

$$\log_{10}\left(\frac{\overline{r}_{\rm h}}{\rm pc}\right) = 1.076 \log_{10}\left(\frac{L_V}{10^6\ L_{V,\odot}}\right) + 0.4314. \tag{5.7}$$

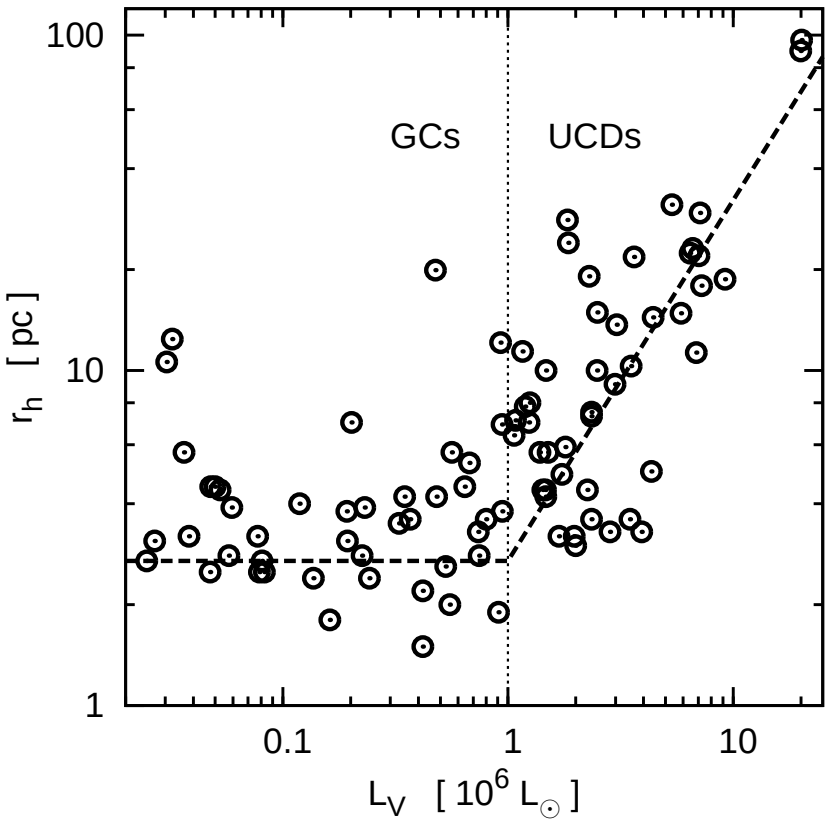

Figure 5.1: The effective half-light radii, $r_{\rm h}$, of GCs and UCDs. The circles show the sample of individual GCs and UCDs from the compilation of Mieske et al. (2008). The dashed line is an estimate of the average $r_{\rm h}$ of GCs and UCDs (cf. Equations 5.6 and 5.7). The vertical dotted line sets the limit between objects that are considered as GCs and objects that are considered as UCDs. Note that the average $r_{\rm h}$ indicated for GCs by the dashed line is lower than the average $r_{\rm h}$ of the GCs shown in this figure. This is because the GCs shown here are mostly GCs of the Milky Way while the dashed line corresponds to the average $r_{\rm h}$ of GCs in the Virgo-cluster. The GCs in the Virgo cluster tend to be more compact than those around the Milky Way.

Note that equality between Equations (5.6) and (5.7) at $L_V = 10^6$ L$_\odot$ was imposed as a secondary condition on the fit of Equation (5.7) to the data. This secondary condition reflects the fact that the $r_{\rm h}$ of GCs are indistinguishable from those of UCDs at $L \approx 10^6$ L$_\odot$ (see Figures 5.1 and 5.2).

5.3.2 Modeling the LMXB-abundance in GCs and UCDs

The origin of LMXBs in GCs and UCDs

Tight binaries consisting of a dark remnant and a low-mass companion can have in principle two different origins:

1. They can be primordial. In this case a tight binary of a high-mass star and a low-mass star have formed already in the star forming event. The high-mass star explodes in a supernova after a few million years leaving behind a dark remnant which can remain bound to its low-mass companion.

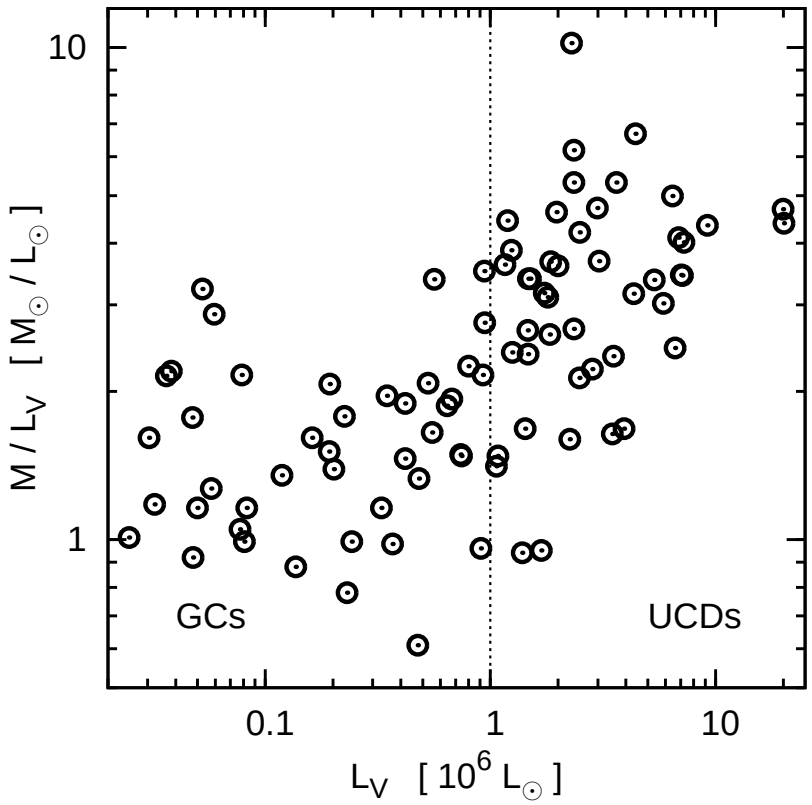

Figure 5.2: The mass-to-light ratios (M/L-ratios) of GCs and UCDs. The circles show the sample of individual GCs and UCDs from the compilation of Mieske et al. (2008). The vertical dotted line sets the limit between objects that are considered as GCs and objects that are considered as UCDs.

2. They have formed through encounters. GCs and UCDs are regions of enormously high stellar density ranging from $10\ \mathrm{M}_\odot\,\mathrm{pc}^{-3}$ to $10^4\ \mathrm{M}_\odot\,\mathrm{pc}^{-3}$ (Dabringhausen et al. 2008). Encounters between dark remnants and low-mass stars are therefore frequent and can lead to the formation of LMXBs due to tidal capture (Verbunt & Hut 1987; Verbunt 2003).

As these formation mechanisms are quite different it is expected that both processes would contribute differently to the LMXB content in GCs and UCDs.

There are however strong arguments against a significant contribution from primordial binaries to the LMXB content of GCs and UCDs:

1. The number of LMXBs in GCs is strongly correlated with the encounter rate and thus clearly linked to it (Jordán A. et al. 2005; Sivakoff et al. 2007).

2. There are several hundred times more LMXBs per unit mass in GCs than in the Galactic field (Verbunt & Hut 1987). The LMXBs in the Galactic field are LMXBs that probably evolved from primordial binaries, since they are in a low-density environment where encounters play no role and most probably formed in star clusters from which they were subsequently ejected. The strong excess of LMXBs in GCs therefore suggests that most LMXBs in GCs form through encounters (Verbunt & Hut 1987).

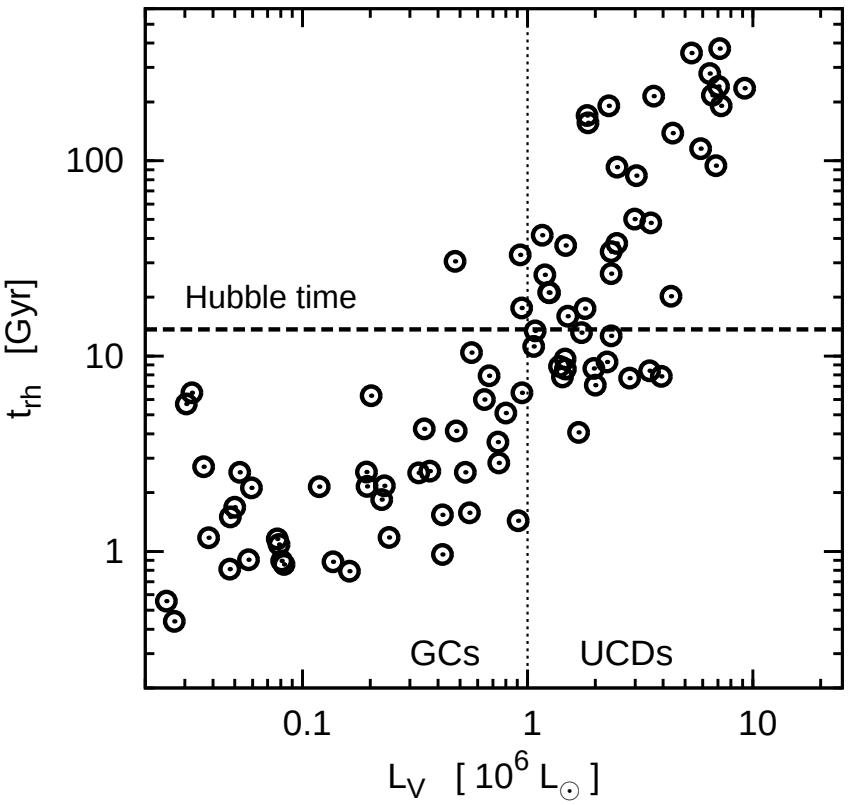

Figure 5.3: The median two-body relaxation times, $t_{\rm rh}$, of GCs and UCDs. The circles show the sample of individual GCs and UCDs from the compilation of Mieske et al. (2008). The dashed horizontal line indicates the age of the Universe, $\tau_{\rm H}$, according to the ΛCDM-model. The vertical dotted line sets the limit between objects that are considered as GCs and objects that are considered as UCDs. Note that $t_{\rm rh} \gtrsim \tau_{\rm H}$ for UCDs. Thus, UCDs can be considered dynamically unevolved (Dabringhausen et al. 2008) and they may therefore be considered as galaxies from a stellar dynamical point of view (Forbes & Kroupa 2011).

The number of encounters relevant for the creation of LMXBs, i.e. encounters where a NS can capture a low-mass star (Verbunt & Hut 1987), can be written as

$$\Gamma \propto \frac{n_{\rm ns}\, n_{\rm s}\, r_{\rm c}^3}{\sigma}, \tag{5.8}$$

where $n_{\rm ns}$ is the number density of NSs, $n_{\rm s}$ is the number density of potential low-mass companion stars, $r_{\rm c}$ is the core radius of the stellar system and σ is the velocity dispersion (Verbunt 2003). The potential companions to a NS in a bright LMXB are stars that come from a rather narrow mass range where stars of a given age leave the main-sequence. At this stage of their evolution, the stars expand rapidly, which makes a high accretion rate on the NS possible, which in turn leads to a high X-ray luminosity.

A more recent study by Ivanova et al. (2008) revealed that tidal capture is not the only dynamical process relevant for the formation of LMXBs. Other dynamical processes like direct collisions between NSs and red giant stars or interactions between stars and existing binaries also play a role and can actually be even more important than tidal captures. However, this does not change the observational finding that the number of LMXBs in GCs scales with Γ (e.g. Jordán A. et al. 2005). Therefore, Γ seems to be an adequate measure for the stellar dynamical

processes that produce LMXBs in general. It is moreover argued in Ivanova et al. (2008) that primordial binaries only make a small contribution to the total population of LMXBs in old GCs.

There are thus strong observational and theoretical motivations for the usage of Γ as a measure for how many LMXBs are expected in GCs and UCDs.

The encounter rate in GCs and UCDs for an invariant SRMF

If only a *single*, invariant mass function for stars and stellar remnants (SRMF) is considered for all stellar systems, then

$$n_{\rm ns} \propto n_{\rm s} \propto \rho_0 \tag{5.9}$$

holds, where ρ_0 is the central mass density. Equation (5.8) can then be rewritten as

$$\Gamma \propto \frac{\rho_0^2\, r_{\rm c}^3}{\sigma} \tag{5.10}$$

by using Equation (5.9).

In order to link the theory on LMXB-formation to the optical properties of observed stellar systems, it is in the following assumed that the mass density of a stellar system follows its luminosity density. The structural parameters derived from the distribution of the light in the stellar system can then be translated directly into statements on the distribution of its mass, i.e. quantities that determine the dynamics of the stellar system.

However, $r_{\rm c}$ is difficult to measure for GCs and UCDs at the distance of the Virgo cluster, as these stellar systems are barely resolved with current instruments. The projected half-light radius $r_{\rm h}$ (and thus the half-mass radius under the assumption that mass follows light) is larger and therefore less difficult to retrieve from the data. For practical purposes, it is therefore useful to assume

$$r_{\rm c} \propto r_{\rm h} \tag{5.11}$$

and

$$\rho_0 \propto \frac{M}{r_{\rm h}^3}, \tag{5.12}$$

where M is the mass of the stellar system. The King profile (King 1962) with its three independent parameters (core radius, tidal radius and central density), is thereby simplified to a density profile with only two independent parameters (half-mass radius and mass). The underlying assumptions are not necessarily true, and indeed, not fulfilled for GCs in the Milky Way since McLaughlin (2000) finds that more luminous GCs tend to be more concentrated. However, regarding the conclusions on how the presence of bright LMXBs is connected to the optical properties of GCs in the Virgo cluster, these assumptions are unproblematic. Using the same concentration for all GCs in their sample Sivakoff et al. (2007) find that they essentially come to the same results as Jordán et al. (2004), who use an individual estimate for the concentration of each GC in their sample.

When dealing with UCDs, replacing $r_{\rm c}$ with $r_{\rm h}$ is even advantageous. The time-scale on which the NSs gather at the centre of the UCD is given as

$$t_{\rm seg} = \frac{\overline{m}}{m_{\rm ns}}\, t_{\rm cc}, \tag{5.13}$$

where $\overline{m} \approx 0.5\ {\rm M}_\odot$ is the mean mass of stars, $m_{\rm ns} \approx 1.35\ {\rm M}_\odot$ is the mass of neutron stars and $t_{\rm cc}$ is the core-collapse time of the UCD without the NSs (Spitzer 1987; Banerjee et al.

2010). If a Plummer sphere (Plummer 1911) is used as an approximation for the density profile of a stellar system, $t_{\rm cc} \approx 15\ t_{\rm rh}$ holds (Baumgardt et al. 2002). With $t_{\rm rh}$ being of the order of a Hubble time for UCDs, Equation (5.13) implies that the distribution of NSs in UCDs still follows the initial distribution of their progenitors. The volume relevant for the formation of LMXBs in a UCD is therefore better measured by $r_{\rm h}$ than by $r_{\rm c}$, provided its stellar population did not *form* mass-segregated. This is because $r_{\rm h}$ represents the size of the whole UCD, whereas $r_{\rm c}$ represents the size of its centre.

Thus, using Equations (5.11) and (5.12), Equation (5.10) can be transformed into

$$\Gamma_{\rm h} \propto \frac{M^2}{r_{\rm h}^3\,\sigma}. \tag{5.14}$$

If the stellar system is also in virial equilibrium,

$$\sigma \propto \rho_0^{0.5}\, r_{\rm h} \propto \frac{M^{0.5}}{r_{\rm h}^{0.5}} \tag{5.15}$$

holds. In this case,

$$\Gamma_{\rm h} \propto \frac{M^{1.5}}{r_{\rm h}^{2.5}} \tag{5.16}$$

follows from Equations (5.14) and (5.15). In contrast to Equation (5.8), Equation (5.16) has only two variables ($M, r_{\rm h}$) instead of four ($n_{\rm s}, n_{\rm ns}, M, r_{\rm c}$).

A further variable can be eliminated by replacing individual values for $r_{\rm h}$ by luminosity-dependent estimates for $r_{\rm h}$, such as Equations (5.6) and (5.7), and noting that the same SRMF for all stellar systems in question implies $M \propto L_V$ for them. This leads to

$$\overline{\Gamma}_{\rm h} \propto \frac{L_V^{1.5}}{\overline{r}_{\rm h}^{2.5}}, \tag{5.17}$$

or, more explicitly by using Equations (5.6), and (5.7), respectively,

$$\log_{10}(\overline{\Gamma}_{\rm h}) = 1.5 \log_{10}\left(\frac{L_V}{10^6\,{\rm L}_\odot}\right) + A \tag{5.18}$$

for GCs (i.e. $L_V < 10^6\ {\rm L}_\odot$), and

$$\log_{10}(\overline{\Gamma}_{\rm h}) = -1.190 \log_{10}\left(\frac{L_V}{10^6\,{\rm L}_\odot}\right) + A \tag{5.19}$$

for UCDs (i.e. $L_V \geq 10^6\ {\rm L}_\odot$). The constant A is the same in Equations (5.18) and (5.19). Note that the transition between Equations (5.18) and (5.19) is continuous due to the continuity of $\overline{r}_{\rm h}$ at $L_V = 10^6\ {\rm L}_\odot$.

Detecting a variable SRMF with LMXBs

For investigating how $\Gamma_{\rm h}$ depends on the IMF, it is useful to consider the ratio between $\Gamma_{\rm h}$ as a function of α_3 and the $\Gamma_{\rm h}$ implied by some reference IMF. This has the advantage that factors, which do not depend on the IMF, cancel. The reference IMF is the canonical IMF in this paper;

a choice that is motivated with the lack of dynamical evolution in UCDs (cf. Section 5.3.1). Using Equation (5.12) thus leads to

$$\frac{\Gamma_{\rm h}(\alpha_3)}{\Gamma_{\rm h}(\alpha_3=2.3)} = \frac{n_{\rm ns}(\alpha_3)}{n_{\rm ns}(\alpha_3=2.3)}\sqrt{\frac{M(\alpha_3=2.3)}{M(\alpha_3)}}, \tag{5.20}$$

if it also assumed that the IMF varies only for stars with $m > m_{\rm to}$, so that also $n_{\rm s}$ is constant. By this last assumption, the luminosity of the UCDs, which is given by observations, stays constant when the IMF of the UCDs is varied. The right side of Equation (5.20) can be calculated if the IMF is specified. In particular,

$$\frac{n_{\rm ns}(\alpha_3)}{n_{\rm ns}(\alpha_3=2.3)} = \frac{\int_{8\ {\rm M}_\odot}^{m_{\rm max*}} \xi(m)\,dm}{\int_{8\ {\rm M}_\odot}^{m_{\rm max*}} \xi_{\rm can}(m)\,dm}, \tag{5.21}$$

and

$$\frac{M(\alpha_3=2.3)}{M(\alpha_3)} = \frac{\int_{0.1\ {\rm M}_\odot}^{m_{\rm max*}} m_{\rm rem}(m)\xi_{\rm can}(m)\,dm}{\int_{0.1\ {\rm M}_\odot}^{m_{\rm max*}} m_{\rm rem}(m)\xi(m)\,dm}, \tag{5.22}$$

where the IMF is normalised using Equation (5.2), $\xi_{\rm can}$ is the canonical IMF and $m_{\rm rem}(m)$ is given by Equation (5.4). Thus, Equation (5.20) quantifies how $\Gamma_{\rm h}$ changes in a stellar system (normalized with $\Gamma_{\rm h}$ for the canonical IMF) if the number of dark remnants and therefore the mass of the stellar system are changed, while its characteristic radius and the number of stars are kept constant.

A difficulty is that $\Gamma_{\rm h}$ of a stellar system cannot be measured directly. However, the actual $\Gamma_{\rm h}$ of a GC or a UCD scales with the rate at which LMXBs are created (see Sec. 5.3.2), which is proportional to the probability P to form an LMXB above a certain brightness limit in a given time. If a sample of GCs or UCDs in a certain luminosity interval is given, a useful estimator for the average P of these GCs or UCDs is the fraction $f_{\rm LMXB}$ of them that have an LMXB above the brightness limit defined by the sensitivity of a given set of observations. Thus,

$$f_{\rm LMXB} \propto P \propto \Gamma_{\rm h}^{\gamma}, \tag{5.23}$$

where the exponent γ accounts for the claims that the LMXB-frequency in GCs and UCDs may not be directly proportional to Γ or $\Gamma_{\rm h}$, but to some power of Γ or $\Gamma_{\rm h}$ (cf. Jordán et al. 2004; Sivakoff et al. 2007).

If the SRMF of UCDs is indeed independent of luminosity, the $f_{\rm LMXB}$ of UCDs in different L_V intervals should all roughly coincide with the prediction from Equation (5.19) for an appropriate choice of the constant A. If however the $f_{\rm LMXB}$ of at least one L_V interval is inconsistent with Equation (5.19) for any choice of A, then this would be evidence for the SRMF changing with the luminosity of the UCDs. This would imply that the IMF of the UCDs changes with luminosity, since the SRMF of UCDs is solely determined by stellar evolution, i.e. a process that does not depend on the size of the system (see Section 5.3.1). Note that the actual value of A in Equations (5.18) and (5.19) has no implications for the physical properties of the observed stellar systems: For a given sample of GCs and UCDs, A depends on the detection limit for an X-ray source or an arbitrarily chosen brightness limit above the detection limit.

Data on the LMXB-frequency in GCs and UCDs

In order to search for a dependency of the IMF in UCDs on their luminosity, we use data published in the upper left panel of figure (6) in Sivakoff et al. (2007). These data provide

the fraction of globular clusters and UCDs, $f_{\rm LMXB}$, hosting an LMXB in a given total z-band magnitude interval.

The results of Sivakoff et al. (2007) were obtained by combining two sets of data.

First, HST images of 11 elliptical galaxies in the Virgo Cluster were used, see Table 1 in Sivakoff et al. (2007). Ten of them are the brightest galaxies observed in the course of the ACS Virgo Cluster Survey (Côté et al. 2004). The eleventh one (NGC 4697) is a similarly bright galaxy that was observed by Sivakoff et al. (2007) with nearly the same observational setup as in the ACS VIrgo Cluster Survey. Using the obtained images, a large number of accompanying GCs and UCDs was identified around each of these galaxies.

Second, Sivakoff et al. (2007) used archival Chandra Observatory X-ray observations of the same galaxies. The setup for the X-ray observations varied widely from galaxy to galaxy, see Table 2 in Sivakoff et al. (2007), which could in principle be problematic.

Sivakoff et al. (2007) find however that the global properties of GCs and UCDs which contain a LMXB are largely unaffected by the varying detection limits for X-ray sources. Also note that the LMXB-frequencies in GCs are well explained by the encounter rates in them (see Section 5.3.3), despite the different detection limits for X-ray sources. This suggests that the encounter rate is indeed a good measure for the rate at which LMXBs of any X-ray luminosity are created. We therefore assume that a large number of GCs and UCDs with an X-ray source is indeed an indicator for a large number of dark remnants in them.

The size of the z-band magnitude intervals in Sivakoff et al. (2007) is chosen such that each of them contains 27 GCs or UCDs with a detected LMXB. This corresponds to a total of at least 100 GCs or UCDs in each of these intervals, since $f_{\rm LMXB} \lesssim 0.2$ in all of them. Thus, $f_{\rm LMXB}$ can be taken as a reliable estimator for the average P to form an LMXB in a GC or a UCD in a given z-band magnitude interval.

For comparing the data on the LMXBs in GCs and UCDs from Sivakoff et al. (2007) to the prediction for the LMXB-frequency in GCs and UCDs formulated in Equations (5.18) and (5.19), z-band magnitudes have to be converted into L_V. For this purpose, z-band luminosities are calculated from z-band magnitudes with

$$L_z = 10^{-0.4(M_z-4.51)}{\rm L}_{\odot,z}, \tag{5.24}$$

where M_z is the absolute z-band magnitude and L_z is z-band luminosity in Solar units (cf. Equation 1 in Sivakoff et al. 2007). Now note that the z-band M/L ratio of GCs in the Virgo-cluster are all close to $\approx 1.5{\rm M}_\odot/L_{\odot,z}$ (Sivakoff et al. 2007), which is essentially identical to the average V-band M/L ratio of the GCs in the Milky Way in Solar units (McLaughlin 2000). This implies that z-band and V-band luminosities of GCs are approximately identical in Solar units. We therefore assume $L_V/L_{\odot,V} = L_z/L_{\odot,z}$ in this paper.

The data from figure (6) in Sivakoff et al. (2007) is shown in Figure 5.4 with the z-band magnitude intervals from Sivakoff et al. (2007) converted into L_V intervals. Three of these intervals are at luminosities $L_V > 10^6$ L$_\odot$, so that the objects in them are UCDs (cf. Section 5.3.1). As the size of the intervals is chosen such that each of them contains 27 objects with an LMXB, 81 UCDs with an LMXB are considered here. The total number of UCDs in the sample from Sivakoff et al. (2007) is about 400, as can be calculated from $f_{\rm LMXB}$ in the according intervals.

For practical purposes, it is useful not to discuss individual values for the $f_{\rm LMXB}$ of UCDs, but to replace them by a continuous function $\overline{P}(L_V)$. This function is obtained by performing a least-squares fit of a linear function to the values for $f_{\rm LMXB}$ in the L_V intervals with the UCDs, leading to

$$\log_{10}(\overline{P}) = a\log_{10}(L_V) + b, \tag{5.25}$$

where the best fitting parameters a and b are given in Tab. (5.1). $\overline{P}$ can be interpreted as an estimate for the average probability for UCDs with a given L_V to host a LMXB brighter than the detection limit. For a meaningful comparison between $\overline{P}$ and $\overline{\Gamma}_{\rm h}$ at different values for L_V, A needs to be gauged. This is done by imposing that $\overline{P}(L_V) = \overline{\Gamma}_{\rm h}(L_V)$ for $L_V = 10^6\ L_{\odot,V}$. The motivation for choosing this condition to fix A is that the stellar populations of systems with this luminosity should be nearly unaffected by dynamical evolution (cf. Section 5.3.1), while their M/L-ratios suggest that their IMF is canonical, in contrast to even more luminous stellar systems (cf. Dabringhausen et al. 2009).

If the rate at which LMXBs are produced in GCs and UCDs is proportional to some power γ of the encounter rate in them, leading to $\overline{P}(L_V) \propto \overline{\Gamma}_{\rm h}^{\gamma}$ (cf. Equations 5.23 and 5.25), Equation (5.20) can be transformed into

$$\frac{\overline{P}(L_V)^{\frac{1}{\gamma}}}{\overline{\Gamma}_{\rm h}(L_V)} = \frac{n_{\rm ns}(\alpha_3)}{n_{\rm ns}(\alpha_3 = 2.3)} \sqrt{\frac{M(\alpha_3 = 2.3)}{M(\alpha_3)}}. \tag{5.26}$$

The left side of Equation (5.26) is then expressed in terms of observable properties of UCDs and the right side only depends on α_3 as a free parameter once $m_{\rm tr}$ is given. Equation (5.26) can therefore be used to estimate the dependency of the IMF of the UCDs as a function of their observed L_V. Since A is chosen such that $\overline{P}(L_V)/\overline{\Gamma}(L_V) = 1$ for stellar systems that are assumed to have formed with the canonical IMF, $\overline{P}(L_V)/\overline{\Gamma}(L_V) > 1$ implies a top-heavy IMF and $\overline{P}(L_V)/\overline{\Gamma}(L_V) < 1$ implies a bottom-heavy IMF.

5.3.3 Results

In order to test for an LMXB-excess and thus a top-heavy IMF in UCDs from the observational data from Sivakoff et al. (2007) we now compare with theoretically expected LMXB-frequencies.

The dynamical formation of LMXBs depends on the density of both dark remnants and low-mass stars (Equation 5.8). In denser star clusters, close encounters are more frequent and the formation of an LMXB is more likely. GCs have a common half-mass radius of a few parsec independent of their luminosity and their stellar mass is on average proportional to their luminosity (McLaughlin 2000). It therefore follows from Equation (5.18) that LMXBs should be hosted predominantly in high-mass GCs if their SRMF does not depend on their stellar mass. The dashed line in Figure 5.4 shows the theoretically expected LMXB frequency for a constant IMF calculated with Equations (5.18) and (5.19) with A chosen such that these equations reproduce the observed LMXB frequency at $L_V = 10^6\ {\rm L}_{\odot}$. The theoretical prediction then matches the observations in the GC regime (i.e. $L_V < 10^6\ {\rm L}_{\odot}$), in agreement with earlier studies on LMXBs in GCs (Jordán A. et al. 2005; Peacock et al. 2010).

At $L_V \approx 10^6\ {\rm L}_{\odot}$, the transition luminosity from GCs to UCDs, both kinds of stellar systems have the same half-mass radius (see Section 5.3.1). However, unlike GCs, UCDs show a luminosity-radius relation such that they become less dense with increasing luminosity (cf. figure 4 in Dabringhausen et al. 2008). Consequently, Equation (5.19) predicts that the capture rate of late-type stars by dark remnants and thus the expected LMXB frequency decreases rapidly with increasing L_V-band luminosity if the SRMF is constant. Note that a constant SRMF in UCDs implies a constant IMF in them due to the lack of dynamical evolution in UCDs (see Section 5.3.1).

In Figure 5.4, the prediction from Equation (5.19) for the LMXB frequency in UCDs with a constant SRMF is shown by the dashed line in the according luminosity range, where A is

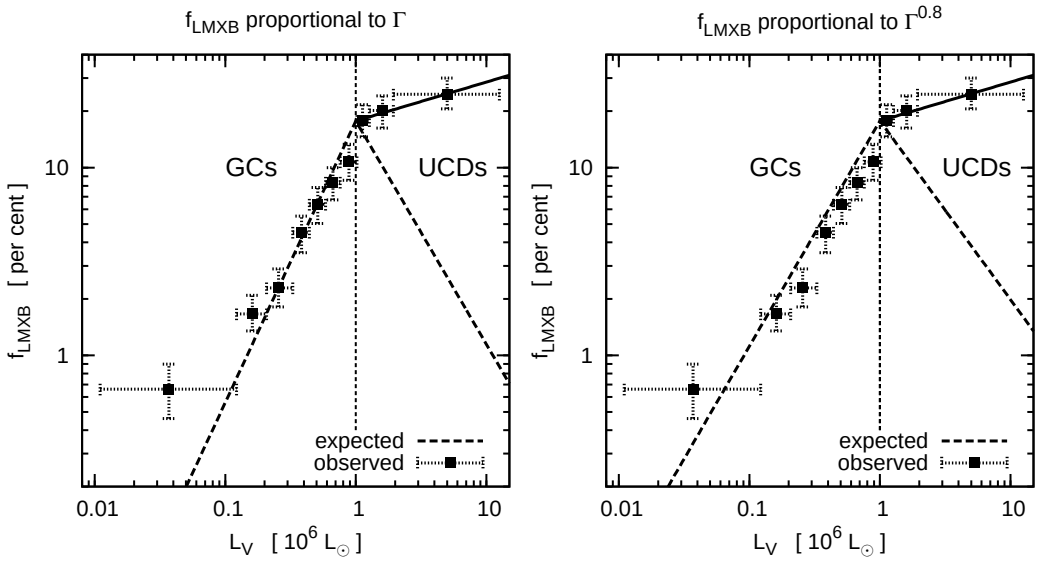

Figure 5.4: The observed LMXB-frequency of GGs and UCDs in comparison to expected frequencies if the IMF was canonical. Plotted are the observed frequencies (squares) of GCs ($L_V < 10^6\ L_{\odot,V}$) and UCDs ($L_V \geq 10^6\ \mathrm{L}_{\odot,V}$) with LMXBs, f_{LMXB}, in the Virgo galaxy cluster as a function of the V-band luminosity, L_V. Each data point contains 27 objects showing the LMXB signal. The data points are identical with the data points in the upper left panel of figure (6) in Sivakoff et al. (2007), except for a rescaling of z-band magnitudes to V-band luminosities. The three brightest data are based on ≈400 UCDs, i.e ≈135 UCDs per bin. The dashed line shows the theoretically expected LMXB-frequency for an invariant canonical IMF with index $\alpha_3 = 2.3$ assuming $f_{\mathrm{LMXB}} \propto \overline{\Gamma}_{\mathrm{h}}$ (left panel) and $f_{\mathrm{LMXB}} \propto \overline{\Gamma}_{\mathrm{h}}^{0.8}$ (right panel). In either case, the theoretically expected LMXB-frequency is significantly too low for UCDs, while for GCs the theoretically expected LMXB-frequency matches the observed LMXB-frequency. The solid line is a fit through the UCD-regime (above $10^6\ \mathrm{L}_{\odot,V}$). From it is derived the variation with luminosity of the IMF index α_3 such that this new model, based on a variable IMF, accounts for the observed f_{LMXB} for $L_V > 10^6\ \mathrm{L}_{\odot,V}$.

chosen such that Equation (5.19) reproduces the observed LMXB frequency at $L_V = 10^6\ \mathrm{L}_{\odot}$. Two cases are considered, namely $f_{\mathrm{LMXB}} \propto \Gamma_{\mathrm{h}}$ and $f_{\mathrm{LMXB}} \propto \Gamma_{\mathrm{h}}^{0.8}$. The second case is closer to the dependency between f_{LMXB} and Γ_{h} reported by Sivakoff et al. (2007). The agreement between the theoretical prediction and and the observed frequency of LMXBs is in either case good for GCs. However, $f_{\mathrm{LMXB}} \propto \Gamma_{\mathrm{h}}^{0.8}$ seems indeed a better fit to the data than $f_{\mathrm{LMXB}} \propto \Gamma_{\mathrm{h}}$. Note that Maccarone & Peacock (2011) find $\Gamma \propto \Gamma_{\mathrm{h}}^{0.8}$ on average for GCs in the Milky Way, which essentially means that the typical ratio between Γ and Γ_{h} depends for these GCs on their mass. This is probably a consequence of the more massive GCs in the MW being more concentrated than the less massive ones (McLaughlin 2000; cf Section 5.3.2), and likely to be the case for the GCs in the Virgo cluster as well.

For UCDs however, the observed LMXB-frequency strongly deviates from the theoretical prediction for a constant SRMF. It is observed that 25 ± 5 per cent of the UCDs with $L_V \approx 5 \times 10^6\ L_{\odot,V}$ have a bright LMXB, while Equation (5.19) suggests a LMXB frequency of about 2 per cent at this luminosity for $f_{\mathrm{LMXB}} \propto \Gamma_{\mathrm{h}}$ and a LMXB frequency of about 3 per cent for $f_{\mathrm{LMXB}} \propto \Gamma_{\mathrm{h}}^{0.8}$. Thus, the expected fraction of LMXBs hosting UCDs is up to ≈ 10 times smaller than observed if all UCDs had the same IMF.

This discrepancy between the data and the model with an invariant (canonical) IMF and the data is highly significant. This cannot be explained with more dark remnants remaining bound

to UCDs due to higher escape velocities. This is because the escape velocity from massive GCs is much higher than the escape velocity from light GCs, since the characteristic radii of GCs do no change with mass, but the encounter rate is nevertheless sufficient for quantifying which fraction of them has a bright LMXB.

The situation is more complicated with the finding that redder GCs and UCDs have more LMXBs than the blue ones, while brighter objects (i.e. the UCDs in particular) tend to be redder than the less luminous ones (Mieske et al. 2006b). Taking color as an indicator for metallicity leads to the interpretation that the LMXB-frequency in GCs and UCDs does not only depend on Γ or $\Gamma_{\rm h}$ but also on metallicity (Jordán et al. 2004; Sivakoff et al. 2007). Note that an increase of metallicity with luminosity and therefore mass of GCs is consistent with theoretical modeling, according to which more massive star clusters retain more processed (i.e. metal-enriched) gas which is turned into subsequent stellar populations (Tenorio-Tagle et al. 2003).

Using metallicity (i.e. color) as a second parameter besides $\Gamma_{\rm h}$ indeed allows a more precise modeling of the probability to find a LMXB in a given GC or UCD than when $\Gamma_{\rm h}$ is assumed to be the sole parameter determining the probability to find a LMXB in that GC or UCD (Sivakoff et al. 2007). The dependency of that probability is however nevertheless almost linear to the encounter rate, while the dependency on the metallicity is much weaker (Jordán et al. 2004; Sivakoff et al. 2007). This may explain why the fraction of GCs with a LMXB is apparently already well explained if only the encounter rate in the GCs is considered (see Figure 5.4) despite the color-luminosity relation for GCs in the Virgo cluster (cf. Mieske et al. 2006b). It is thereby unlikely that the drastic discrepancy between the observed LMXB-frequency in UCDs and the theoretical prediction based on the encounter rate can be explained by an unaccounted metallicity effect, even though the color-luminosity dependency may be somewhat more pronounced for UCDs than for GCs (Mieske et al. 2010).

The conclusion is that the large number of LMXBs in UCDs is best explained by a large number dark remnants as a consequence of a top-heavy IMF in UCDs (and not as a consequence of different escape velocities or metallicities).

For an invariant IMF the theoretical LMXB frequency is highest at a luminosity of $L_V \approx 10^6\ L_{\odot,V}$, because in these systems the present-day stellar density has a maximum and close encounters are most frequent (Figure 4 in Dabringhausen et al. 2008). If the very dense star formation conditions are responsible for a top-heavy IMF then, on first sight, the smallest IMF index α_3 is expected in systems with $L_V \approx 10^6\ L_{\odot,V}$ and not in the most luminous UCDs. However, in systems with a top-heavy IMF stellar feedback is strongly enhanced and rapid gas expulsion leads to an expansion of the UCDs (Dabringhausen et al. 2010). The UCDs revirialise after a few dynamical time scales ($\lesssim$100 Myr) and undergo no further size evolution. Thus, their present day stellar density is the dynamically relevant quantity for producing the LMXB population.

We now determine by what amount the dark remnant content in UCDs has to be increased to get the theoretical LMXB-frequency into agreement with the observed values. For this, Equation (5.26) with $\gamma = 1$ and $\gamma = 0.8$ is used. This equation has α_3 and $m_{\rm tr}$ as parameters (Equation 5.1). In this paper, $m_{\rm tr} = 1\ {\rm M}_\odot$ and $m_{\rm tr} = 5\ {\rm M}_\odot$, so that the influence of the in principle quite arbitrary choice of $m_{\rm tr}$ is tested. Note that with $m_{\rm tr} = 1\ {\rm M}_\odot$, Equation (5.1) describes the family of IMFs that were considered in Dabringhausen et al. (2009). For either choice of $m_{\rm tr}$, the canonical IMF (Kroupa 2001, 2002) corresponds to $\alpha_3 = 2.3$ and a smaller value of α_3 increases the fraction of high-mass stars and subsequent dark remnants. The α_3 that can explain the discrepancy between $\overline{P}(L_V)$ (i.e. the function describing the observed LMXB frequency in UCDs) and $\overline{\Gamma}_{\rm h}(L_V)$ (i.e. the theoretical expectation for the LMXB frequency in UCDs if their

IMF was canonical) at a given L_V can be found by numerically solving Equation (5.26) for α_3 with a given value for $m_{\rm tr}$.

The L_V dependence of α_3 required to bring the model into agreement with the UCD data is plotted as the solid line in Figure 5.5 for $m_{\rm tr} = 1\,{\rm M}_\odot$ and in Fig (5.6) for $m_{\rm tr} = 5\,{\rm M}_\odot$. In either case, the most massive UCDs must have an extremely top-heavy IMF in order to explain their LMXB-excess. The higher $m_{\rm tr}$ is, the more exotic the IMF of UCDs must be in order to explain the number of LMXBs in them. For a given value for $m_{\rm tr}$, it is on the other hand only of minor importance whether $P(L_V)$ is proprotional to $\overline{\Gamma}_{\rm h}$ or proportional to $\overline{\Gamma}_{\rm h}^{0.8}$.

For $m_{\rm tr} = 1\,{\rm M}_\odot$, the independent analysis in this paper leads the same top-heavy IMF as derived from the UCD mass-to-light ratios (Dabringhausen et al. 2009), shown as the dotted line in Figure 5.5. Such a comparison is not meaningful for $m_{\rm tr} = 5\,{\rm M}_\odot$, since the shape thereby assumed for the IMF is different from the IMF considered in Dabringhausen et al. (2009).

The most likely relations between α_3 and $\log_{10}(L_V)$ shown in Figures 5.5 and 5.6 are remarkably close to a linear function,

$$\overline{\alpha_3} = c\log_{10}(L_V) + d. \tag{5.27}$$

The best fitting parameters c and d have been determined from a least-squares fit to 48 sample values calculated from Equation (5.26). These are shown Table 5.1. Probably the best model for the IMF in UCDs is calculated when $f_{\rm LMXB} \propto \Gamma_{\rm h}^{0.8}$ and $m_{\rm tr} = 1\,{\rm M}_\odot$ are assumed. This is because observations suggest a less-than-linear dependency of $f_{\rm LMXB}$ on the encounter rate (Jordán et al. 2004; Sivakoff et al. 2007) and assuming $m_{\rm tr} > 1\,{\rm M}_\odot$ implies even more extreme deviations from the canonical IMF in high-mass UCDs while the IMF is remarkably invariant in open star clusters (Kroupa 2001).

Figure 5.4 suggests that the value of $f_{\rm LMXB}$ for the most luminous UCDs is of central importance for estimating the slope of $\overline{P}(L_V)$ (Equation 5.25) and thus for the α_3 calculated from Equation (5.26). This is because of the distance of these data points to the other data points, which is due to the fact that the corresponding L_V interval is large. In order to estimate an uncertainty to the dependency of α_3 on L_V, we changed the value of $f_{\rm LMXB}$ for the most luminous UCDs ($L_V \gtrsim 2\times10^6\,{\rm L}_\odot$) by 3 times its uncertainty. $\overline{P}(L_V)$ was then recalculated with this new value and used in Equation (5.26). The resulting limits on the dependency of α_3 on L_V are indicated by the limits to the gray area in Figures 5.5 and 5.6. Also the limits of the gray areas are parametrized with linear functions, which are listed in Table 5.1.

The uncertainty of the upper mass limit for stars, $m_{\rm max*}$, has little effect on the results summarized in Table 5.1. This is illustrated with Figure 5.7, where the dependency between L_V and α_3 calculated from Equation (5.26) is shown for $m_{\rm max*} = 150\,{\rm M}_\odot$ (Weidner & Kroupa 2004; Oey & Clarke 2005) and for $m_{\rm max*} = 300\,{\rm M}_\odot$ (Crowther et al. 2010). The two functions are almost identical.

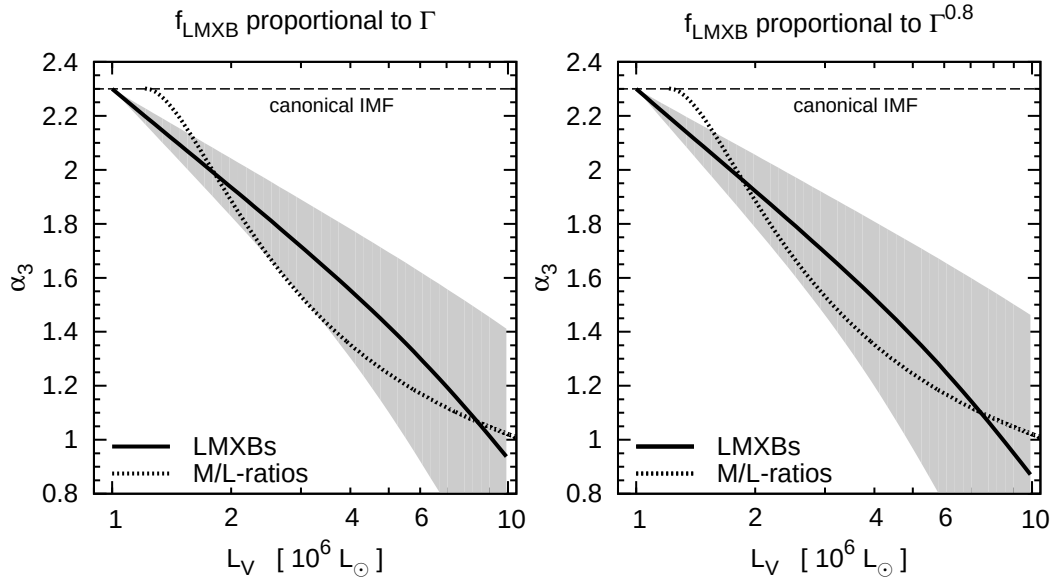

Figure 5.5: The IMF in UCDs for $m_{\rm tr} = 1\,{\rm M}_\odot$. Plotted is the high-mass IMF index, α_3, as a function of the V-band luminosity of the UCDs, L_V for $f_{\rm LMXB} \propto \Gamma_{\rm h}$ leading to $P(L_V) \propto \overline{\Gamma}_{\rm h}$ (left panel) and for $f_{\rm LMXB} \propto \Gamma_{\rm h}^{0.8}$ leading to $P(L_V) \propto \overline{\Gamma}_{\rm h}^{0.8}$ (right panel). The solid line shows the most likely high-mass index required to increase the dark remnant content in UCDs in order to match to observed LMXB-frequency (derived from the solid line in Figure 5.4). The grey shaded area marks an estimate for the $3\,\sigma$ region. The horizontal long dashed line marks the canonical IMF with $\alpha_3 = 2.3$. The dotted line shows the independently calculated high-mass IMF index obtained from the observed mass-to-light ratios of UCDs (Dabringhausen et al. 2009). Simple-to-use fitting relations for the variation of α_3 with L_V can be found in Tab. (5.1).

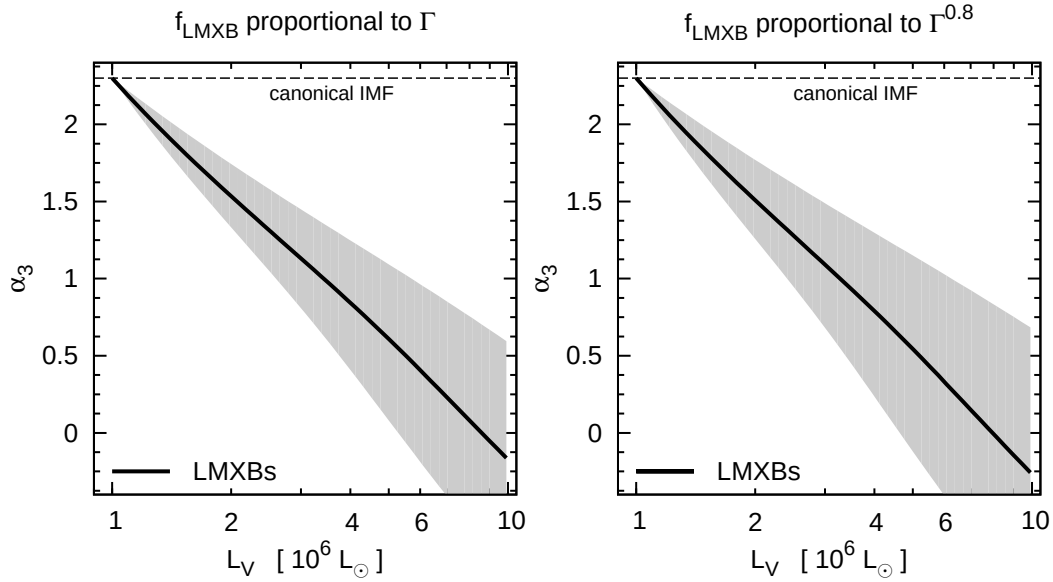

Figure 5.6: The IMF in UCDs for $m_{\rm tr} = 5\,{\rm M}_\odot$, otherwise as Figure 5.5.

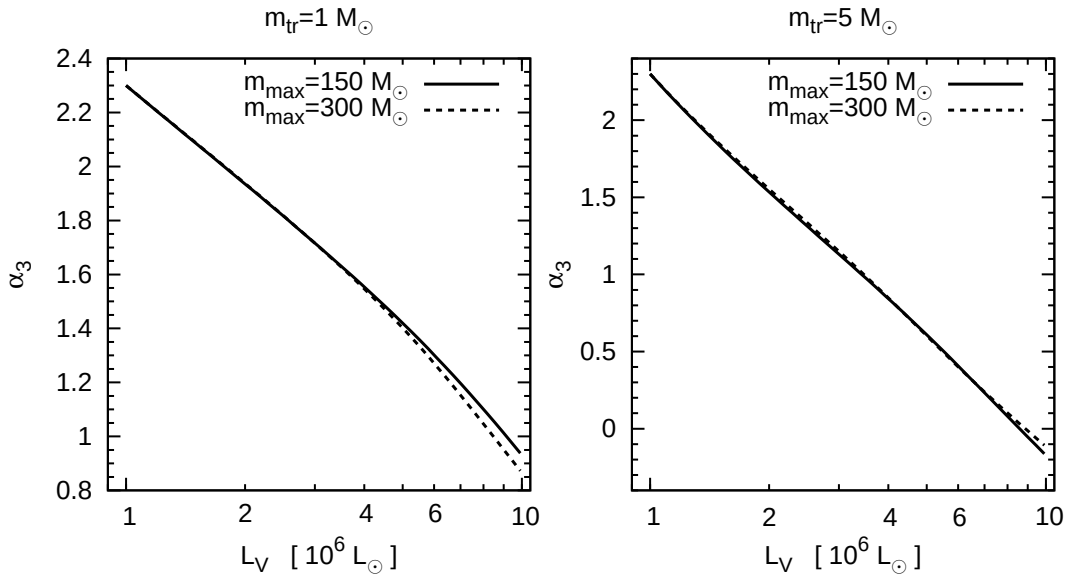

Figure 5.7: The high-mass IMF slope, α_3, as a function of V-band luminosity for different upper mass limits of the IMF, $m_{\rm max*}$ assuming $m_{\rm tr} = 1\,{\rm M}_\odot$ (left panel) or $m_{\rm tr} = 5\,{\rm M}_\odot$ (right panel). The solutions, $\alpha_3(L_V)$, are calculated from Equation (5.26) with $\gamma = 1$, i.e under the assumption that $f_{\rm LMXB} \propto \Gamma_{\rm h}$. Assuming $\gamma = 0.8$ leads however qualitatively to the same results as assuming $\gamma = 1$ (c.f. Figures 5.5 and 5.6). The solid line corresponds in both panels to $m_{\rm max*} = 150\,{\rm M}_\odot$ and is thus identical with the solid line in Figure 5.5, and Figure 5.6, respectively. The dashed lines corresponds to $m_{\rm max*} = 300\,{\rm M}_\odot$.

Table 5.1: The best fitting parameters for linear fits to P and α_3 for different models. The different cases (most likely case, upper limit, lower limit) listed here for every model correspond to different values of P for the UCDs with the highest masses (cf. Sec 5.3.3). Probably the best model for the IMF in UCDs is calculated when $f_{\rm LMXB} \propto \Gamma_{\rm h}^{0.8}$ and $m_{\rm tr} = 1\ {\rm M}_\odot$ are assumed. This is because observations suggest a less-than-linear dependency of $f_{\rm LMXB}$ on the encounter rate (Jordán et al. 2004; Sivakoff et al. 2007) and assuming $m_{\rm tr} > 1\ {\rm M}_\odot$ implies even more extreme deviations from the canonical IMF in high-mass UCDs while the IMF is remarkably invariant in open star clusters (Kroupa 2001). The parameters describing the IMF according to this model are shown in bold face in this table.

	$\log_{10}(\overline{P}) = a\log_{10}(L_V) + b$		$\overline{\alpha_3} = c\log_{10}(L_V) + d$	
model	a	b	c	d
$f_{\rm LMXB} \propto \Gamma_{\rm h}$, $m_{\rm tr} = 1\ {\rm M}_\odot$, most likely case	0.207	1.249	−1.337	2.332
$f_{\rm LMXB} \propto \Gamma_{\rm h}$, $m_{\rm tr} = 1\ {\rm M}_\odot$, upper limit	0.615	1.201	−1.878	2.375
$f_{\rm LMXB} \propto \Gamma_{\rm h}$, $m_{\rm tr} = 1\ {\rm M}_\odot$, lower limit	−0.202	1.298	−0.884	2.396
$f_{\rm LMXB} \propto \Gamma_{\rm h}^{0.8}$, $m_{\rm tr} = 1\ {\rm M}_\odot$, most likely case	0.207	1.249	$\mathbf{-1.402}$	$\mathbf{2.337}$
$f_{\rm LMXB} \propto \Gamma_{\rm h}^{0.8}$, $m_{\rm tr} = 1\ {\rm M}_\odot$, upper limit	0.615	1.201	$\mathbf{-2.089}$	$\mathbf{2.391}$
$f_{\rm LMXB} \propto \Gamma_{\rm h}^{0.8}$, $m_{\rm tr} = 1\ {\rm M}_\odot$, lower limit	−0.202	1.298	$\mathbf{-0.861}$	$\mathbf{2.304}$
$f_{\rm LMXB} \propto \Gamma_{\rm h}$, $m_{\rm tr} = 5\ {\rm M}_\odot$, most likely case	0.207	1.249	−2.415	2.275
$f_{\rm LMXB} \propto \Gamma_{\rm h}$, $m_{\rm tr} = 5\ {\rm M}_\odot$, upper limit	0.615	1.201	−3.169	2.289
$f_{\rm LMXB} \propto \Gamma_{\rm h}$, $m_{\rm tr} = 5\ {\rm M}_\odot$, lower limit	−0.202	1.298	−1.679	2.263
$f_{\rm LMXB} \propto \Gamma_{\rm h}^{0.8}$, $m_{\rm tr} = 5\ {\rm M}_\odot$, most likely case	0.207	1.249	−2.512	2.277
$f_{\rm LMXB} \propto \Gamma_{\rm h}^{0.8}$, $m_{\rm tr} = 5\ {\rm M}_\odot$, upper limit	0.615	1.201	−3.442	2.290
$f_{\rm LMXB} \propto \Gamma_{\rm h}^{0.8}$, $m_{\rm tr} = 5\ {\rm M}_\odot$, lower limit	−0.202	1.298	−1.594	2.263

5.4 The supernova rate in Arp 220

A top-heavy IMF in UCDs can theoretically be understood if UCDs formed as very massive star clusters that were internally heated by infra-red radiation that was trapped inside a molecular cloud massive enough to form a UCD-type star cluster (Murray 2009), or if UCDs formed from molecular clouds that were heated by highly energetic cosmic rays originating from numerous type-II supernovae surrounding those molecular clouds (Papadopoulos 2010; cf. Section 5.1). Both scenarios imply that UCDs are formed during star-bursts, either because of the link between the formation of the most massive star-clusters and high star formation rates (Weidner et al. 2004), or because the cosmic-ray field would only then be intense enough for effective heating of the molecular clouds. Note that likely progenitors of UCDs have actually been observed in star-bursts (Fellhauer & Kroupa 2002a).

Ultra-luminous infra-red galaxies (ULIRGs) are believed to be galaxies with star-bursting regions (Condon et al. 1991). They are thus systems where UCDs are probably forming. If this notion is correct and the IMF in UCDs is top-heavy, the ULIRGs as a whole should have more massive stars than expected for an invariant, canonical IMF. As a consequence, the rate of type II supernovae is expected to be higher.

In the following, we test the hypothesis of a top-heavy IMF in ULIRGs. For this reason, we quantify how the type-II supernova rate (SNR) in a star burst is connected to the star formation in it. Based on this, theoretical predictions for the SNR of Arp 220, which is one of the closest ULIRGs (Lonsdale et al. 2006), are calculated and compared to observations of this stellar system.

The type-II supernova rate (SNR) observed in a stellar system depends on its IMF as well as on its star formation history (SFH), i.e. how the star formation rate in the stellar system has changed with time, because these quantities determine the numbers and ages of stars in given mass intervals. If star formation begins at a time t_0, only stars above a time-dependent mass-limit $m_{\rm low}$ can have completed their evolution at a time $t > t_0$. For stars evolving into SNe, this mass can be approximated (Dabringhausen et al. 2010) by

$$\frac{m_{\rm low}}{\rm M_\odot} = 74.6 \left(\frac{t - t_0}{\rm Myr} - 2.59 \right)^{-0.63} . \tag{5.28}$$

Note that no stars evolve to type-II supernovae (SNe), if $t - t_0 \leq 2.59\,\rm Myr$.

Now consider a time interval $[t, t + \Delta t]$ and stars in a mass interval $[m, m + \Delta m]$, where $m \geq m_{\rm low}$. If the SFR was constant for all $t \geq t_0$, the number of stars evolving into SNe in the given mass interval during the time Δt is equal to the number of new stars that are formed in the same mass interval. Thus,

$$\frac{\Delta \rm SNR}{\rm yr^{-1}} = \frac{\rm SFR}{\rm M_\odot\ yr^{-1}} \int_m^{m+\Delta m} \xi(m)\, dm \tag{5.29}$$

in this case, where $\xi(m)$ is assumed to be given by Equation (5.1) with the normalization defined by Equation (5.3). This normalization keeps the total mass of the stars which are formed per unit time constant.

If Δt is small compared to the time scale on which $m_{\rm low}$ changes, the number of all stars that evolve during Δt can be approximated as

$$\frac{\rm SNR}{\rm yr^{-1}} \approx \frac{\rm SFR}{\rm M_\odot\ yr^{-1}} \int_{m_{\rm low}}^{m_{\rm max*}} \xi(m)\, dm. \tag{5.30}$$

Note that the SFR in Equations (5.29) and (5.30) should be considered an average value over a time-scale $t - t_0$. Variations of the SFR on much shorter time-scales are of no importance here.

The SFR of a ultra-luminous infra-red galaxy (ULIRG) can be estimated as

$$\frac{\mathrm{SFR}}{\mathrm{M_\odot\ yr^{-1}}} = \frac{L_{\mathrm{FIR}}}{5.8 \times 10^9\ \mathrm{L_\odot}}, \tag{5.31}$$

where L_{FIR} is the far infra-red (FIR) luminosity of the ULIRG (Kennicutt 1998).

One of the nearest ULIRGs is Arp 220. Using $L_{\mathrm{FIR}} = 1.41 \times 10^{12}\ \mathrm{L_\odot}$ for Arp 220 (Sanders et al. 2003), Equation (5.31) implies a SFR of $\approx 240\ \mathrm{M_\odot\,yr^{-1}}$ for that galaxy. The SNe in Arp 220 have been observed in a central region with a diameter of $\approx 1\ \mathrm{kpc}$, from where about 40 per cent of its FIR luminosity originates (Soifer et al. 1999). Equation (5.31) thus implies a SFR of $\approx 100\ \mathrm{M_\odot\,yr^{-1}}$ if only this part of Arp 220 is considered. Note that this SFR is consistent with the SFR that has been suggested for a forming UCD if UCDs form on a timescale of approximately 1 Myr (Dabringhausen et al. 2009). Also note that the observed SN in Arp 220 do not seem to distributed evenly over the central part of Arp 220, but to be concentrated in two knots which have a radius ≈ 50 pc each (Lonsdale et al. 2006) (i.e. the size of a UCD). This implies that indeed a major part of the star formation in the central part of Arp 220 takes place within these two knots. This would imply projected star formation densities of a few $10^{-3}\ \mathrm{M_\odot\ yr^{-1}\ pc^{-2}}$ in the knots.

SNRs calculated from Equation (5.30) for a constant SFR of $100\ \mathrm{M_\odot\,yr^{-1}}$ are shown as functions of the high-mass slope of the IMF in Figure 5.8. The two curves correspond to different times at which the star burst was initialized, but the expected number of SN per year (i.e. the SNR) is low in any case. The number of SN that *actually* occur within one year can therefore differ substantially from the calculated SNR, as the frequency of SN over such a time span obeys low-number statistics. Thus, the probability for a certain number of SN to happen within one year is quantified by the Poisson distribution function.

Now consider the case that the star-burst in Arp 220 already lasts for more than 40 Myr. This implies $m_{\mathrm{low}} = 8\ \mathrm{M_\odot}$, so that the number of SNII per year is maximized for the given SFR. The expectation value for the SNII-rate is then about one per year if the IMF was canonical (i.e. $\alpha_3 = 2.3$), but about two per year for a top-heavy IMF with $1 \lesssim \alpha_3 \lesssim 2$, where the SN-rate is only a weak function of α_3 (cf. Figure 5.8). Thus, the probability to actually observe four new SNII in a given year (Lonsdale et al. 2006) is then about two per cent if the IMF is canonical, but about 12 per cent for $1 \lesssim \alpha_3 \lesssim 2$.

A more elaborate discussion of the SNII rate in Arp 220 is obtained by taking into account that stars in a galaxy form in star-clusters of different masses, since m_{max} of the IMF depends on the mass of the star-cluster for low-mass star-clusters. This implies that the integrated galactic IMF (IGIMF) of all star-clusters in Arp 220 combined is not equal to the IMF in its star-clusters.

This IGIMF is given by

$$\begin{aligned} \xi_{\mathrm{IGIMF}}(m) &= \int_{M_{\mathrm{ecl,min}}}^{M_{\mathrm{ecl,max}}(\mathrm{SFR})} \xi(m \leq m_{\mathrm{max}}(M_{\mathrm{ecl}})) \\ &\times \xi_{\mathrm{ecl}}(M_{\mathrm{ecl}})\, dM_{\mathrm{ecl}}, \end{aligned} \tag{5.32}$$

where m is the initial stellar mass, M_{ecl} is the initial stellar mass of a star cluster, $M_{\mathrm{ecl,min}}$ is the minimum mass of newly formed star-clusters, $M_{\mathrm{ecl,max}}(\mathrm{SFR})$ is the SFR-dependent maximum mass of newly formed star-clusters, $\xi(m)$ is the IMF and $\xi_{\mathrm{ecl}}(M_{\mathrm{ecl}})$ is the star-cluster mass

function (Weidner & Kroupa 2005; Weidner et al. 2011). The IGIMF can be parametrized by a multi-power law,

$$\xi_{\rm IGIMF}(m) = k k_i m^{-\alpha_i}, \tag{5.33}$$

with

$$\begin{aligned} \alpha_1 &= 1.3, & 0.1 \leq \frac{m}{\rm M_\odot} < 0.5, \\ \alpha_2 &= 2.3, & 0.5 \leq \frac{m}{\rm M_\odot} < 1, \\ \alpha_{\rm IGIMF} &\in \mathbb{R}, & 1 \leq \frac{m}{\rm M_\odot} \leq m_{\rm max*}, \end{aligned}$$

where the factors k_i ensure that the IGIMF is continuous where the power changes and k is a normalization constant. $\xi_{\rm IGIMF}(m)$ equals 0 if $m < 0.1\,{\rm M_\odot}$ or $m > m_{\rm max*}$, where $m_{\rm max*}$ is the maximum stellar mass. Thus, the IGIMF defined here is equal to the IMF defined by Equation (5.1), except for the high-mass slope and the upper mass limit.

The case of a canonical IMF in all star-clusters, i.e. $\alpha_3 = 2.3$, implies (Weidner & Kroupa 2005) $\alpha_{\rm IGIMF} \gtrsim 3$. The expectation value for the number of SNII per year would then be $\lesssim 0.2$ per year. On the other hand, $\alpha_{\rm IGIMF} \lesssim 2$ is possible, if a varying IMF that becomes more top-heavy with star-cluster mass is considered (Weidner et al. 2011; Kroupa et al. 2011). This implies that the probability to actually observe four new SNII in a given year (Lonsdale et al. 2006) is essentially zero if the IMF is canonical in all star-clusters, but it can still be about 10 per cent if the IMF becomes top-heavy in massive UCD-type star-clusters.

The remnants produced by SNII are neutron stars and black holes. The SNII-rates thereby are an indicator for how many mergers of such remnants can be detected by searching for gravitational waves. Comparing the SN-rate for $\alpha_{\rm IGIMF} = 3$ to the SN-rate for $\alpha_{\rm IGIMF} = 2$ thus suggests that about an order of magnitude more of such events may be expected if the IMF in massive star-clusters is not canonical, but top-heavy. Thus, the hitherto predicted detection rate of about 30 mergers of dark remnants per year (Banerjee et al. 2010) for the upcoming adLIGO-experiment could be too low by an order of magnitude, as an invariant IMF has been used for this estimate.

Further evidence for a top-heavy IMF in star-bursting galaxies is found by Anderson et al. (2011) in Arp 299. They study numbers of different types of supernovae in Arp 299 and conclude from the mass of the appropriate progenitor stars that the IMF is probably top-heavy in that system. Thus, Anderson et al. (2011) qualitatively come to the same conclusion for Arp 299 as we did for Arp 220, while their method is different.

5.5 Star formation densities and the IMF

A top-heavy IMF in UCDs is in-line with different studies concluding a top-heavy IMF in high-redshift star forming galaxies (van Dokkum 2008; Loewenstein 2006). Contrary to this, a recent spectroscopic study of two low-redshift very massive elliptical galaxies suggests a hitherto unseen large population of low-mass stars (van Dokkum & Conroy 2010), which has been predicted as a possible consequence of cooling flows on massive ellipticals (Kroupa & Gilmore 1994). It is on the other hand unlikely that the majority of the UCDs formed in potential wells deeps enough to cause cooling flows.

Also note that the current stellar densities suggest that the star-formation densities (SFDs), i.e. the SFR per volume, of UCDs were very different from the SFDs of elliptical galaxies.

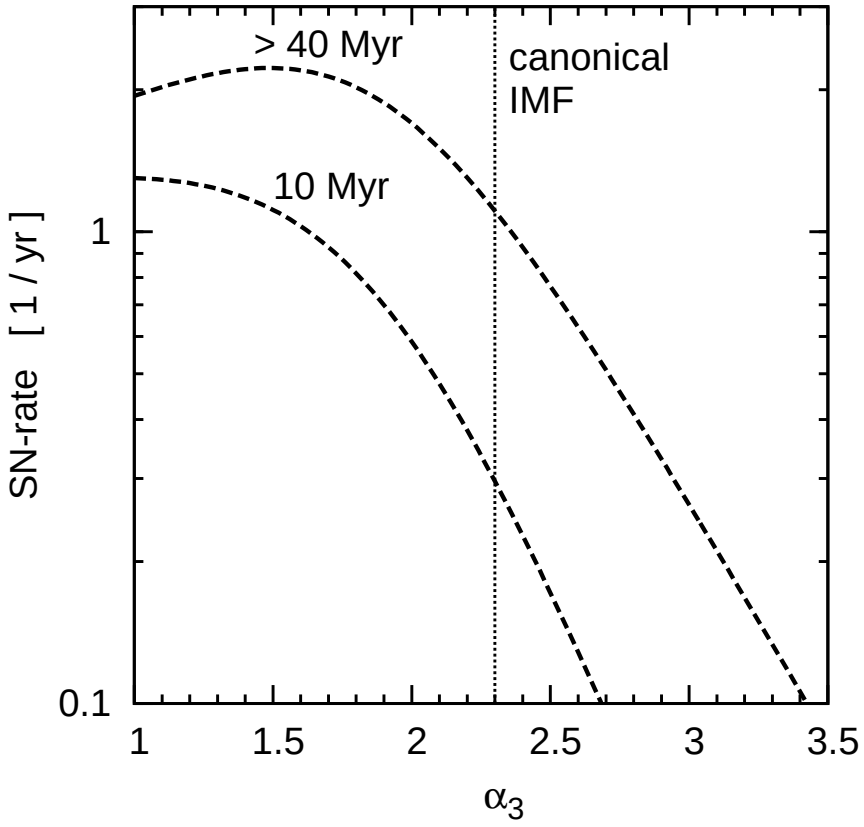

Figure 5.8: The SN-rate in the center of Arp 220. The SN-rates are functions of the slope of the IMF above a stellar mass of $1\,\mathrm{M}_\odot$, α_3, but also depend on the length of the star burst (which is indicated above the corresponding curve). They do not exceed ≈ 1 SN yr^{-1} for the canonical IMF (whose high-mass slope is marked by the dotted vertical line), or ≈ 2 SN yr^{-1} for a top-heavy IMF.

Consider for instance an exemplar present-day UCD with $M = 10^7\,\mathrm{M}_\odot$ and $r_\mathrm{h} = 10\,\mathrm{pc}$ and an exemplar present-day elliptical galaxy with $M = 10^{12}\,\mathrm{M}_\odot$ and $r_\mathrm{h} = 10^4\,\mathrm{pc}$. These values can be considered representative for typical UCDs and massive elliptical galaxies, respectively (cf. figure 4 in Misgeld & Hilker 2011). Star formation is thought to have proceeded quickly in UCDs and massive elliptical galaxies, so that the stellar population of the exemplar UCD may have formed within 10^7 yr (Dabringhausen et al. 2009) and the stellar population of the exemplar elliptical galaxy may have formed within 10^9 yr (Thomas et al. 2005). This leads to a SFR of $1\,\mathrm{M}_\odot\,\mathrm{yr}^{-1}$ for the exemplar UCD and to a SFR of $10^3\,\mathrm{M}_\odot\,\mathrm{yr}^{-1}$ for the exemplar elliptical galaxy. The SFD can be estimated by dividing the SFR by r_h^3, leading to a SFD of $10^{-3}\,\mathrm{M}_\odot\,\mathrm{yr}^{-1}\,\mathrm{pc}^{-3}$ for the exemplar UCD and a SFD of $10^{-9}\,\mathrm{M}_\odot\,\mathrm{yr}^{-1}\,\mathrm{pc}^{-3}$ for the exemplar elliptical galaxy. However, according to Dabringhausen et al. (2010) UCDs must have been even more compact when they formed ($r_\mathrm{h} \approx 1$ pc), since the mass loss following star formation with a top-heavy IMF must have expanded them to their present-day radii. With the masses of UCDs being $10^6\,\mathrm{M}_\odot \lesssim M \lesssim 10^8\,\mathrm{M}_\odot$, their SFRs ranged from $0.1\,\mathrm{M}_\odot\,\mathrm{yr}^{-1}$ to $10\,\mathrm{M}_\odot\,\mathrm{yr}^{-1}$ if they formed within 10 Myr. An initial r_h of 1 pc thereby implies SFDs ranging from $0.1\,\mathrm{M}_\odot\,\mathrm{yr}^{-1}\,\mathrm{pc}^{-3}$ to $10\,\mathrm{M}_\odot\,\mathrm{yr}^{-1}\,\mathrm{pc}^{-3}$. Thus, the SFDs of UCDs can easily be higher by six to ten orders of magnitude than the SFDs of massive elliptical galaxies. Massive ellipticals can therefore not serve as a proxy for the stellar population in UCDs.

It is therefore perhaps the SFD that determines whether the IMF in some region of space becomes top-heavy, and not the overall SFR in a forming stellar system. This is actually consistent

with models why the IMF may become top-heavy: Dabringhausen et al. (2010) argue that the central densities in forming UCDs were so high ($\rho > 10^5\ \mathrm{M}_\odot\, pc^{-3}$) that collisions and perhaps mergers between pre-stellar cores were important in them, in contrast to less massive stellar systems. Likewise, if the heating of molecular clouds by cosmic rays is the process by which the IMF becomes top-heavy (Papadopoulos 2010), it is again not the number, but the number *density* of the surrounding massive stars that makes heating of the molecular cloud effective.

5.6 Conclusion

The dynamical mass-to-light ratios of ultra compact dwarf galaxies (UCDs) are surprisingly high (Haşegan et al. 2005; Dabringhausen et al. 2008; Mieske et al. 2008). This finding was explained by Dabringhausen et al. (2009) with an IMF that has more massive stars than the canonical IMF deduced by Kroupa (2001) from resolved stellar populations in the Milky Way. The high mass-to-light ratio of UCDs is then a consequence of a large population of dark remnants (i.e. neutron stars and black holes) in them.

These dark remnants become visible as X-ray sources if they accrete matter from a low-mass companion star. The rate at which low-mass X-ray binaries (LMXBs) are formed in globular clusters and UCDs scales with the number density of dark remnants (see Section 5.3.2). Data on the fraction of UCDs that harbour a bright X-ray source (Sivakoff et al. 2007) can therefore be used to confirm the presence of a large population of dark remnants in UCDs by a method that does not rely on the fact that dark remnants only increase the mass of a UCD, but not its luminosity. It is shown in this paper that LMXBs in UCDs are indeed up to 10 times more frequent than expected for an invariant, canonical IMF. The overabundance of LMXBs is used to quantify the dependence of the high-mass IMF-slope, α_3, on the luminosity of UCDs. This function is essentially equal to the dependence between the luminosity of the UCDs and their α_3 suggested in Dabringhausen et al. (2009) based on the mass-to-light ratios of UCDs (see Section 5.3.3). Note that the L_V of present-day GCs and UCDs is just one of many properties of such systems. Dependencies of α_3 on their initial mass, initial density and their metallitcity are therefore discussed in Marks et al. (2012).

UCDs can be understood as the most massive star-clusters which only form at extremely high galaxy-wide star formation rates (SFRs) (Weidner & Kroupa 2004). Alternatively, UCDs could form by the merger of gravitationally bound systems of star clusters as they are observed in interacting galaxies (Fellhauer & Kroupa 2002a). In either case, the formation of UCDs would be connected to star-bursts. Given that ultra-luminous infra-red galaxies (ULIRGs) are interpreted as galaxies with star-bursting regions (Condon et al. 1991), they should show indications of a top-heavy IMF as a consequence. The nearest ULIRG is Arp 220. We show that the observed rate of type II supernovae in this ULIRG is indeed highly improbable if the IMF is invariant, but not if the IMF is top-heavy (see Section 5.4).

There are thus three mutually consistent arguments for a top-heavy IMF in UCDs or more generally star-bursting systems. Together with the evidence for the formation of UCDs being connected to star bursts, these arguments imply that the IMF becomes top-heavy in star-bursts (cf. Weidner et al. 2011). This finding stands in contrast to the prevalent notion that the IMF is invariant (Kroupa 2001, 2002; Bastian et al. 2010; Kroupa et al. 2011) and thereby has important implications. For instance, estimates of the SFR of a galaxy based on observations that are sensitive only to high-mass stars and the assumption of an invariant IMF (like Equation 5.31) are too high if the IMF actually is top-heavy. Consequently, estimates for the time scale on which

the population of low-mass star in that galaxy is built up until the gas of the galaxy is depleted become too short. Also the chemical evolution of galaxies is different if the IMF in them can become top-heavy, since the nuclear reactions that occur in a star mainly depend on its mass. This has implications on their content of metals and planetary systems (Ghezzi et al. 2010). Furthermore, as more dark remnants are formed if the IMF is top-heavy, more dark-remnant mergers and thus gravitational-wave emitters should be detected in this case. Finally, the dynamical evolution of star clusters critically depends on the shape of the IMF (Dabringhausen et al. 2010).

Acknowledgments

J.D acknowledges support through DFG-grant KR1635/13 and thanks ESO for financial support via a grant from the Director General Discretionary Fund in 2009. The authors wish to thank Tom Maccarone for some useful comments.

Chapter 6

Dwarf elliptical galaxies as ancient tidal dwarf galaxies

J. Dabringhausen, P. Kroupa, 2013, **MNRAS**, 429, 1858

Abstract:

The formation of tidal dwarf galaxies (TDGs) is triggered by the encounters of already existing galaxies. Their existence is predicted from numerical calculations of encountering galaxies and is also well documented with observations. The numerical calculations on the formation of TDGs furthermore predict that TDGs cannot contain significant amounts of non-baryonic dark matter. In this paper, the first exhaustive sample of TDG-candidates from observations and numerical calculations is gathered from the literature. These stellar systems are gas-rich at the present, but they will probably evolve into gas-poor objects that are indistinguishable from old dwarf elliptical galaxies (dEs) based on their masses and radii. Indeed, known gas-poor TDGs appear as normal dEs. According to the currently prevailing cosmological paradigm, there should also be a population of primordial galaxies that formed within haloes of dark matter in the same mass range. Due to their different composition and origin, it would be expected that objects belonging to that population would have a different structure than TDGs and would thus be distinguishable from them, but such a population cannot be identified from their masses and radii. Moreover, long-lived TDGs could indeed be numerous enough to account for all dEs in the Universe. Downsizing, i.e. that less massive galaxies tend to be younger, would then be a natural consequence of the nature of the dEs. If these claims can be kept up in the light of future observations, the presently prevailing understanding of galaxy formation would need to be revised.

6.1 Introduction

Observations show that encountering galaxies often have bridges of matter connecting them or elongated arcs of matter extending from them (Zwicky 1956). Well known examples are the Antennae Galaxies (NGC 4038 and NGC 4039) and the Mice Galaxies (NGC 4676A and NGC 4676B). Theoretically, the formation of these filamentary structures can be understood by gravitational forces that the encountering galaxies exert on each other (Toomre & Toomre 1972). These gravitational forces lead to a distortion of the galaxies, because strength and direction of an external gravitational force depends on the location within a galaxy. The position-dependent changes of the external force within the galaxy are known as tidal forces, and hence the arcs of matter created by them are called tidal tails.

The disks of spiral galaxies are, due to their extension, particularly sensitive to tidal forces. The tidal tails thereby formed mostly consist of matter coming from the disks of the galaxies, i.e. stars and a considerable amount of gas.

Numerical calculations show that some of the gas in the tidal tails collapses into structures that are bound by their own gravity (Barnes & Hernquist 1992b; Elmegreen et al. 1993; Bournaud 2010). These structures have masses of up to $10^9\,\mathrm{M}_\odot$ (Elmegreen et al. 1993; Bournaud & Duc 2006) and have radii of the order of 1 kpc (Wetzstein et al. 2007; Bournaud et al. 2008). It has also been shown that these objects can survive on a time-scale of 10^9 years and can be sites of long-lasting star formation (Bournaud & Duc 2006; Recchi et al. 2007). With these properties, the structures emerging in the tidal tails can be considered galaxies (cf. Bournaud et al. 2007; Forbes & Kroupa 2011). Due to their size and their origin, such galaxies been named tidal dwarf galaxies (TDGs), and a number of structures that are TDG-candidates have been observed (Mirabel et al. 1992; Monreal-Ibero et al. 2007; Yoshida et al. 2008; Duc P. A. et al. 2011).

However, the formation of the first galaxies in the Universe is driven by non-baryonic cold dark matter (CDM) according to the ΛCDM-model, which is the currently prevailing cosmological model. The CDM is thought to collapse into haloes and thereby to create the gravitational potentials that bind the baryons of the forming galaxies. In order to distinguish them from TDGs, these galaxies are called primordial galaxies.

In contrast to the primordial galaxies, the TDGs are predicted to consist only of baryonic matter, even if the progenitors of the TDGs contained a substantial amount of CDM (Barnes & Hernquist 1992b; Duc et al. 2004; Bournaud & Duc 2006; see also Bournaud 2010 for a theoretical discussion of this finding).

Since only the baryonic matter interacts electromagnetically, CDM and baryonic matter must behave differently. Due to the different composition of the TDGs and the primordial galaxies, it would be natural if these two types of galaxies would constitute populations that are distinguishable by their properties. Thus, observations and theoretical calculations support the notion that there are two types of galaxies, namely primordial galaxies and TDGs. This finding has been termed the 'Dual Dwarf Galaxy Theorem' by Kroupa (2012).

A substantial fraction of the galaxies of the Universe are dwarf elliptical galaxies (dEs). These dEs are of particular interest, because the masses of their stellar populations and their radii would fit to TDGs, but they are usually considered to be the kind of galaxies that forms within CDM-haloes of rather low masses (see, e.g., Li et al. 2010; Guo et al. 2011). Reviews on dEs and how they may have formed are given by Ferguson & Binggeli (1994) and Lisker (2009).

Using a compilation of data on old, dynamically hot stellar systems by Misgeld & Hilker

(2011) on the one hand and a first-time compilation of data from various authors on masses and radii of observed TDG-candidates (observed or from numerical calculations) on the other hand, it is discussed in this paper whether primordial galaxies and TDGs are indeed distinguishable populations, as would be expected. The data used for this comparison is described in Section (6.2). The results are presented and discussed in Sections (6.3) and (6.4). Our conclusions are given in Section (6.5).

6.2 Data

6.2.1 Old stellar systems

Galaxies

Data on the masses and the radii of old elliptical galaxies are taken from Bender et al. (1992) and Bender et al. (1993), Ferrarese et al. (2006), Misgeld et al. (2008) and Misgeld et al. (2009). The data on the dwarf spheroidal galaxies (dSphs) are taken from Table (1) in Misgeld & Hilker (2011), provided an estimate of the mass of their stellar populations, M_*, is available there. This table also lists some compact elliptical galaxies, which are included in the present compilation as well. The catalogues of galaxies in the Hydra I cluster (Misgeld et al. 2008) and galaxies in the Centaurus cluster (Misgeld et al. 2009) comprise a large number of dwarf elliptical galaxies (dEs) and are of particular interest for filling a gap in luminosity between the data from Bender et al. (1992, 1993) and the dSphs from Table (1) in Misgeld & Hilker (2011). The M_* of all mentioned galaxies are calculated from their published luminosities and colours, using the estimates for their stellar mass-to-light ratios published in Misgeld & Hilker (2011). Note that the baryonic masses, M, of these objects are essentially equal to M_* since these kinds of galaxies contain almost no gas or dust (Wiklind et al. 1995; Young L. M. et al. 2011).

GCs and UCDs

Masses and effective radii of globular clusters (GCs) and ultra compact dwarf galaxies (UCDs) are taken from Table (5) in Mieske et al. (2008). Note that the masses listed in that table are mass estimates based on the internal dynamics of the GCs and UCDs (i.e. dynamical masses, $M_{\rm dyn}$) instead of masses estimated from the light and colour of the stellar populations (i.e. M_*). The internal dynamics of GCs and UCDs is however probably not influenced by a hypothetical presence of DM in them, since DM would usually be distributed over larger scales. (Murray 2009; Willman & Strader 2012). A non-Newtonian law of gravity in the limit of weak fields (i.e. the alternative to the dark matter hypothesis) would also leave the dynamics of GCs and UCDs unaffected in most cases (see figure 7 in Kroupa P. et al. 2010). Finally, GCs are free of gas and dust (van Loon et al. 2006), and given the similarities of UCDs to GCs, it is reasonable to assume the same for UCDs. These reasons imply that $M_{\rm dyn} = M_*$ for GCs and UCDs[1].

[1]Note that some authors discuss the elevated M/L_V ratios of UCDs (see, e.g., Haşegan et al. 2005; Dabringhausen et al. 2008; Mieske et al. 2008), which suggest the opposite to be true. The detected difference between the $M_{\rm dyn}$ and the M_* of UCDs is however rather small, even though this deviation probably carries important information on star formation in UCDs (see Dabringhausen et al. 2009, 2012; Marks et al. 2012 and the review by Kroupa et al. 2011).

6.2.2 TDGs

Observed TDG-candidates

Data on the masses and the effective radii of observed TDG-candidates are difficult to obtain and collected from various sources in the literature:

- Miralles-Caballero et al. (2012). The sample from Miralles-Caballero et al. (2012) is an extension of the sample from Monreal-Ibero et al. (2007). The TDG-candidates taken from Miralles-Caballero et al. (2012) are, among all TDG-candidates considered in the present paper, the ones for which the most complete information on masses and radii is available. The data given on the TDG-candidates comprise their equivalent total radii (r), their effective radii ($r_{\rm e}$), their mass estimated from their I-band luminosity using the ages estimated under the assumption of a single star burst (M_I), their mass estimated from their Hα-emission lines ($M_{\rm H\alpha}$), their mass estimated from their I-band luminosity under the assumption that most stars in the TDG-candidates are old ($M_{\rm old}$) and their mass estimated from the internal dynamics of the TDG-candidates ($M_{\rm dyn}$). M_I, $M_{\rm H\alpha}$ and $M_{\rm old}$ are all estimates for M_*, the mass of the stellar population of the TDG-candidate. In oder to have a concrete value for M_*, $M_* = M_I$ is assumed, since estimates for M_* based on optical luminosities are available also for all other TDG-candidates, in contrast to estimates based on Hα-emission. Setting $M_* = M_I$ therefore adds to the homogeneity of the sample of TDG-candidates. The adopted single-burst age is the average of the age estimate derived from photometric data and the age estimate derived from the equivalent width of the Hα-emission. The values are of the order of 10^6 years. Miralles-Caballero et al. (2012) estimate r by adding up the areas of all Hα-emitting regions within a TDG-candidate, leading to a total area $A_{\rm T}$, from which r is calculated from

$$r = \sqrt{\frac{A_{\rm T}}{\pi}}. \tag{6.1}$$

  The average ratio between r and $r_{\rm e}$ of the TDG-candidates in Miralles-Caballero et al. (2012) is 3.5. The standard deviation about this value is 1.1. Simple estimates of $r_{\rm e}$ from r can thereby be calculated from

$$r = (3.5 \pm 1.1) \times r_{\rm e} \tag{6.2}$$

  for other galaxies. Note, however, that Miralles-Caballero et al. (2012) only estimate the effective radius of the dominating knot if a TDG-candidate has more than one star-forming knot. Thus, $r_{\rm e}$ is underestimated for these TDG-candidates.

- Galianni et al. (2010). The TDG-candidates discussed by them have V-band luminosities of 1.6×10^6 $\rm L_\odot$ and 2.6×10^6 $\rm L_\odot$, respectively. By giving estimates for the stellar masses of these TDG-candidates, Galianni et al. (2010) implicitly state that the V-band mass-to-light ratio of the TDG-candidates is 2.5 $\rm M_\odot/L_\odot$, and 2.3 $\rm M_\odot/L_\odot$, respectively. A comparison with single-burst stellar population models (e.g. Maraston 2005) suggests that these assumptions on the M/L_V-ratios of the TDG-candidates discussed in Galianni et al. (2010) are reasonable, since Galianni et al. (2010) conclude from a spectroscopical analysis that the stellar populations of their TDG-candidates are old and have metallicities [Fe/H]> -1, like the ones of old GCs and dSphs. Values for $r_{\rm e}$ have been found by fitting Sérsic-profiles (Sérsic 1963) to the TDG-candidates.

- Yoshida et al. (2008). Photometric data suggests an age of the order of 10^8 years for the star-forming knots they observed (termed 'fireballs' by them). This motivates their assumption of $M_*/L_R = 1\mathrm{M}_\odot/\mathrm{L}_\odot$ for the objects when they calculate the stellar masses of the objects from their R-band luminosities. Values for r_e have been estimated by fitting Gaussian profiles to their luminosity profiles. They are only given collectively as ranging between 200 pc and 300 pc for all observed objects. In order to have a concrete value for the radii, they are set to 250 pc for all fireballs in the present paper.

- Duc et al. (2007). The TDG-candidate identified by them has a stellar population with a mass between $M_* = 3 \times 10^7\ \mathrm{M}_\odot$ and $M_* = 7 \times 10^7\ \mathrm{M}_\odot$, as they find from fitting a modeled stellar population to the spectral energy distribution of the TDG-candidate. In order to have a definite value, $M_* = 5 \times 10^7 \mathrm{M}_\odot$ is assumed in the present paper. Photometric data suggests that most stars in this TDG-candidate formed 3×10^8 years ago and the diameter of the TDG-candidate is given as 4200 pc.

- Bournaud et al. (2007). The stellar masses of the three TDGs discussed in that paper have been estimated from their optical luminosities and models of young stellar populations, since Boquien et al. (2007) estimate ages of less than 5×10^6 years for the stellar populations of these galaxies. The radii given in Bournaud et al. (2007) are the radii up to which rotation curves have been measured. For an estimate of r_e from these radii, equation (6.2) is used in the present paper.

- Tran H. D. et al. (2003). Photometric data suggest an age of $4 - 5 \times 10^6$ for the TDG-candidate discussed in that paper. Its V-band luminosity (corrected for emission lines) then implies $M_* = 6.6 \times 10^5\ \mathrm{M}_\odot$. r_e was estimated by fitting a King model (King 1962) to the surface-brightness profile of the object.

- Hunsberger et al. (1996). The masses of the TDG-candidates listed in that paper are estimated from their R-band luminosities under the assumption that the M_*/L_R ratios of the TDG-candidates is 1 $\mathrm{M}_\odot/\mathrm{L}_\odot$. This M_*/L_R ratio implies an age of the order of 10^8 years for the TDG-candidates. This choice for the age is motivated with Hunsberger et al. (1996) searching for TDG-candidates in Hickson compact groups (Hickson 1982), i.e. in very compact groups of galaxies. Such groups have lifetimes of the order of 10^8 years, within which the formation of TDGs is triggered by the interaction between primordial galaxies belonging to the group. The extension of the TDG-candidates is quantified in Hunsberger et al. (1996) by estimates of their diameters from their projected areas. Estimates of the r_e of the TDG-candidates are calculated in the present paper with equation eq. (6.2).

The adopted properties of the observed TDG-candidates are summarized in Table (A.1) in Appendix (A.3.1).

Note that not all objects in Table (A.1) are confirmed TDGs. The reasons are the following:

- For some young objects, it is doubtful whether they will be stable (cf. Monreal-Ibero et al. 2007; Miralles-Caballero et al. 2012), even though their origin from tidal interactions between primordial galaxies is not disputed.

- Tran H. D. et al. (2003) argue that the TDG-candidate they observed possibly was a stellar supercluster (SSC), i.e. a gravitationally bound complex of star clusters, which

can evolve into a galaxy if a galaxy is defined as a stellar system with a relaxation time larger than a Hubble time (Kroupa 1998; Forbes & Kroupa 2011). In this sense, SSCs can be understood as precursors of TDGs. SSCs are however also seen as likely progenitors of extended star-clusters and UCDs (Fellhauer & Kroupa 2002a,b; Brüns et al. 2011), i.e. objects that are much more compact than the TDG-candidates in Table (A.1) are, including the TDG-candidate discussed by Tran H. D. et al. (2003).

- Yoshida et al. (2008) consider it more likely that the objects they observed formed from gas that was stripped from the probable merger remnant RB 199 due to its motion through the intergalactic medium, rather than from matter ejected by the tidal forces acting between the progenitors of RB 199 during the merger. In order to distinguish the objects they observed from actual TDGs, they termed them 'fireballs'. On the other hand, the fireballs are gas-rich and star-forming, like the TDG-candidates observed by Monreal-Ibero et al. (2007) and Miralles-Caballero et al. (2012). The fireballs are also indistinguishable from the TDG-candidates based on their masses and radii, and both kinds of objects have formed from matter that was previously bound to other galaxies, in contrast to primordial galaxies. Moreover, the arguments by Bournaud (2010) for why TDGs do not contain DM would also hold for galaxies that form from stripped gas. The fireballs are therefore in the following also considered as TDGs, even if the fireballs are not actual TDGs.

In the present paper, we will concentrate on the question how the TDG-candidates will evolve if they are indeed long-lived, self-gravitating structures, as at least some (if not all) of them are. For simplicity, all objects in Table (A.1) will thus be treated like actual, long-lived TDGs in the following. This can be motivated by the finding that they indeed make the impression of a homogeneous sample in Fig. (6.2).

Numerical calculations of TDGs

As a complement to the observed TDG-candidates, numerically calculated TDG-candidates are considered as well. The formation of TDGs during the Newtonian interaction between gas-rich galaxies has been studied with numerical calculations by many authors (e.g. Barnes & Hernquist 1992b; Elmegreen et al. 1993; Barnes & Hernquist 1996; Bournaud & Duc 2006; Wetzstein et al. 2007; Bournaud et al. 2008). Detailed parameters of the resulting objects are however only available for a few exemplary objects, which come from the following sources:

- Bournaud et al. (2008), who show in their figure (5) five TDG-candidates as they appear at the end of their numerical calculation. Values for M_* are given in that figure. In order to calculate estimates for the r_e of these objects, the absolute maximal extension of these objects and the maximal extension along the orthogonal axis were read off from this figure. These values were multiplied in order to obtain an estimate A_T, which was used to calculate an equivalent radius from equation (6.1). These equivalent radii were used to calculate r_e from equation (6.2).

- Wetzstein et al. (2007), who describe the most massive TDG-candidate that formed in their numerical calculation in detail. If the progenitor galaxy of the TDG-candidate is scaled to the Milky Way, the total mass of the TDG-candidate is $M \approx 3.5 \times 10^8\ M_\odot$. About 70 per cent of this mass is gas. Since there is no DM within the TDG-candidate (even though the progenitor galaxy was assumed to reside within a DM-halo), the mass

of the stellar population of the TDG is 30 per cent of its total mass. Fitting Sérsic-profiles (Sérsic 1963) to the calculated TDG-candidate, Wetzstein et al. (2007) estimated that the $r_{\rm e}$ of the stellar population is 700 pc for the adopted scaling. The same procedure holds $r_{\rm e} = 1400$ pc of the gaseous component of the TDG-candidate.

- Barnes & Hernquist (1992b), who describe the most massive TDG that formed in their numerical calculation in detail. If the two progenitor galaxies in the numerical calculation are scaled to the Milky Way, the total mass of the TDG is $M \approx 4 \times 10^8\ M_\odot$. Barnes & Hernquist (1992b) note that there is no DM within the TDG, but they do not distinguish stars and gas in their numerical calculation. It is therefore assumed here that the ratio between gas and stars is the same as in the TDG calculated by Wetzstein et al. (2007). An estimate for $r_{\rm e}$ of this TDG was calculated from the left panel of figure (1) in Barnes & Hernquist (1992b). The TDG shown there has a diameter of $\approx 6.15 \times 10^{-2}$ length units, corresponding to ≈ 2500 pc if the progenitor galaxies are scaled to the Milky Way. Using equation (6.2), this implies $r_{\rm e} \approx 350$ pc.

The adopted properties of the observed TDG-candidates are summarized in Table (A.2).

6.3 Results

6.3.1 Properties of old dynamically hot stellar systems

It is well known that old, dynamically hot (or pressure-supported) stellar systems can be divided into two categories: A star-cluster-like population consisting of GCs and UCDs and a galaxy-like population consisting of normal elliptical galaxies (nEs), dwarf elliptical galaxies (dEs) and dwarf spheroidal galaxies (dSphs) (Gilmore et al. 2007; Forbes et al. 2008; Misgeld & Hilker 2011). Almost every object shown can indeed easily be assigned to one these two populations by its position in Figure (6.1). Exceptions like UCD 3 or M32 are extremely rare (see also Section 6.4.2).

Within these two populations of stellar systems, subpopulations can be identified by changes of the mass-radius relations that characterize these subpopulations. This leads to a distinction between dSphs, dEs and nEs within the galaxy-like population and a distinction between GCs and UCDs within the star-cluster-like population (e.g. Misgeld & Hilker 2011).

The exact locations of the transition from one subpopulation to another is a matter of definition. In the present paper, members of the galaxy-like population are considered dEs if they have a stellar mass $M_* \leq 3 \times 10^9\ \mathrm{M}_\odot$ and nEs otherwise. It is impossible to make a similar distinction between dEs and dSphs (cf. Ferguson & Binggeli 1994). Thus dEs and dSphs will all be referred to as dEs in the following. Taking their M_* to be equal to their total mass (cf. Section 6.2.1), members of the star-cluster-like population are considered GCs if they have a stellar mass $M_* \leq 2 \times 10^6\ \mathrm{M}_\odot$ and UCDs otherwise.

Performing a least-squares fit to dEs with masses $M_* > 10^4\ \mathrm{M}_\odot$, a mass-radius relation for them is quantified as

$$\log_{10}\left(\frac{r_{\rm h}}{\rm pc}\right) = (0.122 \pm 0.013)\log_{10}\left(\frac{M_*}{\mathrm{M}_\odot}\right) + (1.87 \pm 0.10). \quad (6.3)$$

Performing the same kind of fit to dEs with masses $M_* < 10^6\ \mathrm{M}_\odot$ leads to

$$\log_{10}\left(\frac{r_{\rm h}}{\rm pc}\right) = (0.42 \pm 0.08)\log_{10}\left(\frac{M_*}{\mathrm{M}_\odot}\right) + (0.3 \pm 0.3). \quad (6.4)$$

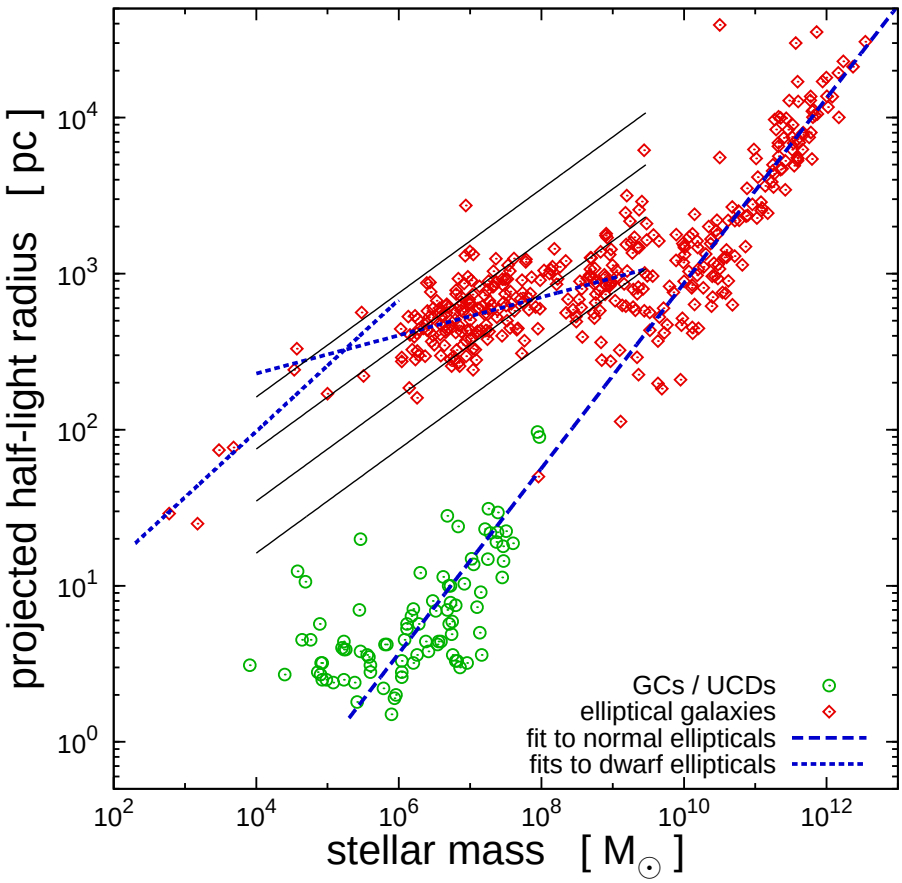

Figure 6.1: The half-light radii of old stellar systems against the mass of their stellar populations, M_* (cf. Section 6.2.1). Provided that the mass of dust, gas and non-baryonic matter is negligible in these systems, the estimates for the mass of their stellar populations are in fact estimates of their total masses. The distinction between GCs and UCDs and elliptical galaxies is as in the literature from which the data is taken. The dashed line is a mass-radius relation obtained through a least-squares fit to (normal) elliptical galaxies with masses $M_* > 3 \times 10^9\ M_\odot$ (cf. equation 6.6), which incidentally also fits well to the UCDs. The dotted lines are mass-radius relations obtained through least-squares fits to (dwarf) elliptical galaxies with masses $10^4\ \mathrm{M}_\odot \leq M_* \leq 3 \times 10^9\ M_\odot$ (cf. equation 6.3), and (dwarf) elliptical galaxies with masses $M_* < 10^6\ \mathrm{M}_\odot$ (cf. equation 6.4), respectively. The thin solid lines indicate constant densities of $\rho = 10^{-3}\ \mathrm{M}_\odot\,\mathrm{pc}^{-3}$, $\rho = 10^{-2}\ \mathrm{M}_\odot\,\mathrm{pc}^{-3}$, $\rho = 0.1\ \mathrm{M}_\odot\,\mathrm{pc}^{-3}$ and $\rho = 1\ \mathrm{M}_\odot\,\mathrm{pc}^{-3}$ from top to bottom.

A constant mean density for galaxies implies

$$\log_{10}\left(\frac{r_\mathrm{h}}{\mathrm{pc}}\right) = \frac{1}{3}\log_{10}\left(\frac{M_*}{\mathrm{M}_\odot}\right) + c, \tag{6.5}$$

where c is a constant. Equation (6.5) is consistent with equation (6.4), so that dEs with very low masses may indeed be characterized by a typical average density. This is however not the case for the more massive dEs. Their typical densities increase with their mass, as is apparent from equation (6.3).

There are however several potential problems with the data on dEs with masses $M_* < 10^6\ \mathrm{M}_\odot$:

1. The data is very sparse in that mass range. The mass-radius relation given by equa-

tion (6.4) is derived from only nine dEs, of which the five most massive ones are also well consistent with mass-radius relation given by equation (6.3).

2. The objects in this mass-range have very low surface brightnesses, so that their $r_{\rm e}$ are difficult to measure.

3. If these objects are pure stellar populations (for instance because they formed as tidal dwarfs and thus contain no DM), they are the most vulnerable to tidal fields that may alter their structure (Kroupa 1997; Metz & Kroupa 2007; Casas et al. 2012, see also Section 6.3.3)

Thus, the apparent steepening of the mass-radius relation for dEs towards lower masses has to be taken with caution.

A least-squares fit to nEs yields

$$\log_{10}\left(\frac{r_{\rm h}}{\rm pc}\right) = (0.593 \pm 0.027)\log_{10}\left(\frac{M_*}{\rm M_\odot}\right) - (2.99 \pm 0.30). \quad (6.6)$$

This mass-radius relation for nEs is consistent with the result in Dabringhausen et al. (2008), even though Dabringhausen et al. (2008) estimated the masses of the nEs from their $r_{\rm h}$ and their velocity dispersions, whereas in this paper their luminosities and colours were used.

UCDs lie along the same mass-radius relation as nEs, even though UCDs belong to the star-cluster-like population while nEs belong to the galaxy-like population (Dabringhausen et al. 2008). Note that UCDs were not included in the fit of equation (6.6) to the data. The mass-radius relation of GCs, in contrast, is essentially flat.

Possible reasons for the transition from dEs to nEs are discussed in Section (6.4.4) and possible reasons for the transition from GCs to UCDs are discussed in Section (6.4.4).

6.3.2 Properties and evolution of TDGs

A comparison of the numerically calculated TDG-candidates with the observed TDG-candidates shows that the estimates of M_* and $r_{\rm e}$ of the calculated TDG-candidates are consistent with the observed ones. If these parameters are however compared to the according present-day parameters of the GCs, UCDs, dEs and nEs (i.e. the stellar systems introduced in Section 6.2.1 and shown in Figure 6.1), the (young) TDG-candidates are on a mass-radius relation below the mass-radius relation for (old) dEs. The old TDGs by Galianni et al. (2010) are however consistent with being typical dEs.

In order to find the actual interrelations between the TDG-candidates and the other stellar systems, it is necessary to estimate what they would look like if they all had the same age. This requires to account for the future evolution of the TDG-candidates listed in Tables (A.1) and (A.2) in the Appendix, since almost all of them have ages of the order of 10^8 years or less, while the objects shown in Figure (6.1) are at least a few 10^9 years old (see Misgeld & Hilker 2011). The age difference between these systems is consistent with the finding that many TDG-candidates show evidence for ongoing star formation, as the Hα-emission from these systems indicates.

The amount of gas is actually very substantial in the three TDG-candidates observed by Bournaud et al. (2007). They estimate the mass of the stars in these TDG-candidates by their luminosity and the amount of gas in them by the strength of their emission lines. They thereby

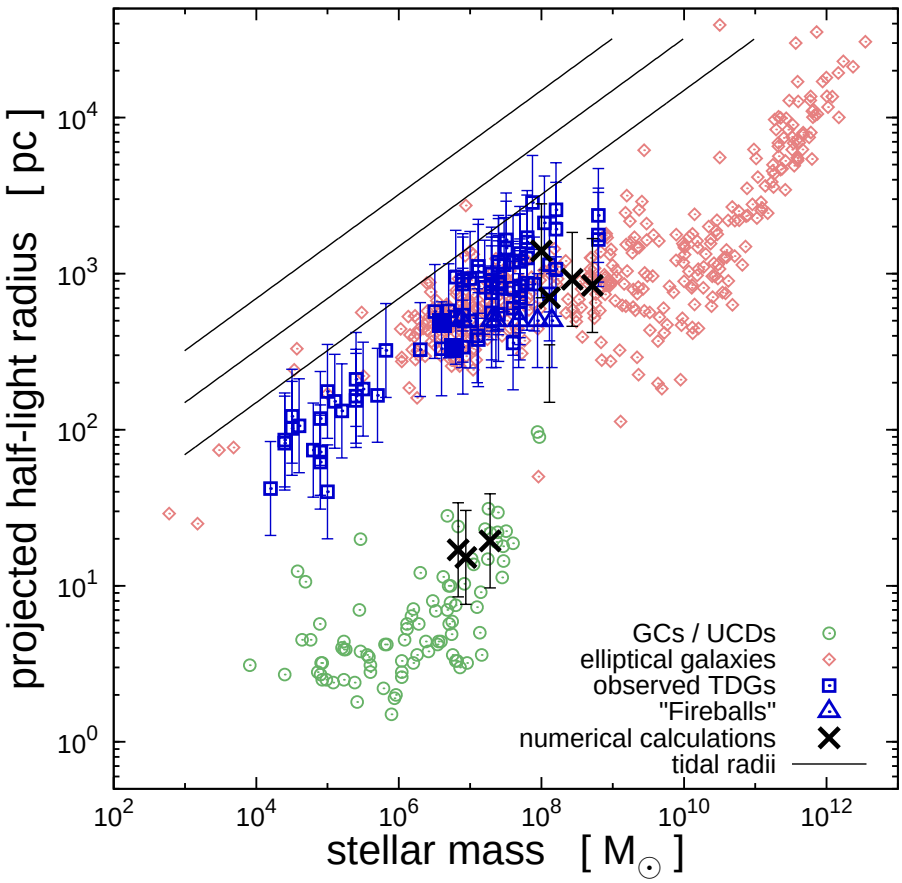

Figure 6.2: Estimates for the final radii of TDG-candidates after their gas has been expelled against estimates of their stellar mass, M_*. The estimates are based on the data on present-day parameters of TDG-candidates (cf. Section 6.2.2 and Table A.1) and on data on TDGs taken from numerical calculations on the formation of TDGs during the encounter of gas-rich galaxies (cf. Section 6.2.2 and Table A.2). Probably the largest uncertainty to the data on the TDG-candidates shown here comes from the poor knowledge on how star-formation and mass-loss will influence the future evolution of the gas-rich present-day TDG-candidates until they possibly resemble old, gas-poor dEs (cf. Section 6.3.2). In order to quantify this uncertainty on the data for the TDG-candidates, the lower limit for future radius of each TDG-candidate is taken to be its present-day radius, which corresponds to no future mass-loss according to equation (6.8). The symbol representing the TDG-candidate is placed at a radius twice its present-day radius, which corresponds to a future mass-loss of half of its present-day mass according to equation (6.8). The upper limit for the radius of each TDG candidate is taken to be four times its present-day radius, which corresponds to a loss of 75 per cent of its present-day mass according to equation (6.8). Thus, the errorbars to the data on the TDG-candidates shown here were not formally calculated from the uncertainties to the observational data, but represent different assumptions on the future evolution of the TDG-candidates. These assumptions are admittedly quite arbitrary, but as they are not very restrictive concerning the future mass-loss (and thus the future evolution) of the TDG-candidates, they are also conservative. The data on old stellar systems presented in Fig. (6.1) are also shown here for comparison. The thin solid lines indicate the tidal radii for stellar systems in the vicinity of a major galaxy 10^5 pc away. The mass of the major galaxy is $M = 10^{10}$ $\mathrm{M}_\odot$, $M = 10^{11}$ $\mathrm{M}_\odot$ and $M = 10^{12}$ $\mathrm{M}_\odot$, from top to bottom.

find that stars make up only about ten per cent of the baryonic mass in each of the TDG-candidates they studied. Such a detailed analysis of their composition has not been made for the

other TDG-candidates discussed in the present paper. It is however likely that the composition of other very young TDG-candidates from Miralles-Caballero et al. (2012) with ages of the order of 10^6 years is similar, especially since the masses derived from their internal dynamics are much higher than the masses derived from the luminosity of their stellar populations. The TDG-candidates discussed by Yoshida et al. (2008) and Duc P. A. et al. (2011) suggest that also TDG-candidates with ages of at least 10^8 years can still contain enough gas to be sites of very recent star-formation. Thus, gas is the principal mass component in many of the TDG-candidates, since they do not contain DM (Barnes & Hernquist 1992b; Bournaud 2010; Kroupa 2012). The fate of the gas in the TDG-candidates is therefore decisive for their future evolution.

The two TDG-candidates studied by Galianni et al. (2010) are the only ones in Table (A.1) that have ages similar to those of the old stellar systems introduced in Section (6.2.1). Like the other old stellar systems, the TDG-candidates show no traces of ongoing star-formation, which suggests that there is no gas left in them. This motivates the assumption that the other TDG-candidates will also have lost their gas once they have reached that age.

There are several processes by which the gas can disappear from the young TDG-candidates on a time-scale of the order of 10^9 years:

1. The conversion of gas into stars.

2. The removal of the gas through heating by massive stars that form in the TDG-candidates.

3. The removal of the gas through ram-pressure stripping when the TDG-candidates move through the intergalactic medium.

More than one of these processes may contribute to the removal of the gas. The first two processes are even intimately linked to each other, since the presence of massive stars implies recent star formation, while the removal of gas through the heating of these massive stars influences further star formation. This interrelation is known as feedback. The second and the third process are similar regarding their effect on the further evolution of the stellar system. Both imply that the TDG-candidate looses mass and in consequence expands (see Kroupa 2008 for a detailed discussion on the effect of mass-loss on stellar systems). However, the actual contribution of each of these processes to the disappearance of the gas in the TDGs is unknown. It is likely to be different for each individual TDG, but according to the models by Recchi et al. (2007), an isolated TDG self-regulates its star-formation such that it is relatively stable against feedback and major blow-outs do not arise.

Let us assume for now that the second and the third process are the most relevant ones for the future evolution of an existing young TDG-candidate, i.e. that it looses much of its mass through the removal of gas, while only little of the gas is converted into stars that add to the existing stellar population of the TDG-candidate. This assumption is motivated by the finding that the gravitational potentials of the TDG-candidates are rather shallow (Bournaud 2010), so that matter can quite easily be removed from them.

If the evolution of a stellar system is primarily driven by mass-loss, it is decisive whether the mass-loss is fast or slow compared to the crossing time of the stellar system. This crossing time can be defined as

$$t_{\rm cr} = \frac{2r_{\rm e}}{\sigma}, \tag{6.7}$$

where $r_{\rm e}$ is the effective radius of the stellar system and σ is its internal velocity dispersion (Kroupa 2008). For the TDG-candidates, typical values for σ are of the order of 10 km/s (see

table 2 in Miralles-Caballero et al. 2012) and typical values for r_e the order of 100 pc (see TableA.1). Noting that 1 km/s is essentially equal to 1 pc/10^6years, the typical crossing times of TDG-candidates are of the order of 10^7 years. The TDG-candidates observed by Yoshida et al. (2008) are of the order of 10^8 years old, but still contain enough gas for star formation. Taking this as evidence that the time scale on which the gas is lost from the TDG-candidates is not less then 10^8 years, the mass-loss would be slow compared to the typical crossing times of the TDG-candidates. In the case of slow (adiabatic) mass loss, the expansion of a stellar system is given by

$$\frac{M_{\rm f}}{M_{\rm i}} = \frac{r_{\rm i}}{r_f}, \tag{6.8}$$

where $M_{\rm f}$ is the final mass of the stellar system, $M_{\rm i}$ is the initial mass of the stellar system, $r_{\rm f}$ is the final radius of the stellar system and $r_{\rm i}$ is the initial radius of the stellar system (Kroupa 2008).

In order to calculate the future expansion of the young TDG-candidates with equation (6.8), $M_{\rm f} = M_*$ and $r_{\rm i} = r_{\rm e}$ is assumed. Two cases are considered here for $M_{\rm i}$, namely $M_{\rm i} = 2M_{\rm f}$ and $M_{\rm i} = 4M_{\rm f}$. Thus, the TDG-candidates are assumed to loose 50 per cent and 75 per cent of their mass through the removal of their gas. That is somewhat less than the amount of gas traced by Bournaud et al. (2007) in TDG-candidates, which reflects the expectation that some of the gas available at the present will not be expelled, but will be converted into stars. The resulting final parameters of the TDGs are shown in Fig. 6.2.

Given the assumptions that were used to calculate them, these estimates for the final values for M_* and $r_{\rm e}$ of the young TDG-candidates can only be approximations. Their overall consistency with the according parameters for the old TDGs discussed by Galianni et al. (2010) and the (old) dEs is however remarkable.

Despite the fact that young TDGs probably mostly consist of gas, it is by no means clear that gas-expulsion is indeed as important as assumed for the estimation of their final parameters as shown in Figure (6.2). Gas expulsion is however not the only process by which the extension of the stellar component of a TDG can grow. According to numerical calculations performed by Recchi et al. (2007), star formation in a TDGs starts at the centre and spreads from there with time.

Whether this buildup of the stellar population of the TDG from the inside to the outside or mass loss is more important for the evolution of its size is unclear at the present. It would however be natural that growth from the inside to the outside is most relevant for the TDGs with the deepest potentials (i.e. the most massive ones), as they are the least vulnerable to mass loss. Thus, young TDGs lie on a mass-radius sequence below the one of old dEs, but the parameters of the TDG-candidates would evolve naturally towards the parameters of dEs as they reach a comparable age.

6.3.3 The tidal radii of the TDGs

A TDG expelled from the interacting or merging progenitor galaxies (cf. Elmegreen et al. 1993) will evolve self-regulated (Recchi et al. 2007) and may become a dwarf irregular galaxy (Hunter et al. 2000). However, if a TDG is bound to a host (either a larger galaxy or a galaxy cluster), its size is limited by its tidal radius. This tidal radius, $r_{\rm tid}$, depends on the mass of the TDG, $M_{\rm gal}$, the mass of the host, $M_{\rm host}$, and the distance between the TDG and its host. For systems that effectively are point masses and obey $M_{\rm host} \gtrsim 10\ M_{\rm gal}$, a good approximation to $r_{\rm tid}$ is given

by (Binney & Tremaine 1987)

$$r_{\rm tid} = \left(\frac{M_{\rm gal}}{3M_{\rm host}}\right)^{\frac{1}{3}} R. \tag{6.9}$$

For given values for R and $M_{\rm host}$, equation (6.9) gives the minimum average density a TDG needs to have in order to be an object kept together by its own gravity. At radii $r > r_{\rm tid}$, matter cannot be bound exclusively to the TDG, but only to the common gravitational potential of the TDG and its host.

Since TDGs form from tidal arms, it is indeed likely that a TDG is bound to a larger structure. This larger structure can be its progenitors or a galaxy cluster in which the TDG formed. The notion of many TDGs remaining bound to their progenitor is supported by the dwarf galaxies bound to the Milky Way, whose disk-like distribution and aligned angular momenta can, as it seems, only be understood if they are ancient TDGs (Kroupa et al. 2005; Metz et al. 2008; Kroupa P. et al. 2010; Pawlowski et al. 2012b,a; Kroupa 2012). For TDGs that remain bound to their progenitor galaxies total masses $10^{10}\,{\rm M}_\odot \lesssim M_{\rm host} \lesssim 10^{12}\,{\rm M}_\odot$ (i.e. the mass of a major galaxy) and distances $R \approx 10^5$ pc would be typical. The tidal radii implied by these parameters are plotted in Fig. 6.2.

If the TDG-candidates introduced in Section (6.2.2) adiabatically loose 75 per cent of their mass (i.e. $M_{\rm i} = 4M_{\rm f}$ in equation 6.8), their radii become similar to the tidal radii shown in Figure (6.2). Thus, the TDG-candidates cannot expand any further if they loose even more mass, provided that the choices of $M_{\rm host}$ and R are appropriate. Note however that a adiabatically expanding TDG would not dissolve completely if its outskirts expand beyond its tidal radius.

Interestingly, the tidal radii shown in figure (6.2) also coincide well with the maximum r_e observed for dEs with stellar masses $M_* \lesssim 10^7{\rm M}_\odot$. This is evidence that tidal fields are indeed relevant for the structure of low-mass galaxies for which dark matter haloes do not play a role, as is very likely to be the case for such galaxies (see Kroupa 2012 and Sections 6.4.1 and 6.4.4). At higher masses, the mass-radius relation for dEs is significantly flatter than a relation implying a constant average density in dEs. Thus, the density of the more massive dEs tends to increase with their mass, so that they are less effected by tidal fields. The reason might be that the galaxies with the lowest masses have the weakest gravitational potentials and therefore are the most vulnerable to mass-loss and subsequent expansion. More massive galaxies might keep more of their initial gas and use it up in star formation, so that they expand less.

Thus, the young TDG-candidates are likely to expand (see Section 6.3.2), but tidal fields are likely to limit this expansion. The young TDG-candidates discussed in this paper would thereby naturally evolve onto the mass-radius relation of dEs and become indistinguishable from them in this respect.

6.4 Discussion

6.4.1 The relation between dEs and TDGs

According to the ΛCDM-model, there are two kinds of galaxies with masses $10^6\,{\rm M}_\odot \lesssim M \lesssim 10^{10}\,{\rm M}_\odot$. The first kind are primordial dwarf galaxies that form within DM-haloes of rather low masses (Li et al. 2010; Guo et al. 2011), as they are predicted in numerical calculations of structure formation in the Universe. The second kind are TDGs, whose formation is predicted in numerical calculations of encountering galaxies that are set up in concordance with the ΛCDM-

model (Barnes & Hernquist 1992b; Bournaud & Duc 2006). This prediction by the ΛCDM-model has been termed the 'Dual Dwarf Galaxy Theorem' by Kroupa (2012).

The 'Dual Dwarf Galaxy Theorem' poses a problem for the ΛCDM-model for several reasons:

1. It would be natural that primordial galaxies containing a substantial amount of CDM have a different structure than old TDGs, which do not contain DM and are of a different origin. Thus, old TDGs and primordial galaxies would be expected to form two distinct populations. Following this argument, the data in Fig. (6.2) suggests that the dEs are old TDGs. The dynamical M/L-ratios in the central parts of dEs with masses $10^8\,\mathrm{M}_\odot \lesssim M_* \lesssim 10^9\mathrm{M}_\odot$ imply that there is little CDM at best in these regions of the dEs (Wolf et al. 2010; Toloba et al. 2011; Forbes et al. 2011). Admittedly, about a (hypothetical) presence of CDM in the outskirts of these galaxies, nothing is known so far from observations. Less massive dEs tend to have seemingly higher M/L-ratios, but this may be due to the disturbance from a tidal field of a neighbouring major galaxy (Kroupa 1997; Casas et al. 2012), or due to Newtonian gravity not being valid in the limit of very weak gravitational fields (see figure 8 in Kroupa P. et al. 2010). UCDs are galaxies according to some definitions of a galaxy (see Forbes & Kroupa 2011 and Section 6.4.2) and have elevated mass-to-light ratios, but a significant amount of CDM in them is very unlikely nevertheless (Murray 2009; Willman & Strader 2012; see also Dabringhausen et al. 2012). Thus, a population of dwarf galaxies that definitively formed within DM-haloes cannot be identified in Fig 6.2.

2. Even if all dEs were galaxies that formed within low-mass CDM-haloes, their number would still be low compared to the predicted number of CDM-haloes in the appropriate mass-range (Moore et al. 1999; Klypin et al. 1999); a finding that has been termed the 'missing satellite problem'. In consequence, mechanisms that would supress the formation of galaxies within most low-mass CDM-haloes were discussed (e.g. Benson et al. 2002; Li et al. 2010). The number of dwarf galaxies that form nevertheless according to such models is however only consistent with the number of observed dwarf galaxies if the existence of TDGs is neglected (Kroupa P. et al. 2010; Kroupa 2012). There is however strong observational evidence for formation of TDGs in encounters between galaxies (e.g Mirabel et al. 1992) and that the TDGs thereby created are numerous (e.g. Hunsberger et al. 1996). Thus, the 'Missing Satellite Problem' persists.

3. The satellite galaxies of the Milky Way form a rotationally (or angular-momentum) supported disk (Kroupa et al. 2005; Metz et al. 2008; Pawlowski et al. 2012b), which would be logical if these galaxies are TDGs, but incomprehensible if they formed as primordial structures in agreement with the ΛCDM-model (Pawlowski et al. 2012a). This implies that all dEs around the Milky Way are in fact ancient TDGs. This finding strengthens the previous two points, namely that firstly all dEs are more likely old TDGs rather than primordial galaxies and that secondly the 'Missing Satellites Problem' thereby is far from being solved within the standard cosmological model.

The notion that all dEs are old TDGs raises the question whether a sufficiently high number could have been produced over the age of the Universe. Concerning this matter, Bournaud & Duc (2006) show in numerical calculations that about 25 per cent of the TDGs initially created in an encounter would survive for more than 2×10^9 years, which corresponds to an average

between 1 and 2 long-lived TDGs per calculated interaction. Okazaki & Taniguchi (2000) argue that a TDG-production at this rate would already be sufficient to account for all dwarf galaxies in the nearby Universe (also see Kroupa P. et al. 2010).

An implication of all dEs being ancient TDGs is that the dynamical M/L-ratios of dEs with masses $M_* \gtrsim 10^8$ $\mathrm{M}_\odot$ must be consistent with the M/L-ratios of pure stellar populations. This can be seen in figure 7 in Misgeld & Hilker (2011), which shows that the internal gravitational acceleration in these dEs is at or above the limit for Milgromian dynamics (Milgrom 1983, see Famaey & McGaugh 2012 for a rewiev), while TDGs do not contain dark matter even if their progenitors did (Barnes & Hernquist 1992b; Bournaud 2010).

Observations of dEs with dynamical masses $M_{\rm dyn} \gtrsim 10^8$ $\mathrm{M}_\odot$ reveal that most of them have dynamical I-band M/L-ratios of $2 \lesssim M_{\rm dyn}/L_I \lesssim 4$ within their effective radii (Wolf et al. 2010). Such $M_{\rm dyn}/L_I$-ratios correspond, for instance, to the M_*/L_I ratios of single-burst stellar populations with a metallicity of [Z/H]$= -0.33$ and ages 5×10^9 yr $< t < 13 \times 10^9$ yr (Maraston 2005). This does not exclude that the actual stellar populations of the dEs shown in Wolf et al. (2010) are more luminous, so that an additional matter component would be needed in order to explain the observed $M_{\rm dyn}/L_I$ ratios. The central $M_{\rm dyn}/L_I$-ratios of the 21 dEs listed in table 7 in Toloba et al. (2011) are however indeed of the same order of magnitude as their central stellar M_*/L_I-ratios. Given that the central M_*/L_I-ratios of these dEs are quite uncertain and in 7 cases higher than the according $M_{\rm dyn}/L_I$-ratios, there is moreover no compelling evidence that $M_{\rm dyn} > M_*$ holds for them. Thus, observations do indeed support the notion that the dynamics of the central region of dEs is consistent with Newtonian dynamics, even if little or no dark matter is present there.

The typical $M_{\rm dyn}/L$-ratios of dEs with masses $M_* \lesssim 10^8$ (often referred to as dSphs in the literature, but see Ferguson & Binggeli 1994 and Section 6.3.1) strongly increase with decreasing mass (cf. figure 4 in Wolf et al. 2010). This makes them inconsistent with the assumption that dEs with masses $M_* \lesssim 10^8$ are pure stellar populations that are in virial equilibrium and obey to Newtonian dynamics. However, being less tightly bound than the more massive dEs (cf. figure 7 in Misgeld & Hilker 2011), these dEs are more likely to be disturbed by tidal fields, which would lead to seemingly high $M_{\rm dyn}/L$-ratios if the dEs are assumed to be in virial equilibrium (Kroupa 1997; McGaugh & Wolf 2010; Casas et al. 2012). Moreover, the internal accelerations in low-mass dEs are in the regime where Milgromian dynamics (Milgrom 1983) would be relevant (cf. figure 7 in Misgeld & Hilker 2011). Note that Milgromian dynamics would also explain the remarkably high dynamical masses of the TDG-candidates discussed by Bournaud et al. (2007), which cannot be explained with the baryonic matter found in these galaxies, even though numerical experiments strongly predict the absence of DM in TDGs (e.g. Barnes & Hernquist 1992b; Gentile et al. 2007; Bournaud 2010). Thus, also low-mass dEs can be understood as dark-matter free TDGs, if they are not in virial equilibrium or if their internal dynamics is non-Newtonian.

It has also been established from observations that less luminous elliptical galaxies (i.e. dEs) tend to be bluer than more luminous elliptical galaxies (i.e. nEs). This colour-magnitude relation exists, because less luminous elliptical galaxies tend to be younger and less metal-rich than more massive elliptical galaxies (Gallazzi et al. 2006).

If the notion of all dEs being old TDGs is correct, and nEs are primordial galaxies, the dEs would tend to be younger than the nEs because the dEs could as a matter of principle only form after the formation of the first primordial galaxies. Thus, this scenario would naturally explain 'downsizing', i.e. that the least massive galaxies tend to have the youngest stellar populations, although they should be the oldest galaxies according to the ΛCDM model (see, e.g.,

Cimatti A. et al. 2004).

Understanding why the dEs tend to be less metal-rich than nEs is less intuitive under the premise that dEs are old TDGs. This is because the dEs would have formed from pre-enriched material if they are not primordial objects. However, the old TDGs have formed at a time when the primordial galaxies were less self-enriched than they are today. Old low-mass and metal-poor dEs can therefore be understood as TDGs that formed from matter that was scarcely pre-enriched and in which self-enrichment was not very effective. The low-mass dEs are indeed less tightly bound than the more massive dEs and nEs, as figure 7 in Misgeld & Hilker (2011) indicates. Thus, the low-mass dEs are may have been more likely to loose the gas expelled by evolving stars, while high-mass dEs and nEs may have been more likely to reprocess it. This would explain why the typical metallicity of dEs increases with their mass, no matter whether they are ancient TDGs or not.

Thus, so far the properties of the dEs seem to be consistent with them being old TDGs. This would, however, imply that there are no primordial galaxies with stellar masses $M_* \lesssim 10^{10}\,\mathrm{M}_\odot$, which would be inconsistent with the ΛCDM-model (Kroupa P. et al. 2010; Kroupa 2012). This may be evidence for the ΛCDM-model needing to be replaced with a cosmological model where the apparent need for DM as an explanation for the internal dynamics of galaxies is replaced with a non-Newtonian law of gravity in the ultra-weak field limit. An excellent example of such a law of gravity is provided by Milgromian dynamics (Milgrom 1983).

6.4.2 The relation between UCDs and TDGs

The highly resolved numerical calculation of the merger of two galaxies performed by Bournaud et al. (2008) implies that two types of stellar systems are created during the merger:

1. pressure-supported stellar systems with masses $10^5\,\mathrm{M}_\odot < M_* < 10^7\,\mathrm{M}_\odot$ and diameters between 10 and 100 pc. Bournaud et al. (2008) identifies this type of stellar system with the super star clusters (SSCs) discussed by Kroupa (1998), i.e. complexes of star clusters that are kept together by mutual gravitational forces. Possible SSCs have been observed by Whitmore & Schweizer (1995) and they will evolve into objects that observers would classify as UCDs (Kroupa 1998; Fellhauer & Kroupa 2002a) or extended star-clusters (Fellhauer & Kroupa 2002b; Brüns et al. 2011).

2. rotating stellar systems with masses $10^8\,\mathrm{M}_\odot < M_* < 10^9\,\mathrm{M}_\odot$ and diameters of a few 10^3 pc. This type of stellar system has been identified with 'classical' TDGs by Bournaud et al. (2008). Candidates for observed TDGs are listed in Table (A.1), and may evolve into dEs (see Sections 6.3.2 and 6.3.3).

The properties of the stellar systems that form during a merger of galaxies according to the numerical calculations by Bournaud et al. (2008) are therefore consistent with observations, as is also illustrated in Figure (6.2). This consistency with the observations includes the lack of objects intermediate to SSCs and 'classical' TDGs. Given the probable future evolution of these objects, their absence translates into the absence of objects intermediate to UCDs and dEs, which is illustrated with Figure (6.1).

Thus, the numerical calculation by Bournaud et al. (2008) correctly reproduces the mass spectrum and the sizes of objects forming during a galaxy merger. This is strong evidence for the physical processes included in the model (gas dynamics, stellar dynamics, star formation law) being sufficient and their implementation in the numerical code being adequate for the overall

description of a galaxy merger. A detailed understanding of why two distinct types of objects are formed during the merger (namely SSCs and TDGs) is however still missing. Given the apparent link to physical processes, it nevertheless stands to reason to distinguish galaxies from star-clusters by their different structure, i.e. by the gap between a star-cluster-like population (to which the UCDs belong) and a galaxy-like population (to which the TDGs belong). This is essentially equivalent to the distinction between star-clusters and galaxies proposed by Gilmore et al. (2007).

Note however that there are also other ways to define a galaxy (see Forbes & Kroupa 2011). The choice of the definition is decisive for the classification of UCDs and their progenitors.

If a galaxy is defined as a stellar system whose dynamics cannot be explained with its baryons obeying Newton's laws of gravity (Willman & Strader 2012), UCDs[2] and SSCs are star-clusters. The internal properties of even one of the most massive UCDs have indeed been argued to be consistent with it being an extremely massive star cluster (Frank et al. 2011).

If a galaxy is defined as a stellar system whose relaxation time at its half-mass radius, t, is longer than the age of the universe, $\tau_{\rm H}$, (Kroupa 1998, 2012), most UCDs and SSCs are galaxies. Thus, the numerical calculations performed by Bournaud et al. (2008) would predict the formation of two different kinds of tidal galaxies according to this definition of a galaxy. Note however that this definition implies that any stellar system will become a star-cluster at some point of time by the aging of the universe.

In essence, each of the proposed definitions is based on a property that is typical for a galaxy. By choosing a certain definition, the importance of the according property is emphasized. Defining a galaxy as a stellar system with $t_{\rm rh} > \tau_{\rm H}$ emphasizes the fact that such systems cannot have evolved dynamically through two-body encounters at the present, which has important implications for how to model the dynamical evolution of such systems effectively (Kroupa 2012). Defining a galaxy by its extension, or by the impossibility to explain its dynamics with its baryonic matter and the Newtonian laws of gravity, emphasizes a fundamental physical difference of these systems.

6.4.3 The GCs of dEs

It is known that dEs usually are surrounded by GC systems. Typical sizes of these GC systems range from a few GCs to about 100 GCs. Not considering the total number of GCs in these systems, but the number of GCs per unit luminosity of their host galaxy, the GC systems of some low-luminosity dEs are actually large in comparison to other galaxies (Peng E. et al. 2008).

If dEs are ancient TDGs, their GCs can have formed in different ways:

1. The numerical calculation by Bournaud et al. (2008) suggests that during a galaxy merger GCs and TDGs are created at the same time. If they are formed within the same phase-space volume, a forming TDG might capture forming GCs within its gravitational field.

2. SSCs, which are possible progenitors of TDGs, are highly substructured. While most of the subsystems quickly merge into an object that would be identified as a UCD or a TDG

[2]The elevated M/L_V ratios of UCDs (Haşegan et al. 2005; Dabringhausen et al. 2008; Mieske et al. 2008) are probably not due to CDM or non-Newtonian gravity (see Section 6.2.1), but to the presence of a large population of neutron stars and stellar-mass black holes in UCDs, which is the consequence of a top-heavy stellar initial mass function in UCDs which formed as a major star-burst (Dabringhausen et al. 2009, 2012; Marks et al. 2012).

by observers, some subsystems may survive on a timescale of 10^9 years (see figure 11 in Fellhauer et al. 2002) and might qualify as GCs.

3. According to Weidner et al. (2004), the mass of the most massive star-clusters that can form within a stellar system depends on the star formation rate of that stellar system. If the initial star formation rate in the TDGs was high enough, GCs may have formed during the evolution of the TDG as its most massive star-clusters. In contrast to the first two scenarios, this scenario implies that the GCs are younger than its host.

In any case, GC-candidates should be very common around TDG-candidates of any age, if the dEs are old TDGs and if their GC-systems form early during their evolution. As these GCs would have formed from pre-processed matter, they would tend to be more metal-rich than GCs that formed with the formation of a primordial galaxy. This stands in contrast with the finding that dEs tend to have a higher fraction of blue GCs than nEs, which could be interpreted as the GCs of dEs tending to be less metal-rich than the GCs of nEs (cf. figure 8 in Peng E. et al. 2008). Note however that the bluer colour of the GCs belonging to dEs could also indicate a lower age. This would be natural if the nEs are primordial galaxies while the dEs are old TDGs (and thus younger than nEs) and if the GCs formed together with their host galaxies. Moreover, metal-enrichment might not have proceeded very far in the progenitor galaxies when the progenitors of present-day dEs possibly have formed as TDGs (cf. Section 6.4.1). Thus, finding GC-candidates in a systematic search around TDG-candidates would be supportive evidence for the dEs being old TDGs.

If no GC-candidates are found around young TDG-candidates, this could be explained in different ways:

1. Only the dEs with very few or no GCs are ancient TDGs.

2. GCs form rather late during the evolution of a young TDG into a dE.

3. Marks & Kroupa (2010) note that metal-rich GCs form with larger radii. These GCs are thus more susceptible to destruction than the GCs that formed at the age of ancient TDG-formation, which arguably formed from matter that was barely pre-enriched. Presently forming TDGs may thus have a small specific frequency of GCs.

Note however that the case of finding no GC-candidates around TDG-candidates does not seem very likely, considering the substructure found in SSCs and the TDG-candidates discussed in Miralles-Caballero et al. (2012) and the possibility that some of these substructures may survive for a long time according to Fellhauer et al. (2002).

6.4.4 Mass-radius relations

In the following, possible reasons for the mass-radius relations described in Section (6.3.1) are discussed.

The mass-radius relation of nEs and UCDs

The mass-radius relation for UCDs and nEs is very remarkable because it bridges the gap between the galaxy-like population and the star-cluster-like population (cf. Section 6.4.2). The common mass-radius relation suggests that the overall structure of UCDs and nEs was shaped

by a process that is relevant for both types of stellar systems, even though the formation of objects intermediate to UCDs and nEs is inhibited. As spheroidal systems with little or no substructure and primarily old stellar populations, UCDs and nEs share indeed many similarities, despite being separated by the size gap noted by Gilmore et al. (2007). Since there is most probably no CDM in UCDs (cf. Section 6.4.2), considering UCDs and nEs as similar objects at different masses argues against the presence of DM in nEs. In fact, strong evidence for the absence of CDM in galaxies has already been found by Disney et al. (2008).

The process that shaped UCDs and nEs could be monolithic collapse, i.e. that the stellar systems form rapidly by the collapse of a single gas cloud. If the mass of a cloud is sufficient for the formation of a UCD, it becomes optically thick for infrared radiation during the collapse, which leads to internal heating. This internal heating halts the collapse and Murray (2009) finds that the radius at which the collapse is halted depends on the mass of the cloud. This dependency is quantified as

$$\log(r_{\rm h}) \propto 0.6\log(M_*), \tag{6.10}$$

i.e. up to a constant by the same mass-radius dependency that was found for nEs and UCDs from their observed parameters (cf. Dabringhausen et al. 2008; Misgeld & Hilker 2011 and equation 6.6). Note that Murray (2009) only discusses the difference between GCs and UCDs. However, if monolithic collapse is the reason for the mass-radius relation of UCDs, the fact that nEs and bulges[3] lie on the same mass-radius relation suggests that they also formed through monolithic collapse. Monolithic collapse has indeed already been considered for the formation of nEs and bulges (e.g. Elmegreen 1999; Sanders 2008).

As an extension to the model of pure monolithic collapse, it can be assumed that the gas clouds formed substructures while they collapsed. The present-day UCDs and nEs would then have formed by the merging of these substructures, as discussed in the literature for UCDs (e.g. Kroupa 1998; Fellhauer & Kroupa 2002a; Brüns et al. 2011).

The mass-radius relation of GCs

The members of the star-cluster-like population lie an a mass-radius relation that changes its slope at a mass $M_* \approx 2 \times 10^6\ M_\odot$. This change of the slope marks the transition from GCs to UCDs. (Haşegan et al. 2005; Mieske et al. 2008).

The progenitors of UCDs were gas clouds above a certain mass threshold, at which gas clouds become optically thick for infrared radiation when they collapse and form stellar systems. They follow equation (6.10). The progenitors of GCs and open star clusters like the Plejades or the Orion Nebula Cluster would be gas clouds that remained transparent for infrared radiation because their masses were below the threshold (Murray 2009; see also Section 6.4.4). Such clouds collapse to sizes of 0.1 pc (Marks & Kroupa 2012), which is the observed size of dense cloud cores that are thought to be the progenitors of low-mass star clusters (Bergin & Tafalla 2007). The 0.1 pc scale may be set by the width of filaments within molecular clouds. Star formation is observed in the filaments if the mass per unit length exceeds a critical value (André Ph. et al. 2010).

Thus, there is no fundamental difference between the progenitors of present-day GCs and the progenitors of present-day UCDs, except for their mass, which has implications for their evolution. A common origin of both types of stellar systems is indeed implied by the continuous

[3]Note that the location of bulges within the fundamental plane suggests that they are essentially identical to nEs (e.g. Bender et al. 1992).

transition between GCs and UCDs. This common origin may be that they have formed during the interaction between galaxies, which is not only a likely trigger for the formation of UCDs (Fellhauer & Kroupa 2002a), but also for the formation of 'classical' GCs (Zepf & Whitmore 1993). Thus, UCDs can be understood as the most massive GCs (Mieske et al. 2012).

Such an origin would make UCDs and GCs similar to TDGs. This makes it even harder to understand why the radii of TDGs are about an order of magnitude larger than the radii of GCs and UCDs of comparable mass (see Fig 6.2), so that GCs and UCDs on the one hand and TDGs on the other hand are distinct populations of stellar systems (cf. Section 6.4.2).

The mass-radius relation of dEs

At a stellar mass $M_* \approx 10^{10}\,\mathrm{M}_\odot$, the mass-radius relation for dEs branches of from the mass-radius relation defined by nEs and UCDs. In the context of the ΛCDM-model, this can heuristically, but not quantitatively be understood if the dEs are primordial galaxies, of which some formed the nEs by hierarchical merging (cf. White & Rees 1978; Aarseth & Fall 1980; Kauffmann et al. 1993; Springel et al. 2005).

However, in the light of the arguments given in Sections (6.4.1) and (6.4.4), it seems to be more likely that the nEs are primordial objects that formed through the monolithic collapse of gas clouds (see Section 6.4.4), while the dEs are secondary objects that formed as TDGs (see Section 6.4.1). The difference between the mass-radius relation for dEs and the mass-radius relation for nEs would then nevertheless indicate the transition between a primordial and a secondary population of galaxies.

6.5 Conclusion

6.5.1 The nature of old pressure-supported stellar systems

In this paper, the largest existing catalogue of young TDG-candidates is collated and their relation to old pressure-supported stellar systems is discussed. The old stellar systems can be categorized into three groups:

- dEs, which follow a mass-radius relation quantified by equation (6.3) for $10^4\,\mathrm{M}_\odot < M_* < 3\times10^9\,\mathrm{M}_\odot$, with a steepening for very low-mass dEs. The properties of these galaxies are best explained with them being ancient TDGs. The reason is that there is plenty of evidence for the existence of young TDGs, both observational (e.g. Zwicky 1956; Mirabel et al. 1992; Duc P. A. et al. 2011; Miralles-Caballero et al. 2012) and theoretical (e.g. Barnes & Hernquist 1992b; Bournaud & Duc 2006). These systems would naturally evolve onto the mass-radius sequence defined by the dEs if they survive for a long enough time (see Sections 6.3.2 and 6.3.3) and Okazaki & Taniguchi (2000) have shown that already a rather low production rate of TDGs per galaxy encounter would be sufficient to account for all observed dEs (see Section 6.4.1). Note that TDGs cannot contain a significant amount of CDM (Barnes & Hernquist 1992a; Bournaud 2010; Kroupa 2012). Consequently, this would also be true for the dEs if they are TDGs. Dynamical M/L-ratios derived from spectroscopic measurements indeed suggest that there is little or no CDM in the central parts of dEs with stellar masses $M_* \gtrsim 10^8\,\mathrm{M}_\odot$ (Forbes et al. 2011; Toloba et al. 2011). At the present, no similar claim can be made for the outskirts of dEs due to the lack of suitable data. The M/L-ratios of dEs with lower masses are

much higher in many cases, but this does not necessarily indicate that these galaxies are dominated by CDM. The extreme M/L-ratios of these galaxies may also indicate that the assumption of virial equilibrium is not valid for them (Kroupa 1997; McGaugh & Wolf 2010; Casas et al. 2012) or that the laws of gravity have to be modified in the limit of weak gravitational fields (Hernandez et al. 2010; McGaugh & Wolf 2010; Kroupa P. et al. 2010; Famaey & McGaugh 2012; Kroupa 2012).

- nEs, which follow a mass-radius relation quantified by equation (6.6) for $M_* > 3 \times 10^9\,\mathrm{M}_\odot$. Surprisingly, the UCDs lie along the same mass-radius relation (see Section 6.3.1), which suggests that the structure of nEs and UCDs was shaped by the same process. This process may be the formation of stellar systems by monolithic collapse of gas clouds (see Section 6.4.4), since this process can explain the mass-radius relation for UCDs (Murray 2009). This would make nEs primordial galaxies. The rapid formation that monolithic collapse implies for the nEs is consistent with the chemical properties of the nEs, namely their large alpha-element enrichment (Thomas et al. 2005; Recchi et al. 2009). Also the trend of the nEs being older than the dEs (Cowie et al. 1996; Gavazzi et al. 2002; Thomas et al. 2005; Recchi et al. 2009) can easily be explained if nEs are indeed primordial objects and dEs are old TDGs, which can only form after a population of primordial galaxies has formed already. This finding is much more difficult to understand if nEs are built up from dEs via hierarchical merging.

- GCs and UCDs, which lie along a continuous mass-radius sequence that changes its slope at a mass $M_* \approx 2 \times 10^6\,\mathrm{M}_\odot$ (see, e.g., Mieske et al. 2008). GCs and UCDs might well be the same kind of object (e.g. Mieske et al. 2012), which would also explain why the formation of GCs and UCDs alike seems to be connected to the interaction between gas-rich galaxies (see Zepf & Whitmore 1993 for GCs and, e.g., Fellhauer & Kroupa 2002a for UCDs). This would make GCs and UCDs similar to the TDG-candidates in Tables (A.1) and (A.2) as well, and thus to probable progenitors of dEs (see Figure 6.2). GCs and UCDs are however much more compact than dEs (see Figure 6.1) and their probable progenitors listed in Tables (A.1) and (A.2). This indicates a fundamental difference between GCs and UCDs on the one hand and dEs on the other hand (cf. Gilmore et al. 2007; Misgeld & Hilker 2011), even if all of them owe their existence to the interactions between galaxies. Interestingly, a difference between likely progenitors of GCs and extended TDGs has apparently been reproduced by Bournaud et al. (2008) in a numerical calculation of the interaction between gas-rich galaxies. It is however still not understood how the different physical processes implemented in the calculation by Bournaud et al. (2008) actually lead to the formation of two distinct types of objects from the matter in tidal tails.

In effect, the observational evidence suggests that all kinds of old pressure-supported stellar systems do not contain CDM.

6.5.2 Implications for cosmology

Currently, there are two competing schools of thought in cosmology, i.e. the attempt to describe the Universe and its evolution as a whole. These schools of thought are best distinguished by the conclusions they draw from the fact that general relativity (GR) cannot explain the dynamics of galaxies, if only their visible, baryonic matter is taken into account.

- According to the first (and at the present dominant) school of thought, GR is an exact formulation of the laws of gravity on all size scales and mass scales. The fact that the dynamics of most galaxies cannot be explained with GR from their baryonic matter would then indicate the presence of unseen, non-baryonic matter in these galaxies. Extensions of the standard model of particle physics predict particles that would be candidates for this kind of dark matter, but experiments with the aim to detect such particles have not been successful so far. The ΛCDM-model is nevertheless widely accepted, because GR has passed many experimental tests, and because the ΛCDM-model is a good description of the Universe on large scales (but see Kroupa 2012).

- According to the second school of thought, the dynamics of galaxies is not evidence for the presence of DM in them, but indicates that GR has to be modified in the limit of very weak space-time curvature. This approach has indeed been extremely successful in describing the properties of galaxies (see Famaey & McGaugh 2012 for a rewiev).

A prediction from the ΛCDM-model is the 'Dual Dwarf Galaxy Theorem', which states the coexistence of primordial dwarf galaxies and TDGs at masses $M_* \lesssim 10^{10}\ \mathrm{M}_\odot$ (Kroupa P. et al. 2010; Kroupa 2012). The primordial dwarf galaxies would have formed within CDM-haloes, while the TDGs cannot contain CDM. Thus, the primordial dwarf galaxies and the TDGs would have very different matter compositions, which strongly suggests that they should fall into two easily distinguishable groups. Two groups of objects in the appropriate mass-range can indeed be identified in Figure (6.1), namely the UCDs and the dEs. However, according to the conclusions presented in Section (6.5.1), neither the dEs nor the UCDs seem to be populations of primordial dwarf galaxies within CDM-haloes, but rather populations of objects whose formation was triggered by the tidal interaction between gas-rich galaxies. Thus, the conclusions presented in Section (6.5.1) support the second school of thought, according to which the ΛCDM-model needs to be replaced by a cosmological model that is based on a new theory of gravity.

Note however that the data on TDG-candidates used here (see Tables A.1 and A.2) is gathered from different previous publications and is thus based on observations with different instruments, and different numerical calculations, respectively. Moreover, the methods by which the listed parameters have been estimated are in some cases rather crude (cf. Sections 6.2.2 and 6.2.2). In order to put our conclusions on a stronger footing, it would be advisable to re-evaluate the existent raw data on TDG-candidates in an effort to make the data as comparable as possible, or even to make a new observational survey of the TDG-candidates.

Acknowlegdements

The authors thank R. C. Brüns for helpful comments. JD aknowledges support through DFG grant KR1635/13 and a grant for PhD-students from the University of Bonn.

Chapter 7

The mass function of CDM-halo masses

Section 3 in P. Kroupa et al., 2010, **A&A**, 523, 23

Abstract:

According to the currently prevailing cosmological model, the concordance cosmological model (CCM), most of the matter in the Universe is non-baryonic old dark matter (CDM). Numerical simulations based on the CCM predict that the CDM would collapse into CDM-haloes of various masses as the Universe evolves into its current state. These CDM-haloes are the sites where the first galaxies form according to the CCM. However, if every CDM-halo contained a galaxy, the Milky Way would have many more satellite galaxies. This finding has been termed the 'missing satellite problem' by theorists. In order to solve the 'missing satellites problem', models that explain why most low-mass CDM-haloes would contain no baryons and thus no galaxy have been developed. These models lead to a mass-function of luminous CDM-haloes (i.e. CDM-haloes that contain a galaxy). Using Monte-Carlo modelling, it is tested here whether the mass function of luminous CDM-haloes that was derived by Li et al. (2010) is not only qualitatively, but also quantitatively consistent with the mass function of the satellite galaxies of the Milky Way. The hypothesis that the satellite galaxies of the Milky Way have been drawn from the mass function derived by Li et al. (2010) is thereby rejected with more than 95 per cent confidence. Thus, the 'missing satellites problem' persists also with state-of-the-art modelling.

7.1 Introduction

One of the predictions of the ΛCDM hypothesis is the self-similarity of DM-halos down to (at least) the mass range of dwarf galaxies, i.e. that massive halos contain sub-halos of lesser mass, but with the same structure in a statistical sense (Moore et al. 1999; for a major review see Del Popolo & Yesilyurt 2007). The mass function of these sub-halos is, up to a critical mass $M_{\rm crit}$, very well approximated by

$$\xi_{\rm sub}(M_{\rm vir}) = \frac{dN}{dM_{\rm vir}} \propto M_{\rm vir}^{-1.9}, \tag{7.1}$$

where dN is the number of sub-halos in the mass interval $M_{\rm vir}, M_{\rm vir} + dM_{\rm vir}$ (Gao et al. 2004). $M_{\rm crit}$ is given by $M_{\rm vir} \approx 0.01 M_{\rm h}$ where $M_{\rm h}$ is the virial mass of the hosting CDM-halo. The virial mass, $M_{\rm vir}$, is defined by

$$M_{\rm vir} = \frac{4\pi}{3} \Delta_{\rm vir} \rho_0 r_{\rm vir}^3, \tag{7.2}$$

where ρ_0 is the critical density of the universe and $\Delta_{\rm vir}$ is a factor such that $\Delta_{\rm vir}\rho_0$ is the critical density at which matter collapses into a virialised halo, despite the overall expansion of the universe. The virial radius $r_{\rm vir}$ is thereby determined by the density profile of the collapsed CDM-halo. For $M_{\rm vir} > 0.01\, M_{\rm h}$, the mass function steepens (Gao et al. 2004), so that it is effectively cut off at a mass $M_{\rm max}$ (see Eq. 7.3 below). It is reasonable to identify $M_{\rm max}$ with the mass of the most massive sub-halo, which must be larger than $M_{\rm crit}$, where the mass function begins to deviate from Eq. 7.1 and smaller than M_h, the mass of the host-halo. Thus, $M_{\rm crit} < M_{\rm max} < M_h$.

Thus, a halo with $M_{\rm vir} \approx 10^{12}\, M_\odot$, like the one that is thought to be the host of the MW, should have a population of sub-halos spanning several orders of magnitude in mass. It is well known that, in consequence, a steep sub-halo mass function like Eq. 7.1 predicts many more low-mass sub-halos than the number of observed faint MW satellites (Moore et al. 1999; Klypin et al. 1999), a finding commonly referred to as the "missing satellites problem". Efforts to solve this problem rely on physical processes that could either clear CDM-halos of all baryons or inhibit their gathering in them in the first place, and that would affect low-mass halos preferentially (e.g. Moore et al. 2006; Li et al. 2010; Section 2 in Kroupa P. et al. 2010). More specifically, Li et al. (2010) find that the mass function of luminous halos, $\xi_{\rm lum}(M_{\rm vir})$, would essentially be flat for $10^7 M_\odot \leq M_{\rm vir} < 10^9 M_\odot$. All sub-halos with $M_{\rm vir} \geq 10^9 M_\odot$ would keep baryons and therefore $\xi_{\rm lum}(M_{\rm vir}) = \xi_{\rm sub}(M_{\rm vir})$ in this mass range. Thus, the mass function of *luminous sub-halos* can be written as

$$\xi_{\rm lum}(M_{\rm vir}) = k k_i M_{\rm vir}^{-\alpha_i}, \tag{7.3}$$

with

$$\begin{array}{lll} \alpha_1 = 0, & k_1 = 1, & 10^7 \leq \frac{M_{\rm vir}}{M_\odot} < 10^9, \\ \alpha_2 = 1.9, & k_2 = k_1\,(10^9)^{\alpha_2 - \alpha_1}, & 10^9 \leq \frac{M_{\rm vir}}{M_\odot} \leq M_{\rm max}, \end{array}$$

where the factors k_i ensure that $\xi_{\rm vir}(M_{\rm vir})$ is continuous where the power changes and k is a normalisation constant chosen such that

$$\int_{10^7}^{M_{\rm max}} \xi_{\rm vir}(M_{\rm vir})\, dM_{\rm vir} = 1. \tag{7.4}$$

From a mathematical point of view, Eq. 7.3 is the probability distribution of luminous sub-halos. Note that the luminous sub-halo mass function proposed in Moore et al. (2006) is very

similar to the one in Li et al. (2010). In the high-mass part, it has the same slope as the mass function for all sub-halos and flattens in the low-mass part (cf. fig. 3 in Moore et al. 2006). The lower mass limit for luminous halos is however suggested to be $M_{\rm vir} \approx 10^8\,M_\odot$ in Moore et al. (2006). Note also that the mass function of *all sub-halos* has $\alpha_1 \approx \alpha_2 \approx 1.9$ (Gao et al. 2004).

7.2 NFW-halos

It is well established by now that the density profiles of galaxy-sized CDM-halos are similar to a universal law proposed by Navarro et al. (1997). It is given as

$$\rho_{\rm NFW}(r) = \frac{\delta_c \rho_0}{r/r_{\rm s}\,(1+r/r_{\rm s})^2}, \tag{7.5}$$

where r is the distance from the centre of the halo and ρ_0 is the critical density of the universe, while the characteristic radius $r_{\rm s}$ and δ_c are mass-dependent parameters.

By integrating $\rho_{\rm NFW}(r)$ over a volume, the total mass of CDM within this volume is obtained. Thus,

$$M(r) = \int_0^r \rho(r') 4\pi r'^2\, dr' \tag{7.6}$$

is the mass of CDM contained within a sphere with radius r around the centre of the CDM-halo, and $M(r) = M_{\rm vir}$ for $r = r_{\rm vir}$. Performing the integration on the right-hand side of Eq. 7.6 and introducing the concentration parameter $c = r_{\rm vir}/r_{\rm s}$ leads to

$$M(r) = \frac{4\pi\rho_0\delta_c r_{\rm vir}^3}{c^3}\,\left[\frac{r_{\rm vir}}{r_{\rm vir}+c\,r} + \ln\left(1+\frac{c\,r}{r_{\rm vir}}\right) - 1\right]. \tag{7.7}$$

Note that δ_c can be expressed in terms of c,

$$\delta_c = \frac{\Delta_{\rm vir}}{3}\frac{c^3}{\ln(1+c) - c/(1+c)}, \tag{7.8}$$

as can be verified by setting $r = r_{\rm vir}$ in Eq. 7.7 and substituting $M(r_{\rm vir}) = M_{\rm vir}$ by Eq. 7.2.

If the halo is luminous, it is evident that $M(r)$ is smaller than the *total* mass included within r, M_r. However, assuming that the MW satellites are in virial equilibrium and that their dynamics is Newtonian, the mass-to-light ratios calculated for them are generally high and imply that they are DM-dominated and thus, $M(r) = M_r$ would be a good approximation. This relation is therefore adopted for the present discussion. Note in particular that $M(r = 0.3{\rm kpc}) = M_{0.3{\rm kpc}}$ in this approximation.

In principle, the parameters ρ_0 (Navarro et al. 1997), c (Bullock et al. 2001) and $\Delta_{\rm vir}$ (Mainini et al. 2003) depend on the redshift z but for the purpose of the present paper only $z = 0$ needs to be considered, as this is valid for the local universe. Thus,

$$\rho_0 = \frac{3H_0^2}{8\pi G}, \tag{7.9}$$

with the Hubble constant $H_0 = 71\,{\rm km\,s^{-1}\,Mpc^{-1}}$ (Spergel D. N. et al. 2007), $\Delta_{\rm vir} \simeq 98$ for ΛCDM-cosmology (Mainini et al. 2003), and

$$\log_{10}(\overline{c}) = 2.31 - 0.109\log_{10}\left(\frac{M_{\rm vir}}{M_\odot}\right), \tag{7.10}$$

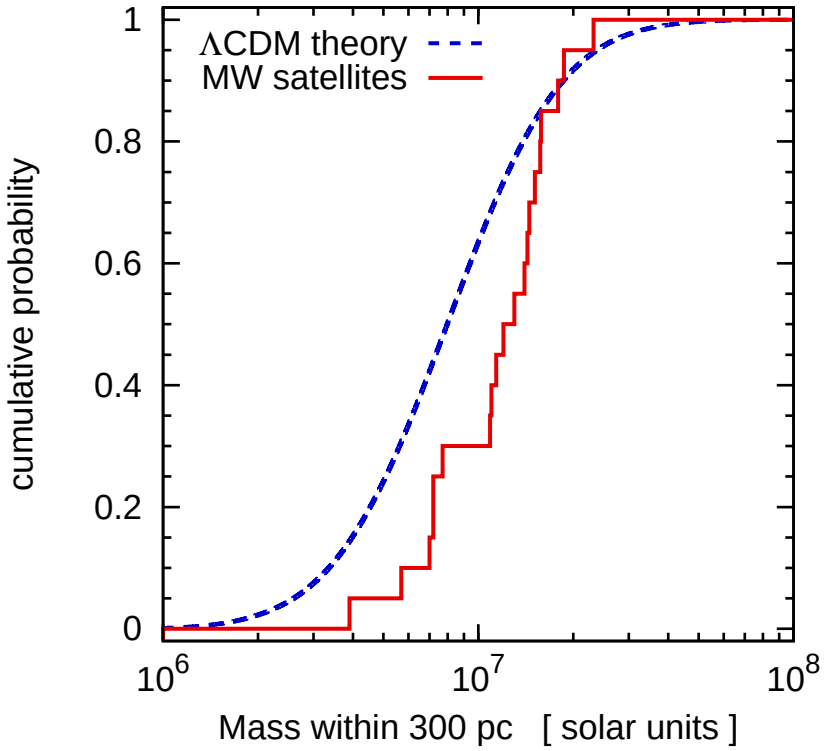

Figure 7.1: The 'overpredicting luminous satellite problem'. The cumulative distribution function for the mass within the central 300 pc, $M_{0.3\mathrm{kpc}}$, of the MW satellites (solid line) and the cumulative distribution function for $M_{0.3\mathrm{kpc}}$ of a sample of 10^6 CDM-halos picked from the parent distribution of luminous sub-halos (Eq. 7.3, dashed line). The null hypothesis is that the MW satellite $M_{0.3\mathrm{kpc}}$ masses are drawn from this parent distribution. The maximum distance between the two curves is 0.333 so that the null hypothesis can be discarded with 99.1 per cent confidence.

where $\overline{c}$ is the expectation value of c as a function of M_{vir}. Thus, $\overline{c}$ decreases slowly with M_{vir}, while the scatter of the actual c is rather large, being

$$\sigma_{\log_{10} c} = 0.174 \tag{7.11}$$

(Macciò et al. 2007). Note that the only caveat here is that the NFW profile is used to integrate the mass, while the now-preferred Einasto profile (Navarro et al. 2010, Section 1 in Kroupa P. et al. 2010) makes only a small difference in the central parts.

7.3 Probing the ΛCDM hypothesis with $M_{0.3\mathrm{kpc}}$

Strigari et al. (2008) use stellar motions in 18 MW satellites for calculating their mass within the central 300 pc, $M_{0.3\mathrm{kpc}}$. They assume the satellites to be in virial equilibrium and that Newtonian dynamics can be applied to them. The sample from Strigari et al. (2008) can be enlarged to 20 satellites by including the Large Magellanic Cloud (LMC) and the Small Magellanic Cloud (SMC), since van der Marel et al. (2002) estimated the mass of the LMC within the innermost 8.9 kpc, M_{LMC}, using the same assumptions as Strigari et al. (2008). This implies $M_{\mathrm{LMC}} = (8.7 \pm 4.3) \times 10^9\, M_\odot$, of which the major part would have to be DM. Eqs. 7.2, 7.7, 7.8 and 7.10 have been used to create tabulated expectation values of $M(r)$ for NFW-halos with different M_{vir} and it can thereby be seen that for a typical NFW-halo with $M(r = 8.9\,\mathrm{kpc}) =$

$8.7 \times 10^9\,M_\odot$, $M(r = 0.3\,\mathrm{kpc}) = 2.13 \times 10^7\,M_\odot = M_{0.3\mathrm{kpc}}$ and $M_{\mathrm{vir}} = 1.2 \times 10^{11}\,M_\odot$. Noting that the SMC has about 1/10 of the mass of the LMC (Kallivayalil et al. 2006), the virial mass of its halo can be estimated as $M_{\mathrm{vir}} = 1.2 \times 10^{10}\,M_\odot$, corresponding to $M_{0.3\mathrm{kpc}} = 1.51 \times 10^7\,M_\odot$.

In order to test the shape of the MW satellite distribution function against the shape of the distribution of the $M_{0.3\mathrm{kpc}}$ values of the MW-satellites, artificial samples of 10^6 $M_{0.3\mathrm{kpc}}$ masses are generated in concordance with the ΛCDM hypothesis, using Monte-Carlo simulations. As noted in Sect. 7.2, $M_{0.3\mathrm{kpc}}$ is well approximated by $M(r = 0.3\mathrm{kpc})$ in a CDM-dominated galaxy, $M(r = 0.3\mathrm{kpc})$ can be calculated if M_{vir} and c are given, and the expectation value for c is a function of M_{vir}. The first step is therefore to choose a value for M_{vir} using uniform random deviates and the probability distribution of luminous halos given in Eq. 7.3 (see e.g. chapter 7.2 in Press et al. 1992 for details). The next step is to attribute a value for $\log_{10}(c)$ to the chosen M_{vir}. This is done by multiplying Eq. 7.11 with a Gaussian random deviate and adding the result to the value for $\log_{10}(\overline{c})$, which is calculated from Eq. 7.10. After transforming $\log_{10}(c)$ to c, $M_{0.3\mathrm{kpc}} = M(r = 0.3\mathrm{kpc})$ of the given halo can be calculated from Eq. 7.7, using Eq. 7.2 and Eq. 7.8. These steps are repeated, until a sample of 10^6 $M_{0.3\mathrm{kpc}}$ values is generated.

If two samples are given, the maximum distance between their cumulative distribution functions, D, can be calculated. Performing the KS-test, this quantity allows to estimate how likely it is that they are drawn from the same distribution function. The null hypothesis is that the observed satellite galaxies are drawn from the theoretically calculated mass function of luminous halos; the parent distribution is thus assumed to be the mass function of $M(0.3\mathrm{kpc})$ values of luminous sub-halos according to the ΛCDM hypothesis. Setting M_{max} in Eq. 7.3 to $10^{11} M_\odot$, which is approximately the mass estimated for the CDM-halo of the LMC, and taking $M_{\mathrm{min}} = 10^7\,M_\odot$, leads to $D = 0.333$. According to the KS-test, given the parent distribution the probability for an even larger distance is 0.011. This means that the null hypothesis can be excluded with 98.9 per cent confidence. Both cumulative distributions are shown in Fig. 7.1[1].

Omitting the LMC and SMC from the observational sample but keeping $M_{\mathrm{min}} = 10^7\,M_\odot$ and $M_{\mathrm{max}} = 10^{11}\,M_\odot$ in the theoretical sample yields $D = 0.294$ leading to exclusion of the null hypothesis with a confidence of 95.5 per cent. Additionally setting $M_{\mathrm{max}} = 4 \times 10^{10}\,M_\odot$, yields $D = 0.301$, leading to exclusion of the null hypothesis with a confidence of 96.3 per cent. A mass of $4 \times 10^{10}\,M_\odot$ equals the M_{vir} that corresponds to the most massive $M_{0.3\mathrm{kpc}}$ in the sample by Strigari et al. (2008), i.e. the most massive sub-halo except the haloes of the Magellanic Clouds. The latter two tests thus comprise a homogeneous mass-sample of observed satellites as compiled by Strigari et al. (2008).

The fact that the mass function is expected to steepen at $M_{\mathrm{crit}} = 0.01\,M_{\mathrm{h}}$ even increases the discrepancy between the ΛCDM hypothesis and the observations. Returning the LMC and SMC back into the observational sample and cutting off $\xi_{\mathrm{sub}}(M_{\mathrm{vir}})$ at $M_{\mathrm{max}} = 10^{10} M_\odot$ (with $M_{\mathrm{min}} = 10^7\,M_\odot$), which would be close to M_{crit} for the CDM-halo of the MW (see Sect. 7.1), and one order of magnitude below the estimated mass of the CDM-halo of the LMC, implies $D = 0.359$ and an exclusion with 99.5 per cent confidence.

On the other hand, setting $M_{\mathrm{max}} = 10^{12}\,M_\odot$ (with $M_{\mathrm{min}} = 10^7\,M_\odot$) leads to $D = 0.329$ and an exclusion with 98.8 per cent confidence. Any reasonable uncertainty to the actual value of M_{max} can therefore be excluded as an explanation for the discrepancy between the observed

[1]Monte Carlo experiments are used to quantify the confidence values for the KS-tests: Drawing the corresponding number of sub-halo masses (e.g. 20 as in this case) from Eq. 7.3, D' is calculated. This is repeated 10^5 times. Counting of D' values gives the fraction of cases when $D' > D$, where D is the actually obtained D' value from the data (e.g. $D = 0.333$ in this case). These fractions are reported here as likelihood values, and are about half as large as the probability values obtained using approximate methods, as e.g. in Press et al. (1992).

sample of $M_{0.3\,\mathrm{kpc}}$ and a sample generated based on the ΛCDM hypothesis. As a consequence, the same is true for the uncertainty to the actual mass of the halo of the MW, M_{h}, since M_{max} is linked to M_{h} (see Sect. 7.1).

Thus M_{max} is kept at $10^{11}\,M_{\odot}$ in the following. Setting the lower limit of $\xi_{\mathrm{lum}}(M_{\mathrm{vir}})$ from $10^{7}\,M_{\odot}$ to $10^{8}\,M_{\odot}$ then leads to $D = 0.319$ and an exclusion of the null-hypothesis with a confidence of 98.4 per cent confidence. $10^{8}\,M_{\odot}$ is the M_{vir} suggested by the lowest $M_{0.3\mathrm{kpc}}$ in the sample from Strigari et al. (2008). Note that the likelihood decreases with decreasing M_{max}. This is due to the overabundance of $M_{0.3\,\mathrm{kpc}} \approx 10^{7}\,M_{\odot}$ halos becoming more prominent in the observational sample.

Strigari et al. (2008) suggest that $\xi_{\mathrm{lum}}(M_{\mathrm{vir}})$ might even be cut off below a mass of $\approx 10^{9} M_{\odot}$, either because halos below that mass do not contain baryons or do not form at all. Indeed, modifying $\xi_{\mathrm{lum}}(M_{\mathrm{vir}})$ given by Eq. 7.3 accordingly, results in an agreement between the theoretical distribution and the data ($D = 0.188$ with exclusion confidence of only 70 per cent). A $\xi_{\mathrm{lum}}(M_{\mathrm{vir}})$ with a lower mass limit of $10^{9}\,M_{\odot}$ is however in disagreement with the ΛCDM hypothesis, since the limiting mass below which all CDM-halos are dark ought to be two orders of magnitude lower according to Li et al. (2010).

Note, that the recently newly derived reduced mass of Hercules (Adén et al. 2009) does not affect the calculated likelihoods nor the conclusions reached here.

7.4 Conclusion

In *summary*, the mass distribution of the putative DM halos of observed satellites can be understood in terms of the ΛCDM hypothesis with at most 4.5 per cent likelihood. Assuming the dSph satellites are in virial equilibrium and Newtonian dynamics to be valid, the observationally deduced DM halo masses of the MW satellites show a significant overabundance of $M_{0.3\mathrm{kpc}} \approx 10^{7}\,M_{\odot}$ halos and a lack of less-massive values compared to the theoretically calculated distribution for luminous sub-halos, despite much effort to solve the "common-mass-scale" problem (Sect. 2 in Kroupa P. et al. 2010).

Chapter 8

Outlook

8.1 Further observational tests for the hypothesis of a top-heavy IMF in UCDs

It was suggested in Chapters 3, 4 and 5 that UCDs form with a top-heavy IMF due to the conditions under which star formation takes place in UCDs. Given the fundamental importance of the IMF in astrophysics, further tests of this scenario seem advisable. Methods by which this can be done are given below.

8.1.1 Testing the hypothesis that LMXBs in GCs and UCDs are formed through close dynamical encounters.

Based on the hypothesis that essentially all LMXBs in GCs and UCDs are formed through encounters between star and stellar remnants, Dabringhausen et al. (2012) found that the IMF in UCDs varies with their mass. This underlying hypothesis could be tested with the GCs in the Milky Way, since it has already been noted by Katz (1975) that the GCs in the Milky Way harbor numerous X-ray sources and further studies have revealed more probable LMXBs. A census of these can therefore be taken from the existing literature. Also age estimates have been published for a number of the GCs in the Milky Way (Salaris & Weiss 2002). Using these age estimates for the GCs, their masses M and their half-mass radii $r_{\rm h}$, the number of crossing times that have passed can be calculated. The number of crossing times is a measure for the frequency of stellar encounters. Thus, there should be a correlation between the number of LMXB in a GC and the number of its crossing times. Moreover, this correlation should be such that it would be consistent with the GCs having no LMXBs at zero crossing times, if their population of LMXBs indeed originates from close encounters between low-mass stars and neutron stars.

Such a study on the dependency between the LMXB-frequency in GCs and the age of the host-GCs would be complementary to a recent study by Zhang et al. (2012) on the dependency of the LMXB-frequency in galaxies and the age of the host-galaxies. Zhang et al. (2012) remove the LMXBs in GCs from their sample, in order to obtain a sample of LMXBs that was not formed dynamically through interactions between stars. They therefore investigate to what extent the LMXB-frequency depends on the aging of stars in a binary population that is not changed through encounters. The study proposed here, in contrast, will rely on GCs as systems where dynamical interactions between stars are relevant, in order to confirm that the number of LMXBs in GCs indeed primarily depends on the dynamical evolution they have experienced.

The number of GCs, for which both an age estimate and deep X-ray observations exists, is unlikely to be large. The statistical analysis of the LMXB-distribution in GCs with their age will therefore be made using the percentile-percentile plots described by Maschberger & Kroupa (2009). If this statistical tool is used, no information on the GC-age distribution is lost, in contrast to methods that include binning of the data. The methods introduced by Maschberger & Kroupa (2009) therefore allow sound conclusions also from rather small samples.

An increase of the LMXB-frequency in GCs with the age of the GCs would also open a new perspective on the well known dependency between the color of extra-Galactic GCs and the probability to find a bright LMXB in them. This probability is the larger the redder these GCs are (Jordán et al. 2004; Sivakoff et al. 2007). The prevailing interpretation is that the color of these GCs reflects their metallicity, so that more metal rich (i.e. redder) GCs have more LMXBs (e.g. Jordán et al. 2004). There is however a degeneracy between the integrated color of a stellar population and its age or metallicity. Equal-age stellar populations are redder if they are more metal-rich, and stellar populations with the same metallicity are redder if they are older (Worthey 1994). This degeneracy has not been considered so far in the context of the dependency between the frequency of bright LMXBs in GCs and their color. A dependency between age and LMXB-frequency is however very natural if LMXBs in GCs are mainly created by close encounters between stars and dark remnants. Using stellar population models, we therefore intend to quantify how the LMXB-frequency in GCs depends on their age, if their color is taken as a tracer of their age.

8.1.2 Testing the hypothesis of a top-heavy IMF with an extended study on LMXBs in UCDs.

Dabringhausen et al. (2012) have argued from the fraction of UCDs with a bright X-ray source (interpreted as a LMXB) that the IMF in UCDs is top-heavy. While the data they use is based on a rather large sample of UCDs (≈ 400), a weak point in their analysis is that the data is grouped in only three luminosity bins. Information on the luminosities of the individual UCDs is thereby lost, which otherwise could have been used with more powerful statistical techniques.

It is therefore worthwhile to further test the results using other, more detailed data. This data can be searched for in the wealth of literature on the connection between LMXBs and globular clusters (e.g. Blanton et al. 2001; Maccarone et al. 2003; Sarazin et al. 2003; Woodley et al. 2008; Fabbiano et al. 2010; Paolillo et al. 2011). The reason why these studies are useful for studies for my work is that they usually include UCDs, even though they are not distinguished from GCs. It has indeed been argued that before that UCDs might be the most massive GCs (Mieske et al. 2008, 2012).

The statistical methods described in Maschberger & Kroupa (2009) can be applied on the sample of GCs and UCDs with a LMXB collected from the literature. The results reported in Dabringhausen et al. (2012) should thereby be confirmed, if the IMF is indeed top-heavy in UCDs. The general idea is to model the luminosity distribution of GCs and UCDs using typical observed parameters of GCs and UCDs and different assumptions on how the IMF of UCDs depends on their luminosity. This leads to different hypotheses on the luminosity distributions of GCs and UCDs with a bright X-ray source that indicates a LMXB. Whether these hypotheses are consistent with the observed luminosity distribution of GCs and UCDs can be tested with the percentile-percentile plots introduced by Maschberger & Kroupa (2009).

Given that with the methods described in Maschberger & Kroupa (2009) no information on the luminosity distribution of the considered objects is lost (in contrast to methods where

the objects are gathered in luminosity bins), they allow sound conclusions also from rather small samples. Therefore also a dependency of the LMXB-frequency and thus the IMF on the environment could be tested for with the methods from Maschberger & Kroupa (2009): Does the IMF in UCDs depend on wether they are associated with a galaxy cluster or a field galaxy? Does the luminosity and the type of the host galaxy of UCDs play a role for their IMF? Answering such questions could give further insights on the conditions under which the IMF becomes top-heavy (if at all).

The case of the Fornax Galaxy Cluster is of particular interest. UCDs in the Fornax Galaxy Cluster have lower M/L ratios than UCDs in the Virgo Galaxy Cluster (Mieske et al. 2008) and are consistent with having a canonical IMF (Chilingarian et al. 2008). It is therefore expected that they also have a lower incidence of LMXBs than the UCDs in the Virgo Galaxy Cluster. This can be tested with the data on the Fornax Galaxy Cluster from Paolillo et al. (2011).

8.1.3 Testing the hypothesis of a bottom-heavy IMF in UCDs.

Provided that LMXBs in UCDs are formed through close dynamical encounters between dark remnants and low-mass stars, an overabundance of LMXBs can either be due to an overabundance of dark remnants (i.e. a top-heavy IMF, see Dabringhausen et al. 2009; Murray 2009) or to an overabundance of low-mass stars (i.e. a bottom-heavy IMF, see Mieske & Kroupa 2008).

The low-mass stars that could be part of a bright LMXB in a UCD are the most massive stars (near $1\ \mathrm{M}_\odot$) that have not yet completed their evolution. They are therefore the brightest stars in a UCD also at optical wavelengths. The observed typical M/L_V-ratios of UCDs thereby set strong constrains on the size of such a population and on the possible shape of a bottom-heavy IMF. It is likely that a bottom-heavy IMF can only fulfill the constraints set by the overabundance of LMXBs in UCDs and the M/L_V-ratios of UCDs at the same time if the luminosity of a great number of possible low-mass companions in LMXBs is balanced by population of faint stars which would have to be introduced as an additional parameter to the model. This kind of fine-tuning would make a bottom-heavy IMF an improbable explanation for the observed properties of UCDs. However, for a more conclusive statement, it has to be quantified how a bottom-heavy IMF could explain simultaneously the elevated M/L_V-ratios and the LMXB-excess of UCDs.

8.1.4 Quantifying the spectra of young UCDs at high redshifts.

Given that UCDs probably were very compact when they formed and that their stellar population formed quickly, they must have been extremely bright when they were young. This is due to a large population of massive stars that had not yet evolved shortly after the formation of the UCD.

Consider, for instance, a UCD with an initial mass of $10^8\ \mathrm{M}_\odot$ and an elliptical galaxy with a mass of $10^{12}\ \mathrm{M}_\odot$. Given the short lifetime of the most massive stars, the star formation rate (SFR) is decisive for how many of them populate a stellar system at a given time. Thus, the luminosity of a young, star-forming stellar system is largely determined by the SFR, since the most massive stars are also the most luminous ones. If the star formation took 10^6 years in the UCD (cf. Dabringhausen et al. 2009) and 10^9 years in the elliptical galaxy (cf. Thomas et al. 2005), the SFR was $100\ \mathrm{M}_\odot\,\mathrm{yr}^{-1}$ for the UCD and $10^3\ \mathrm{M}_\odot\,\mathrm{yr}^{-1}$ for the elliptical galaxy. The young elliptical galaxy would thus be about ten times brighter than the young UCD if they both had the same IMF. However, stars with masses $\gtrsim 15\ \mathrm{M}_\odot$ are about a hundred times more

numerous for a top-heavy IMF with $\alpha_3 \approx 1$ than for a canonical IMF ($\alpha_3 = \alpha_2 = 2.3$; see Fig. 1.1 for a definition of α_3). While massive UCDs may indeed have top-heavy IMFs, the IMF of elliptical galaxies was even suggested to be bottom-heavy by van Dokkum & Conroy (2010). A young UCDs with a mass of $M = 10^8\,\mathrm{M}_\odot$ may therefore be as luminous as a young major elliptical galaxy with $M = 10^{12}\,\mathrm{M}_\odot$.

Now consider the radii of elliptical galaxies and UCDs. An elliptical galaxy with $M = 10^{12}\,\mathrm{M}_\odot$ typically has a half-light radius of $\approx 5 \times 10^3$ pc (cf. Dabringhausen et al. 2008), while a UCD with an initial mass of $M = 10^8\,\mathrm{M}_\odot$ may have evolved from an object with an initial radius of 5 pc if the probable mass loss of the UCD is taken into account (cf. Dabringhausen et al. 2010).This leads to a central star formation surface density of $\Sigma_{SFR} \approx 2\,\mathrm{M}_\odot\,\mathrm{pc}^{-2}\,\mathrm{yr}^{-1}$ for the young UCD and a central star formation surface density of $\Sigma_{SFR} \approx 2 \times 10^{-5}\,\mathrm{M}_\odot\,\mathrm{pc}^{-2}\,\mathrm{yr}^{-1}$ for the young elliptical galaxy.

Thus, a young UCD with a luminosity similar to that of a young massive elliptical galaxy would have had a surface brightness 10^5 times higher than that of a young elliptical galaxy. With a given telescope, a young massive UCD would therefore be much easier to detect than a young major elliptical galaxy of equal luminosity. Consequently, young UCDs should be observable as bright point sources up to the same distances at which bright galaxies can be observed (i.e. at redshifts $z \lesssim 10$), provided they formed as early as galaxies. If UCDs form through the interaction of galaxies (Fellhauer & Kroupa 2002a), they would also form at rather low redshifts, which would make their detection easier. With the current knowledge on UCDs, a complete failure in finding young UCDs at any redshift would be an unexpected, but therefore even more intriguing result. Such a result would exclude the formation of UCDs in starbursts, despite the evidence for α-enrichment in UCDs (Evstigneeva et al. 2007) and the evidence for top-heavy IMFs in UCDs (Dabringhausen et al. 2009, 2012), which are understandable as a consequence of extremely high densities in the young UCDs (Kroupa et al. 2011).

However, in order to distinguish the young UCDs from other point sources, their spectral properties have to be known. These properties depend on the star formation history (SFH) of the UCD, the age of its stellar population, its metallicity and the redshift. Finally, the spectral properties of a UCD also depend on its IMF.

The strategy for predicting what a distant UCD would look like to an observer is a follows. First, the time-evolution of the spectrum of the UCDs in their rest-frame needs to be calculated for a grid of probable SFHs, metallicities and IMFs. This task can be performed with the publicly available stellar evolution codes PEGASE and STARBURST99. Assuming an expansion history of the Universe (for instance, the expansion history predicted by the ΛCDM model) and an age for the UCD, the effect of redshift on these spectra can be calculated. The result would be a grid of UCD spectra whose parameters are the SFH, age, metallicity, and IMF of the UCDs. Note that also integrated colors in different passbands can be calculated from these spectra. While they do not contain as much information as a full spectrum, the advantage of such integrated colors is that they are simpler to observe. Observed spectra of point sources can then be compared to this grid which would allow conclusions on the properties of UCDs.

Alternatively, such a grid of UCD spectra can also be used to test cosmological models. If a sample of distant UCDs is observed, the properties of their stellar populations (SFH, age, metallicity, IMF) can be chosen such that they agree with parameters typical for UCDs in the Local Universe. Their spectra can then be compared with modeled spectra for different choices of the matter density Ω_M and the vacuum density Ω_Λ in the Universe, which imply different expansion histories of the Universe.

8.1.5 Quantifying the SNII frequency in young UCDs.

Dabringhausen et al. (2009) suggested that a massive UCD forms stars with a total mass of $10^8\ \mathrm{M}_\odot$ within 10 Myr and therefore has an average SFR of $100\ \mathrm{M}_\odot\,\mathrm{yr}^{-1}$. With these parameters, up to one type II supernova (SNII) per year would be expected in such a stellar system in the inertial frame of the UCD (cf. Fig. 8 in Dabringhausen et al. 2012). The brightest SNII have a B-band peak luminosity $L_{\mathrm{peak}} > 5 \times 10^9\ \mathrm{L}_\odot$. Thus, SNII can become brighter than a small spiral galaxy like M 33 ($L_B \approx 5 \times 10^9\ \mathrm{L}_\odot$, cf. Karachentsev et al. 2004), but remain dimmer than a large spiral galaxy like M 31 ($L_B \approx 6.7 \times 10^{10}\ \mathrm{L}_\odot$, cf. Karachentsev et al. 2004). With such luminosities, SNII will be observable to redshifts $z \lesssim 8$ with the upcoming European Extremely Large Telescope (E-ELT), while currently only SNII with $z \lesssim 1$ are observed (Hook, I. M. 2005). Thus, SNII in high-redshift UCDs can be observed in a couple of years. A given SNII cannot be detected for very long, as the timespan in which it exceeds 10 per cent of its peak luminosity is only about 100 days in their inertial frame (Doggett & Branch 1985).

Thus, SNII are bright enough to be detected to very large distances in the near future, and in a given UCD they are rare enough to produce clear variations of their luminosity (which would not be the case, if the typical time between two SNII is shorter than the characteristic timescale on which the luminosity of a SNII changes).

The probability to find a SNII near the maximum of its brightness in a UCD can be estimated for a given mass, IMF and age of the UCD. This is because the mass and the IMF determines the number of massive stars that formed in that UCD and the age determines the number of stars that are about to complete their evolution. The most massive UCDs should be bright enough to narrow down their ages, luminosities and IMFs by using the modeled spectra created earlier. Based on the best-fitting models, the total number of UCDs with a SNII near the maximum of its brightness can be estimated. This number can be checked by observing a sample of candidates for bright and young UCDs and observing the same sample again (at least) one year later. After one year, enough time should have passed also in the inertial frame of the UCDs for a significant change of the luminosity of a SNII. The luminosity variations of the candidate UCDs between the first and the second observation would therefore allow to estimate the number of SNII that have faded and the number of new SNII since the first observation.

Appendix A

Appendix

A.1 Statistical tests

A.1.1 Pearson's test for the goodness of fit

Pearson's test for the goodness of fit (Bhattacharyya & Johnson 1977) can be used for deciding whether the frequency of a certain result for a measurement that has been performed on n objects deviates significantly from an expected frequency. For the special case that only two results A and B can be the outcome of each measurement (A could be for example a result higher than a theoretical expectation and B the opposite case), result A will have occurred j times and result B $n - j$ times. The probability of this outcome can now be calculated if a certain probability p for the case A as the result of a measurement is assumed. A useful measure for this is given by the equation

$$\chi^2 = \frac{(j - pn)^2}{pn} + \frac{((n - j) - (1 - p)n)^2}{(1 - p)n}. \tag{A.1}$$

There are tabulated values for χ^2 (e.g. table 6 in the appendix of Bhattacharyya & Johnson 1977) which make it possible to read off the probability for χ^2 being higher than some value for a series of measurements, if the hypothesis for the probability p is correct. (The degree of freedom is one in this case.)

A.1.2 The sign test

The sign test (Bhattacharyya & Johnson 1977) is specifically designed for a small number of pairs of values, (X_1, X_2), and is supposed to detect whether there is a significant trend for X_2 being larger or smaller than X_1 or not. X_1 and X_2 could be two measurements under different conditions (e.g. other instruments), or X_1 could be a value inferred from an observation, while X_2 is the theoretical prediction for this value. If the conditions under which X_1 and X_2 were obtained do not result into systematically larger or smaller values for X_2 compared to X_1, the probability for X_1 being larger than X_2 is 0.5. The probability that $X_2 > X_1$ for j out of n pairs of values is then given by the binomial distribution.

A.2 The total mass of the remnants

We explicitly note the terms with $m > m_{\rm to}$ that arise from the integration of the right hand side of eq. (3.6), if eq. (3.8) is inserted for $m_{\rm rem}(m)$.

The contribution of the white dwarfs to $M_{\rm m}$, $M_{\rm m,WD}$, can be written as

$$\begin{aligned}\frac{M_{\rm m,WD,v}}{\rm M_\odot} =& \frac{0.109\,k_3}{2-\alpha_3} \times (8^{2-\alpha_3} - m_{\rm to}^{2-\alpha_3}) \\ &+ \frac{0.394\,k_3}{1-\alpha_3} \times (8^{1-\alpha_3} - m_{\rm to}^{1-\alpha_3}),\end{aligned} \tag{A.2}$$

with the masses of the stars in Solar units. $m_{\rm to}$ was argued to be $\approx 1\,\rm M_\odot$ in Section 3.3.1.

The contribution of neutron stars to $M_{\rm m}$, $M_{\rm m,NS}$, can be written as

$$\frac{M_{\rm m,NS}}{\rm M_\odot} = \frac{1.35\,k_3}{1-\alpha_3} \times (25^{1-\alpha_3} - 8^{1-\alpha_3}). \tag{A.3}$$

The contribution of the remnants of stars with initial masses higher than $25\,\rm M_\odot$ to $M_{\rm m}$, $M_{\rm m,BH}$, can be written as

$$\frac{M_{\rm m,WD,v}}{\rm M_\odot} = \frac{0.1\,k_3}{2-\alpha_3} \times (m_{\rm max}^{2-\alpha_3} - 25^{2-\alpha_3}). \tag{A.4}$$

A.3 Data on tidal dwarf galaxies

A.3.1 Data on observed tidal dwarf galaxies

Table A.1: Data on observed TDG-candidates, as described in Section (6.2.2). Listed are the identification of the object as in the source paper, its half-light radius ($r_{\rm e}$), its equivalent radius (r; cf. equation 6.1), the mass of its stellar population estimated from its optical luminosity (M_*), the mass of its stellar population estimated from its Hα-emission lines (M_α), the mass of its stellar population under the assumption that the stellar population is a mix of old and young stars ($M_{\rm old}$), the mass of the object estimated from its internal dynamics ($M_{\rm dyn}$), the age of its stellar population assuming a single star burst and finally the reference to the source of the data (1: Hunsberger et al. 1996; 2: Tran H. D. et al. 2003; 3: Bournaud et al. 2007; 4: Duc et al. 2007; 5: Yoshida et al. 2008; 6: Galianni et al. 2010; 7: Miralles-Caballero et al. 2012). If the value for $r_{\rm e}$ is given in brackets, it has not been given in the literature, but was calculated here using equations (6.1) and (6.2).

identification	$r_{\rm e}$ [pc]	r [pc]	M_* [$\mathrm{M}_\odot$]	$M_{\rm H\alpha}$ [$\mathrm{M}_\odot$]	$M_{\rm old}$ [$\mathrm{M}_\odot$]	$M_{\rm dyn}$ [$\mathrm{M}_\odot$]	t years	source
HCG 01b 1	(1283)	4490	1.6×10^8	–	–	–	some 10^8	1
HCG 01b 2	(563)	1970	2.5×10^7	–	–	–	some 10^8	1
HCG 01b 3	(1180)	4130	6.3×10^8	–	–	–	some 10^8	1
HCG 16a 1	(271)	950	7.9×10^6	–	–	–	some 10^8	1
HCG 16a 2	(286)	1000	3.2×10^6	–	–	–	some 10^8	1
HCG 16a 3	(163)	570	2.0×10^6	–	–	–	some 10^8	1
HCG 26b 1	(962)	3370	1.6×10^8	–	–	–	some 10^8	1
HCG 26b 2	(797)	2790	6.3×10^7	–	–	–	some 10^8	1
HCG 26b 3	(823)	2880	3.2×10^7	–	–	–	some 10^8	1
HCG 31a N 1	(389)	1360	5.0×10^7	–	–	–	some 10^8	1
HCG 31a N 2	(351)	1230	5.0×10^7	–	–	–	some 10^8	1
HCG 31a N 3	(189)	660	1.3×10^7	–	–	–	some 10^8	1
HCG 31c N	(180)	630	4.0×10^7	–	–	–	some 10^8	1
HCG 31a S 1	(169)	590	7.9×10^6	–	–	–	some 10^8	1
HCG 31a S 2	(371)	1300	1.3×10^8	–	–	–	some 10^8	1
HCG 38b N	(591)	2070	4.0×10^7	–	–	–	some 10^8	1
HCG 38b S	(429)	1500	7.9×10^7	–	–	–	some 10^8	1
HCG 92c 1	(474)	1660	6.3×10^6	–	–	–	some 10^8	1
HCG 92c 2	(429)	1500	7.9×10^6	–	–	–	some 10^8	1
HCG 92c 3	(289)	1010	5.0×10^6	–	–	–	some 10^8	1

HCG 92c 4	(557)	1950	1.3×10^7	–	–	–	some 10^8	1
HCG 92c 5	(409)	1430	1.6×10^7	–	–	–	some 10^8	1
HCG 92c 6	(263)	920	6.3×10^6	–	–	–	some 10^8	1
HCG 92c 7	(466)	1630	1.0×10^7	–	–	–	some 10^8	1
HCG 92c 8	(451)	1580	2.0×10^7	–	–	–	some 10^8	1
HCG 92c 9	(517)	1810	1.3×10^7	–	–	–	some 10^8	1
HCG 92c 10	(429)	1500	2.0×10^7	–	–	–	some 10^8	1
HCG 92c 11	(451)	1580	7.9×10^6	–	–	–	some 10^8	1
HCG 92c 12	(591)	2070	2.5×10^7	–	–	–	some 10^8	1
HCG 92c 13	(603)	2110	5.0×10^7	–	–	–	some 10^8	1
HCG 92b S 1	(403)	1410	4.0×10^7	–	–	–	some 10^8	1
HCG 92b S 2	(280)	980	2.0×10^7	–	–	–	some 10^8	1
HCG 92b S 3	(434)	1520	6.3×10^7	–	–	–	some 10^8	1
HCG 92b S 4	(569)	1990	1.3×10^8	–	–	–	some 10^8	1
HCG 92b S 5	(377)	1320	2.0×10^7	–	–	–	some 10^8	1
HCG 92b N 1	(497)	1740	2.0×10^7	–	–	–	some 10^8	1
HCG 92b N 2	(534)	1870	1.6×10^8	–	–	–	some 10^8	1
HCG 92b N 3	(406)	1420	2.5×10^7	–	–	–	some 10^8	1
HCG 92d S 1	(417)	1460	5.0×10^7	–	–	–	some 10^8	1
HCG 92d S 2	(274)	960	2.5×10^7	–	–	–	some 10^8	1
HCG 92d N 1	(429)	1500	2.5×10^7	–	–	–	some 10^8	1
HCG 92d N 2	(249)	870	1.0×10^7	–	–	–	some 10^8	1
HCG 92d N 3	(300)	1050	4.0×10^7	–	–	–	some 10^8	1
HCG 92d N 4	(440)	1540	2.5×10^7	–	–	–	some 10^8	1
HCG 96c E	(674)	2360	5.0×10^7	–	–	–	some 10^8	1
HCG 96a W 1	(729)	2550	3.2×10^7	–	–	–	some 10^8	1
HCG 96a W 2	(631)	2210	6.3×10^7	–	–	–	some 10^8	1
UGC 10214 SSC	161	–	6.6×10^5	–	–	–	$4 - 5 \times 10^6$	2
NGC5291N	(1057)	3700	1.1×10^8	–	–	3.0×10^9	$< 5 \times 10^6$	3
NGC5291S	(1429)	5000	7.5×10^7	–	–	2.7×10^9	$< 5 \times 10^6$	3
NGC5291SW	(571)	2000	3.0×10^7	–	–	1.2×10^9	$< 5 \times 10^6$	3

VCC 2062	(600)	2100	5.0×10^7	–	–	3.5×10^8	3×10^8	4
RB 199 Knot 1	250	–	8.8×10^7	–	–	–	some 10^8	5
RB 199 Knot 2	250	–	1.4×10^8	–	–	–	some 10^8	5
RB 199 Knot 3	250	–	4.8×10^7	–	–	–	some 10^8	5
RB 199 Knot 4	250	–	7.6×10^6	–	–	–	some 10^8	5
RB 199 Knot 5	250	–	2.3×10^7	–	–	–	some 10^8	5
RB 199 Knot 6	250	–	2.0×10^7	–	–	–	some 10^8	5
NGC 1097 Knot A	336	–	6.0×10^6	–	–	–	some 10^9	6
NGC 1097 Knot B	482	–	4.0×10^6	–	–	–	some 10^9	6
IRAS 04315−0840 1	38	166	7.9×10^4	2.5×10^5	6.3×10^5	3.2×10^7	4.6×10^6	7
IRAS 04315−0840 2	21	93	1.6×10^4	6.3×10^5	3.2×10^5	6.3×10^7	7.0×10^6	7
IRAS 06076−2139 1	77	306	2.5×10^5	7.9×10^5	–	1.0×10^8	4.2×10^6	7
IRAS 06076−2139 2	59	283	7.9×10^4	2.5×10^5	–	1.0×10^8	4.5×10^6	7
IRAS 06076−2139 3	53	121	4.0×10^4	1.3×10^5	4.0×10^5	7.9×10^7	5.4×10^6	7
IRAS 06076−2139 4	51	116	3.2×10^4	1.0×10^5	–	1.0×10^8	4.8×10^6	7
IRAS 06076−2139 5	41	89	2.5×10^4	1.3×10^5	–	4.0×10^7	4.9×10^6	7
IRAS 06076−2139 6	66	137	1.6×10^5	7.9×10^5	–	–	4.9×10^6	7
IRAS 07027−6011 S 1	31	127	7.9×10^4	4.0×10^5	–	7.9×10^7	3.6×10^6	7
IRAS 07027−6011 S 2	61	186	3.2×10^4	4.0×10^4	–	–	3.2×10^6	7
IRAS 08572+3915 N	105	405	2.5×10^5	7.9×10^5	–	5.0×10^8	4.0×10^6	7
IRAS 08572+3915 SE 3	76	322	1.3×10^5	1.3×10^5	1.3×10^6	–	4.9×10^6	7
IRAS 08572+3915 SE 4	191	312	3.2×10^5	1.3×10^6	3.2×10^6	–	5.9×10^6	7
IRAS F10038−3338 3	43	269	2.5×10^4	3.2×10^4	5.0×10^5	4.0×10^7	3.6×10^6	7
IRAS F10038−3338 4	88	252	1.0×10^5	1.6×10^5	1.0×10^6	1.6×10^8	4.9×10^6	7
IRAS 12112+0305 1	200	887	1.3×10^7	2.0×10^7	1.0×10^8	2.5×10^9	4.3×10^6	7
IRAS 12112+0305 4	82	288	2.5×10^5	1.3×10^6	–	–	4.2×10^6	7
IRAS 14348−1447 1	280	909	5.0×10^7	1.3×10^8	3.2×10^8	2.0×10^9	4.4×10^6	7
IRAS 15250+3609 1	165	627	4.0×10^6	5.0×10^6	3.2×10^7	2.0×10^9	5.3×10^6	7
IRAS F18093−5744 N	20	74	1.0×10^5	6.3×10^5	–	7.9×10^7	5.1×10^6	7
IRAS F18093−5744 C	37	78	6.3×10^4	1.6×10^5	5.0×10^5	4.0×10^7	4.9×10^6	7
IRAS 23128−5919	83	376	5.0×10^5	1.3×10^6	3.2×10^6	1.0×10^9	4.8×10^6	7

IRAS 16007+3743 R1	828	–	6.3×10^8	–	–	6.3×10^9	7.1×10^6	7
IRAS 16007+3743 R2	884	–	6.3×10^8	–	–	1.0×10^{10}	5.4×10^6	7
IRAS 16007+3743 R3	851	–	6.3×10^7	–	–	1.3×10^{10}	6.4×10^6	7

A.3.2 Results from numerical calculations on the formation of tidal dwarf galaxies

Table A.2: Data on TDGs that were found in numerical calculations of encounters between gas-rich galaxies as described in Section (6.2.2). Listed are the effective radius of each TDG ($r_{\rm e}$), and if available its size (given through diameters along two orthogonal axes), the mass of its stellar population (M_*), its total mass (M), the time at the end of the calculation (t) and finally the reference to the source of the data (1: Bournaud et al. 2008; 2: Wetzstein et al. 2007; 3: Barnes & Hernquist 1992b). The value of M_* for the TDG from Barnes & Hernquist (1992b) is an estimate based on M.

$r_{\rm e}$ [pc]	size [pc] × [pc]	M_* [$\mathrm{M}_\odot$]	M [$\mathrm{M}_\odot$]	t years	source
8.5	61×46	6.8×10^6	–	9.5×10^8	1
7.6	63×35	8.7×10^6	–	9.5×10^8	1
9.7	46×78	1.9×10^7	–	9.5×10^8	1
460	3700×2200	2.7×10^8	–	9.5×10^8	1
420	4500×1500	5.2×10^8	–	9.5×10^8	1
700	–	1.0×10^8	3.5×10^8	1.2×10^8	2
229	–	(1.3×10^8)	4.0×10^8	7.5×10^8	3

Acknowledgements

Over the last couple of years, I received a lot of support from different people. Their help was was essential for the success of my PhD project and therefore I would like to thank them.

First of all, I would like to thank my PhD supervisor Pavel Kroupa for his support, guidance and feedback. He was always ready to discuss my work and thereby greatly improved it.

Of course, many other people also deserve thanks for their feedback, their support and stimulating discussions with them. For this, I would like to thank the (past and present) members of the stellar populations and dynamics research group, and in particular (in alphabetical order) Holger Baumgardt, Benoit Famaey, Michael Fellhauer, Michael Hilker, Michael Marks, Thomas Maschberger, Steffen Mieske, Soroush Nasoudi-Shoar, Jan Pflamm-Altenburg, Marcel Pawlowski and Ylva Schuberth.

Moreover, I would like to thank Steffen Mieske for being my host during a two-month studentship at ESO in Santiago de Chile, as well as Klaas de Boer and Pavel Kroupa for supporting my application for a stipend from Bonn University that financed my last year as a PhD student.

Finally, I would like to thank my parents, to whom I am indebted for their constant support over the years.

Bibliography

Aarseth, S. J. & Fall, S. M. 1980, ApJ, 236, 43

Adams, F. C. & Fatuzzo, M. 1996, ApJ, 464, 256

Adén, D., Wilkinson, M. I., Read, J. I., et al. 2009, ApJ, 706, L150

Anderson, J. P., Habergham, S. M., & James, P. A. 2011, MNRAS, 416, 567

André Ph. et al. 2010, A&A, 518, L102

Annibali, F., Bressan, A., Rampazzo, R., Zeilinger, W. W., & Danese, L. 2007, A&A, 463, 455

Baes, M., Sil'chenko, O. K., Moiseev, A. V., & Manakova, E. A. 2007, A&A, 467, 991

Ballero, S. K., Kroupa, P., & Matteucci, F. 2007, A&A, 467, 117

Banerjee, S., Baumgardt, H., & Kroupa, P. 2010, MNRAS, 402, 371

Banerjee, S., Kroupa, P., & Oh, S. 2012, ApJ, 746, 15

Barmby, P., Huchra, J. P., Brodie, J. P., et al. 2000, AJ, 119, 727

Barnes, J. E. & Hernquist, L. 1992a, ARA&A, 30, 705

Barnes, J. E. & Hernquist, L. 1992b, Nature, 360, 715

Barnes, J. E. & Hernquist, L. 1996, ApJ, 471, 115

Bassino, L. P., Muzzio, J. C., & Rabolli, M. 1994, ApJ, 431, 634

Bastian, N., Covey, K. R., & Meyer, M. R. 2010, ARA&A, 48, 339

Baugh, C. M., Lacey, C. G., Frenk, C. S., et al. 2005, MNRAS, 356, 1191

Baumgardt, H., Hut, P., & Heggie, D. C. 2002, MNRAS, 336, 1069

Baumgardt, H. & Kroupa, P. 2007, MNRAS, 380, 1589

Baumgardt, H., Kroupa, P., & Parmentier, G. 2008, MNRAS, 384, 1231

Baumgardt, H. & Makino, J. 2003, MNRAS, 340, 227

Baumgardt, H., Makino, J., Hut, P., McMillan, S., & Portegies Zwart, S. 2003, ApJ, 589, L25

Baumgardt, H. & Mieske, S. 2008, MNRAS, 391, 942

Bekki, K., Couch, W. J., Drinkwater, M. J., & Shioya, Y. 2003, MNRAS, 344, 399

Bender, R., Burstein, D., & Faber, S. M. 1992, ApJ, 399, 462

Bender, R., Burstein, D., & Faber, S. M. 1993, ApJ, 411, 153

Benson, A. J., Lacey, C. G., Baugh, C. M., Cole, S., & Frenk, C. S. 2002, MNRAS, 333, 156

Bergin, E. A. & Tafalla, M. 2007, ARA&A, 45, 339

Bhattacharyya, G. & Johnson, R. 1977, Statistical Concepts and Methods (Wiley & Sons, New York NY)

Binney, J. & Tremaine, S. 1987, Galactic dynamics (Princeton University Press)

Blanton, E. L., Sarazin, C. L., & Irwin, J. A. 2001, ApJ, 552, 106

Blumenthal, G. R., Faber, S. M., Flores, R., & Primack, J. R. 1986, ApJ, 301, 27

Boily, C. M. & Kroupa, P. 2003, MNRAS, 338, 673

Bonnell, I. A. & Bate, M. R. 2002, MNRAS, 336, 659

Bonnell, I. A., Bate, M. R., & Zinnecker, H. 1998, MNRAS, 298, 93

Boquien, M., Duc, P.-A., Braine, J., et al. 2007, A&A, 467, 93

Borch, A., Spurzem, R., & Hurley, J. 2007, ArXiv e-prints, 704

Bournaud, F. 2010, Advances in Astronomy, 2010

Bournaud, F. & Duc, P.-A. 2006, A&A, 456, 481

Bournaud, F., Duc, P.-A., Brinks, E., et al. 2007, Science, 316, 1166

Bournaud, F., Duc, P.-A., & Emsellem, E. 2008, MNRAS, 389, L8

Brown, G. E., Heger, A., Langer, N., et al. 2001, New Astronomy, 6, 457

Brüns, R. C., Kroupa, P., Fellhauer, M., Metz, M., & Assmann, P. 2011, A&A, 529, 138

Bruzual, G. & Charlot, S. 2003, MNRAS, 344, 1000

Bullock, J. S., Kolatt, T. S., Sigad, Y., et al. 2001, MNRAS, 321, 559

Burstein, D., Bender, R., Faber, S., & Nolthenius, R. 1997, AJ, 114, 1365

Cappellari M. et al. 2006, MNRAS, 366, 1126

Cappellari M. et al. 2012, Nature, 484, 485

Carney, B. W. 1996, Publications of the Astronomical Society of the Pacific, 108, 900

Carroll, B. W. & Ostlie, D. A. 1996, An Introduction to Modern Astrophysics (Addison-Wesley, Reading, MA)

Casares, J. 2007, in IAU Symposium, Vol. 238, IAU Symposium, ed. V. Karas & G. Matt, 3–12

Casas, R. A., Arias, V., Peña Ramírez, K., & Kroupa, P. 2012, MNRAS, 424, 1941

Chabrier, G. 2001, ApJ, 554, 1274

Chabrier, G. 2003, PASP, 115, 763

Chandar, R., Whitmore, B., & Lee, M. G. 2004, ApJ, 611, 220

Chary, R.-R. 2008, ApJ, 680, 32

Chevalier, R. A. & Clegg, A. W. 1985, Nature, 317, 44

Chilingarian, I. V., Cayatte, V., & Bergond, G. 2008, MNRAS, 390, 906

Cimatti A. et al. 2004, Nature, 430, 184

Clark, P. C., Klessen, R. S., & Bonnell, I. A. 2007, MNRAS, 379, 57

Combes, F., Young, L. M., & Bureau, M. 2007, MNRAS, 377, 1795

Condon, J. J., Huang, Z., Yin, Q. F., & Thuan, T. X. 1991, ApJ, 378, 65

Côté, P., Blakeslee, J. P., Ferrarese, L., et al. 2004, ApJS, 153, 223

Cowie, L. L., Songaila, A., Hu, E. M., & Cohen, J. G. 1996, AJ, 112, 839

Crowther, P. A., Schnurr, O., Hirschi, R., et al. 2010, MNRAS, 408, 731

Dabringhausen, J., Fellhauer, M., & Kroupa, P. 2010, MNRAS, 403, 1054

Dabringhausen, J., Hilker, M., & Kroupa, P. 2008, MNRAS, 386, 864

Dabringhausen, J., Kroupa, P., & Baumgardt, H. 2009, MNRAS, 394, 1529

Dabringhausen, J., Kroupa, P., Pflamm-Altenburg, J., & Mieske, S. 2012, ApJ, 747, 72

D'Antona, F. & Caloi, V. 2004, ApJ, 611, 871

D'Antona, F., Ventura, P., & Caloi, V. 2007, in Astronomical Society of the Pacific Conference Series, Vol. 374, From Stars to Galaxies: Building the Pieces to Build Up the Universe, ed. A. Vallenari, R. Tantalo, L. Portinari, & A. Moretti, 155

De Marchi, G., Paresce, F., & Pulone, L. 2007, ApJ, 656, L65

Decressin, T., Baumgardt, H., & Kroupa, P. 2008, A&A, 492, 101

Decressin, T., Charbonnel, C., & Meynet, G. 2007, A&A, 475, 859

Del Popolo, A. & Yesilyurt, I. S. 2007, Astronomy Reports, 51, 709

Disney, M. J., Romano, J. D., Garcia-Appadoo, D. A., et al. 2008, Nature, 455, 1082

Doggett, J. B. & Branch, D. 1985, AJ, 90, 2303

Drinkwater, M. J., Gregg, M. D., Couch, W. J., et al. 2004, Publications of the Astronomical Society of Australia, 21, 375

Drinkwater, M. J., Gregg, M. D., Hilker, M., et al. 2003, Nature, 423, 519

Drinkwater, M. J., Jones, J. B., Gregg, M. D., & Phillipps, S. 2000, Publications of the Astronomical Society of Australia, 17, 227

Duc, P.-A., Bournaud, F., & Masset, F. 2004, A&A, 427, 803

Duc, P.-A., Braine, J., Lisenfeld, U., Brinks, E., & Boquien, M. 2007, A&A, 475, 187

Duc P. A. et al. 2011, MNRAS, 417, 863

Elmegreen, B. G. 1997, ApJ, 486, 944

Elmegreen, B. G. 1999, ApJ, 517, 103

Elmegreen, B. G. 2000, ApJ, 530, 277

Elmegreen, B. G. & Efremov, Y. N. 1997, ApJ, 480, 235

Elmegreen, B. G., Kaufman, M., & Thomasson, M. 1993, ApJ, 412, 90

et al., M. H. 2007, ApJ, 669, 1024

Evstigneeva, E. A., Gregg, M. D., Drinkwater, M. J., & Hilker, M. 2007, AJ, 133, 1722

Fabbiano, G., Brassington, N. J., Lentati, L., et al. 2010, ApJ, 725, 1824

Famaey, B. & McGaugh, S. S. 2012, Living Reviews in Relativity, 15, 10

Fellhauer, M., Baumgardt, H., Kroupa, P., & Spurzem, R. 2002, Celestial Mechanics and Dynamical Astronomy, 82, 113

Fellhauer, M. & Kroupa, P. 2002a, MNRAS, 330, 642

Fellhauer, M. & Kroupa, P. 2002b, AJ, 124, 2006

Fellhauer, M. & Kroupa, P. 2005a, MNRAS, 359, 223

Fellhauer, M. & Kroupa, P. 2005b, ApJ, 630, 879

Fellhauer, M. & Kroupa, P. 2006, MNRAS, 367, 1577

Fellhauer, M., Kroupa, P., Baumgardt, H., et al. 2000, New Astronomy, 5, 305

Ferguson, H. C. & Binggeli, B. 1994, A&ARv, 6, 67

Ferrarese, L., Côté, P., Jordán, A., et al. 2006, ApJS, 164, 334

Figer, D. F. 2004, in Astronomical Society of the Pacific Conference Series, Vol. 322, The Formation and Evolution of Massive Young Star Clusters, ed. H. J. G. L. M. Lamers, L. J. Smith, & A. Nota (Astronomical Society of the Pacific, San Francisco, CA), 49

Figer, D. F. 2005, Nature, 434, 192

Figer, D. F., Najarro, F., Morris, M., et al. 1998, ApJ, 506, 384

Forbes, D. A. & Kroupa, P. 2011, PASA, 28, 77

Forbes, D. A., Lasky, P., Graham, A. W., & Spitler, L. 2008, MNRAS, 389, 1924

Forbes, D. A., Spitler, L. R., Graham, A. W., et al. 2011, MNRAS, 413, 2665

Frank, M. J., Hilker, M., Mieske, S., et al. 2011, MNRAS, 414, L70

Galianni, P., Patat, F., Higdon, J. L., Mieske, S., & Kroupa, P. 2010, A&A, 521, 20

Gallazzi, A., Charlot, S., Brinchmann, J., & White, S. D. M. 2006, MNRAS, 370, 1106

Gallazzi, A., Charlot, S., Brinchmann, J., White, S. D. M., & Tremonti, C. A. 2005, MNRAS, 362, 41

Gao, L., White, S. D. M., Jenkins, A., Stoehr, F., & Springel, V. 2004, MNRAS, 355, 819

Gavazzi, G., Bonfanti, C., Sanvito, G., Boselli, A., & Scodeggio, M. 2002, ApJ, 576, 135

Geha, M., Guhathakurta, P., & van der Marel, R. P. 2003, AJ, 126, 1794

Gentile, G., Famaey, B., Combes, F., et al. 2007, A&A, 472, 25

Gesicki, K., Acker, A., & Zijlstra, A. A. 2003, A&A, 400, 957

Ghezzi, L., Cunha, K., Smith, V. V., et al. 2010, ApJ, 720, 1290

Gilmore, G., Wilkinson, M. I., Wyse, R. F. G., et al. 2007, ApJ, 663, 948

Goerdt, T., Moore, B., Kazantzidis, S., et al. 2008, MNRAS, 385, 2136

Goodwin, S. P. 2009, Ap&SS, 324, 259

Goodwin, S. P., Kroupa, P., Goodman, A., & Burkert, A. 2007, in Protostars and Planets V, ed. B. Reipurth, D. Jewitt, & K. Keil (Univ. Arizona Press, Tucson AZ), 133–147

Graham, A. W., Merritt, D., Moore, B., Diemand, J., & Terzić, B. 2006, AJ, 132, 2711

Gratton, R., Sneden, C., & Carretta, E. 2004, ARA&A, 42, 385

Greggio, L. 2005, A&A, 441, 1055

Guo, Q., White, S., Boylan-Kolchin, M., et al. 2011, MNRAS, 413, 101

Haşegan, M., Jordán, A., Côté, P., et al. 2005, ApJ, 627, 203

Harris, W. E. 1976, AJ, 81, 1095

Harris, W. E. 1996, AJ, 112, 1487

Harris, W. E., Whitmore, B. C., Karakla, D., et al. 2006, ApJ, 636, 90

Hartmann, L., Ballesteros-Paredes, J., & Bergin, E. A. 2001, ApJ, 562, 852

Heggie, D. & Hut, P. 2003, The Gravitational Million-Body Problem: A Multidisciplinary Approach to Star Cluster Dynamics (Cambridge University Press, Cambrigde)

Hernandez, X., Mendoza, S., Suarez, T., & Bernal, T. 2010, A&A, 514, A101

Hickson, P. 1982, ApJ, 255, 382

Hilker, M., Baumgardt, H., Infante, L., et al. 2007, A&A, 463, 119

Hilker, M., Infante, L., Vieira, G., Kissler-Patig, M., & Richtler, T. 1999, A&AS, 134, 75

Hilker, M., Kayser, A., Richtler, T., & Willemsen, P. 2004, A&A, 422, L9

Hilker, M., Mieske, S., & Infante, L. 2003, A&A, 397, L9

Hilker, M. & Richtler, T. 2000, A&A, 362, 895

Hills, J. G. 1980, ApJ, 235, 986

Hook, I. M., ed. 2005, The Science Case for the European Extremely Large Telescope: The next step in mankind's quest for the Universe

Hunsberger, S. D., Charlton, J. C., & Zaritsky, D. 1996, ApJ, 462, 50

Hunter, D. A., Hunsberger, S. D., & Roye, E. W. 2000, ApJ, 542, 137

Ibata, R. A., Lewis, G. F., Conn, A. R., et al. 2013, Nature, 493, 62

Ivanova, N., Heinke, C. O., Rasio, F. A., Belczynski, K., & Fregeau, J. M. 2008, MNRAS, 386, 553

Jordán, A., Côté, P., Ferrarese, L., et al. 2004, ApJ, 613, 279

Jordán A. et al. 2005, ApJ, 634, 1002

Jordán A. et al. 2007, ApJS, 171, 101

Kalirai, J. S., Hansen, B. M. S., Kelson, D. D., et al. 2008, ApJ, 676, 594

Kallivayalil, N., van der Marel, R. P., & Alcock, C. 2006, ApJ, 652, 1213

Karachentsev, I. D., Karachentseva, V. E., Huchtmeier, W. K., & Makarov, D. I. 2004, AJ, 127, 2031

Katz, J. I. 1975, Nature, 253, 698

Kauffmann, G., White, S. D. M., & Guiderdoni, B. 1993, MNRAS, 264, 201

Kawamura, A., Onishi, T., Yonekura, Y., et al. 1998, ApJS, 117, 387

Kayser, A., Hilker, M., Richtler, T., & Willemsen, P. G. 2006, A&A, 458, 777

Kennicutt, Jr., R. C. 1998, ApJ, 498, 541

King, I. 1962, AJ, 67, 471

King, I. R. 1966, AJ, 71, 276

Kissler-Patig, M., Brodie, J. P., Schroder, L. L., et al. 1998, AJ, 115, 105

Klypin, A., Kravtsov, A. V., Valenzuela, O., & Prada, F. 1999, ApJ, 522, 82

Koester, D. & Reimers, D. 1996, A&A, 313, 810

Kormendy, J. 1985, ApJ, 295, 73

Kroupa, P. 1997, New Astronomy, 2, 139

Kroupa, P. 1998, MNRAS, 300, 200

Kroupa, P. 2001, MNRAS, 322, 231

Kroupa, P. 2002, Science, 295, 82

Kroupa, P. 2007, ArXiv Astrophysics e-prints

Kroupa, P. 2008, in Lecture Notes in Physics, Vol. 760, The Cambridge N-Body Lectures, ed. S. J. Aarseth, C. A. Tout, & R. A. Mardling (Springer Verlag, Berlin), 181

Kroupa, P. 2012, ArXiv e-prints, 1204.2546

Kroupa, P., Aarseth, S., & Hurley, J. 2001, MNRAS, 321, 699

Kroupa, P. & Gilmore, G. F. 1994, MNRAS, 269, 655

Kroupa, P., Theis, C., & Boily, C. M. 2005, A&A, 431, 517

Kroupa, P., Tout, C. A., & Gilmore, G. 1993, MNRAS, 262, 545

Kroupa, P. & Weidner, C. 2003, ApJ, 598, 1076

Kroupa, P., Weidner, C., Pflamm-Altenburg, J., et al. 2011, ArXiv e-prints

Kroupa P. et al. 2010, A&A, 523, 32

Kruijssen, J. M. D. 2008, A&A, 486, L21

Kruijssen, J. M. D. & Lamers, H. J. G. L. M. 2008, A&A, 490, 151

Kumar, B., Sagar, R., & Melnick, J. 2008, MNRAS, 386, 1380

Lada, C. J. & Lada, E. A. 2003, ARA&A, 41, 57

Larsen, S. S., Forbes, D. A., & Brodie, J. P. 2001, MNRAS, 327, 1116

Larson, R. B. 1998, MNRAS, 301, 569

Li, Y.-S., De Lucia, G., & Helmi, A. 2010, MNRAS, 401, 2036

Lisker, T. 2009, Astronomische Nachrichten, 330, 1043

Loewenstein, M. 2006, ApJ, 648, 230

Lonsdale, C. J., Diamond, P. J., Thrall, H., Smith, H. E., & Lonsdale, C. J. 2006, ApJ, 647, 185

Lyne, A. G. & Lorimer, D. R. 1994, Nature, 369, 127

Maccarone, T. J., Kundu, A., & Zepf, S. E. 2003, ApJ, 586, 814

Maccarone, T. J. & Peacock, M. B. 2011, MNRAS, 415, 1875

Macciò, A. V., Dutton, A. A., van den Bosch, F. C., et al. 2007, MNRAS, 378, 55

Mainini, R., Macciò, A. V., Bonometto, S. A., & Klypin, A. 2003, ApJ, 599, 24

Maraston, C. 2005, MNRAS, 362, 799

Maraston, C., Bastian, N., Saglia, R. P., et al. 2004, A&A, 416, 467

Marks, M. & Kroupa, P. 2010, MNRAS, 406, 2000

Marks, M. & Kroupa, P. 2012, A&A, 543, A8

Marks, M., Kroupa, P., & Baumgardt, H. 2008, MNRAS, 386, 2047

Marks, M., Kroupa, P., Dabringhausen, J., & Pawlowski, M. S. 2012, MNRAS, 422, 2246

Maschberger, T. & Kroupa, P. 2009, MNRAS, 395, 931

Massey, P. 1998, in Astronomical Society of the Pacific Conference Series, Vol. 142, The Stellar Initial Mass Function (38th Herstmonceux Conference), ed. G. Gilmore & D. Howell, 17–44

Massey, P. & Hunter, D. A. 1998, ApJ, 493, 180

Mateo, M. L. 1998, ARA&A, 36, 435

Matteucci, F. & Greggio, L. 1986, A&A, 154, 279

Matteucci, F. & Recchi, S. 2001, ApJ, 558, 351

McConnachie, A. W. & Irwin, M. J. 2006, MNRAS, 365, 1263

McConnachie, A. W., Irwin, M. J., Ferguson, A. M. N., et al. 2005, MNRAS, 356, 979

McGaugh, S. S. & Wolf, J. 2010, ApJ, 722, 248

McLaughlin, D. E. 2000, ApJ, 539, 618

McLaughlin, D. E. & van der Marel, R. P. 2005, ApJS, 161, 304

Melioli, C. & de Gouveia Dal Pino, E. M. 2004, A&A, 424, 817

Metz, M. & Kroupa, P. 2007, MNRAS, 376, 387

Metz, M., Kroupa, P., & Jerjen, H. 2009, MNRAS, 394, 2223

Metz, M., Kroupa, P., & Libeskind, N. I. 2008, ApJ, 680, 287

Meylan, G., Sarajedini, A., Jablonka, P., et al. 2001, AJ, 122, 830

Mieske, S., Hilker, M., & Infante, L. 2002, A&A, 383, 823

Mieske, S., Hilker, M., & Infante, L. 2004, A&A, 418, 445

Mieske, S., Hilker, M., Infante, L., & Jordán, A. 2006a, AJ, 131, 2442

Mieske, S., Hilker, M., Jordán, A., Infante, L., & Kissler-Patig, M. 2007, A&A, 472, 111

Mieske, S., Hilker, M., Jordán, A., et al. 2008, A&A, 487, 921

Mieske, S., Hilker, M., & Misgeld, I. 2012, A&A, 537, A3

Mieske, S., Jordán, A., Côté, P., et al. 2006b, ApJ, 653, 193

Mieske, S., Jordán, A., Côté, P., et al. 2010, ApJ, 710, 1672

Mieske, S. & Kroupa, P. 2008, ApJ, 677, 276

Milgrom, M. 1983, ApJ, 270, 365

Mirabel, I. F., Dottori, H., & Lutz, D. 1992, A&A, 256, L19

Miralles-Caballero, D., Colina, L., & Arribas, S. 2012, A&A, 538, A61

Misgeld, I. & Hilker, M. 2011, MNRAS, 414, 3699

Misgeld, I., Hilker, M., & Mieske, S. 2009, A&A, 496, 683

Misgeld, I., Mieske, S., & Hilker, M. 2008, A&A, 486, 697

Monreal-Ibero, A., Colina, L., Arribas, S., & García-Marín, M. 2007, A&A, 472, 421

Moore, B., Diemand, J., Madau, P., Zemp, M., & Stadel, J. 2006, MNRAS, 368, 563

Moore, B., Ghigna, S., Governato, F., et al. 1999, ApJL, 524, L19

Murray, N. 2009, ApJ, 691, 946

Murray, S. D. & Lin, D. N. C. 1996, ApJ, 467, 728

Nagashima, M., Lacey, C. G., Baugh, C. M., Frenk, C. S., & Cole, S. 2005, MNRAS, 358, 1247

Navarro, J. F., Frenk, C. S., & White, S. D. M. 1997, ApJ, 490, 493

Navarro, J. F., Ludlow, A., Springel, V., et al. 2010, MNRAS, 402, 21

Nomoto, K., Tominaga, N., Umeda, H., Kobayashi, C., & Maeda, K. 2006, Nuclear Physics A, 777, 424

Oey, M. S. & Clarke, C. J. 2005, ApJ, 620, 43

Okazaki, T. & Taniguchi, Y. 2000, ApJ, 543, 149

Paolillo, M., Puzia, T. H., Goudfrooij, P., et al. 2011, ApJ, 736, 90

Papadopoulos, P. P. 2010, ApJ, 720, 226

Pawlowski, M. S., Kroupa, P., Angus, G., et al. 2012a, MNRAS, 424, 80

Pawlowski, M. S., Pflamm-Altenburg, J., & Kroupa, P. 2012b, MNRAS, 2990

Peacock, M. B., Maccarone, T. J., Kundu, A., & Zepf, S. E. 2010, MNRAS, 407, 2611

Peng E. et al. 2008, ApJ, 681, 197

Pflamm-Altenburg, J. & Kroupa, P. 2006, MNRAS, 373, 295

Phillipps, S., Drinkwater, M. J., Gregg, M. D., & Jones, J. B. 2001, ApJ, 560, 201

Plummer, H. C. 1911, MNRAS, 71, 460

Prantzos, N. & Charbonnel, C. 2006, A&A, 458, 135

Press, W. H., Teukolsky, S. A., Vetterling, W. T., & Flannery, B. P. 1992, Numerical recipes in C. The art of scientific computing, 2nd ed. (Cambridge University Press, Cambridge)

Prosser, C. F., Stauffer, J. R., Hartmann, L., et al. 1994, ApJ, 421, 517

Recchi, S., Calura, F., & Kroupa, P. 2009, A&A, 499, 711

Recchi, S., Matteucci, F., & D'Ercole, A. 2001, MNRAS, 322, 800

Recchi, S., Theis, C., Kroupa, P., & Hensler, G. 2007, A&A, 470, L5

Rejkuba, M., Dubath, P., Minniti, D., & Meylan, G. 2007, A&A, 469, 147

Richtler, T. 2003, in Lecture Notes in Physics, Berlin Springer Verlag, Vol. 635, Stellar Candles for the Extragalactic Distance Scale, ed. D. Alloin & W. Gieren, 281–305

Salaris, M. & Weiss, A. 2002, A&A, 388, 492

Salpeter, E. E. 1955, ApJ, 121, 161

Sanders, D. B., Mazzarella, J. M., Kim, D., Surace, J. A., & Soifer, B. T. 2003, AJ, 126, 1607

Sanders, R. H. 2008, MNRAS, 386, 1588

Sarazin, C. L., Kundu, A., Irwin, J. A., et al. 2003, ApJ, 595, 743

Schaller, G., Schaerer, D., Meynet, G., & Maeder, A. 1992, A&AS, 96, 269

Sérsic, J. L. 1963, Boletin de la Asociacion Argentina de Astronomia La Plata Argentina, 6, 41

Simon, J. D. & Geha, M. 2007, ApJ, 670, 313

Sivakoff, G. R., Jordán, A., Sarazin, C. L., et al. 2007, ApJ, 660, 1246

Soifer, B. T., Neugebauer, G., Matthews, K., et al. 1999, ApJ, 513, 207

Spergel D. N. et al. 2007, ApJS, 170, 377

Spitzer, L. 1987, Dynamical evolution of globular clusters (Princeton, NJ: Princeton University Press)

Spitzer, L. J. & Hart, M. H. 1971, ApJ, 164, 399

Springel, V., White, S. D. M., Jenkins, A., et al. 2005, Nature, 435, 629

Strigari, L. E., Bullock, J. S., Kaplinghat, M., et al. 2008, Nature, 454, 1096

Tantalo, R., Chiosi, C., & Bressan, A. 1998, A&A, 333, 419

Tenorio-Tagle, G., Palouš, J., Silich, S., Medina-Tanco, G. A., & Muñoz-Tuñón, C. 2003, A&A, 411, 397

Tenorio-Tagle, G., Wünsch, R., Silich, S., & Palouš, J. 2007, ApJ, 658, 1196

Thies, I. & Kroupa, P. 2007, ArXiv e-prints, 708

Thomas, D., Maraston, C., & Bender, R. 2003, MNRAS, 339, 897

Thomas, D., Maraston, C., Bender, R., & Mendes de Oliveira, C. 2005, ApJ, 621, 673

Thorsett, S. E. & Chakrabarty, D. 1999, ApJ, 512, 288

Toloba, E., Boselli, A., Cenarro, A. J., et al. 2011, A&A, 526, A114

Toomre, A. & Toomre, J. 1972, ApJ, 178, 623

Tortora, C., Napolitano, N. R., Romanowsky, A. J., Capaccioli, M., & Covone, G. 2009, MNRAS, 396, 1132

Trager, S. C., Faber, S. M., Worthey, G., & González, J. J. 2000, AJ, 119, 1645

Tran H. D. et al. 2003, ApJ, 585, 750

van de Ven, G., van den Bosch, R. C. E., Verolme, E. K., & de Zeeuw, P. T. 2006, A&A, 445, 513

van der Marel, R. P., Alves, D. R., Hardy, E., & Suntzeff, N. B. 2002, AJ, 124, 2639

van Dokkum, P. G. 2008, ApJ, 674, 29

van Dokkum, P. G. & Conroy, C. 2010, Nature, 468, 940

van Loon, J. T., Stanimirović, S., Evans, A., & Muller, E. 2006, MNRAS, 365, 1277

VandenBerg, D. A. 2000, ApJS, 129, 315

Verbunt, F. 2003, in Astronomical Society of the Pacific Conference Series, Vol. 296, New Horizons in Globular Cluster Astronomy, ed. G. Piotto, G. Meylan, S. G. Djorgovski, & M. Riello, 245–+

Verbunt, F. & Hut, P. 1987, in IAU Symposium, Vol. 125, The Origin and Evolution of Neutron Stars, ed. D. J. Helfand & J.-H. Huang, 187–197

Villanova S. et al. 2007, ApJ, 663, 296

Wehner, E. M. H. & Harris, W. E. 2007, ApJ, 668, L35

Weidner, C. & Kroupa, P. 2004, MNRAS, 348, 187

Weidner, C. & Kroupa, P. 2005, ApJ, 625, 754

Weidner, C. & Kroupa, P. 2006, MNRAS, 365, 1333

Weidner, C., Kroupa, P., & Bonnell, I. A. D. 2010, MNRAS, 401, 275

Weidner, C., Kroupa, P., & Larsen, S. S. 2004, MNRAS, 350, 1503

Weidner, C., Kroupa, P., & Pflamm-Altenburg, J. 2011, MNRAS, 979

Weilbacher, P. M., Duc, P.-A., Fritze v. Alvensleben, U., Martin, P., & Fricke, K. J. 2000, A&A, 358, 819

Wetzstein, M., Naab, T., & Burkert, A. 2007, MNRAS, 375, 805

Whelan, J. & Iben, I. J. 1973, ApJ, 186, 1007

White, S. D. M. & Rees, M. J. 1978, MNRAS, 183, 341

Whitmore, B. C. & Schweizer, F. 1995, AJ, 109, 960

Wiklind, T., Combes, F., & Henkel, C. 1995, A&A, 297, 643

Willman, B. & Strader, J. 2012, AJ, 144, 76

Wolf, J., Martinez, G. D., Bullock, J. S., et al. 2010, MNRAS, 406, 1220

Woodley, K. A., Raychaudhury, S., Kraft, R. P., et al. 2008, ApJ, 682, 199

Woosley, S. E. 1987, in IAU Symposium, Vol. 125, The Origin and Evolution of Neutron Stars, ed. D. J. Helfand & J.-H. Huang, 255–270

Woosley, S. E., Heger, A., & Weaver, T. A. 2002, Reviews of Modern Physics, 74, 1015

Worthey, G. 1994, ApJS, 95, 107

Wu, X. 2007, ArXiv Astrophysics e-prints

Wuchterl, G. & Tscharnuter, W. M. 2003, A&A, 398, 1081

Xin, Y., Deng, L., & Han, Z. W. 2007, ApJ, 660, 319

Yoon, S.-J., Yi, S. K., & Lee, Y.-W. 2006, Science, 311, 1129

Yoshida, M., Yagi, M., Komiyama, Y., et al. 2008, ApJ, 688, 918

Young L. M. et al. 2011, MNRAS, 414, 940

Zepf, S. E. & Whitmore, B. C. 1993, ApJ, 418, 72

Zhang, Z., Gilfanov, M., & Bogdan, A. 2012, ArXiv e-prints

Zinnecker, H., Keable, C. J., Dunlop, J. S., Cannon, R. D., & Griffiths, W. K. 1988, in IAU Symposium, Vol. 126, The Harlow-Shapley Symposium on Globular Cluster Systems in Galaxies, ed. J. E. Grindlay & A. G. D. Philip, 603–604

Zwicky, F. 1956, Ergebnisse der exakten Naturwissenschaften, 29, 344